– Dissertation –

submitted to the
Combined Faculties of the Natural Sciences and Mathematics
of the Ruperto-Carola University of Heidelberg, Germany
for the degree of
Doctor of Natural Sciences

Put forward by
Aaron Held
born in: Freiburg i. Br. (Germany)
oral examination: December 11th, 2019

2019

From particle physics to black holes:
The predictive power of asymptotic safety

Referees: Prof. Dr. Astrid Eichhorn
Prof. Dr. Tilman Plehn

Acknowledgements

I had the amazing opportunity to experience science as collaborative and fun. For this, I am most grateful to all researchers that have participated in and provided guidance during the research leading to this thesis. In particular, I am grateful to all the current and former group members of the now delocalizing quantum-gravity group of Astrid Eichhorn. Above all, I want to thank Astrid for providing such a stimulating scientific atmosphere, always caring about all of our individual development, and leading all of us to deliver our very possible best.
I would also like to thank my wife, my family, and friends that have provided a home for me to come to and find new strength and acceptance of what I do.

While this thesis presents my own view and a broader context of all results, a large part of the material covered in this thesis is based on published work in collaboration with other scientists. For the convenience of the reader, I list these publications in reversed chronological order and refer to the sections in which they are discussed:

- [1] "Predictive power of grand unification from quantum gravity," A. Eichhorn, A. Held and C. Wetterich, arXiv:1909.07318 [hep-th], see Sec. 6.
- [2] "Asymptotic safety, string theory and the weak gravity conjecture," S. de Alwis, A. Eichhorn, A. Held, J. M. Pawlowski, M. Schiffer and F. Versteegen, Phys. Lett. B. 798 (2019) 134991, see Sec. 5.
- [3] "Asymptotic safety casts its shadow," A. Held and R. Gold and A. Eichhorn, JCAP 1906 (2019) 029, see Sec. 7.
- [4] "Higgs-mass bound and fermionic dark matter," A. Held and R. Sondenheimer, JHEP 1902 (2019) 166, see Sec. 3.
- [5] "Mass difference for charged quarks from asymptotically safe quantum gravity," A. Eichhorn and A. Held, Phys.Rev.Lett. 121 (2018) no.15, 151302, see Sec. 5.
- [6] "Asymptotic safety in the dark," A. Eichhorn, A. Held and P. V. Griend, JHEP 1808 (2018) 147, see Sec. 3.
- [7] "Quantum-gravity predictions for the fine-structure constant," A. Eichhorn, A. Held and C. Wetterich, Phys. Lett. B782 (2018) 198-201, see Sec. 6.
- [8] "Top mass from asymptotic safety," A. Eichhorn and A. Held, Phys. Lett. B777 (2018) 217-221, see Sec. 4.
- [9] "Viability of quantum-gravity induced ultraviolet completions for matter," A. Eichhorn and A. Held, Phys. Rev. D96 (2017) no.8, 086025, see Sec. 4.
- [10] "Is scale-invariance in gauge-Yukawa systems compatible with the graviton?," N. Christiansen, A. Eichhorn and A. Held, Phys. Rev. D96 (2017) no.8, 084021, see Sec. 3.

The following sections contain work from ongoing collaborations to be published in the future:

- "Quark masses and mixings in a minimal, parameterized ultraviolet completion of the Standard Model" in collaboration with Reinhard Alkofer, Astrid Eichhorn, Carlos M. Nieto, Roberto Percacci, and Markus Schröfl, see Sec. 5.

Abstract

At the Planck scale, matter, space, and time fluctuate collectively. This thesis explores the phenomenology of a suggested joint theory of quantum gravity and matter. The discovery of the Higgs boson has completed the Standard Model of particle physics, realizing a delicate balance of the measured masses and couplings for which the Higgs potential provides a strong hint for Planckian quantum scale symmetry. The latter could also tame gravitational and Abelian interactions and render both General Relativity and the Standard Model asymptotically safe.

A pivotal weak-gravity mechanism could facilitate a gravitationally induced UV-completion of the Standard Model. Within this scenario, the asymptotic-safety paradigm potentially enhances the predictive power of the Standard Model. It could uniquely fix the Abelian gauge and various Yukawa couplings from first principles. We uncover mechanisms which could link the mass difference of top and bottom quark to their charge ratio, could dynamically favor small Dirac neutrino masses, and might allows for phenomenologically appealing transitions between different fixed points of the CKM-mixing matrix. In the absence of intermediate scales, those Planckian predictions are connected to the electroweak scale by Renormalization Group flows. This could permit testing quantum gravity at accessible energy scales.
Thereupon, we generalize the paradigm of quantum scale symmetry and the associated enhanced predictivity to grand unification where it potentially restores the predictivity of the complicated chain of spontaneous symmetry breaking.

Asymptotically safe quantum fluctuations could also resolve the singularity at the center of black holes. We obtain the shadow boundary for non-spinning and spinning regular black holes. In comparing to the shadow image obtained by the Event Horizon Telescope, we find that horizonless objects can not yet be excluded.

An der Planckskala fluktuieren Materie, Raum und Zeit gemeinsam. Die vorliegende Doktorarbeit erforscht die Phenomenologie einer möglichen gemeinsamen Quantentheore von Gravitation und Materie. Die Entdeckung des Higgs-Bosons hat das Standardmodell der Teilchenphysik so vervollständigt, dass eine empfindliche Balance der gemessenen Massen und Kopplungen, für welche das Higgspotential einen starken Hinweis auf Plancksche Quantum-Skalensymmetrie liefert, realisiert ist. Letztere könnte zudem die Gravitations- und Abelsche Wechselwirkung zähmen und sich damit sowohl Allgemeine Relativitätstheorie, als auch das Standardmodell als asymptotisch sicher erweisen.

Ein zentraler Mechanismus, der der schwachen Gravitation, könnte eine gravitationsinduzierte UV-Vervollständigung des Standardmodells ermöglichen. Innerhalb dieses Szenarios erhöht das Paradigma der asymptotischen Sicherheit potentiell die Vorhersagekraft des Standardmodells. Es könnte die Abelsche Eichkopplung und verschiedene Yukawakopplungen fundamental fixieren. Wir legen Mechanismen frei, welche die Massendifferenz von Top- und Bottomquark mit ihrer Ladungsdifferenz verknüpen, dynamisch eine kleine Dirac-Neutrinomasse bevorzugen und phenomenologisch attraktive Übergänge zwischen unterschiedlichen Fixpunkten der CKM-Matrizen erlauben könnten. In Abwesenheit intermediärer Skalen verbinden Renormierungsgruppenflüsse diese Planckschen Vorhersagen mit der elektroschwachen Skala. Dies könnte Tests der Quantengravitation auf erreicharen Energieskalen erlauben.
Im Weiteren verallgemeinern wir das Paradigma der Quantenskaleninvarianz und die damit verbundene erhöhte Vorhersagekraft für Modelle der großen Vereinigung, in welchen diese potentiell die Prädiktivität der komplizierten spontanen Symmetriebrechungskette wiederherstellt.

Des Weiteren könnten asymptotisch sichere Quantenfluktuationen die Singularität im Zentrum Schwarzer Löcher aufheben. Wir bestimmen den Schattenumriss nichtrotierender und rotierender, regulärer Schwarzer Löcher. Durch Vergleich mit dem Schattenbild des Event Horizon Teleskops stellen wir fest, dass Objekte ohne Horizont noch nicht ausgeschlossen werden können.

Conventions

We work in natural units in which Planck's constant $\hbar$ and the speed of light c are set by $\hbar = c = 1$. Also, we use the $(-,+,+,+)$ metric-convention.

The predictivity of scale-invariant regimes will be integral much of the physics presented here. The following two sets of terminology – despite putting different emphasis – are equivalent, respectively:

- positive critical exponent, i.e., $\theta > 0$ — relevant — ultraviolet (UV)-attractive infrared (IR)-repulsive — predicted direction,
- negative critical exponent, i.e., $\theta > 0$ — irrelevant — infrared (IR)-attractive ultraviolet (UV)-repulsive — free parameter.

While all abbreviations and symbols will be consistently introduced in the main text, we provide a compendium of the most frequently used ones for reference.

Frequently used abbreviations

AS	Asymptotic safety
ASSM	Asymptotically safe Standard Model
CKM	Cabibbo-Kobayashi-Maskawa
FP	Fixed point
EFT	Effective field theory
GFP	Gaußian fixed point
GR	General Relativity
GUT	Grand unified theory
IR	Infrared
ΛCDM	Λ-Cold-Dark-Matter (cosmology)
MSAS	Maximally symmetric asymptotic safety
NGFP	non-Gaußian fixed point
νSM	Standard Model including ν_R
QFT	Quantum Field Theory
QM	Quantum Mechanics
RG	Renormalization Group
SM	Standard Model (of particle physics)
UV	Ultraviolet

Frequently used symbols

For non-marginal operators, "barred" couplings denote the dimensionful version, e.g. $\overline{G}$, and "unbarred" couplings the dimensionless version, e.g., G.

$\alpha_g = g^2/(4\pi)$	squared gauge coupling (GUT conventions)
$\alpha_y = y^2/(4\pi)$	squared gauge coupling (GUT conventions)
$\tilde{\alpha}_g = g^2/(4\pi)^2$	squared gauge coupling (SM conventions)
G	Newton coupling (dimensionless)
g_i	gauge couplings
k	RG scale
Λ	Cosmological constant (dimensionless)
λ_i	quartic couplings
M_{Planck}	Planck scale / Planck mass
μ	physical RG scale
y_i	Yukawa couplings

Contents

Motivation **1**

I Quantizing gravity: An asymptotically safe review **3**

1 Where to expect new physics? **4**
1.1 The Standard-Model desert conjecture 5
1.1.1 The Standard Model and unexplained phenomena in particle physics . . . 6
1.1.2 General Relativity and riddles of cosmological evolution 12
1.1.3 What constitutes dark matter? 14
1.2 Field theories predicting their own breakdown 15
1.2.1 Singularities of General Relativity 15
1.2.2 Singularities of the Standard Model 16
1.3 The perturbative quantization of gravity 17
1.3.1 Renormalizable quadratic gravity and unitarity 18
1.3.2 What next? Different branches of quantum gravity 19

2 Fixed points and the status of renormalizing gravity **21**
2.1 A brief introduction to non-perturbative renormalization 21
2.2 Weinbergs asymptotic-safety paradigm 23
2.2.1 Approximation schemes to the full effective action 24
2.2.2 UV and IR fixed points for a single coupling: Conformal window for QCD 25
2.2.3 Fixed points for multiple couplings 26
2.3 Mechanisms for asymptotic safety 28
2.3.1 Classical vs quantum scaling 28
2.3.2 Balance of fermionic and bosonic fluctuations 29
2.3.3 Balance of different loop orders: the Litim-Sannino fixed point 30
2.4 The Reuter fixed-point of asymptotically safe quantum gravity 31
2.4.1 The near-canonical-scaling conjecture 33
2.4.2 The Einstein-Hilbert truncation and the classical limit 33
2.4.3 Evidence for the near-canonical-scaling conjecture 35
2.4.4 Towards infinite-dimensional theory space 35
2.5 Outstanding questions in asymptotically safe gravity 36

II Bridging the gap: Particle physics and Planckian scale symmetry **37**

3 Beyond the Standard Model: New physics – new problems **38**
3.1 The Higgs potential as a window into new physics 38
3.1.1 The Higgs-potential and (fermionic) dark matter 38
3.1.2 Fermionic dark matter and the Standard-Model Higgs potential 42
3.2 Asymptotic safety at a large number of degrees of freedom 45
3.2.1 Litim-Sannino fixed points and gravitational corrections 45
3.2.2 Effective asymptotic safety and predictivity for Litim-Sannino models . . 47

4 Matter in asymptotically safe gravity: structure and symmetry 50
4.1 Maximally symmetric asymtotic safety . . . 50
4.1.1 Matter fluctuations and the potential loss of asymptotic safety of gravity . 53
4.1.2 A weak-gravity mechanism: The propagator of gravitational fluctuations . 54
4.1.3 The scalar-fermion sector of MSAS . . . 56
4.2 Weak-gravity bound: gravitationally induced matter interactions . . . 59
4.3 Viability bound: emergence of a non-trivial low-energy sector . . . 60
4.3.1 Constraints on higher-order gravitational parameter space . . . 62
4.4 The fixed-point structure of marginal Standard-Model couplings . . . 63
4.4.1 Gravitationally induced anomalous dimensions . . . 63
4.4.2 Upper bound structures for global-symmetry reducing couplings . . . 63
4.5 Towards an asymptotically safe UV completion for the Standard Model . . . 64
4.5.1 Yukawa couplings and a viable phenomenology . . . 65
4.5.2 Upper bound for the top mass from asymptotic safety . . . 66
4.5.3 First trajectories of an asymptotically safe Standard Model . . . 68
4.5.4 Systematic errors and convergence . . . 69

5 The asymptotically safe Standard Model (ASSM) 71
5.1 Standard-Model UV-completion from dimensional reduction . . . 71
5.2 Gauge couplings and upper bounds from asymptotic safety . . . 73
5.3 Single-generation Yukawa fixed-points . . . 73
5.3.1 Mass-difference for charged quarks from asymptotic safety . . . 74
5.3.2 Dynamically vanishing Dirac-neutrino masses from scale-invariance . . . 77
5.4 Fixed-point structure in multiple generations . . . 80
5.4.1 Analytical results and mechanisms for two generations . . . 81
5.4.2 Three-generation CKM-mixing angles and scale-invariance . . . 84
5.5 Effective asymptotic safety of quantum gravity . . . 85

6 Unified asymptotic safety 87
6.1 Motivation: why unify? . . . 88
6.1.1 Unification of quarks and leptons and charge quantization . . . 88
6.1.2 Gauge unification, proton decay and $SO(10)$ breaking chains . . . 90
6.1.3 Fermion masses in $SO(10)$ unification . . . 92
6.1.4 Unification and asymptotic freedom . . . 93
6.2 Minimal GUTs and a lack of predictivity . . . 94
6.3 Losing asymptotically freedom and gaining asymptotic safety . . . 96
6.3.1 Complete asymptotic freedom in the presence of gravity . . . 97
6.3.2 Asymptotic safety at the boundary of complete asymptotic freedom . . . 98
6.3.3 Asymptotically safe gauge-Yukawa sector of minimal SU(5) . . . 99
6.4 Restoring predictivity for GUTs: asymptotically safe potentials . . . 100
6.4.1 Planck-induced GUT-symmetry breaking: a simple toy model . . . 100
6.4.2 Quartic couplings and the direction of symmetry breaking . . . 102

III New horizons:
Black-hole physics as a potential window into quantum gravity 105

7 Shadows without singularities 106
7.1 Singularity resolution in quantum gravity 106
7.1.1 Renormalization-Group improved black holes 106
7.1.2 Singularity resolution from other quantum-gravity models 108
7.2 Spherically-symmetric and singularity-free shadows 108
7.3 A dent in singularity-free Kerr spacetime 111

Conclusions 118

Outlook 120

Appendix 123

A Standard-Model parameters and couplings 124

B Fermionic Higgs-portal model: Supplementary material 125
B.1 β-functions for the fermionic Higgs-portal model 125
B.2 Convergence properties of the asymptotically safe fixed point 127
B.3 Fiducial Standard-Model to mimic the Higgs potential 127

C Matter in asymptotically safe gravity: Supplementary material 129
C.1 Diagramatic expansion of the flow equation 129
C.2 Threshold integrals 130
C.3 Bounds on gravitational parameter space 133
C.4 Suppression of matter-mediated effects 134

D CKM running in three generations 136

E RG-flow of the scalar potential in a simple gauge-Yukawa model 137

F Ray tracing in regular spacetimes 138
F.1 Simple Ray Tracer: A mathematica package 138
F.2 Secondary features in the shadow boundary for near-critical $\tilde{\gamma}$ 141

References 142

Motivation

Quantum gravity is an attempt to unify Quantum Mechanics and General Relativity. On the one hand, General Relativity describes how spacetime is curved by the objects within, much like a trampoline surface is stretched by a heavy object. On the other hand, Quantum Mechanics requires fundamental particles to not be fully localized. So what happens, if an object is small enough to be quantum and energetic enough to curve space and time? If, for instance, two electrons were to collide at extremely high center-of-mass energy, the collision would significantly curve the surrounding spacetime. But, since the electrons are quantized, spacetime itself should then be quantized, too. The effect of quantized matter on spacetime can usually be neglected since the associated energy scale – the Planck scale – is enormous. In fact, if a single proton were to reach this regime, it would have to burn through the entire planet's natural oil reserve. Nevertheless, the last decade offered two great experimental breakthroughs in fundamental physics: the discovery of the Higgs boson and first glimpses of the strong curvature regime. And both come with the profound and possibly surprising implication that Planck-scale physics might not be completely out of reach after all.

The discovery of the Higgs boson completes the Standard Model of particle physics such that it extends consistently up to the Planck scale, i.e., a huge desert is realized. The measured Higgs-mass value realizes a delicate balance for which the Higgs potential could be perfectly flat at Planckian energies. The latter provides a strong hint for a new asymptotic form of symmetry referred to as scale invariance. The desert scenario is supported by the persisting absence of any new physics in the vicinity of present particle masses: no sign of supersymmetry, no dark-matter candidate, no statistically significant deviations of the Standard Model at all. This leads us to consider the tentatively implied alternative, namely that our picture of the universe might be complete – all the way up to the Planck scale.

On the other hand, neither the Standard Model nor General Relativity is consistent beyond the Planck scale. The electromagnetic force within the Standard Model is infinitely screened at the transplanckian Landau pole. Similarly, General Relativity is plagued by transplanckian singularities as well. These occur at the center of its black-hole solutions. A resolution of these inconsistencies becomes an even more pressing issue in light of the second great experimental breakthrough of this decade. The Event Horizon Telescope captured humanities' first image of a shadow at the center of galaxies and the LIGO collaboration detected gravitational waves of compact binary mergers. These extraordinary advances into the strong-curvature regime firmly establish black-hole-like compact objects as the stable final state of gravitational collapse. They offer novel probes of horizon-scale physics and put the singularities of General Relativity into the spotlight of attention. Possible modified gravitational dynamics in this previously unexplored regime might carry traces of singularity-resolving modifications of General Relativity.

The significance of the Planck scale in all of the above motivates the main synthesis of this doctoral thesis: It takes two outstanding physical problems, (i) the lack of direct experiments to constrain quantum gravity and (ii) the implied absence of new physics at accessible energy scales, and brings them together under the combined framework of quantum scale symmetry. The consistency of the SM allows to reconstruct the running of its marginal couplings all the way up from the electroweak to the Planck scale which could establish a unique link between quantum gravity and observable physics. Hinging on the experimentally suggested Planckian

scale invariance, the theoretical framework of asymptotic safety elevates this hint to the central paradigm of quantum scale symmetry. Just like discrete symmetries cause crystals to grow in specific patterns, scale symmetry could relate different running couplings and thereby enhance the predictivity of fundamental physics. The implied relations for fundamental couplings in particle physics and modified gravity could allow to test this theoretical framework at colliders and with strong-curvature observations of black holes.

This Ph.D. thesis is split into three parts: Part I, containing Sec. 1-2, is mostly introductory, while the Part II (Sec. 3-6) and III (Sec. 7) encompass original material on quantum-gravity phenomenology in particle and black-hole physics, respectively. To help guide the reader through this thesis we provide abstracts at the beginning of each of the sections containing original material and offer intermediate conclusions where useful.

Sec. 1 will elaborate on the presented motivation. It will review current experimental evidence for unexplained phenomena beyond the Standard Model and General Relativity, focusing on possible Planckian solutions. We invite the reader to consider this rather unusual perspective. We proceed to look more closely at the singular behavior of both theories which will naturally also take us to an introduction to the fundamental problem of quantizing the gravitational force. Sec. 2 makes an effort to present a concise but accessible introduction to the technical framework of the (functional) Renormalization Group and the asymptotic-safety paradigm. While introducing the latter, we emphasize the phenomenology and the predictive power of scale invariance. These will be indispensable concepts to an understanding of the results in Part II.

Sec. 3 sidetracks from the Planckian scale symmetry. It explores asymptotic safety in the context of non-gravitational models at subplanckian scales. In a broader context, it exemplifies how delicately the Standard-Model balance reacts to new physics at intermediate scales. It highlights that asymptotic safety can also remain predictive as an effective field theory.
Sec. 4 and 5 make up the heart of this thesis and examine the phenomenology and enhanced predictive power of the asymptotic-safety paradigm for quantum gravity and matter. These two sections complement each other: Sec. 4 presents non-perturbative functional RG calculations to determine the contributions of asymptotically safe gravitational fluctuations to the Standard Model and its Yukawa couplings, in particular. In contrast, Sec. 5 relies on a small set of well-motivated assumptions and thereupon searches for the most predictive form of quantum scale invariance within a fully perturbative setup.
Sec. 6 goes beyond the Standard Model. It generalizes the potential quantum scale symmetry to theories of grand unification. This is particularly appealing since the latter could remain without any free parameters. It bears the potential to restore predictivity to otherwise undetermined symmetry-breaking chains. We initiate a program to explore whether an asymptotically safe grand-unification model can reproduce the Standard Model.

Finally, Part III (Sec. 7) moves to the topic of singularity resolution. We pioneer in exploring the modifications of the shadow boundary of spinning and non-spinning spacetimes due to singularity-resolving physics tied to local curvature scales. While such singularity-free spacetimes can be motivated from asymptotic safety and other quantum-gravity models, their most appealing phenomenology arises when the singularity-resolving physics is probed more generally. Within our parameterization, we find that current data from the Event Horizon Telescope is not yet able to exclude the possibility of horizonless compact objects.

Part I

Quantizing gravity: An asymptotically safe review

1 Where to expect new physics?

Modern-day fundamental physics has bifurcated into quantum physics, which was developed into the Standard Model of particle physics (SM), and gravitational physics, beautifully described by General Relativity (GR). This reflects the arguably most conspicuous shortcoming of our understanding of Nature – it is also the main focus of this thesis. We can – and most often do – look at these two regimes of fundamental physics separately because of their vastly separated fundamental scales. So where do we expect quantum gravity?

The fundamental constant of quantum physics is the Planck constant[1]

$$\hbar = 6.62607015 \times 10^{-34} \, \frac{kg\, m^2}{s} \, . \tag{1.1}$$

Its units are [energy]×[time]. Whenever a physical system reaches such energies in a corresponding time interval, or equivalently momenta on corresponding length scales, it is subject to quantum fluctuations. All associated phenomena can nowadays be described consistently by the laws of quantum mechanics (or its relativistic extension, i.e., Quantum Field Theory). In short: $\hbar$ sets the scale at which quantum physics becomes important.
Gravitational physics is set by a different fundamental constant, Newton's constant[2],

$$\overline{G} = 6.6743(15) \times 10^{-11} \, \frac{m^3}{kg\, s^2} \, . \tag{1.2}$$

Its units can be expressed as [force]×[distance]/[mass^2] and it measures how large the gravitational forces are that two objects with specified masses at a given distance exert on each other. In short: $\overline{G}$ sets the scale at which gravitational physics becomes important.
Both quantum and gravitational theory share another fundamental constant: the speed of light[3],

$$c = 2.99792458 \times 10^{8} \, \frac{m}{s} \, , \tag{1.3}$$

The speed of light unifies quantum mechanics and special relativity into Quantum Field Theory (QFT) and equates the gravitational force with geometry to form GR.

Combining these three fundamental constants, one can infer characteristic units of all physical quantities such as (Planck) length, (Planck) time and (Planck) energy[4].

$$l_{\text{Planck}} = t_{\text{Planck}} \, c = \sqrt{\frac{\hbar \, \overline{G}}{c^3}} \, , \qquad M_{\text{Planck}} = p_{\text{Planck}}/c = E_{\text{Planck}}/c^2 = \sqrt{\frac{\hbar \, c}{\overline{G}}} \, . \tag{1.4}$$

Equating $c \equiv 1$, i.e., implicitly measuring all velocities in units of the speed of light, identifies units of length and time, as well as those of mass, momentum and energy.
Characteristic units for QFT and GR are found by also equating the respective other fundamental constant. In QFT, the so-called *natural units* are set by $\hbar = c = 1$ (and $k_B = \epsilon_0 = 1$). In

[1] Since 2018, the value of $\hbar$ is decided upon as an exact definition, part of the SI units, and replaces the definition of a kg [11].

[2] $\overline{G}$ is not part of the definition of SI units. The above value is the CODATA recommended value [12].

[3] The value of c is again part of the definition of SI units and thus exact.

[4] To describe temperature one needs an additional constant, the Boltzman constant $k_B = 1.380649 \times 10^{-23} \, J/K$. Similarly, to describe processes involving electromagnetic (as well as weak or strong) forces one requires the corresponding coupling constant.

GR, the so-called *geometerized units* are set by $\overline{G} = c = 1$. *Planck units*, the characteristic units of quantum gravity are set by $\overline{G} = \hbar = c = 1$. In natural units, the Planck energy (or equivalently Planck mass or momentum) corresponds to an enormously large scale of

$$E_{\text{Planck}} = \sqrt{\frac{\hbar\, c^5}{\overline{G}}} \approx 1.2209 \times 10^{19}\ \text{GeV}\ . \tag{1.5}$$

In comparison, the most energetic current collider experiments at the Large Hadron Collider (LHC) run at a center-of-mass energy of 1.3×10^4 GeV [13]. Even astrophysical observations of ultra-high energy neutrinos only reach $\sim 10^6$ GeV [14]. As a consequence, gravitational effects are suppressed by 15 (13) orders of magnitude. Similar estimates demonstrate that direct quantum effects are highly suppressed in all of gravitational physics accessible to experiment to date.
It is misleading to expect quantum gravitational effects if only one of these scales is reached. For instance, we surpass the Planck mass, $M_{\text{Planck}} \sim 22\,\mu g$, in most everyday processes. To expect quantum gravity, *all* scales involved in a physical process must become Planckian. Put differently, one can identify the following non-Planckian limits:

- gravity is negligible whenever $\frac{\text{length}}{\text{mass}} \gg \frac{\overline{G}}{c^2}$,
- quantum effects are negligible whenever length $\times$ mass $\gg \hbar$.

Both of the above limits are tremendously successful descriptions of all measured physical processes in each of the respective regimes of physics. Their unification into a quantum theory of gravity remains a century-long challenge for fundamental theoretical physics.

The following introductory chapter advocates the possibility that our subplanckian understanding of Nature could be complete. This rather radical viewpoint is suggested by the current absence of unexplained experimental signatures. We will review current experimental evidence for unexplained phenomena in both particle and gravitational physics, with particular focus on solutions which can be attributed to Planckian scales, see Sec. 1.1. Despite subplanckian completeness, Landau poles in QFT and singularities in GR constitute glaring theoretical shortcomings, indicating that our understanding of transplanckian scales is incomplete, see Sec. 1.2. Together this motivates the Planck scale as the next scale at which new physics is truly required. Sec. 1.3 briefly reviews why a standard perturbative quantization of GR fails and how different quantum-gravity approaches emerged from there.

1.1 The Standard-Model desert conjecture

While GR and the SM are tremendously successful descriptions of Nature, there are a few measured phenomena which cannot be explained within these theories. We will group them into (i) particle physics, (ii) gravitational physics, and (iii) the shared riddle of Dark Matter. Along the way, we will briefly introduce basic concepts from GR and the SM which will become important later on. The discussion is presented from a somewhat unusual vantage point: Most theoretical models to explain observed indications for new physics are deliberately built according to the principles of (a) being minimal in adding new parameters and degrees of freedom, and (b) constructing new physics which is detectable by current or near-future observations. See, e.g., [15, 16] for examples of beyond Standard Model (BSM) constructions which obey these principles. A growing body of observational evidence, some of which is collected below, disfavors the second model-building principle. We will, therefore, replace the principle of associating

BSM physics with a nearby energy scale (electroweak scale model-building) with the attempt to associate all new physics with the Planck scale (quantum scale symmetry). The latter, as we will argue in Sec. 1.2, is a fundamental scale at which new physics is required anyhow. Along those lines, we will now discuss unexplained observations and possible Planckian solutions. It is quite striking that this allows for the consistent possibility of (almost) no new subplanckian physics.

1.1.1 The Standard Model and unexplained phenomena in particle physics

Within the framework of group theory and modern QFT, for which we refer to the many available textbooks [17–20], the SM is characterized by (i) its gauge group

$$\mathcal{G}_{\rm SM} = SU(3) \otimes SU(2)_L \otimes U(1)_Y \,, \tag{1.6}$$

(ii) its three generations, i.e., $i = \{1, 2, 3\}$, of group-theoretic fermionic matter content, cf. Tab. 1,

$$\mathcal{F}_{\rm SM} = \underbrace{(\mathbf{1},\mathbf{2})_{(-1/2)}}_{L_L^{(i)}=(\nu_L^{(i)},e_L^{(i)})} \oplus \underbrace{(\mathbf{1},\mathbf{1})_{(1)}}_{e_R^{(i)}} \oplus \underbrace{(\mathbf{3},\mathbf{2})_{(1/6)}}_{Q_L^{(i)}=(u_L^{(i)},d_L^{(i)})} \oplus \underbrace{(\overline{\mathbf{3}},\mathbf{1})_{(-2/3)}}_{u_R^{(i)}} \oplus \underbrace{(\overline{\mathbf{3}},\mathbf{1})_{(1/3)}}_{d_R^{(i)}} \,, \tag{1.7}$$

i.e., the left-handed quark and lepton SU(2)-doublets $Q_L^{(i)}$ and $L_L^{(i)}$, as well es the right-handed SU(2)-singlets $u_R^{(i)}$, $d_R^{(i)}$ and $e_R^{(i)}$. Here, $(\mathbf{a},\mathbf{b})_{(c)}$ refer to the dimension $\mathbf{a}$ of the $SU(3)$ representation, the dimension $\mathbf{b}$ of the $SU(2)$ representation, and the $U(1)$ hypercharge c of the field. Additionally, the SM contains a single complex scalar field, the Higgs-doublet H, i.e.,

$$\mathcal{S}_{\rm SM} = (\mathbf{1},\mathbf{2})_{-1/2} \,. \tag{1.8}$$

Finally and (iii), the SM realizes all possible perturbatively renormalizable couplings c_i and in addition a scalar mass term for H. These correspond to free parameters and have to be determined from experiment.

An important and non-trivial feature of the SM is its cancellation of gauge anomalies. An anomaly is a symmetry (global or gauged) which is broken by quantum fluctuations. For gauge symmetries, these anomalies are problematic because they would excite longitudinal gauge degrees of freedom which induce unitarity violations. At the renormalizable level, gauge theories couple to two charged matter fields with one gauge boson. Hence, anomalies are most straightforwardly understood as arising from triangle diagrams with three external gauge bosons and internal matter loops, cf., e.g. [20, Ch.30]. The absence of gauge anomalies thus translates into conditions on the sum of traces over three generators of the respective matter representations. For the SM, the non-trivial relations can be summarized as

$$\begin{aligned}
U(1)_Y^3 &: && (2\,Y_L^3 - Y_e^3) + 3(2Y_Q^3 - Y_u^3 - Y_d^3) = 0 \,, \\
SU(3)^2U(1)_Y &: && (2Y_Q^3 - Y_u^3 - Y_d^3) = 0 \,, \\
SU(2)^2U(1)_Y &: && (2Y_L^3 + 3Y_Q) = 0 \,, \\
\mathrm{grav}^2U(1)_Y &: && (2\,Y_L - Y_e) + 3(2Y_Q - Y_u - Y_d) = 0 \,.
\end{aligned} \tag{1.9}$$

Here, we have generalized the hypercharges (lower-indexed numbers) in Eq. (1.7) to arbitrary values. In fact, we can now see, that the hypercharge assignments of the SM are not arbitrary.

	lepton doublet $L_L = (\mathbf{1},\mathbf{2})_{(-1/2)}$	quark doublet $Q_L = (\mathbf{3},\mathbf{2})_{(1/6)}$	lepton singlet $E_R = (\mathbf{1},\mathbf{1})_{(1)}$	up-type singlet $U_R = (\overline{\mathbf{3}},\mathbf{1})_{(-2/3)}$	down-type singlet $D_R = (\overline{\mathbf{3}},\mathbf{1})_{(1/3)}$
1st	$\begin{pmatrix}\nu_e\\ e_L\end{pmatrix}$	$\begin{pmatrix}u_L\\ d_L\end{pmatrix}$	e_R	u_R	d_R
2nd	$\begin{pmatrix}\nu_\mu\\ \mu_L\end{pmatrix}$	$\begin{pmatrix}c_L\\ s_L\end{pmatrix}$	μ_R	c_R	s_R
3rd	$\begin{pmatrix}\nu_\tau\\ \tau_L\end{pmatrix}$	$\begin{pmatrix}t_L\\ b_L\end{pmatrix}$	τ_R	t_R	b_R

Table 1: Three generations of group-theoretic matter content of the SM, with $SU(2)$ structure shown explicitly in vector notation.

Reducing the above set of anomaly constraints gives two families of solutions

$$(i): \qquad \text{const} = 2\,Y_L = Y_e = -6\,Y_Q = -\frac{3}{2}\,Y_u = 3\,Y_d\,, \tag{1.10}$$

$$(ii): \qquad \text{const} = Y_u = -Y_d\,, \quad Y_L = Y_Q = Y_e = 0\,. \tag{1.11}$$

Reinstating the SM hypercharges realizes the first solution. An arbitrary constant can be absorbed by a rescaling of the measured charge. Thereby, anomaly cancellation implies charge quantization in the SM [21–24]. For now, it remains a mystery of the SM, why the first and not the second solution (which would be equally viable in terms of anomalies) is realized, cf. Sec. 6 for a review of anomaly cancellation in grand unified theories.

The couplings of the SM can be measured (or at least be systematically constrained) in scattering experiments. We summarize the experimental values and respective couplings at a common energy scale in Tab. 9 in App. A[5]. Being central to Part II of this thesis, these coupling values will serve – unless stated otherwise – as reference values. For now, we conclude that the SM has 19 free parameters.
The concept of the Renormalization Group (RG) will be properly discussed in Sec. 2.1. At this point, it suffices to state that quantum fluctuations introduce an energy dependence of all SM couplings in Tab. 9. Denoting this energy scale by k, the scale dependence of the SM couplings, collectively denoted by c_i, is captured by the respective β-functions, i.e.,

$$k\,\partial_k\,c_i = \beta^{(1)}_{c_i} + (\text{higher-loop contributions})\,, \tag{1.12}$$

where $^{(1)}$ denotes the universal 1-loop contribution to the running of couplings. Fig. 1 presents the resulting 1-loop running of the SM couplings. The energy-scale dependence in Fig. 1 uncovers three unexpected features and one riddle of the SM which are quite uniquely tied to the particular set of experimentally measured values.

(i) Remarkably, the running develops no pathologies up to transplanckian scales.

(ii) The gauge couplings (far-left panel in Fig. 1) almost unify in a single point only a few orders below the Planck scale.

[5] For simplicity, we use a 1-loop renormalization group (RG) scheme properly defined in [25]. For state-of-the-art RG equations, we refer to [26].

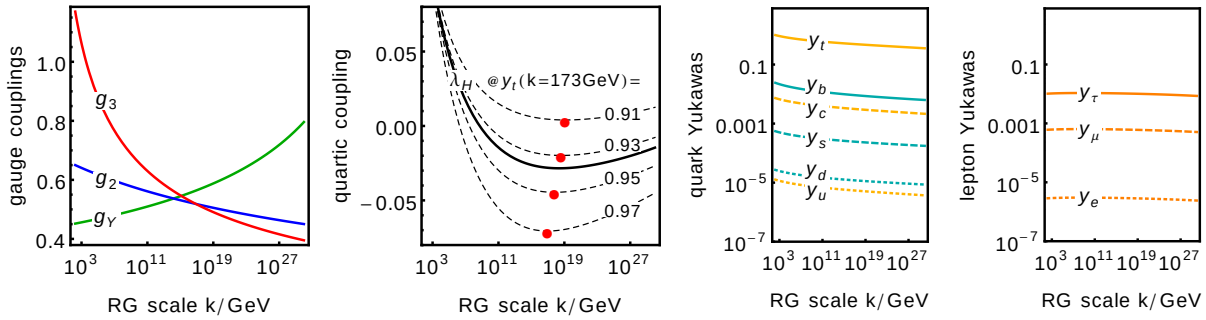

Figure 1: 1-loop running of SM, gauge, quark Yukawa, lepton Yukawa and Higgs quartic from left to right respectively, couplings with initial conditions as in Tab. 9. We refrain from showing the running of CKM-matrix elements, as it is negligibly small, cf. Sec. 5.4. The Higgs-mass parameter scales linearly and $\theta_{\rm QCD}$ is consistently set to 0. The quartic coupling depends critically on the measured value of y_t (dashed lines in the left-middle panel), see main text. The red dots denote the minimum of the running quartic coupling.

(iii) The quartic coupling becomes almost flat and develops a minimum close to the Planck scale (inner-left panel in Fig. 1). Its dip below zero is partially an artifact of the simple 1-loop approximation and moreover depends very sensitively on the measured top-mass value. In fact, recent data is consistent (1σ) with an exact zero at the Planck scale [27, 28].

(iv) The Standard-Model Yukawa couplings of both the quarks (middle-right panel in Fig. 1) and leptons (far-right panel in Fig. 1) exhibit a significant hierarchy.

The lack of any pathologies or poles (i) highlights the theoretical consistency of the SM up to the Planck scale and beyond. For the Abelian hypercharge coupling, the far-left panel in Fig. 1 already signals the onset of a divergence – the transplanckian Landau pole, cf. Sec. 1.2.2. Gravitationally induced scale symmetry could provide a Planckian solution to this theoretical inconsistency, cf. Sec. 5. (ii) suggests gauge coupling unification in the vicinity of the Planck scale, cf. Sec. 6. Moreover, (iii) points to scale invariance of the Planckian Higgs potential. We emphasize that all these features are a rather particular consequence of the measured values: Doubling the measured value of g_Y, results in a subplanckian divergence, not to mention that it invalidates gauge coupling unification. The Higgs potential is even more sensitive: a different top-mass value, a few percent off from the measured value, decides whether Planckian scale invariance is realized or not. Hence, the experimentally observed SM coupling values all seem to point to the Planck scale as a very special fundamental scale, see Sec. 4-6. In Sec. 5, we attempt to connect Planckian scale symmetry to the riddle of quark and lepton mass-hierarchies.

Stability of the Standard Model vacuum and the Planck scale. The scale-dependent Higgs-quartic coupling $\lambda_{\rm H}$ (left-middle panel in Fig. 1) might turn to negative values and thereby generate a second vacuum of the Standard-Model Higgs potential at very high energies. The value of this metastability scale depends very sensitively on the top-Yukawa coupling y_t and therefore on the measured top mass value [29–33]. A top mass of a few GeV higher or lower shifts the metastability scale by many orders of magnitude. Current experimental data is consistent with instability, metastability as well as absolute stability of the Higgs potential [27, 28] (cf. dashed lines in the left-middle panel of Fig. 1). Vanishing $\lambda_{\rm H}$ at the Planck scale thus fixes the ratio of top mass and Higgs mass, which has been exploited to predict the latter [34].
The following secondary observation though does not depend on the measured top-mass value. Fixing all other Standard-Model parameters at their (comparatively well measured) values, the

minimum of the Higgs potential (red dots in the left-middle panel of Fig. 1) depends solely on the top mass M_t and the Higgs mass M_H. For each Higgs mass, demanding that the minimum occurs at $\lambda_H = 0$, i.e., that the Higgs quartic-coupling and its scale dependence both vanish at the same scale, singles out a particular high-energy scale $k_{\beta_\lambda=0=\lambda}(M_H)$ (and with it a given top mass value). Strikingly, this scale is the Planck scale. Put differently, demanding that not only $\lambda_H(M_{\text{Planck}}) = 0$ but also $\beta_{\lambda_H}(M_{\text{Planck}}) = 0$ fixes *two independent* moments of the Higgs potential. These two can be used to fix the top mass and the Higgs mass *independently* [35]. Vice versa and given that the experimental values are known, it can be interpreted as a strong hint for scale invariance at the Planck scale which motivates Part II of this thesis.

Neutrino masses and mixing. The only true requirement for new physics below the Planck scale are massive neutrinos. The latter are required by neutrino oscillations[6]. As for the case of quark mixing, the oscillations are attributed to a misalignment of the eigenstates of the kinetic basis (associated with gauge-interactions), and the mass basis (in the case of Dirac neutrino-masses associated with Yukawa-interactions). Without explicit mass terms, such a misalignment is not possible – the neutrinos are flavor-locked. Vanishing neutrino masses are thus in contradiction to the observation of neutrino oscillations. Or at least, there is no currently known mechanism for oscillations without a mass term. We will be concise in the following summary and refer to, e.g., [52, 53] for extensive reviews of the topic.
Before addressing the SM, it is instructive to consider a generic Weyl decomposed Dirac fermion $\psi = \psi_L^T + \psi_R$, which we conveniently write in vector notation $N^T = (\psi_L^T,\ \mathcal{C}\bar{\psi}_R)$, where $\mathcal{C}$ is the charge conjugation operator transforming $\psi \to -i\gamma_2\psi^* \equiv \mathcal{C}\psi$ and γ_μ denote the Dirac matrices. The $\psi_{L/R}$ can be interpreted as their own anti-particles [54] and thereby admit for multiple possible mass terms – the usual Dirac mass, a Majorana mass, or a mixture of both, i.e.,

$$\mathcal{L}_{\text{mass}} = \frac{1}{2} N^T \mathcal{C}^\dagger \underbrace{\begin{bmatrix} m_L & m_D \\ m_D & m_R \end{bmatrix}}_{\equiv M} N + \text{h.c.} = \underbrace{-m_D\, \bar{\psi}_R \psi_L}_{\text{Dirac mass}} \underbrace{+\frac{1}{2} m_L\, \psi_L^T \mathcal{C}^\dagger \psi_L}_{\text{left-handed Majorana}} \underbrace{+\frac{1}{2} m_R\, \psi_R^T \mathcal{C}^\dagger \psi_R}_{\text{right-handed Majorana}} + \text{h.c.}\,, \tag{1.13}$$

where we have defined the mass matrix M[7]. A left-handed Majorana mass term, just as well as a Dirac mass term, violates the $SU(2)_L$ gauge symmetry. Both mass terms are thus not allowed in the SM. Additionally, Majorana mass terms also violate global U(1) symmetries, i.e., they violate lepton number conservation[8]. In case of a real (complex) mass matrix M, CP is conserved (broken).
In the SM, the three generations of left-handed neutrinos ν_i are part of the left-handed lepton doublet $L_{Li} = (\nu_{Li}, e_{Li})$ where $i = (e, \mu, \tau)$ for electron-, muon- and tau-neutrino. They are electrically neutral, and thus both, a unique astrophysical messenger, and very hard to detect. But they participate in the weak interactions and are hence referred to as 'active' neutrinos[9].

[6] The prediction of neutrino oscillations [36, 37] was experimentally confirmed by an overwhelming number of observations of solar [38–45], atmospheric [46, 47], reactor [48, 49], and accelerator neutrinos [50, 51], rewarded a Nobel prize, given to representatives of the SuperKamiokande and SNO collaborations.

[7] Dirac himself originally dismissed Majorana mass terms because they violate parity, but Wu and Yang noticed that this had never been tested experimentally. The now-famous 'Wu experiment'[55] indeed discovered parity violations of the weak force. Chien-Shiung Wu was not officially recognized while the discovery of parity violations earned Lee and Yang the Nobel Prize for Physics in 1957.

[8] This can be seen by transforming the Majorana mass term under $\psi \to e^{i\alpha}\psi$ (and $\mathcal{C}\psi \to e^{-i\alpha}\mathcal{C}\psi$) with $\alpha \in \mathbb{R}$.

[9] Active neutrinos also have non-vanishing $U(1)_Y$-hypercharge such that $Q_{\text{em}}(\nu_{Li}) \equiv T_{\text{L3}} + Y = 0$, cf. Eq. (1.7).

Such 'active' neutrinos can neither have a direct Dirac nor a Majorana mass term, without either violating renormalizability or gauge symmetry.[10] The question of Dirac or Majorana mass is thus irrelevant for the conclusion that neutrino masses require a minimal extension of the SM[11].

The arguably straightforward and minimal extension of the SM to allow for neutrino mass terms is the inclusion of three generations of right-handed neutrino singlets, i.e., $\mathcal{F}_{\nu\text{SM}} = \mathcal{F}_{\text{SM}} \oplus (\overline{\mathbf{1}}, 1)_{(0)}$, referred to as the minimally extended Standard Model or νSM [58, 59]. The right-handed neutrinos do not carry any SM charge and are hence referred to as 'sterile'. Firstly, such sterile neutrinos do not modify the conclusions about anomaly cancellations. Secondly, they are not protected by any gauge symmetry, so they admit for both right-handed Majorana masses and Dirac mass-terms via Yukawa couplings with the left-handed fermions. Neutrino masses in the νSM are thus naturally an unknown combination of Dirac and Majorana mass. Oscillation experiments provide indirect evidence for neutrino masses and measure the squared mass-difference between neutrinos [49, 51] and the leptonic PMNS mixing angles [37, 60][12]. All constraints apply only to active neutrino masses. Sterile right-handed neutrinos can be arbitrarily heavy.

The mass Lagrangian in Eq. (1.13) can be diagonalized by a unitary transformation $N = U\,n$, which defines the mass eigenstates $n^T = (\nu_{1L}^T, \nu_{2L}^T)$ by the condition that

$$U^T\, M\, U = \begin{bmatrix} m_1 & 0 \\ 0 & m_2 \end{bmatrix} . \tag{1.14}$$

Without CP violations (real M), U is orthogonal and the mass eigenstates become

$$m_{1/2} = \frac{1}{2}\left(m_L + m_R \mp \sqrt{(m_L - m_R)^2 + 4\, m_D^2} \right) . \tag{1.15}$$

In the SM, $m_L = 0$ is required to preserve gauge invariance. If additionally $m_D \ll m_R$, the see-saw mechanism [68–71] is realized. The name is intuitively understood when expanding Eq. (1.15) for small m_D which splits the physical masses m_1 and m_2, i.e.,

$$m_2 = m_R + \mathcal{O}(m_D^2) , \quad m_1 = -\frac{m_D^2}{m_R^2} + \mathcal{O}(m_D^4) , \qquad \text{for:} \quad m_L = 0 \quad \text{and} \quad m_D \ll m_R . \tag{1.16}$$

The right-handed Majorana-mass scale not only sets $m_2 \approx m_R$, but also parametrically suppresses $m_1 \sim m_D^2/m_R^2$. Provided a large Majorana-mass scale m_R for the sterile right-handed neutrino, it offers an explanation for tiny neutrino masses even in presence of a Dirac mass m_D generated by Yukawa couplings of the same order of magnitude as those of the SM quarks. The see-saw mechanism invites us to speculate about very-high-energy new-physics scales which set

[10] For nonrenormalizable Weinberg operators which can generate mass terms in the context of effective field theory (EFT), we refer to [56].

[11] The pure-Dirac mass limit is distinguished from non-zero Majorana mass terms by Lepton-number conservation. The detection of any lepton-number violating processes such as neutrinoless double-beta decay [57] would signify a Majorana nature of neutrinos, even though additional Dirac-mass terms remain possible.

[12] While lower mass bounds can be inferred, these experiments give no upper bound on the overall neutrino mass scale. Ongoing direct mass searches, see, e.g., [61, 62] constrain Majorana masses to below 120 – 250 meV [63], potentially to be improved to the $\approx$ 25 meV region by future experiments [64]. Assuming the validity of the νSM, in conjunction with the ΛCDM standard model of cosmology, as well as a thermal production of stable neutrinos, CMB measurements constrain the overall neutrino mass to $\sum_j m_j < 170\,\text{meV}$ [65, 66], with projected future constraints at $\sum_j m_j < 20\,\text{meV}$ [67].

m_R, and thereby explain the non-observation of m_2 and the smallness of m_1. One such scale is the grand unification scale, cf. Sec. 6. Another naturally very large scale would be the Planck scale itself, cf. 5. We conclude by noting that a minimal extension of the SM by three generations of right-handed neutrino singlets suffices to incorporate all neutrino observations.

Matter anti-matter asymmetry. A more subtle requirement for new physics is the observed matter anti-matter or baryon asymmetry of the universe (BAU)[13]. Baryon asymmetry is related to CPT invariance. Before the conjectured [72] and subsequently observed BAU [73, 74], it was assumed that all physical processes are invariant under simultaneous mirroring of position (parity P), momentum (time T) and charge (C). Indeed, any process which is to result in baryon asymmetry needs to violate CPT. This is reflected in the famous Sakharov conditions [75] according to which the BAU requires

1. Violation of baryon number: Obviously, producing an asymmetry in the number of baryons requires a process which violates the corresponding conserved charge.

2. C and P violations: if either C or P were conserved, the reverse process would occur with equal probability and no net asymmetry could develop.

3. Departure from thermal equilibrium: All processes in thermal equilibrium are time reversal. A departure from thermal equilibrium is thus equivalent to time irreversibility.

In principle, the SM and its electroweak phase transition fulfill all the Sakharov conditions [76, 77][14]. But, neither are CP-violations from SM CKM-mixing strong enough [82–89], nor is the electroweak phase transition close enough to first order, i.e., out of equilibrium [83, 90, 91]. The latter is related to the Higgs mass being heavier that ~ 70 GeV [92, 93]. Both of these shortcomings can be overcome by BSM physics [94, 95]: see [96, 97] for possible BAU in the context of the νSM [98], as well as [99–101] for baryon-number violations in the context of GUT-scale proton decay, cf. Sec. 6.
The Sakharov conditions are sufficient conditions for generating a matter anti-matter asymmetry [102], at least in the framework of QFT. They are not necessary though, see [102, Sec. 4-7]. For instance, a charge-violating but baryon-number conserving decay into heavy and light baryons and anti-baryons in the vicinity of a black hole [103][15] is one of the potential examples violating the Sakharov conditions, see, e.g., [104, 105]. It might thus be misleading to interpret the BAU as an unmistakable sign of new physics – even more so of new physics close to the electroweak scale.

A comment on fine-tuning and naturalness. The standard argument in favor of new physics at the electroweak scale is the fine-tuning problem associated with the Higgs mass-parameter. The latter has to be chosen with 17 digit precision to arrange for the large separation between the electroweak and the Planck scale. It is important to distinguish between

[13] Explaining the BAU by specific initial conditions of the universe is impossible if the SM is embedded into a standard inflationary cosmology. Inflation washes out any such initial condition. Concurrently, this implies that any explanation must be post-inflationary.

[14] See [78–80] for non-perturbative baryon-number violating sphaleron processes, and [15, Sec. IV.1] and [81] for accessible reviews.

[15] If the decay widths are distinct due to charge-symmetry violations and the heavy partners are more likely to be trapped by the black hole horizon, a net asymmetry could be generated. Baryon number is conserved by all particle physics processes but dynamically broken in the vicinity of black holes. Strictly speaking the black-hole horizons simply separate baryons and anti-baryons and the overall universe is still matter anti-matter symmetric.

radiative stability against higher-loop corrections (which might well be a technical problem of our ignorance expanding in a perturbation series around low-energy physics) and the fact that physics drastically changes if an input parameter is slightly modified (fine-tuning).
The technical question of radiative stability depends on whether the small parameter at hand is protected by symmetry and therefore technically natural [106]. This is the case for small Yukawa couplings or fermion masses but not for the Higgs mass. Independent of technical naturalness, there exist renormalization schemes such as dimensional regularization or the use of a dilaton scalar field which avoid any new quadratic divergences at higher loop orders in the perturbative expansion. The small parameter has to be fine-tuned only once. While fine-tuning remains, the question of radiative stability thus depends on the technical choice of RG scheme and is thus an unphysical problem.
One may still wonder why, given a particular theoretical model of our universe with a set of input parameters, the experiment has determined one (or multiple) of these parameters at a vastly different order of magnitude from all others. This usually occurs if the separation of two scales in the RG-flow of the theory depends on a power-law running parameter. While this calls for an explanation, this explanation need not occur at nearby scales, see, e.g. [107] for a possible scenario which does not explain the large separation of the electroweak and the Planck scale but successfully diverts it to the transplanckian regime. For a discussion of fine-tuning we refer to [108] and remain with the conclusion that while an explanation for different physical scales is always desirable, this by no means requires any new physics close to the electroweak scale.

1.1.2 General Relativity and riddles of cosmological evolution

Similar to the SM, all astrophysical data is currently consistently described by GR. This includes the exciting first glimpses into the strong-curvature regime and the first image of a black hole [109–114]. GR is a classical field theory of the spacetime $g_{\mu\nu}$ metric itself. It is governed by the Einstein-Hilbert action

$$S_{\mathrm{GR}} = \frac{1}{16\pi\overline{G}} \int_x \sqrt{g}\,(2\overline{\Lambda} - R) + \int_x \sqrt{g}\,\mathcal{L}_{\mathrm{matter}}\,, \tag{1.17}$$

where $\overline{G}$ and $\overline{\Lambda}$ denote the Newton coupling and the cosmological constant, respectively, $\sqrt{g} = \sqrt{\det(-g)}$ denotes the metric determinant, and R is the curvature scalar The Einstein field equations are obtained by varying S_{GR} with respect to the fundamental field $g_{\mu\nu}$, i.e.,

$$R_{\mu\nu} - \frac{1}{2} R\, g_{\mu\nu} + \overline{\Lambda} g_{\mu\nu} = 8\pi\overline{G}\, T_{\mu\nu}\,, \tag{1.18}$$

where $T_{\mu\nu}$ is the energy-momentum tensor of the matter part of the theory, i.e.,

$$T_{\mu\nu} \equiv \frac{-2}{\sqrt{g}} \frac{\delta(\sqrt{g}\mathcal{L}_{\mathrm{matter}})}{\delta\, g^{\mu\nu}} = -2\frac{\delta \mathcal{L}_{\mathrm{matter}}}{\delta\, g^{\mu\nu}} + g_{\mu\nu}\,\mathcal{L}_{\mathrm{matter}}\,. \tag{1.19}$$

The Einstein-Hilbert action, and equivalently GR, is the unique local action of a diffeomorphism invariant metric field which generates linearized second-order equations of motion of only the a massless spin-2 field. In the appropriate weak-field limit, the theory reduces to Newtonian mechanics and $\overline{G}_{\mathrm{N}}$ governs the non-relativistic laws of gravitational motion. In combination with the Ostrogradsky theorem, which disfavors higher-derivative equations of motion, this can be used to argue that GR is unique, cf. Sec. 1.3.1.

The Standard Model of cosmology (ΛCDM). This thesis will not have much to say about cosmology, so the following section is very brief and we refer to, e.g. [115], for a more complete introduction to cosmology. Observations have confirmed that the universe is spatially homogeneous and isotropic at large scales such that, apart from perturbations, cosmological evolution is described by the symmetry-reduced FRW metric [116–118], i.e.,

$$ds^2 = -dt^2 + \frac{a^2(t)}{1 - K\,r^2} + a^2(t)\,r^2\,d\Omega^2 \,, \tag{1.20}$$

where t is the cosmological time, $a(t)$ the scale factor and $K = 0$, $K > 0$, and $K < 0$ indicate vanishing, positive, or negative curvature, respectively. Solving the dynamics of GR, cf. Eq. (1.18), for a perfect-fluid matter content $T_{\mu\nu} = \rho\,u_\mu u_\nu + p(u_\mu u_\nu + g_{\mu\nu})$ with pressure p, densitiy ρ and fluid velocity field u, results in the cosmological field equations

$$H^2 \equiv \left(\frac{\dot{a}}{a}\right)^2 = \frac{8\pi G}{3}\rho - \frac{K}{a^2} \,, \qquad \frac{\ddot{a}}{a} = -\frac{4\pi G}{3}(\rho + 3p) \,, \tag{1.21}$$

supplemented by $\dot{\rho} + 3\,H(\rho + p) = 0$ (continuity equation). Here, the Hubble constant H was introduced and dots denote derivatives with respect to cosmological time. Solving Eqs. (1.21) requires a microscopic equation of state. ΛCDM cosmology [119–121] is driven by a barotropic, i.e., $p_i/\rho_i = w_i = \text{const.}$, combination of baryonic matter ($w_m = 0$), photons ($w_\gamma = 1/3$), neutrinos ($w_\nu = -1/3$), cold dark matter ($w_{\text{CDM}} = 0$), and a cosmological constant ($w_\Lambda = -1$), for which the FRW Eqs. (1.21) imply

$$H^2 = H_0^2 \sum_i \Omega_i^{(0)} \left(\frac{a_o}{a}\right)^{3(1+w_i)} \,. \tag{1.22}$$

Here, H_0 and a_0 are the Hubble constant and scale factor at the present time. From astrophysical observations, one infers that at the present day the visible matter density is $\Omega_m = 0.046 \pm 0.002$. Within GR, an additional dark matter density $\Omega_{\text{DM}} = 0.23 \pm 0.01$ is required, cf. below. Finally, the observed current(late)-time expansion [122–125] of the universe requires a cosmological constant with density $\Omega_\Lambda = 0.73 \pm 0.02$. Accepting another huge fine-tuning problem, it is sufficient to associate this to an evenly distributed vacuum energy parameterized by Λ in the action of GR[16]. Despite fine-tuning, Occam's razor certainly favors a cosmological constant as the simplest model since current observations only provide a single data point. This would change if a dynamical cosmological constant were to be observed, see e.g. [129].

Cosmic initial conditions and inflation A priori, any cosmological evolution can have arbitrary initial conditions. To that respect, near-flatness, -homogeneity, and -isotropy of the cosmological evolution, which have been spectacularly verified by the observation of the cosmic microwave background (CMB), are very special and call for an explanation. The standard explanation is a period of inflation [130–135] in which the Universe expands faster than local lightcones. Thereby, the observable cosmological horizon only extends to a patch of the Universe all of which has originally been in close causal contact and which is therefore very homogeneous and isotropic.
Many inflationary models can successfully fit the observed cosmological perturbations in the CMB power spectrum with a small set of free parameters [136–139]. Any scalar field – referred to as inflaton – with a suitable potential can source inflation. The predictivity of inflation can

[16] Other possibilities include the addition of a new scalar field (quintessence [126, 127], cf. [128] for a review).

be improved if the inflaton is identified with a scalar field of separate physical significance such as the Higgs, see e.g. [140] for a recent summary. Alternatively, inflation might also be driven by a large R^2 coupling in an effective gravitational action at inflationary scales [130, 141] possibly sourced by quantum fluctuations. Both options are candidates for a viable cosmological period of inflation without requiring any additional fundamental physics.

1.1.3 What constitutes dark matter?

Dark matter can be defined as all components of the universe which obey a baryonic equation of state, cf. Eq. (1.22), but has – until now – only been detected in observations of gravitational physics. The first signature of dark matter resulted from the observed flattening of the rotational velocity of spiral galaxies with growing distance to the galactic center [142, 143]. Given the distribution of visible matter within a galaxy, one would expect a faster falloff.
The requirement of dark matter can be averted by postulating modified gravitational dynamics at galactic scales. Such modified Newtonian dynamics (MoND) are disfavored in comparison to dark matter, for instance, by (i) the observed CMB angular power spectrum [125], (ii) baryon acoustic oscillations (BAO) [125], and (iii) the observation of a local displacement of the gravitational and visible center of mass within a recent collision of two galaxy clusters [144].
A plethora of new particles has been suggested as dark-matter candidates. Following the electroweak-scale model-building paradigm, many of them have been tied to the TeV scale, but this is by no means necessary. Sterile right-handed neutrinos provide for an excellent dark-matter candidate [145]. The summary below will focus on dark-matter candidates which do not require any new physics beyond the (ν)SM.

Primordial black holes and other baryonic dark-matter candidates. Depending on the particular inflationary model, gravitational collapse of densely populated regions of space during the early cosmological history may have formed primordial black holes [146–154]. A possible window between microlensing and wide-binary constraints [155, 156] might even suggest that the observed gravitational waves [157] could originate from primordial black-holes which make up dark matter [158–160]. This proposal remains a viable dark matter candidate [161] and can potentially be ruled out by non-observation of FRB echos [162] or GRB echos [163].
For small primordial black holes, Hawking radiation becomes increasingly significant. As they evaporate to reach Planckian mass scales, the semiclassical description breaks down and most quantum-gravity models give indications for a Planck-size stable black-hole remnant, cf. Sec. 7. Primordial black-hole remnants could be produced during inflation [164–170], cf. [171] for a production proposal in Higgs inflation.

Conclusion

In summary, all new physics can be attributed to Planckian or transplanckian energies. In some cases, such as for the seesaw-mechanism of neutrino masses, the absence of proton decay, and the Higgs potential, theoretical solutions even point to scales in the vicinity of the Planck scale. Put differently, one should maybe not be surprised if the current absence of new physics at the TeV scale persists.

1.2 Field theories predicting their own breakdown

Having argued that no new physics is required up to the Planck scale, why do we need new physics at all? For instance, Newtonian mechanics was and still is a complete theory without internal inconsistencies. By now, of course, we know it fails when confronted with experimental reality. But, there is no intrinsic reason for its failure and Newton could not have known better. Fortunately or unfortunately, both GR and the SM are not such theories. Black-hole singularities in GR, as well as Landau poles in the SM, indicate a breakdown at transplanckian scales.

1.2.1 Singularities of General Relativity

As it is sufficient to discuss the main properties of singularities, we will stick to static spherically symmetric solutions of the field equations. Given a general such ansatz for the metric, i.e.,

$$ds^2 = -f(r)\,dt^2 + g(r)\,dr^2 + r^2\,d\Omega^2\,, \quad \text{with} \quad d\Omega^2 = d\theta^2 + \sin^2\theta\,d\varphi^2\,, \tag{1.23}$$

the Einstein field equations (1.18) in combination with a correct weak-field limit require

$$f(r) = g(r)^{-1} = \left(1 - \frac{2\bar{G}\,M}{r}\right)\,. \tag{1.24}$$

The one-parameter family of solutions is parameterized by the mass of the central object M – the Schwarzschild black hole [172], see also [173]. The metric is singular at $r = r_s \equiv 2\bar{G}\,M$ and at $r = 0$. The singular point at $r = r_s$ is connected to the black hole's defining property – the event horizon. Since a singular metric component is a coordinate-dependent statement, a proper definition has to be given via geodesics. An event horizon is a boundary surface in spacetime such that no two events separated by the boundary can in the future be in causal contact[17].

To the contrary, the divergence at $r = 0$ is not a coordinate but rather a physical singularity[18]. This can be observed by calculating a curvature invariant such as the Kretschman scalar[19]

$$K = R_{\mu\nu\rho\sigma}R^{\mu\nu\rho\sigma} = \frac{48\,\overline{G}^2\,M^2}{r^6} \xrightarrow{r\to 0} \infty\,. \tag{1.25}$$

By definition curvature invariants are coordinate invariant objects. Hence, the singularity at $r = 0$ is a physical prediction of GR. Two comments are in order, to appreciate the severity of such singularities. Firstly, Schwarzschild spacetime is not an isolated solution but the stable final state of spherically-symmetric gravitational collapse [174, 175]. Also, less-symmetric spacetimes collapse to generalized black-hole spacetimes, all of which feature singularities.
Secondly, the singularity of Schwarzschild spacetime is hidden behind an event horizon. Hence, unphysical implications from the singularity can never impact any outside observer. It has therefore been conjectured that Nature veils all physical singularities behind horizons [176][20]. If true,

[17] An event horizon is thus a global property of spacetime and its determination requires knowledge about the entire future spacetime. For dynamical spacetimes, the notion of an apparent horizon as the boundary surface separating inwards and outwards directed light rays is more suitable. This thesis is only concerned with static black-hole spacetimes for which the notions of an apparent and an event horizon coincide, cf. Sec. 7.

[18] The big-bang singularity poses a similar divergence.

[19] Schwarzschild spacetime is Ricci flat, i.e., the Ricci curvature vanishes everywhere. Hence the lowest curvature invariant is not a useful criterion.

[20] The weak (strong) version of the cosmic censorship conjecture states that no external observer at spatial infinity (no observer at all) can see the singularity, i.e., is connected to it by a lightlike geodesic.

such cosmic censorship would remove all physical phenomena associated with new physics in the vicinity of singularities from the experimentally accessible part of Nature. By now counterexamples, i.e., matter configurations that can collapse to form naked singularities unprotected by horizons have been constructed, see, e.g., [177–180][21].

In summary, GR predicts curvature singularities, thus predicting its own breakdown. Some new physics can be expected to avoid the divergence. In the vicinity of singularities, length, mass, density, and curvature eventually reach the Planck scale. Physics close to singularities thus enters the regime of quantum gravity which could resolve the singularity, cf. Sec. 7.

1.2.2 Singularities of the Standard Model

In quantum mechanics and QFT alike, unitary time evolution corresponds to conservation of probability and is an indispensable requirement for any physically meaningful theory. In the context of effective field theories (EFTs) [56, 183–188][22], unitarity provides a quantitative framework to determine the cutoff scale at which new physics is necessary.

The optical theorem and tree-level unitarity. For a QFT to preserve probability, its scattering matrix (S-matrix) S has to be unitary on the physical Hilbert space of asymptotic states. This implies (see e.g. [20, Ch.24] for a derivation) the generalized optical theorem which relates matrix elements at 1-loop level (or more generally at loop order $n+1$) to tree-level ones (or more generally of loop order n). It allows for the exploration of unitarity order by order in perturbations theory. Hence, if tree-level unitarity breaks down, probability is no longer conserved – at least not in perturbation theory. At the respective scale, new physics is necessary to preserve unitarity, either in the form of new degrees of freedom or in the form of a non-perturbative restoration of unitarity.
As a direct physical consequence of the optical theorem, one finds partial wave unitarity bounds (related to the Froissart bound [190]). For the special case of $2 \to 2$ elastic scattering, unitarity bounds the s-channel tree-level amplitude $\mathcal{M}_{2\to2}(s)$, i.e.,

$$|\mathcal{M}_{2\to2}(s)| < 1 \,. \tag{1.26}$$

This allows for a simple estimate of the scale of new physics in EFTs.

New physics at the breakdown of unitarity. We take Fermi's theory of weak interactions [191] as an example. In the simple case of a single generation of leptons, i.e., for a Lagrangian $\mathcal{L} = -G_F/\sqrt{2}(\bar{\nu}\gamma_\mu(1-\gamma_5)e)(\bar{e}\gamma^\mu(1-\gamma_5)\nu)$, the partial-wave unitarity bound in Eq. (1.26) constrains the center-of-mass energy E_{cm} of the scattering amplitude $\mathcal{M}_{(\nu e\to\nu e)}(s)$, i.e.,

$$E_{\text{cm}} = \sqrt{s} < \left(\frac{2\pi\sqrt{2}}{G_F}\right)^{1/2} \,. \tag{1.27}$$

Having measured Fermi's constant at $G_F \approx 1.17 \times 10^{-5}\ \text{GeV}^{-2}$, unitarity requires new physics at or below 870 GeV. The underlying reason is that Fermi's theory of weak interactions is

[21] These configurations can be constructed from matter obeying the null-energy condition. The remaining objections to such solutions are whether they form a null set, whether configurations with non-vanishing pressure exist, whether they are stable [181], and whether all such naked-singularity forming configurations correspond to ill-posed initial value problems [182].

[22] See [189] for a recent review of the SM as an EFT (SMEFT).

non-renormalizable and that cross sections grow faster than $\log^2(E_{\rm cm})$ (Froissart bound [190]). By now we know that the required new physics manifests in weak gauge-bosons. Subsequently, similar unitarity bounds also demand the existence of the Higgs boson (or the onset of other new physics close to the electroweak scale)[23].

Absence of unitarity bounds for the Standard Model. With the discovery of the Higgs-boson [199, 200] at a mass of $M_H = 125 \pm 0.5$ GeV, the SM is completed into a perturbatively renormalizable theory. Hence, there are no tree-level unitarity bounds which indicate that new physics is required beyond the SM[24]. As discussed in Sec. 1.1.1, cf. Fig. 1, the SM develops no subplanckian pathologies, even if loop-corrections are included.

The U(1) Landau pole. Nevertheless, ignoring gravitational contributions and blindly extrapolating the SM running couplings beyond the Planck scale, results in transplanckian divergences. The onset of the first such divergence can be observed for the U(1) gauge coupling g_Y in the far-left panel of Fig. 1. Integrating its 1-loop running $k\partial_k\, g_Y = \beta_{g_Y} = b_Y\, g_Y^3/(16\pi^2)$ with $b_Y = 41/6 > 0$ characterizing the screening behavior of matter fluctuations, cf. Sec. 5.1, results in an energy scale k dependence

$$g_Y^2(k) = \frac{g_Y^2(k_0)}{1 - \frac{41}{96\pi^2} g_Y^2(k_0)\, \log(k/k_0)}\,. \tag{1.28}$$

Clearly, the coupling diverges once $k = k_0\, \exp(96\pi^2/(41\, g_Y(k_0)^2))$. Plugging in the experimental low-energy value $g_Y(k_0 = 173\,\text{GeV}) = 0.35$ yields the so-called Landau pole at $k \approx 10^{41}$ GeV [202]. The corresponding triviality problem has been confirmed beyond perturbation theory [203–205]. Similar poles can also occur for all Yukawa and the Higgs quartic coupling. The Landau-pole divergence occurring first is a result of the specific measured SM parameters[25].

We conclude that while there is no demand for new physics below the Planck scale, the SM develops singularities when extrapolated beyond the Planck scale. As we will argue in the upcoming section, the Planck scale implies new physics in the gravitational sector anyways. The simplest answer would thus be that a proper theory of quantum gravity should resolve not only the singularities of GR but also those of the SM.

1.3 The perturbative quantization of gravity

Standard lore tells that since the Newton coupling $\overline{G}$ has negative mass dimension -2, GR is power-counting non-renormalizable. An actual proof on perturbative non-renormalizability is difficult though because new divergences could miraculously cancel at every loop order. And indeed, pure Einstein gravity turns out to not require any counterterm at 1-loop level [214]. Including matter, 1-loop renormalizability is lost. At 2-loop order, even pure gravity requires a counterterm, although just a single one [215]. Following [216], all of this can be understood

[23] As an alternative to the original Glashow-Weinberg-Salam [192–194] gauge-theory construction, the principle of unitarity bounds provides another route to the SM [195–198].

[24] In fact, one can also reformulate the logarithmic divergence of the U(1) Landau pole in terms of a partial-wave unitarity bound [201]. Ignoring the breakdown of perturbation theory, one thereby recovers, for instance for $(\nu\, e \to \nu\, e)$ weak-gauge-boson exchange, a logarithmic unitarity bound and thus a transplanckian cutoff scale close to the U(1) Landau pole.

[25] Prior to measurement, the possible subplanckian Landau pole for the Higgs-quartic coupling was used to constrain the Higgs mass to below 180 GeV [206–213].

by means of (i) dimensional analysis, (ii) gauge invariance, see, e.g., [217] for a background-field method treatment of gravity, and (iii) demanding on-shell conditions. Furthermore, we demand that the counterterms be local. To do so, one expands the action of GR, cf. Eq. (1.17), in (perturbatively small) metric fluctuations $h_{\mu\nu}$ around a flat background $\delta_{\mu\nu}$

$$g_{\mu\nu} = \delta_{\mu\nu} + \epsilon\, h_{\mu\nu} \,, \qquad \text{with} \quad \epsilon = \sqrt{8\pi\, \overline{G}} \,, \tag{1.29}$$

where $\epsilon^2 \sim \overline{G}$ is the perturbative expansion parameter. By dimensional analysis we conclude that every loop order ϵ^{2n} requires counterterms of mass dimension $-[\overline{G}^n] = -n[\overline{G}] = 2n$.
For pure gravity at 1-loop order, there are 3 such invariants with mass dimension 4, i.e.,

$$\Delta S_{\text{1-loop}} = \int d^4x\sqrt{g}\, \left[c_1\, R^2 + c_2\, R_{\mu\nu}R^{\mu\nu} + c_3\, R_{\mu\nu\rho\sigma}R^{\mu\nu\rho\sigma}\right] \,, \tag{1.30}$$

where R, $R_{\mu\nu}$, and $R_{\mu\nu\rho\sigma}$ are the Ricci scalar, Ricci tensor, and Riemann tensor, respectively. But, Einsteins equations (1.18) in vacuum require $R = 0$ and thereby also $R_{\mu\nu} = 0$, on shell. In four dimensions the only remaining counterterm $R_{\mu\nu\rho\sigma}R^{\mu\nu\rho\sigma}$ can be expressed by the two vanishing ones by means of a topological invariant $\int_x \sqrt{g}(R^2 - 4\, R_{\mu\nu}R^{\mu\nu} + R_{\mu\nu\rho\sigma}R^{\mu\nu\rho\sigma}) = 0$. To conclude, all three counterterms at 1-loop level have to vanish on shell in four dimensions. The resulting 1-loop renormalizability of vacuum GR is confirmed by explicit calculation [214][26].

1.3.1 Renormalizable quadratic gravity and unitarity

The seemingly obvious outcome is that GR is non-renormalizable. This conclusion is altered if one treats the 1-loop counterterms, cf. Eq. (1.30), as independent couplings, i.e., also allows for a finite part in the c_i. This leads to the quadratic gravity action

$$S_{\text{QG}} = \int d^4x\sqrt{g}\, \left[a\, R^2 + b\, R_{\mu\nu}R^{\mu\nu}\right] \,, \tag{1.31}$$

where the 4D-topological invariant has been exploited to remove the third independent term. For the special case of $a = -b/3$ the theory reduces to Weyl-invariant or conformal gravity[27]. Explicit calculations confirm that pure quadratic gravity S_{QG} and even the combination $S_{\text{EH}} + S_{\text{QG}}$ (henceforth called quadratic gravity) define perturbatively renormalizable [221] and for particular coupling values even asymptotically free [222, 223] quantum field theories[28].

Unitarity violations in quadratic gravity. If quadratic gravity is perturbatively renormalizable, why not adopt it as the quantum theory of gravity? Upon linearizing quadratic gravity,

[26] At 2-loop, the counting of independent invariants of mass dimension 6 is more involved but results in only a single non-vanishing counterterm after the use of the on-shell equations of motion. It is named after Goroff and Sagnotti who performed the explicit 2-loop calculation first [215]. It is likely but remains an open question whether more counterterms arise at higher loop order.

[27] This particular version of quadratic gravity is not only invariant under diffeomorphism symmetry but also under Weyl conformal transformations $g_{\mu\nu}(x) \to e^{2\sigma(x)}g_{\mu\nu}(x)$. It has been argued [218–220] that conformal gravity (and thus also the more general quadratic gravity theory) could reproduce the observed gravitational physics. Certainly, they admit the Schwarzschild solution and therefore also the Newtonian weak-field limit. However, stability, even in the classical theory, see below, remains an open issue.

[28] Concerning power counting, it is quite intuitive that this action is renormalizable since, in 4D, its couplings are marginal, i.e., have vanishing mass dimension. Although this turns out to be true, this is a deceptive argument because the concept of power-counting renormalizability only applies to theories with quadratic propagators (as in counting powers of momenta). To the contrary, pure quadratic gravity has quartic propagators since R^2 and $R_{\mu\nu}R^{\mu\nu}$ contain four derivatives each. See below, for a relation to unitarity and the Ostrogradky theorem. Given the different powers of momenta in the propagator the usual power counting does *not* apply.

the Ricci scalar R and the trace-free Ricci-tensor $R_{\mu\nu} - 1/4\, g_{\mu\nu} R$ give rise to a massive spin-0 and a massive spin-2 degree of freedom in addition to the usual massless spin-2 graviton [221]. While these massive modes (in particular the massive spin-2 mode) guarantee renormalizability, the massive spin-2 mode and the graviton have opposite-sign kinetic terms. Already at the classical level, this results in a linearly unstable Hamiltonian (Ostrogradsky instability [224]), at least within the linear theory. In the quantized theory, the massive spin-2 mode resurfaces as a potentially problematic negative-norm state. It is ghost-like, i.e., it propagates positive (negative) energy backward (forward) in time, while the graviton propagates negative (positive) energy forward (backward) in time, see [225]. It remains an open issue whether the spin-2 ghost is stable and should be considered as part of the asymptotic spectrum [226–233]. If so, possible unitarity violations could lead to a breakdown of quantized quadratic gravity at high scales.

Quantum gravity as an effective field theory with Planckian cutoff. Assuming that the ghost is part of the asymptotic spectrum, quantized GR can still be treated as an EFT [234], see [235] for a review. Using graviton-mediated s-channel scattering of a scalar field ($\phi\,\phi \to \phi\,\phi$) as a simple approximation to estimate the scale of new physics, one finds the following partial-wave unitarity bound, see, e.g., [236, 237],

$$|\mathcal{M}_{(\phi\,\phi\to\phi\,\phi)}(s)| \sim \frac{s}{8\pi\,\bar{G}} \sim \frac{E_{\rm cm}}{M_{\rm Planck}} < 1\,. \tag{1.32}$$

Against the backdrop of no clear new signs for subplanckian new physics within the SM, this advocates the Planck scale $M_{\rm Planck} \sim 10^{19}$ GeV as the next scale of new physics.

1.3.2 What next? Different branches of quantum gravity

A viable quantum theory of gravity must – at least in some effective IR limit – recover a *4D, Lorentzian, local, causal and unitary, perturbatively renormalizable QFT of the metric which reproduces continuum GR at tree level*. But, as we have seen, a straightforward perturbative quantization leads to a conflict between renormalizability and unitarity, cf. Sec. 1.3 and 1.3.1. Most quantum-gravity approaches can be characterized by loosening one of the above principles while insisting on others. In the absence of direct experimental signatures, each such approach is equally justified and part of a more general effort to find a quantum theory of gravity.

- Arguably, quadratic gravity is the most conservative quantum gravity ansatz. As previously mentioned, the massive spin-2 ghost might not be part of the asymptotic spectrum of perturbatively renormalizable quadratic gravity [226–233]. Even if this promising possibility can be formally established in the future, the corresponding quantum gravity theory typically contains Planckian causality violations. Further, the theory is still phrased as a Euclidean and not Lorentzian QFT. The required Wick rotation remains non-trivial.

- Another ansatz to consolidate unitarity and renormalizability is to include infinitely many higher-derivative terms which resum into an entire and thus invertible function without additional poles in the propagator [238–241]. Such theories give up on the principle of locality and it remains unclear how predictivity amongst the a priori infinitely many different entire functions should be restored.

- One such principle to restore predictivity is Weinberg's asymptotic safety paradigm [242]. It conjectures (and systematically verifies) the existence of an RG fixed point and the corresponding Reuter universality class [243]. If realized, quantum scale-symmetry fixes

infinitely many higher-order curvature terms (or equivalently the infinitely many higher moments of the entire function) in terms of a finite set of lower-order ones. The asymptotic-safety paradigm is at the heart of this thesis, cf. Sec. 2. As for the previous two branches of quantum-gravity, it remains within the realm of Euclidean QFT. Consequentially, Wick-rotation and unitarity persist as non-trivial open issues.

- String theory, see, e.g., [244, 245] for a textbook series, abandons the demand for 4 space-time dimensions and the QFT-framework.
- Loop quantum gravity, see, e.g., [246] for reviews, at least in its original formulations, imposes a fundamentally discrete area spectrum.
- Causal set theory [247] – the arguably only truly Lorentzian theory of spacetime – also relies on a fundamental discreteness scale.
- Alternatively, such discrete quantization procedures can be interpreted as a non-fundamental and lattice-like approach to regularize spacetime. This technical notion of discreteness includes dynamical triangulation, see [248] for a recent review. It is the hope that as the cutoff is removed, i.e., the fundamental discreteness scale taken to zero, these models recover a corresponding continuum field theory similar to asymptotic safety.

Conclusion.

On the one hand, we have established the Planck scale as the next scale at which new fundamental physics is truly expected. On the other hand, we have laid out that perturbative renormalizability and unitarity seem contradictive in quantum gravity, whereupon many different branches of quantum gravity have emerged – all potentially equally viable. To help guide these theoretical efforts to realize a more complete theory of quantum gravity, some contact with observation is absolutely crucial. In combination with the tentative hint for Planckian scale symmetry obtained from the values of masses and couplings in the SM, cf. Sec. 1.1.1, this provides two strong incentives to explore physics at the Planck scale and its possible link to observation, see Part II of this thesis.

2 Fixed points and the status of renormalizing gravity

Without profound explanation, we stated in Sec. 1 that the couplings of a QFT vary with scale. Renormalization is a procedure to ensure that physical quantities described at the scale μ_0 do not depend on the scale μ at which its fundamental degrees of freedom are set. For physics at μ_0 to remain unchanged, the couplings have to change (be renormalized) as μ is varied. This change is captured by the Wilsonian Renormalization Group (RG) [249–252][29].
Physically meaningful renormalization proceeds from high energies (UV) to low energies (IR), i.e., from many microscopic to fewer macroscopic degrees of freedom. Most of physics relies on the powerful principle that some information from more microscopic physics is unnecessary for a description of macroscopic scales, while other information is crucial: QCD is irrelevant once the quarks are confined inside an atom; atoms themselves become irrelevant once bound in molecules; single molecules are irrelevant to describing the motion of a car or a fluid. Nevertheless, some microscopic properties are decisive in determining, for instance, which molecules can form a car and which others can form a fluid. The RG gives a mathematical framework to determine which degrees of freedom are relevant and which others are irrelevant.

2.1 A brief introduction to non-perturbative renormalization

As QFTs incorporate infinitely many degrees of freedom, the RG flow describes the continuous integrating out of momenta at scales above the energy scale k. The associated theory space is spanned by the dimensionless versions c_i of all (possibly) dimensionful couplings $\bar{c}_i$ of the QFT. The RG flow in theory space can be expressed by continuous differential equations – the Callan-Symanzik beta functions [253, 254],

$$\beta_i = k\,\partial_k \bar{c}_i = -d_{c_i}\, c_i + k\,\partial_k c_i \,. \tag{2.1}$$

If the couplings at hand only dress marginal operators $\mathcal{O}_i$ whose canonical dimension $[\mathcal{O}_i]$ equals the inverse spacetime dimension $-D$, s.t., $c_i = \bar{c}_i$, the RG flow can be inferred from calculating diagrams in a standard perturbative loop expansion of the QFT. If, however, non-marginal operators for which $d_{c_i} = D - [\mathcal{O}_i] \neq 0$ and thus $c_i = \bar{c}_i/k^{d_{c_i}}$ are included, a proper description of the RG flow requires non-perturbative methods.

The flow equation. The non-perturbative method of choice in this thesis is the functional RG [255], see also [256–258]. Its governing equation can be derived from whithin the path-integral approach to Euclidean QFT. The D-dimensional Euclidean path integral is defined by the generating functional Z, or equivalently the effective action Γ[30], i.e.,

$$Z[J] \equiv e^{W[J]} \equiv \int \mathcal{D}\varphi\, e^{-S[\varphi]+J\cdot\varphi} \,, \quad \text{or equivalently} \quad \Gamma[\phi] = \sup_J \left(J\cdot\phi - W[J]\right) \,. \tag{2.2}$$

Here, we restrict the discussion to a simple scalar field φ with a fundamental action $S[\varphi]$ but the following results generalize to fermions [259–261], gauge fields [262–264], and gravity [264]. In Eq. (2.2), $J\cdot\varphi \equiv \int d^D x\, J(x)\phi(x)$ denotes a source term where we use the shorthand notation

[29] Kadanoff developed a coarse-graining picture of grouping degrees of freedom at smaller length scales into an effective degree of freedom at larger length scales, see [249] in which this block-spinning is applied to the Ising model. Wilson developed this physical picture into a differential language applicable to general (statistical and quantum) field theories [250, 251], see [252] for a review and a connection to QFT.

[30] The effective action Γ removes redundant information about reducible correlation functions contained in the generating functional Z.

of functional calculus, $\phi = \langle\varphi\rangle$ corresponds to the expectation value of φ, and $\sup_J$ denotes the supremum in the Legendre transformation. The effective action $\Gamma[\phi]$ derives its name from the corresponding quantum equation of motion resembling the classical equation of motion

$$\frac{\delta\Gamma[\phi]}{\delta\phi(x)} = J(x) \qquad \longleftrightarrow \qquad \frac{\delta S[\varphi]}{\delta\varphi(x)} = 0\,. \tag{2.3}$$

Solving such equations amounts to solving the path integral of the QFT by integrating out all quantum fluctuations at once. Following the Wilsonian RG picture, one can instead integrate out quantum fluctuations step by step. To do so, one regulates the above expressions by an artificial mass-like cutoff term $\Delta S_k[\varphi]$, i.e.,

$$\begin{aligned} &Z_k[J] \equiv e^{W_k[J]} \equiv \int \mathcal{D}\varphi\, e^{-S[\varphi]-\Delta S_k[\varphi]+J\cdot\varphi}\,, \qquad \Gamma_k[\phi] = \sup_J\left(J\cdot\phi - W_k[J]\right) + \Delta S_k[\varphi]\,, \\ &\text{where} \quad \Delta S_k[\varphi] = \frac{1}{2}\int \frac{d^Dq}{(2\pi)^2}\varphi(-q)\,R_k(q)\,\varphi(q)\,, \end{aligned} \tag{2.4}$$

and R_k – the regulator – should satisfy the following three properties: (i) $R_k(q^2/k^2 \to 0) > 0$ to ensure that it properly regulates IR modes; (ii) $R_k(k^2/q^2 \to 0) = 0$ to ensure that the scale-dependent effective action converges to the full effective action, i.e., $\Gamma_k \to \Gamma$ for $k \to 0$; and (iii) $R_{k\to\infty}(q^2) \to \infty$ to ensure that by use of a saddle-point approximation one recovers the fundamental action, i.e., $\Gamma_k \to S$, for $k \to \infty$.
Having introduced the regulating scale k, on can derive an a priori exact functional RG equation [255], see also [265–267]. It governs the flow $S \to \Gamma_k \to \Gamma$, i.e.,

$$k\partial_k\Gamma_k[\phi] = \frac{1}{2}\mathrm{Tr}\left[\frac{1}{\Gamma_k^{(2)}[\phi] + R_k}\,k\partial_k R_k\right] \quad = \quad \frac{1}{2}$$

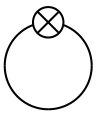

, (2.5)

The second equality expresses the flow equation (2.5) in diagramatic form. As for a usual Feynman diagram, the looped line corresponds to an internal propagator. In crucial distinction to the Feynman diagrams involving bare propagators only, the term $1/(\Gamma_k^{(2)}[\phi] + R_k)$ and the corresponding diagramatic line represent the fully dressed regulated propagator including all quantum fluctuations above k. Here, $\Gamma_k^{(2)}[\phi]$ denotes the second functional derivative of $\Gamma_k[\phi]$ with respect to ϕ. As a consequence, the flow equation is structurally a 1-loop equation. The $\otimes$ denotes the regulator insertion $k\partial_k R_k$.
Eq. (2.5) is formally exact but as an infinite dimensional integro-differential equation not exactly solvable in practice. Instead, $\Gamma_k[\phi]$ can be expanded in systematic truncations, cf. Sec. 2.2.1. At each order – by taking functional derivatives on both sides of Eq. (2.5), projecting appropriately, and setting all remaining fields to zero – the RG flow of couplings in front of specific operators contained in Γ_k can be extracted. Most importantly, Eq. (2.5) thereby breaks down the hard problem of solving a full QFT path integral to the much more feasible task of solving differential equations. Given a proper expansion scheme, the obtained approximate RG flow converges to the full RG flow with growing order of the respective truncation. At $k = 0$, the result is independent of the regulator. In practice, and at intermediate k, residual regulator dependence provides an approximation to the systematic error at finite truncation order.

Physical scales. Ideally, the RG-flow is fully solved down to $k = 0$, incorporating all energy scales μ_i of the physical process of interest. RG running with the physical scales μ_i can then be

studied in the obtained quantum effective action Γ at $k = 0$. This requires to still solve non-local integro-differential equations. For physical processes involving only a single physical energy scale μ, an identification $\mu = k$ seems justified since there simply are no other scales present. In those cases, the RG scale k can be regarded as the physical energy scale of the process. Part II of this thesis, which is concerned with single-scale particle physics at the center-of-mass energy of collider processes, will always implicitly assume this identification. In part III, which is devoted to studies of black holes, multiple physical scales might complicate the picture.

Other non-perturbative methods. The functional RG is by no means the only non-perturbative method to explore RG flows and their fixed points. Other methods include the lattice approach to quantum gravity, i.e., dynamical triangulations, both Euclidean (EDT)[268–276] and causal (CDT) [277–280], see [248] for a recent review, the LQG spin-foam [281–285] renormalization [286–288] as well as LQG Hamiltonian renormalization [289], and holographic renormalization [290]. Recent generalizations of the flow equation (2.5) to background-independent [291–295] tensor models and to Lorentzian spacetime [296, 297] – see also [298] for a formulation of the functional RG in Lorentzian signature – are particularly important for progress in studying possible fixed points of quantum gravity.
Whenever these different renormalization schemes agree on the physical assumptions, e.g., whether they physically break Lorentz invariance, they should eventually lead to the same physical statements about the quantized and renormalized theory. Thereby non-perturbative RG-flows can provide novel points of contact and promise joint progress within the quantum-gravity community.

2.2 Weinbergs asymptotic-safety paradigm

This section introduces the concept of fixed points of the RG flow. Fixed points dominate the RG flow of field theories. Close to a fixed point an enhanced scale symmetry results in universal scaling properties. These determine phase transitions in condensed matter physics, cf. [25, 299] for textbooks. Partial fixed points play a key role in the SM of particle physics [300–303]. Moreover, cf. Sec. 1, indications for Planckian scale symmetry tentatively point to a fundamental and joint fixed point for quantum gravity and the SM, cf. Sec. 4 and 5.
The following discussion covers both asymptotic freedom and asymptotic safety. It encompasses the notion of UV and IR fixed-points and clarifies this terminology for a multi- or infinite-dimensional coupling space. In the Wilsonian EFT picture, the coupling space of any QFT is infinite-dimensional. The RG flow, cf. Sec. 2.1, defines a vector field on this theory space. Attractors and sources within this vector field define special points – so-called fixed points – in theory space at which the QFT becomes scale-invariant. In this abstract picture,

- asymptotic freedom [304] of trajectories in theory space restores classical scale-invariance at a fixed point for which all couplings vanish;
- asymptotic safety [242] of trajectories in theory space generates a novel form of quantum scale-invariance at a fixed point for which some couplings remain finite.

Therefore, asymptotic freedom is a special case of asymptotic safety. Typically, the terms are only used for fixed points which are not fully IR-attractive. To introduce the concepts of fixed points and attractive eigendirections more rigorously, we reduce the infinite-dimensional couplings space – first to one and then to finite dimensions, cf., Sec. 2.2.2 and Sec. 2.2.3, respectively. In specific theories, a meaningful reduction requires an ordering principle in the

infinite-dimensional space of couplings. One such ordering principle is perturbation theory around the free fixed point and the corresponding canonical power-counting. For now, we will simply assume that such an ordering principle exists and that it defines a meaningful truncation scheme. Only after introducing asymptotically safe gravity, cf. Sec. 2.4, will we return to the limit of infinite-dimensional coupling space, cf. Sec. 2.4.4.

Finally, the RG defines a preferred direction of the flow, namely from the UV to the IR. Physically, this represents the loss of information when integrating out degrees of freedom, cf. Sec. 2.1. Mathematically, it is reflected in the fact that the Renormalization Group, despite its name, is not actually a group, but a semi-group only, see, e.g., [260]. In any case, the UV-to-IR arrow of the flow cannot be reversed in full theory space. This property is lost in finite-dimensional truncations in which the flow can be tracked in both directions equivalently. Crucially, only one direction can be extended to recover the infinite-dimensional case. This "arrow of information loss" also makes a crucial distinction in the significance of IR and UV attractive directions: every physically meaningful fixed point must exhibit a finite number of UV-attractive and therefore an infinite number of IR-attractive directions. Otherwise, no meaningful IR-directed flow towards this fixed can be established.

2.2.1 Approximation schemes to the full effective action

In general, the scale-dependent effective action $\Gamma_k[\Phi]$ for a specified field content Φ contains (i) arbitrary functions of all possible invariants $\mathcal{O}_i$ formed from the field content, each potentially dressed by (ii) an arbitrary function of spacetime derivatives. We can schematically write

$$\Gamma_k = \int d^D x \sum_{i,j} \mathcal{F}_i\left(\mathcal{O}_i, \Delta_j\right) , \tag{2.6}$$

where the Δ_j denote the derivative operators acting on the invariants $\mathcal{O}_i$. For the special case of a single-component scalar field, there is only one such invariant. In the case of gravity, already the task of finding a basis in curvature invariants is very non-trivial [305].
As a result of this general expansion, the flow equation (2.5) remains an infinite-dimensional integro-differential equation (IDE). Additional systematic expansions can be employed to reduce the complexity and obtain more feasible truncations of the RG flow.

- **Vertex expansion:** This scheme expands the continuous functions of all possible field invariants in a set of fluctuating fields $\delta\Phi$. At truncation order n, this comprises an M_n-dimensional basis set of all possible such vertex structures, i.e.,

$$\Gamma_k = \sum_{n=1}^{\infty} \frac{1}{n!} \int d^D x_1 \dots d^D x_n \sum_{m=1}^{M_n} \Gamma_k^{(n,m)}(x_1, \dots, x_n) \mathcal{O}^{(n,m)}(\delta\Phi_1, \dots, \delta\Phi_n) . \tag{2.7}$$

  This expansion retains the full momentum dependence of the vertex function or form factors $\Gamma_k^{(n,m)}$. Although now of finite order, the flow equation remains an IDE.

- **Derivative expansion:** Contrary to an expansion in field invariants, the derivative expansion truncates the arbitrary functions of momenta but retains full functions of the field invariants, i.e.,

$$\Gamma_k = \int d^D x \sum_{j=0}^{\infty} \left(\Delta_i\right)^j F_j(\mathcal{O}_i) . \tag{2.8}$$

Here, $F_0 \equiv V$ corresponds to the effective potential and the lowest order to the local-potential approximation [265]. At each finite order, this scheme reduces the integro-differential equation (IDE) to a set of partial differential equations (PDEs).

- **Combined expansion:** Expanding both the operator and derivative structure to finite order reduces the scale dependence of the effective action to a finite set of couplings. The flow equation collapses to a set of ordinary differential equations (ODEs) – the β-functions.

In the following two sections we will define asymptotic safety for such finite-dimensional truncations of infinite-dimensional theory space.

2.2.2 UV and IR fixed points for a single coupling: Conformal window for QCD

Given a single coupling α and its RG flow $\beta_\alpha = k\,\partial_k \alpha$, the set of all fixed points $\alpha_*^{(i)}$ with $i = 1, \ldots, n$ is defined by $\beta_\alpha(\alpha = \alpha_*^{(i)}) = 0$. We assume that β_α is continuous. For the special case without a fixed point, the coupling diverges both in the UV and the IR. If there exists a single fixed point, the theory will approach it either towards the UV or towards the IR. This defines the critical exponent

$$\theta_*^{(i)} = -\partial_\alpha \beta_\alpha\big|_{\alpha=\alpha_*^{(i)}} . \tag{2.9}$$

For $\theta_*^{(i)} < 0$ ($\theta_*^{(i)} > 0$), the fixed point is IR (UV) attractive and thus defines an IR (UV) complete theory for all values of α. For any finite $n \geqslant 2$, it is unambiguous to define theories which are both UV- and IR-complete. Because β_α is a continuous function, the critical exponents of its fixed points must alternate in sign. Thus, each pair of two neighboring fixed points, $g_*^{(i)}$ and $g_*^{(i\pm1)}$, automatically defines such a UV- and IR-complete window of coupling values[31].

The arguably most famous example is the conformal window of $SU(N)$ non-Abelian gauge theories. The perturbative 2-loop RG flow for the gauge coupling $\alpha = g^2/(4\pi)^2$, cf. [306], reads

$$\beta_\alpha = -B\,\alpha^2 - C\,\alpha^3 + \mathcal{O}(\alpha^4) . \tag{2.10}$$

B and C depend on the matter content, see [307]. In general, there are two fixed points with corresponding critical exponents

$$\alpha_*^{(1)} = 0, \qquad \theta_*^{(1)} = -B \qquad \text{and} \qquad \alpha_*^{(2)} = -B/C, \qquad \theta_*^{(2)} = B . \tag{2.11}$$

Fixed points at $\alpha < 0$ correspond to imaginary values of g and thus have no direct physical meaning. For $B > 0$ and $C > 0$ the theory has only one physical fixed point at $\alpha_* = 0$ which is UV-attractive. Hence, the theory is UV-complete (asymptotically free) for any value of $\alpha > 0$ which does not invalidate perturbation theory[32]. For $N = 3$ and N_F fermions in the fundamental representation, this case is realized for $N_F < 8.05$. At $N_F = 8.05$ the sign of C flips, i.e., $C < 0$. As long as $B > 0$, the non-vanishing fixed point $\alpha_*^{(2)}$ is physical and IR attractive. This is the Banks-Zaks fixed point [307, 308], cf. Fig. 2. Now, the theory is both IR- and UV-complete. $B > 0$ remains positive up to the famous value $N_F = 16.5$ which signals the (complete) loss of asymptotic freedom. In fact, already at $16.5 > N_F > 8.05$ asymptotic freedom is restricted to $\alpha < \alpha_*^{(2)}$ because the Banks-Zaks fixed point screens larger values, cf. Fig. 2. For $N_F > 16.5$, only the fixed point at $\alpha_*^{(1)}$ is physical, but now it is IR-attractive for all coupling values. The

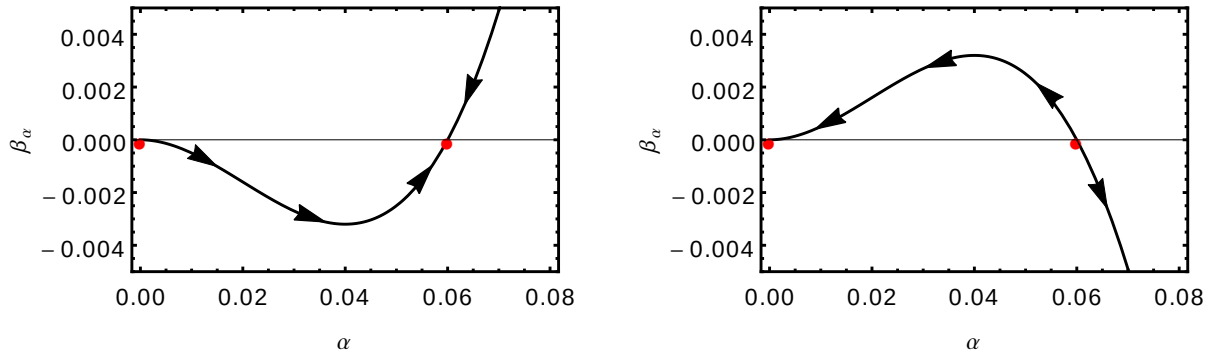

Figure 2: β-function of the squared gauge coupling. Red dots mark the fixed points. Arrows point towards the IR. Left-hand panel: UV- and IR-complete trajectory between a vanishing UV and a non-vanishing IR fixed point for $N_f = 12$. Right-hand panel: UV- and IR-complete trajectory between a non-vanishing UV and a vanishing IR fixed point. This case (e.g., $B = -6$, $C = 100$) cannot be realized in a single-coupling gauge theory.

resulting theory has a triviality problem, cf. Sec. 1.2.2.
The other mixed case of $B < 0$ and $C > 0$ corresponds to the first example of a UV-attractive fixed point at non-vanishing coupling value. This sign-combination cannot be achieved for any $N_F > 0$. Nevertheless, the right-hand panel in Fig. 2 depicts this situation for the artificial case of $B = -6$ and $C = 100$. This form of asymptotic safety can be realized in gauge-Yukawa theories with multiple couplings, cf. [309] as well as Sec. 2.3.

2.2.3 Fixed points for multiple couplings

For a single coupling, each fixed point can be unambiguously classified as either a UV or an IR fixed-point. Such unambiguous cases *can* persist for theories with finitely many couplings, but this need not be the case to define an asymptotically safe theory. Transitioning from a finite to an infinite number of couplings, every physical fixed point must at some point acquire infinitely many IR-attractive directions anyways, i.e., every physical fixed point is mostly an IR fixed point.

Given a (finite) set of couplings λ_i and their truncated flow $\beta_i = k\partial_k\lambda_i$, a fixed point is defined as a set of couplings $\lambda_* = \{\lambda_{i*}\}$ for which all $\beta_i(\lambda_*) = 0$. To determine UV/IR attractivity, it is sufficient to linearize the flow around the fixed point λ_*, i.e.,

$$\beta_i = \sum_j \mathcal{M}_{ij}\,(\lambda_i(k) - \lambda_{i*}) \qquad \Longrightarrow \qquad \lambda_i(k) = \lambda_{i*} + \sum_j C_j \times (\mathbf{V}_j)_i \left(\frac{k}{k_0}\right)^{-\theta_j}\,, \tag{2.12}$$

where $\mathcal{M}_{ij}$ is the stability matrix and the critical exponents θ_j are its negative eigenvalues. The associated eigenvectors $\mathbf{V}_j$ span the corresponding basis. The C_j are the constants of integration. Every positive (negative) critical exponent corresponds to a UV-attractive (IR-attractive) direction[33].
Along the UV-attractive directions, the set of constants $\{C_j|\theta_j > 0\}$, parameterizes the departure

[31] The two boundary windows for $g < g_*^{(1)}$ and $g > g_*^{(n)}$ remain UV or IR divergent, respectively.
[32] The opposite case of $B < 0$ and $C < 0$ defines a theory which is always IR-complete.
[33] There are many equivalent terminologies for this linearized attractivity. UV-attractive, IR-repulsive, and relevant directions are interchangeably used for positive critical exponents. IR-attractive, UV-repulsive, and irrelevant directions are used to describe negative critical exponents. Also, the definition of the sign in θ_j is arbitrary and some of the literature uses the opposite definition.

from the scale-invariant fixed point towards the IR. These directions span the *critical hypersurface* $\mathcal{T}(\lambda_*)$ associated to the fixed point λ_*. This constitutes a special hypersurface because the flow towards the IR along all other directions attracts trajectories towards this surface. This is reflected by the set of integration constants $\{C_j|\theta_j < 0\}$ becoming less and less important towards the IR. We are now in a position to rigorously define an asymptotically safe fixed point:

- For a theory space which is expandable in a (possibly infinite-dimensional) basis of couplings, a fixed point is asymptotically safe if it has at least one but at most a finite number of UV-attractive directions in this basis.

It is merely a convention to exclude fully IR-attractive fixed points. Every asymptotically safe fixed point λ_* defines a special set of theories which emanate from it. They correspond to the critical hypersurface $\mathcal{T}(\lambda_*)$. Its dimension is determined by the number of UV-attractive directions. Whether it is unbound and extends to infinite coupling values depends on the presence of other fixed points and possible physical poles. In any case, $\mathcal{T}(\lambda_*)$ defines the set of all asymptotically safe theories associated with this λ_*. By definition, asymptotically safe theories are predictive since only a finite set of initial conditions $\{C_j|\theta_j > 0\}$ has to be fixed by experiment to fully determine them. We will refer to this as *fundamental asymptotic safety*.

The qualifying term 'fundamental' is added because the predictivity of an asymptotically safe fixed point reaches beyond the fundamental theories which it defines. Indeed, the attractivity properties of the fixed point extend to its entire critical hypersurface. Any trajectory within the basin of attraction of the fixed point λ_* – not screened by other fixed points or by poles – will be attracted to the critical hypersurface $\mathcal{T}(\lambda_*)$. Towards the IR, any such non-fundamental theory will more and more resemble one of the fundamentally asymptotically-safe theories. Hence, these theories exhibit *effective asymptotic safety*. A perturbative Wilsonian EFT corresponds to the special case of effective asymptotic safety around the free fixed point – one could refer to it as effective asymptotic freedom.

To discuss the above concepts for specific examples, we use the most general β-functions of two couplings λ_1 and λ_2 up to second order in a combined expansion, i.e.,

$$\beta_1 = a_1\,\lambda_1 + b_1\,\lambda_1^2 + c_1\,\lambda_1\,\lambda_2 + d_1\,\lambda_2 + e_1\,\lambda_2^2 + \mathcal{O}(\lambda_i^2)\,, \tag{2.13}$$

$$\beta_2 = a_2\,\lambda_2 + b_2\,\lambda_2^2 + c_2\,\lambda_1\,\lambda_2 + d_2\,\lambda_1 + e_2\,\lambda_1^2 + \mathcal{O}(\lambda_i^2)\,, \tag{2.14}$$

Obviously, the system has 4 fixed points, some of which can lie in the complex plane. Also, for special relations between the coefficients, the fixed points can be degenerate or moved to ∞. Although they can be the cause of collisions in the real plane, $d_{1/2}$ and $e_{1/2}$ merely shift the fixed points around. For $d_{1/2} = e_{1/2} = 0$, the fixed points take a simple analytical form

$$\mathrm{FP}^{\lambda_1\lambda_2}_{\circ\circ} = (\lambda_1 = 0,\ \lambda_2 = 0)\,, \tag{2.15}$$

$$\mathrm{FP}^{\lambda_1\lambda_2}_{\bullet\circ} = (\lambda_1 = -a_1/b_1,\ \lambda_2 = 0)\,, \tag{2.16}$$

$$\mathrm{FP}^{\lambda_1\lambda_2}_{\circ\bullet} = (\lambda_1 = 0,\ \lambda_2 = -a_2/b_2)\,, \tag{2.17}$$

$$\mathrm{FP}^{\lambda_1\lambda_2}_{\bullet\bullet} = \left(\lambda_1 = \frac{a_2\,c_1 - a_1\,b_2}{b_1\,b_2 - c_1\,c_2},\ \lambda_2 = \frac{a_1\,c_2 - a_2\,b_1}{b_1\,b_2 - c_1\,c_2}\right)\,. \tag{2.18}$$

The nomenclature indicates which couplings take vanishing (empty circle $\circ$) or non-vanishing (filled circle $\bullet$) values. Whenever all 4 fixed points are real, the critical exponents of the

Gaußian $\mathrm{FP}^{\lambda_1\lambda_2}_{\bigcirc\bigcirc}$ determines all other ones. For instance, if the $\mathrm{FP}^{\lambda_1\lambda_2}_{\bigcirc\bigcirc}$ is fully UV-attractive, each transition to a nonvanishing fixed-point value flips one associated critical exponent to become IR-attractive. This simply follows from continuity of the flow. This is a generic property of such systems and will serve to easily discern many of the main results of this thesis.
In fact, the schematic system in Eq. (2.13) already contains much of the essence of the results to come. We notice that the transition $\widetilde{\beta}_i \equiv \beta_i \, \lambda_i$ does not change the fixed-point structure or the sign of the critical exponents. It merely adds to the degeneracy of the Gaußian FP (and changes the magnitude of the critical exponents). With this understanding, we can indeed identify the following physical mechanisms of how non-vanishing fixed points can arise:

- **Classical vs. quantum**: The terms a_i in β_i correspond to classical scaling, cf. Eq. (2.1) as can be understood intuitively: When integrating β_i, a linear term corresponds to a power-law running of λ_i in the vicinity of $\lambda_i = 0$. This is the prototypical EFT scaling of couplings associated with canonically (ir)relevant operators. The terms b_i, e_i and c_i correspond to lowest-order quantum self-interactions, quantum mixing, and quantum induction by another coupling, respectively. Provided the signs work out, any of the latter terms can balance against the classical one. This mechanism is explicitly discussed in Sec. 2.3.1.

- **Competing degrees of freedom**: If the classical contribution vanishes, i.e., $a_i = 0$, the different quantum fluctuations b_i, e_i and c_i can still balance against each other. The prime example of this is the competition of fermionic and bosonic fluctuations since the Grassmannian nature of fermions contributes a relative sign in loops.

- **Balancing loop orders**: Finally, with the transition to $\widetilde{\beta}_i$, Eq. (2.13) also represents adjacent loop-orders. This was exemplified in case of a single coupling in the last section and holds for multiple couplings, provided the right signs. Both, the Banks-Zaks, cf. Sec. 2.2.2, as well as the Litim-Sannino fixed point, cf., [309] and Sec. 2.3, are such examples.

2.3 Mechanisms for asymptotic safety

We will now discuss the above mechanisms in more detail.

2.3.1 Classical vs quantum scaling

The question of whether a coupling is marginal or not depends on the dimension of the quantum field theory. Fixed points arising from the balance of classical and quantum scaling can thus potentially be connected to asymptotically free, perturbatively renormalizable theories in another dimension.

Perturbatively renormalizable quantum field theories in their critical dimension. Given a general set of quantum fields Φ, potentially obeying global or even local symmetries, each invariant $\mathcal{O}(\Phi)$ built from these fields defines a renormalizable field theory in the corresponding critical dimension d_c. The critical dimension can be obtained by dimensional analysis of a Lagrangian with kinetic term and interaction term corresponding to $\mathcal{O}(\Phi)$, i.e.,

$$\mathcal{L} = \Phi_i \mathcal{D} \, \Phi_i + \bar{\lambda}_{\mathcal{O}} \, \mathcal{O}(\Phi) \, , \tag{2.19}$$

where $\mathcal{D}$ is a derivative operator which defines the kinetic term. E.g., for fermionic fields, $[\mathcal{D}] = [\mathcal{D}_F] = 1$ has mass dimension one, while for bosonic fields $[\mathcal{D}] = [\mathcal{D}_B] = 2$ has mass

dimension two. Since the action – which corresponds to integration of the Lagrangian over D spacetime dimensions – has to be dimensionless, the Lagrangian has to be of mass dimension D. Hence, the mass dimension of the fundamental fields is $[\Phi_i] = (D - [\mathcal{D}])/2$, i.e., $[\Phi_i] = (D-2)/2$ for bosons and $[\Phi_i] = (D-1)/2$ for fermions. Therefore, one can infer the mass dimension of $\mathcal{O}(\Phi)$. The critical dimension D_c is the one in which $[\mathcal{O}(\Phi)] = D_c$, and the corresponding coupling $[\bar{\lambda}_{\mathcal{O}}] = 0$ is marginal.
The running of such couplings, i.e., $\beta_{\bar{\lambda}_{\mathcal{O}}} = k\partial_k \bar{\lambda}_{\mathcal{O}}$, is (1-loop) 2-loop universal in (massive) massless RG-schemes, see e.g., [18]. It can, for instance, be obtained within perturbation theory. A negative (positive) sign of the leading-order antiscreening (screening) quantum self-interactions

$$\beta_{\lambda_{\mathcal{O}}} = \pm \# \lambda_{\mathcal{O}}^2 \quad + \text{higher order} \,, \tag{2.20}$$

determines whether the coupling is asymptotically free (or Landau-pole like). In such a way one can classify all quantum field theories (at least those with a single interaction) by whether they are screening ($+\#\lambda_{\mathcal{O}}^2$ in Eq. (2.20)) or antiscreening ($-\#\lambda_{\mathcal{O}}^2$ in Eq. (2.20)) in their respective critical dimension.

Theories away from their upper and/or lower critical dimension. Perturbation by a small parameter, i.e., moving to $D = D_c \pm \epsilon$, and introducing the corresponding dimensionless coupling $\lambda_{\mathcal{O}} = \bar{\lambda}_{\mathcal{O}} k^{\mp\epsilon}$, generalizes the above β-function to arbitrary dimension, i.e.,

$$\beta_{\lambda_{\mathcal{O}}} = \mp \epsilon \lambda_{\mathcal{O}} \pm \# \lambda_{\mathcal{O}}^2 + \text{higher order} \,, \tag{2.21}$$

where, a priori, the first $\mp$ refers to above and below D_c, while the second $\pm$ refers to antiscreening and screening leading-order quantum fluctuations. It is instructive to combine the signs in the above fashion since this selects the cases in which a non-vanishing fixed point is generated at

$$\lambda_{\mathcal{O}\,*} = \epsilon/\# \,. \tag{2.22}$$

- A quantum field theory with an antiscreeing self-interaction – which is therefore asymptotically free in its critical dimension – develops an interacting fixed point with a UV-attractive direction above its critical dimension.
- A quantum field theory with a screening self-interaction – which is therefore Landau-pole like in its critical dimension – develops an interacting fixed point with an IR-attractive direction below its critical dimension.

In condensed-matter physics, universality classes can be generated by this mechanism. One thereby defines the upper (lower) critical dimension of a universality class. This includes the famous screening Wilson-Fisher fixed point [310] with $D_c = 4$, the anti-screening Gross-Neveu universality class [311] with $D_c = 2$, asymptotically free (anti-screening) Yang-Mills theory [312] with $D_c = 4$, and potentially antiscreening quantum gravity with $D_c = 2$, see below.

2.3.2 Balance of fermionic and bosonic fluctuations

For theories in their critical dimension, put differently, for perturbatively renormalizable theories, there is no canonical contribution for the running of couplings because such theories are classically scale-invariant. Nevertheless, classical scale invariance is broken by quantum effects. It can either be restored, if all quantum contributions vanish (asymptotic freedom) or if they cancel against each other (asymptotic safety).

Such a cancellation can be realized by the balance of contributions from different interacting fields Φ_1 and Φ_2, schematically,

$$\beta_\lambda = \beta_\lambda^{\Phi_1} - \beta_\lambda^{\Phi_2} \,, \tag{2.23}$$

where $\beta_\lambda^{\Phi_{1/2}} > 0$. A prime example is the balance of fluctuations from bosonic and fermionic superpartners in supersymmetric field theories [313–315][34]. Even without the presence of supersymmetry bosonic and fermionic quantum fluctuations can cancel against each other at particular coupling values λ_*, see [316–318] for the possibility of asymptotic safety in simple Higgs-Yukawa systems, and [6] as well as Sec. 3.1 for a possible four-dimensional example of asymptotic safety via competing degrees of freedom.

2.3.3 Balance of different loop orders: the Litim-Sannino fixed point

Another mechanism to generate asymptotic safety within the critical dimension of a theory is the cancellation of different orders, e.g., 1-loop against 2-loop terms [309]. By construction, these asymptotically safe fixed points violate perturbative loop ordering at low order. Any such fixed point should thus be verified at higher order in the perturbative expansion, see [319].
It is non-trivial to construct such perturbative asymptotically safe theories in $D = 4$, mainly because the balance has to hold not just for one coupling, but for all renormalizable couplings of the given field content. The first successful realization of asymptotic safety in $D = 4$ is a non-Abelian $SU(N_C)$ gauge-Yukawa theory [309] for large-N_C (growing with the number of gauge fields) and large-N_F (number of fermions), i.e., in the Veneziano limit [320]. In this limit one takes both $N_C \to \infty$ and $N_F \to \infty$, while keeping a particular ratio fixed to define an arbitrarily small perturbative parameter

$$\epsilon \equiv \frac{N_F}{N_C} - \frac{11}{2} \,. \tag{2.24}$$

The corresponding Litim-Sannino fixed points will be discussed in the context of gravitational corrections and effective asymptotic safety in Sec. 3.2. As we shall see, asymptotic safety is generated by a combination of the mechanisms of balancing different loop orders and competing degrees of freedom.

The fixed-point mechansim is based on a non-Abelian gauge coupling g, or the more convenient definition[35] $\tilde{\alpha}_g = \frac{N_C\, g^2}{(4\pi)^2}$. In its β-function (to second loop order), i.e.,

$$\beta_{\tilde{\alpha}_g} = -B\,\tilde{\alpha}_g^2 + C\,\tilde{\alpha}_g^3 \,, \tag{2.25}$$

the negative sign indicates the antiscreening character of the leading-order contribution associated to asymptotic freedom. This holds as long as antiscreening gauge self-interactions dominate over fermionic matter fluctuations, i.e., as long as $B > 0$. If, in addition, $C > 0$, then a non-vanishing fixed point arises at

$$\tilde{\alpha}_{g\,*} = B/C \,. \tag{2.26}$$

[34] In supersymmetry this type of quantum scale-invariance is usually not discussed in the context of fixed points, but rather as a theory which never departs from quantum scale-invariance.

[35] We denote this definition by $\tilde{\alpha}_g$ to distinguish it from the similar definition $\alpha_g = g^2/(4\pi)$ commonly used in the context of grand unification.

Whenever antiscreening is lost – because of too many matter degrees of freedom – at leading order ($\tilde{\alpha}_g^2$), i.e., $B < 0$, but restored at next-to-leading order ($\tilde{\alpha}_g^3$), i.e., $C < 0$, this fixed point inherits the UV-attractive nature of asymptotic freedom and can thus serve to UV-complete the theory.
It has been proven [309, 321, 322] that $C < 0$ is only possible in the presence of Yukawa interactions[36]. In turn, this requires a mechanism to generate an asymptotically safe (or free) fixed point for the Yukawa coupling y itself. Again, we introduce $\tilde{\alpha}_y = \frac{N_F\, y^2}{(4\pi)^2}$, for which the β-function to leading (1-loop) order reads,

$$\beta_{\tilde{\alpha}_y} = E\,\tilde{\alpha}_y^2 - F\,\tilde{\alpha}_g\,\tilde{\alpha}_y\ . \tag{2.27}$$

A non-trivial fixed point in the Yukawa sector can be generated by the competition of bosonic gauge fields and fermionic fields, i.e.,

$$\tilde{\alpha}_{y\,*} = \frac{F}{E}\tilde{\alpha}_g\ . \tag{2.28}$$

See [321, 322, 324] for generalizations to an arbitrary number of Yukawa couplings, to semi-simple gauge groups, and to supersymmetry [325, 326].

2.4 The Reuter fixed-point of asymptotically safe quantum gravity

We have discussed two perturbative mechanisms of how asymptotically safe theories can arise within the critical dimension of a given theory: (i) via competing degrees of freedom and (ii) via cancellations of different (adjacent) loop orders. Moreover, (iii) moving away from the critical dimension allows to generate non-vanishing fixed points by balancing classical against quantum scaling. In physical – therefore integer – dimensions, this automatically requires some degree of non-perturbativity because an $\mathcal{O}(1)$ classical contribution needs to be balanced by quantum effects. Non-perturbative techniques ranging from resummation [327], lattice simulations [328], to the functional RG [265, 329, 330], have gathered substantial evidence for several non-trivial universality classes that realize quantum scale-invariance in condensed matter theories. In this context, a possible asymptotically safe fixed point for quantum gravity appears as just one of many realizations of this mechanism[37].

The asymptotic-safety program, cf. [331, 332] for recent textbooks and [333, 334] for reviews, investigates the possibility of a non-perturbative fixed point for Euclidian quantum gravity. The question whether – and if so, how – Euclidean and Lorentzian asymptotically safe gravity are related is subject to active research, see [335–339]. This thesis will investigate only the Euclidean theory.

As discussed in Sec 2.2, the asymptotic-safety paradigm involves all (infinitely many) operators allowed by symmetry. Canonical scaling and therefore perturbative renormalizability guarantees a powerful principle to single out a finite subset of these operators which are important for quantization around the Gaussian fixed point – the classically relevant and classically

[36] See also [323] for a proof that non-Abelian gauge interactions are required to generate *perturbative* asymptotically free or safe fixed points.

[37] As we have argued in Sec. 2.2, every physical fixed point must be mainly an IR fixed point. Hence, the statement that universality classes have only been explored for IR- and not UV-fixed points is meaningless. Nevertheless, quantum gravity makes for a very particular example because of its dynamical background and Lorentzian origin.

marginal couplings.
For Euclidean quantum gravity, the canonical dimension of operators can be obtained knowing that the metric is a dimensionless field, i.e., $[g_{\mu\nu}] = 0$. For instance, the Ricci scalar which involves two spacetime derivatives has mass dimension 2. We schematically write a general gravitational action ordered in a power series of curvature invariants and derivatives by

$$S_{\text{gravity}} = \int d^D x \sqrt{-g} \frac{1}{16\pi \bar{G}} \left(R - 2\bar{\Lambda}\right) + \int d^D x \sqrt{-g} \sum_{n>1, m\geq 0, i} \bar{\alpha}^{(i)}_{(n,m)} \mathcal{O}^{(i)} \left(\mathcal{R}^n, \Box^m\right) . \tag{2.29}$$

The first term is the Einstein-Hilbert action with dimensionful couplings $\bar{G}$ and $\bar{\Lambda}$. The second term denotes a series expansion in curvature invariants $\mathcal{R}^n$ and derivatives $\Box^m$. The 0^{th} and 1^{st} order are contained in the Einstein-Hilbert term. The three curvature invariants (two in $D = 4$, see Sec. 1.3) at 2^{nd} order define the quadratic-gravity action, cf. Eq. (1.31) in Sec. 1.3. Here, we are only concerned with the canonical dimensionality of the couplings, i.e.,

$$[\bar{\Lambda}] = 2 , \quad [\bar{G}] = 2 - D , \quad [\bar{\alpha}^{(i)}_{(n,m)}] = D - 2(n+m) . \tag{2.30}$$

Resembling a mass-term, the cosmological constant corresponds to a relevant direction in every dimension. The Newton coupling $\bar{G}$ becomes more (canonically) irrelevant with growing dimension[38]. To the contrary, higher-order gravitational couplings $\bar{\alpha}^{(i)}_{(n,m)}$ become increasingly (canonically) relevant with growing dimension. The Newton coupling is marginal in $D = 2$, in which Einstein gravity is perturbatively renormalizable. With growing and even dimensionality, other perturbatively renormalizable gravitational theories may be defined via higher curvature invariants at the level $(n+m) = D/2$. For obvious reasons, an example of particular importance is quadratic gravity in $D = 4$, cf. Sec. 1.3.
Focusing only on $\bar{G}$, the β-function of its dimensionless counterpart $G = \bar{G}k^2$ in $D = 2 + \epsilon$ takes precisely the form discussed in the context of non-vanishing fixed points from a balance of classical and quantum scaling, cf. Sec. 2.3.1. For convenience, we recapitulate its form,

$$\beta_G = \epsilon\, G - \beta_G^{(1-loop)}\, G^2 + \mathcal{O}(G^3) . \tag{2.31}$$

The 1-loop coefficient reads $\beta_G^{(1-loop)} = (25-c)/24\pi$, where the central charge c parameterizes the matter content of the theory [242, 340, 341]. It is universal (meaning RG-scheme independent) in $D = 2$ but non-universal for $D \neq 2$, and found to be antiscreening, i.e., $\beta_G^{(1-loop)} > 0$, unless too much fluctuating matter, i.e., $c < 25$, is included[39]. The antiscreening property of gravity leads to an asymptotically safe fixed point and corresponding critical exponent

$$G_* = \epsilon / \beta_G^{(1-loop)} , \qquad \theta = \epsilon . \tag{2.32}$$

Hence, the quantum critical exponent θ becomes more relevant with increasing dimension $2 + \epsilon > 0$. This is in contrast to the canonical dimension which drops with increasing dimension. Asymptotic safety thus necessarily implies that the quantum scaling of the dimensionless Newton coupling G differs considerably from canonical scaling.
In the remainder of this section we will (i) extend to the conjectured set of relevant directions

[38] We cannot naively redefine $\bar{\alpha}_0 = 1/(16\pi\bar{G})$ to be a relevant couplings in $D = 4$. This is connected to $\bar{G}$ entering the equations of motion, i.e., the Einstein equations, cf. (1.18), and a proper connection to IR dynamics.

[39] See [342] for two-loop results within the ϵ-expansion. Unfortunately, the latter are not sufficient to consistently obtain the second order in the ϵ-expansion.

at the Reuter fixed point in $D = 4$ and formulate the corresponding near-canonical-scaling conjecture in Sec. 2.4.1, (ii) match the Einstein-Hilbert truncation in the presence of matter to a viable infrared limit, see Sec. 2.4.2, (iii) discuss a posteriori evidence for and thereby justify the near-canonical-scaling conjecture in Sec. 2.4.3, and finally (iv) review how to extend finite-dimensional truncations to an infinite-dimensional expansion, see Sec. 2.4.4.

2.4.1 The near-canonical-scaling conjecture

The symmetries of a theory (such as diffeomorphism symmetry for GR) are insufficient to limit the respective EFT to a finite set of admissible interactions[40]. The powerful principle of renormalizability is able to close that gap. Perturbative renormalizability around the free fixed point singles out a finite set of relevant and marginal interactions to span a hypersurface of renormalizable theories. The ϵ-expansion around $D_c \pm \epsilon$ suggests non-perturbative fixed points in adjacent dimensions. Exploring asymptotic safety, cf. 2.2 amounts to conjecturing a non-perturbative principle to limit the set of all UV-attractive directions, i.e., free parameters. This conjecture is justified a posteriori through non-perturbative techniques. In the case of quantum gravity the asymptotic-safety conjecture can be stated as:

> *The UV-attractive sector of the Reuter universality class of 4D quantum gravity is restricted to the 2 couplings of GR, cf. Eq.* (1.17)*, and the 2 independent couplings of quadratic gravity, cf. Eq.* (1.31)*. All other canonically irrelevant couplings remain IR-attractive at the Reuter fixed point. Their inclusion is important for quantitative convergence, but does not introduce additional free parameters.*

The conjecture states that canonical dimensionality is still a useful ordering principle to identify the UV-attractive couplings. As we shall see in Sec. 2.4.3, there is substantial evidence for the conjecture. For now, its validity shall be assumed to discuss the resulting physical consequences. The main aim of the following section is to present the physics of asymptotically safe gravity in the most accessible way. Remarkably, for most of the physical mechanisms $S_{\rm GR}$ is sufficient. The influence of $S_{\rm QG}$ will thus only be discussed if necessary.

2.4.2 The Einstein-Hilbert truncation and the classical limit

When treating (quantum) gravity as a QFT, the gravitational couplings are subject to renormalization and therefore vary with energy scale k. Differently to the Standard Model couplings, gravitational couplings exhibit a canonical power-law running. The running of dimensionless gravitational couplings G and Λ, governed by their β-functions, can be approximated by truncated functional Renormalization Group studies [343]

$$\beta_G = 2\,G + \mathcal{A}(\Lambda)\,G^2\,, \qquad \beta_\Lambda = -2\Lambda + \mathcal{A}(\Lambda)\,G\,\Lambda + \mathcal{B}(\Lambda)G\,, \tag{2.33}$$

where $\mathcal{A}(\Lambda)$ and $\mathcal{B}(\Lambda)$ are threshold functions. Their value depend on the choice of truncation, on how to close the flow with respect to the background spacetime [344–346], on how to split the metric into background and fluctuation field [347–349], and on the choice of regulator [350]. Physically, they depend on the matter content [343] of the theory. Explicit truncated expressions including Standard-Model matter can, for instance, be found in [338, 343, 351]. Expanding $\mathcal{A}(\Lambda)$

[40] One exciting exception are purely fermionic theories in which the Grassmannian nature of n fundamental fields causes all interactions involving more than one of each such fields, i.e., interactions with $m > n$ fields, to vanish.

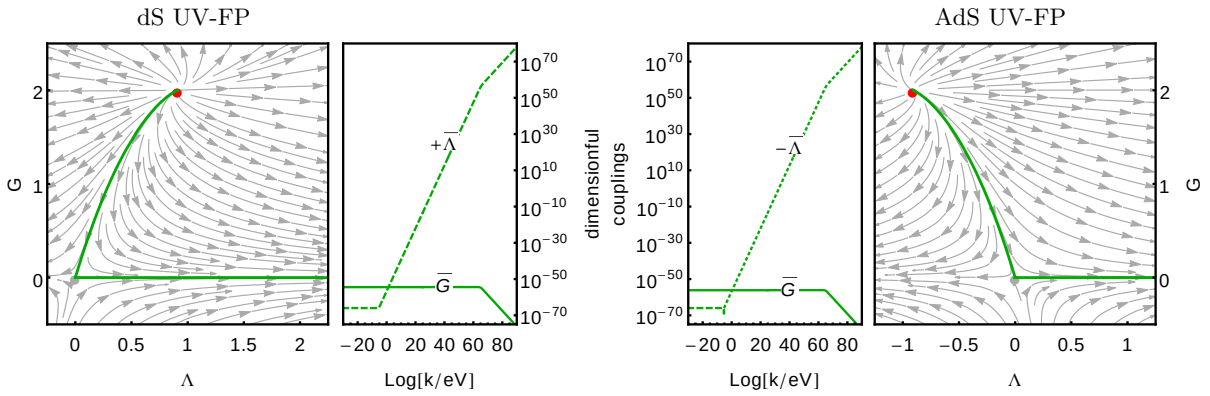

Figure 3: Stream plots (outer panels): RG-flow emanating from the gravitational UV fixed-point (red dot) in the UV-de-Sitter (left two panels, $\mathcal{N}_{\rm eff} = -1$, $\widetilde{\mathcal{N}}_{\rm eff} = 1$) and the UV-anti-de-Sitter (right two panels, $\mathcal{N}_{\rm eff} = -1$, $\widetilde{\mathcal{N}}_{\rm eff} = -1$) case. Running dimensionful couplings (inner panels): trajectories matching viable IR-values for G (continuous) and $|\Lambda|$ (dashed when positive, dotted when negative) in the infrared. These trajectories are also marked as thick green lines in the stream plots.

and $\mathcal{B}(\Lambda)$ to zeroth and first order in Λ respectively, results in the following schematic form, which is sufficient to discuss the qualitative physics, i.e.,

$$\beta_G = 2\,G + \mathcal{N}_{\rm eff}\,G^2\,, \qquad \beta_\Lambda = -2\Lambda + \widetilde{\mathcal{N}}_{\rm eff}\,G + \left(\mathcal{N}_{\rm eff} + \frac{17}{6\pi}\right) G\,\Lambda\,. \tag{2.34}$$

These exhibit a Gaussian (GFP) and a non-Gaussian (NGFP) fixed point, i.e.,

$$G^{*\rm GFP} = \Lambda^{*\rm GFP} = 0\,, \qquad \theta_1^{*\rm GFP} = 2\,,\ \theta_2^{*\rm GFP} = -2\,. \tag{2.35}$$

$$G^{*\rm NGFP} = -\frac{2}{\mathcal{N}_{\rm eff}}\,,\ \ \Lambda^{*\rm NGFP} = -\frac{6\pi\,\widetilde{\mathcal{N}}_{\rm eff}}{12\pi\,\mathcal{N}_{\rm eff} + 17}\,, \qquad \theta_1^{*\rm NGFP} = 2\,,\ \theta_2^{*\rm NGFP} = \frac{17}{3\pi\,\mathcal{N}_{\rm eff}} + 4\,. \tag{2.36}$$

$\mathcal{N}_{\rm eff}$ and $\widetilde{\mathcal{N}}_{\rm eff}$ depend crucially on the matter content of the theory, cf. [338, 343, 351–357] and Sec. 4. The asymptotic-safety scenario interprets the NGFP as a UV fixed point for quantum gravity.

Due to a topological obstruction in the flow, RG-trajectories cannot cross from positive to negative G. Therefore, $\mathcal{N}_{\rm eff} < 0$ is required to allow for trajectories connecting the UV-fixed point to viable IR-physics with positive G. The cosmological constant on the other hand can cross from de Sitter (dS), i.e., $\Lambda > 0$, to anti de Sitter (AdS), i.e., $\Lambda < 0$, and vice versa without obstruction [2]. In particular, the flow can connect a classical scaling regime with a positive cosmological constant with both a UV-de-Sitter as well as a UV-anti-de-Sitter phase.

For $\mathcal{N}_{\rm eff} = -1$ and $\widetilde{\mathcal{N}}_{\rm eff} = 1$ ($\widetilde{\mathcal{N}}_{\rm eff} = -1$), the UV-fixed point lies at positive (negative) Λ, cf. left-hand (right-hand) panel in Fig. 3. In both cases, the UV-fixed point is UV-attractive in both directions. This allows to reach the measured values of the Newton coupling and cosmological constant, i.e., $\overline{G}(k \approx 10^{-5}\,\text{eV}) \sim 10^{-57}\,\text{eV}^{-2}$ measured at laboratory scales and $\overline{\Lambda}(k \approx 10^{-33}\,\text{eV}) \sim 10^{-66}\,\text{eV}^2$ measured at Hubble scales.

Both cases exhibit three distinct scaling regimes. Beyond the Planck scale, the flow is dominated by fixed-point scaling of the NGFP for which the dimensionless couplings are constant and the dimensionful couplings scale with their canonical dimension, i.e., $\bar{G} \sim 1/k^2$ and $\bar{\Lambda} \sim k^2$. At $k \approx M_{\rm Planck}$, the flow departs from the fixed point and the Newton coupling quickly freezes out. After a rapid transition, the flow approaches the GFP and exhibits EFT scaling, i.e., both dimensionless couplings scale $\sim k^2$ and hence $\bar{G} \approx$ const. and $\bar{\Lambda} \sim k^4$. At $k_{\rm EFT} \approx 10^{-5}\,\text{eV}$, see also

[358], the flow starts to scale away from the GFP and the dimensionfull cosmological constant freezes out. In the corresponding classical scaling regime, both $\bar{G} \approx$ const. and $\bar{\Lambda} \approx$ const..

A running cosmological constant at CMB scales. Having fixed the running of G and Λ by two measurements, the RG-trajectories are uniquely fixed *at all scales*. The cosmological constant transitions between EFT and classical scaling at $k_{\rm EFT} \approx 10^{-5}\,\text{eV}$, i.e., roughly at the CMB scale of $2.725\,K = 2.36 \times 10^{-4}$ eV which could be a rephrasing of the coincidence problem [359]. Consequently, the asymptotically safe cosmological constant measured at CMB scales might differ from the one measured at Hubble scales. The scale $k_{\rm EFT} \approx 10^{-5}\,\text{eV}$ only depends on the relative order of magnitude of the gravitational fixed point values $|G^{*\rm NGFP}/\Lambda^{*\rm NGFP}|$ and not on their precise values. On the other hand, the location of the asymptotically safe NGFP impacts the eigenvectors at the GFP and thereby decides whether the cosmological constant is larger or turns negative at energy scales above the CMB scale. Cautioning that the presented RG-flow is approximate, such properties might be observable with present experimental technology.

Quadratic-gravity couplings and cosmology. Truncations of asymptotic safety including both invariants at the curvature-squared level and the corresponding quadratic-gravity couplings, cf. Eq. (1.31), have been investigated in [360–364], see Sec. 2.4.3 for truncations projecting onto a single quadratic invariant. All truncations find at least one UV-attractive direction which overlaps with the R^2-direction. This is of phenomenological significance because a large value of the R^2-coupling α at inflationary scales can drive Starobinsky inflation [130, 141]. Since α is associated with a free parameter of asymptotically safe gravity, its flow can be matched to the one that drives inflation [358]. The inclusion of the R^2-term does not affect the above conclusions.

2.4.3 Evidence for the near-canonical-scaling conjecture

The RG flow of entire functions $f(R)$, cf. [348, 365, 366][41] results in a PDE of the general form

$$f'''(R) = \mathcal{F}(f'(R), f''(R), R)\,. \tag{2.37}$$

The latter can be expanded in powers of R to recover a polynomial expansion in a tower of high-order invariants $c_n\,R^n$ [368–370]. The asymptotically safe fixed point persists at all orders and no further UV-attractve directions are introduced at any order of $R^{n>2}$ up to $n = 70$ [370]. This provides a strong a posteriori justification for the asymptotic-safety conjecture in Sec. 2.4.1 and suggests that – except for the Newton coupling G – canonical power counting still provides an ordering principle for the non-perturbative renormalization of quantum gravity.

2.4.4 Towards infinite-dimensional theory space

Extending truncations to infinite dimensions corresponds to finding global solutions to the PDE (2.37). The fixed-point solution $f_*(R)$ should be smooth and singularity-free (moveable singularity) for any $R > 0$ to define a physically meaningful fundamental action[42]. If an asymptotically

[41] See also [367] for projections on different quadratic-curvature invariants. Since these analyses evaluate the flow on a spherical background, the different quadratic-curvature invariants cannot be disentangled. While changing the operator structure on the left-hand side of the flow equation (2.5), the right-hand side thus always projects on the same structure.

[42] A discontinuous regulator as in [371] can introduce artificial discontinuities in the fixed-point solution $f_*(R)$.

safe fixed point is realized, $f_*(R>0)$ at fixed R should be determined by a finite number of free parameters only. The dimensionality of the solution of Eq. (2.37) is reduced by fixed singularities corresponding to simple poles in $\mathcal{F}$. If the number of independent fixed singularities outgrows the order of the differential equation, no global solutions exist. Whether the asymptotically safe fixed point persists in infinite-dimensional truncations, depends on the singularity structure, possible symmetry identities relating different simple poles, and the influence of the regulator and is subject of current research [372–377].

2.5 Outstanding questions in asymptotically safe gravity

Background independence and Ward identities. The derivation of the flow equation (2.5) for quantum gravity [264] requires to introduce a background metric $\bar{g}_{\mu\nu}$ with respect to which the regulator[43] and the gauge-fixing term can be defined. The metric is thus split $g_{\mu\nu} = \bar{g}_{\mu\nu} + h_{\mu\nu}$ into background and fluctuation $h_{\mu\nu}$, see [378] and [344, 379] for an alternative exponential and a geometrical metric split, respectively. The obtained RG flow remains fully background independent only if all backgrounds are treated on an equal footing. To the contrary, most results of the last Sec. 2.4 were obtained by identifying background and fluctuation fields to close the flow equation. Generalizing results to bi-metric truncations [380, 381] is a focus of current investigations [345, 382, 383]. In particluar, the dynamics of the RG flow should be driven by the fluctuation metric [384–386]. The RG-flow of Ward identities [387, 388] restores background independence for scalar fields [389], cf. [390–393] for similar efforts in quantum gravity.

Wick rotation to Lorentzian signature. Wick rotation from Euclidean to Lorentzian signature is non-trivial in quantum gravity. It depends on possible additional poles in the propagator[44] and it is unclear whether Euclidean and Lorentzian quantum gravity are related. In the ADM decomposition [394], in which Wick-rotation is better behaved, RG flows tentatively suggest that asymptotic safety persists [335–337]. See also [298, 395] for formulations of the functional RG in Lorentzian signature and [296, 297] for a flow equation of a Lorentzian Causal-Sets discretization for quantum gravity.

A link to observation. These outstanding conceptual questions are supplemented by the need for quantum-gravity phenomenology. The main difficulty in connecting quantum gravity to experiment is to find ways to overcome the scale suppression by the huge ratio $M_{\text{Planck}}/M_{\text{ew}} \sim 10^{16}$. For instance, all $R^{n>2}$-level higher-order couplings predicted by the asymptotically safe fixed point, cf. Sec. 2.4.3, are increasingly suppressed by $(M_{\text{ew}}/M_{\text{Planck}})^{2n}$ and thus unobservably tiny at experimentally accessible scales. To the contrary, marginal couplings only run logarithmically, see Fig. 1. Provided the (SM) desert conjecture holds as indicated by experiment, cf. Sec. 1, the set of marginal couplings serves as a unique kind of theoretical microscope into the quantum-gravity regime. This includes (i) the couplings of quadratic gravity, cf. Eq. (1.31), (ii) the non-minimal Higgs-curvature coupling $\xi\, H^\dagger H\, R^2$, (iii) and *all* the Standard-Model couplings. In Part II of this thesis we will investigate this unique link between the Planck and the electroweak scale. Part III will explore black holes as another potential window into quantum gravity.

[43] Integrating out modes from high to low momentum requires a background with respect to which one can define what is meant by large or small momentum. See Sec. 2.1 for approaches to define the RG flow in a background independent manner.

[44] See Sec. 1.3.1 for the related question of unitarity.

Part II
Bridging the gap: Particle physics and Planckian scale symmetry

The Standard-Model is consistent up to the Planck scale and the Higgs potential hints at Planckian scale-invariance. New physics can easily spoil this delicate balance. This is exemplified here for a Higgs-portal coupling to fermionic dark matter for which asymptotic safety might be realized without gravity. Such non-gravitational matter fixed-points should be analyzed from the perspective of effective asymptotic safety with a Planckian cutoff scale. The remaining effective predictivity is discussed for the fermionic Higgs-portal model as well as for Litim-Sannino type Standard-Model extensions.

3 Beyond the Standard Model: New physics – new problems

The experimental values of SM couplings give hints for scale symmetry at the Planck scale, cf. Sec. 1, and a natural candidate is a scale-invariant theory of quantum gravity, cf. Sec. 2. Before investigating this exciting prospect in Sec. 4 and 5, we explore two other possibilities to generate asymptotic safety, i.e., scale-invariance in the presence of quantum fluctuations, in sectors of the SM without gravity[45]. The following two examples also demonstrate the difficulty of adding predictive beyond SM physics which does not destroy the subplanckian consistency of the Standard Model.

3.1 The Higgs potential as a window into new physics

Uncertainties in the top-mass measurement and its conversion to the running Yukawa coupling significantly influence the Higgs potential. Experimental values are therefore consistent with both, a near-Planckian metastability scale or scale-invariance at $M_{\rm Planck}$ [32, 396, 397][46]. The second possibility provides a strong hint for Planckian scale symmetry [29, 34], in particular, for an asymptotically safe Standard Model (ASSM) in the presence of gravity, cf. Sec. 4 and 5. In any case, the corresponding Higgs-stability bound – and with it the validity of the SM up to Planckian or inflationary scales – is very sensitive to new physics [140, 403–407, 407–410]. Moreover, if the dark-matter puzzle, contrary to alternatives presented in Sec. 1.1.1, implies a new fundamental particle, the Higgs provides a natural portal to the dark sector, see, e.g., [411–417][47].

3.1.1 The Higgs-potential and (fermionic) dark matter

Here, we present the first evidence for an asymptotically safe fixed-point in a toy model containing an $O(N)$ scalar ϕ and N_f Dirac fermions ψ endowed with a $U(N_f)$ flavor symmetry [6]. To lowest order in power counting, fermions and bosons are coupled by a perturbatively non-renormalizable portal coupling

$$\mathcal{L}_{\rm HP} \sim \bar{\lambda}_{h\psi}\, \bar{\psi}\, \psi\, \phi\, \phi\,. \tag{3.1}$$

[45] A SM UV-completion can also be achieved by completely asymptotically free grand unification, cf. Sec. 6.

[46] Novel ATLAS [27] and CMS [28] run-II data points towards Planckian scale invariance. The significant shift in the measured top-pole mass compared to the PDG'18 world average [398] originates from the previously unheeded difference between the pole-mass and the Monte-Carlo mass. HL-LHC data [399, 400], as well as future collider [401, 402] proposals will be able to better distinguish between these two scenarios.

[47] Any form of particle dark matter (DM) can only couple to SM fields via operators like (DM-DM)(SM-SM). If only one DM or SM field were involved in the interaction, dark matter (or SM matter) would decay. Also, dark matter – by definition – is typically not charged under the SM gauge group. The lowest-dimensional operator of such type will thus always be a coupling to the scalar Higgs. In particular, a Higgs-portal to a dark scalar even provides a perturbatively renormalizable operator.

A renormalizable Yukawa coupling would violate the scalar $O(N)$ symmetry. Phenomenologically, a similar Higgs-portal coupling to uncharged fermions is a candidate for dark-matter searches. The functional-RG calculation to determine the corresponding β-functions [6] is delegated into App. B.1. We will explore a combination of the mechanisms presented in Sec. 2.3.1 and 2.3.2 to generate asymptotic safety in this model. If the asymptotically safe fixed point can be verified in extended truncations, it predicts the portal coupling in terms of the scalar quartic-coupling and the respective masses. Once established, this and similar theoretical predictions could inform experimental dark-matter searches.
We approximate the full theory space by a lowest-order derivative expansion, cf., Sec. 2.2.1, i.e., by the truncated effective action

$$\Gamma_k = \int d^dx \Big[i \sum_{j=1}^{N_f} \bar{\psi}^j (Z_\psi \not{\partial}) \psi^j + \frac{1}{2} Z_\phi \sum_{a=1}^{N} \partial_\mu \phi^a \partial^\mu \phi^a + i \sum_{j=1}^{N_f} \bar{\psi}^j \psi^j \bar{V}(\rho) + \bar{U}(\rho) \Big] , \tag{3.2}$$

where $\rho = \frac{1}{2} \sum_{a=1}^{N} \phi^a \phi^a$ is the radial scalar mode. $\bar{V}(\rho)$ and $\bar{U}(\rho)$ denote functions of the scalar field and $Z_{\phi/\psi}(k)$ denote the scalar and fermionic wave-function renormalization. This corresponds to the local-potential approximation, cf. Sec. 2.2.1 as well as, e.g., [265]. We transition to renormalized fields and dimensionless couplings/potentials by

$$\begin{aligned} &\eta_\phi = -\partial_t \ln Z_\phi \,, \quad \eta_\psi = -\partial_t \ln Z_\psi \,, \quad \widetilde{\phi} = Z_\phi^{1/2} \, \phi \,, \quad \widetilde{\psi} = Z_\psi^{1/2} \, \phi \,, \quad \widetilde{\rho} = Z_\phi \, k^{-2} \, \rho \,, \\ &U(\widetilde{\rho}) = k^{-4} \bar{U}(\rho) \,, \quad V(\widetilde{\rho}) = k^{-4} \bar{V}(\rho) \,, \end{aligned} \tag{3.3}$$

where we will drop the "$\sim$" in the following. One can expand the potentials in the symmetric (SYM) or spontaneously broken (SSB) phase, i.e.,

$$U_{\mathrm{SYM}}(\rho) = \sum_{n=1}^{N_U} \frac{\lambda_{2n}}{n!} \rho^n \,, \qquad V_{\mathrm{SYM}}(\rho) = \sum_{m=0}^{N_V} \frac{\lambda_{2m}^{(\mathrm{V})}}{m!} \rho^n \,, \tag{3.4}$$

$$U_{\mathrm{SSB}}(\rho) = \sum_{n=1}^{N_U} \frac{\lambda_{2n}}{n!} (\rho - \kappa)^n \,, \qquad V_{\mathrm{SSB}}(\rho) = \sum_{m=0}^{N_V} \frac{\lambda_{2m}^{(\mathrm{V})}}{m!} (\rho - \kappa)^n \,, \tag{3.5}$$

where κ denotes the dimensionless vacuum expectation value of the broken phase. The scalar and fermionic masses are identified with $m_\phi = \lambda_2$ and $m_\psi = \lambda_0^{(\mathrm{V})}$. λ_4 corresponds to the quartic, and $\lambda_{h\psi} = \lambda_2^{(\mathrm{V})}$ to the portal coupling. The general β-functions are presented in App. B.1. The mechanism to generate asymptotic safety in this model is manifest already at order $N_U = 2$ and $N_V = 1$ with $\eta_\phi = \eta_\psi = 0$ in the symmetric phase, for which the β functions read

$$\beta_{\lambda_{h\psi}} = \lambda_{h\psi} + \frac{3\lambda_4 \, \lambda_{h\psi}}{16\pi^2 (1+m_\phi^2)^3} + \frac{m_\psi \, \lambda_{h\psi}^2 (2 + m_\psi^2 + m_\phi^2)}{8\pi^2 (1+m_\phi^2)^2 (1+m_\psi^2)^2} \,, \tag{3.6}$$

$$\beta_{\lambda_4} = \frac{9\lambda_4^2}{16\pi^2 (1+m_\phi^2)^3} + \frac{\lambda_{h\psi}^2}{4\pi^2 (1+m_\psi^2)^2} - \frac{m_\psi^2 \, \lambda_{h\psi}^2}{\pi^2 (1+m_\psi^2)^3} \,, \tag{3.7}$$

$$\beta_{m_\psi} = -m_\psi - \frac{\lambda_{h\psi}}{32\pi^2 (1+m_\phi^2)^2} \,, \tag{3.8}$$

$$\beta_{m_\phi^2} = -2m_\phi^2 + \frac{m_\psi \lambda_{h\psi}}{4\pi^2 (1+m_\psi^2)^2} - \frac{3\lambda_4}{32\pi^2 (1+m_\phi^2)^2} \,. \tag{3.9}$$

The non-trivial denominators arise from functional RG mass-thresholds, decoupling the respective degrees of freedom at $k \approx m_i$. Setting the thresholds to one, recovers the universal 1-loop

	$m_{\psi *}$	$m^2_{\phi *}\,(\kappa^*)$	λ_{4*}	$\lambda_{h\psi *}$	η_ϕ	θ_1	θ_2	θ_3	θ_4
$\mathrm{SSB}'_{(20,1)}$	18.3	$2\cdot 10^{-3}$	129.4	-9497	0.50	12.54	3.71	1.71	-1.90
$\mathrm{SSB}_{(20,1)}$	24.8	$2\cdot 10^{-3}$	143.4	-12280	-	11.77	4.26	1.20	-0.99
$\mathrm{SYM}_{(20,1)}$	4.61	-0.45	25.3	-438	-	2.2 + i 2.1	2.2 - i 2.1	0.56	-4.70

Table 2: Fixed-point values of the masses and quartic couplings, the four leading critical exponents in the local potential approximation (LPA) of the symmetric and symmetry-broken expansion, $\mathrm{SYM}_{(20,1)}$ and $\mathrm{SSB}_{(20,1)}$ respectively, as well as the improved local-potential approximation (LPA') in the symmetry-broken parameterization, i.e., $\mathrm{SYM}'_{(20,1)}$, where we also give the scalar anomalous dimension η_ϕ, see also App. B.2.

result for β_{λ_4}[48].

Generating asymptotic safety. The asymptotic-safety mechanism in this scalar-fermion portal model combines those of Sec. 2.3.1 and 2.3.2. The running of the marginal quartic in β_{λ_4}, cf., Eq. (3.7), receives contributions from bosonic (first term) and fermionic (second and third term) quantum fluctuations. For large fermionic mass $|m_\psi| > 1/3$, these fluctuations have opposite sign. Hence, they can balance to generate a non-trivial zero in β_{λ_4}. The masses as well as the portal coupling are not marginal and already run classically, see the respective first terms in Eqs. (3.6), (3.8), and (3.9). The respective canonical dimensions can balance against quantum fluctuations if the couplings are sufficiently non-perturbative and $\lambda_{h\psi} < 0$.

Convergence properties. The fixed point arising in the lowest non-trivial order in the symmetric expansion, i.e., $\mathrm{SYM}_{(2,1)}$, has three UV-attractive and one IR-attractive direction. Here, the first and second index denote the order N_U of the expansion of U and the order N_V of the expansion of V. At the fixed point, $m^2_\phi < 0$ which signals a symmetry-broken regime. Indeed the same fixed point can be obtained in the symmetry-broken expansion $\mathrm{SSB}_{(2,1)}$, in which its vacuum expectation value is positive, i.e., $\kappa > 0$. This is expected since the fixed point realizes a symmetry-broken phase. In both expansions of the potential $U(\rho)$, the fixed point can be tracked to high order N_U. Tab. 2 lists the fixed-point values for λ_4, $\lambda_{h\psi}$, m_ψ, and m^2_ϕ (or equivalently κ in the SSB expansion) as well as the four most relevant critical exponents at $N_U = 20$. All other critical exponents remain IR-attractive at each order in N_U.
In the SYM expansion, fixed-point values and critical exponents converge very fast, cf. Fig. 35 in App. B.2. In the SSB expansion, convergence is less fast, cf. Fig. 34 in App. B.2. In particular, the UV-attractive critical exponents drift to larger positive values and converge only very slowly. Nevertheless, no further UV-attractive direction arises. At first sight, this is unexpected. Since the fixed point lies in the symmetry-broken regime, one expects better convergence when expanding around a non-trivial vacuum expectation value. We point out that while the scalar fixed-point potential U_* is clearly in the symmetry-broken phase, the same need not be true for the portal fixed-point potential V_*. The slow convergence might signal that the symmetry-broken parameterization does not capture the properties of V_*. More definite statements about the convergence and existence of the fixed point thus require to explore larger truncations in the fermionic sector. In particular, this includes four-fermion interactions dressed by further scalar potentials.

Phenomenological implications. For an effective field theory without a fixed point, the two masses (m_ϕ and m_ψ) and the two couplings (λ_4 and $\lambda_{h\psi}$) all correspond to free parameters. To

[48] The other couplings are dimensionful and thus scheme dependent.

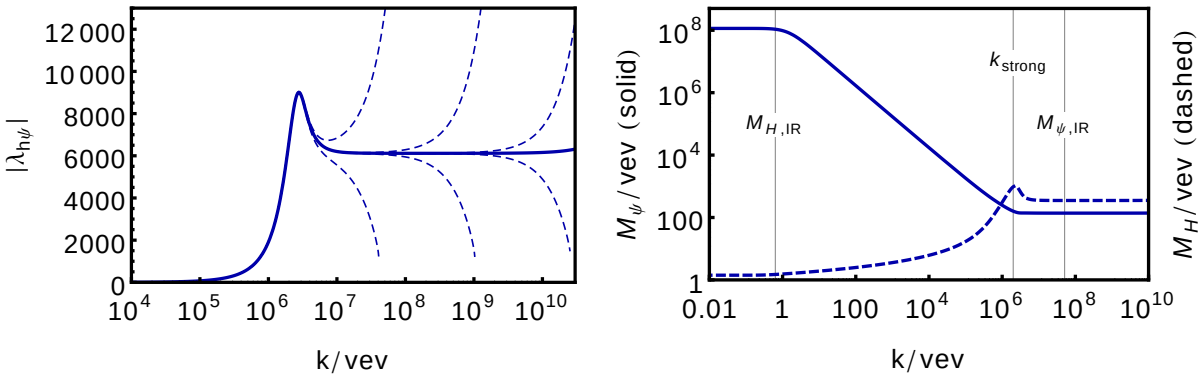

Figure 4: Left-hand panel: RG evolution of the portal coupling $\lambda_{h\psi}$ from $k_{\rm UV} = 10^{10}$ vev down to the IR $k_{\rm UV} = 10^4$ vev. All values at $k_{\rm UV}$ within the plotted range (and beyond) are attracted to a very narrow IR window. This effectively predicts $\lambda_{h\psi,\rm IR}$. The relevant couplings are chose such that $\text{vev}^2 = 2\kappa_{\rm IR} = 0.2$, $M_{H,\rm IR}/\text{vev} = 1.44$ and $M_{\psi,\rm IR}/\text{vev} = 1.13 \times 10^8$.
Right-hand panel: Running physical masses $M_H/\text{vev}(k)$ (dashed) and $M_\psi/\text{vev}(k)$ (solid) on the same RG trajectory. Above $M_{\psi,\rm IR}$, the flow is dominated by the asymptotically safe fixed point. At $M_{\psi,\rm IR}$, the dark fermions decouple dynamically and the flow departs from the fixed point. Below $M_{H,\rm IR}$, the bosonic degree of freedom decouples as well and the flow enters the IR-scaling regime in which all masses freeze out.

the contrary, the asymptotically safe fixed point features only three UV-attractive directions. The critical hypersurface of all admissible IR is therefore only three-dimensional. Consequently, asymptotic safety predicts a relation amongst the four couplings, e.g., $\lambda_{h\psi}(m_\phi, m_\psi, \lambda_4)$. Interpreting the scalar sector as the SM Higgs sector, its mass m_ϕ and quartic coupling λ_4 are fixed by the electroweak vacuum expectation (vev) value and the Higgs mass M_H, respectively. This implies a – possibly complicated but fixed – relation $\lambda_{h\psi}(m_\psi)$ between the portal coupling and the dark-fermion mass.

Despite the neglected SM gauge structure, the present model (for $N_f = N = 1$) closely resembles a single dark fermion coupled to the SM Higgs. For $N = 1$ there are no remaining scalar Goldstone modes and below $k_{\rm IR} < \max\left(M_{\phi,\rm IR}, M_{\psi,\rm IR}\right)$ the RG flow freezes out completely[49].

We demonstrate the predictive power for the lowest non-trivial truncation order, cf. Eqs. (3.6)-(3.8), and in the symmetry-broken phase. The three free UV-initial conditions at some high scale $k_{\rm UV}$ are chosen such that $\text{vev}^2 = 2\bar{\kappa}(k \to 0) = 0.2$, $M_{H,\rm IR}/\text{vev} = \sqrt{\lambda_4}(k \to 0) = 1.44$ and $M_{\psi,\rm IR}/\text{vev} = \bar{m}_\psi/\sqrt{2\bar{\kappa}}(k \to 0) = 1.13 \times 10^8$ after complete freezeout. The first identification simply sets the units in which dimensionful quantities are measured. Here, we choose to measure everything in units of the vev. The right-hand panel in Fig. 4 shows the freezeout of the two masses after the RG flow has dropped below all thresholds. The left-hand panel of Fig. 4 shows explicitly that the low-energy value of $\lambda_{h\psi}$ is determined by the asymptotically safe scaling regime.

When interpreting the asymptotically safe fixed point as fundamental, i.e., removing the cutoff $k_{\rm UV} \to \infty$, the prediction becomes exact. In any asymptotic-safety scenario not including gravity, we strongly advocate the perspective of effective asymptotic safety instead, since pushing the cutoff beyond $M_{\rm Planck}$ is meaningless. Hence, we initialize the flow in a large range of $\lambda_{h\psi}(k_{\rm UV})$ values at some high but subplanckian $k_{\rm UV}$. In the present model, the degree of effective predictivity is very high because the corresponding critical exponent is $\mathcal{O}(1)$. As a result, the IR-attractive direction of the asymptotically safe fixed point maps a large window of UV-values

[49] In the Standard Model one would remain with a perturbative running due to the massless photon, and above $\Lambda_{\rm QCD}$ also with massless gluons.

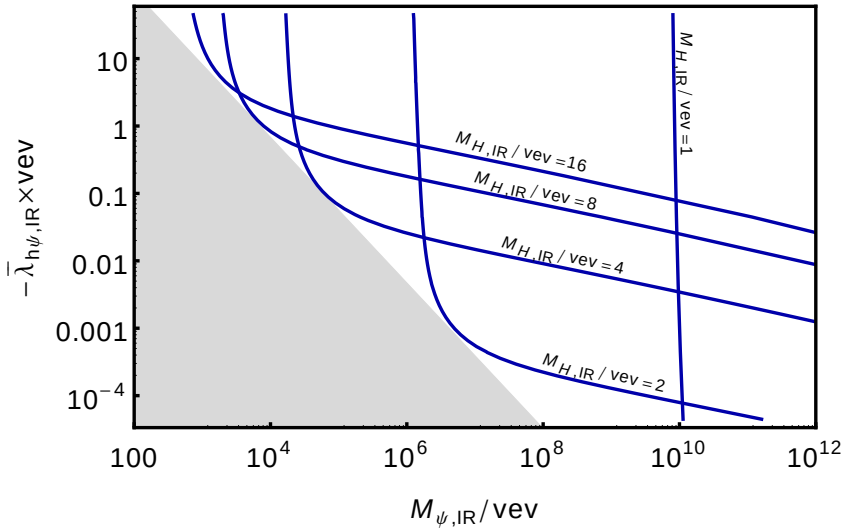

Figure 5: Relation between the Higgs-portal coupling $\bar{\lambda}_{h\psi,\mathrm{IR}}\mathrm{vev}$ and the dark-fermion mass $M_{\psi,\mathrm{IR}}/\mathrm{vev}$ implied by effective asymptotic safety. All dimensionfull quantities are measured in units of the VEV which we fix to $\mathrm{vev}^2 = 2\kappa_{\mathrm{IR}} = 0.2$. We show cases for different scalar masses $M_{H,\mathrm{IR}}/\mathrm{vev}$. The gray-shaded region at small coupling and small dark-fermion mass cannot be reached within the present truncation.

to an extremely narrow IR-window, cf. left-hand panel in Fig. 4. Effective asymptotic safety can hardly be distinguished from fundamental asymptotic safety.
In Fig. 5, we vary the fermion mass $M_{\psi,\mathrm{IR}}$ to obtain a relation between the two phenomenologically unknown parameters $\lambda_{h\psi}$ and $M_{\psi,\mathrm{IR}}$ and obtain a rather robust conclusion. *The asymptotically safe fixed point of the scalar-fermion system predicts that fermionic dark matter cannot be weakly coupled and light at the same time.* Once the asymptotically safe fixed point is more rigorously established, such conclusions can serve as a guidance principle for model building and experimental searches.

3.1.2 Fermionic dark matter and the Standard-Model Higgs potential

The asymptotically safe fixed point of the above scalar-fermion portal model requires strong dynamics and future studies are required to establish its existence. From a more conservative viewpoint, any departure from the perturbative regime can be interpreted as a signal for the onset of unknown new physics that is out of reach of the EFT of the presently considered degrees of freedom. The region of validity of an EFT can be defined as the parameter space in which all dimensionless combinations of the EFT couplings remain perturbatively small. For the above portal model, this requires[50] that the scalar quartic coupling $\lambda_H < 4\pi$, and that the dimensionless combination of fermion mass and portal coupling $\bar{\lambda}_{h\psi}\,\bar{m}_\psi < 4\pi$. This defines an EFT cutoff scale. For the SM, as discussed in Sec. 1.1.1, it lies at transplanckian values, i.e., $\Lambda_{\mathrm{EFT}}^{(\mathrm{SM})} \approx 10^{41}\ \mathrm{GeV} \gg M_{\mathrm{Planck}}$.
A second possibly problematic scale can arise from the Standard Model Higgs potential. If the latter develops a second high-energy vacuum expectation value (VEV), the electroweak-scale vacuum could be metastable and might decay [29, 31, 397, 405, 418–420]. In the perturbative picture, such a second VEV develops due to a zero-crossing in the running of the quartic coupling

[50] The exact value of 4π is somewhat arbitrary. But, unless there exists a fixed point just outside the thereby defined EFT, any $\mathcal{O}(1)$ number will lead to similar conclusions.

λ_H. Due to large experimental uncertainties in the top-mass measurement, it remains unclear whether the Standard Model develops a subplanckian metastability scale, cf. Sec. 1.1.1 and the discussion at the beginning of Sec. 3.1. Assuming a metastability scale, we extend the above Higgs-portal model by a Yukawa coupling (again dressed with a scalar potential) and a fiducial gauge sector to mimic the running SM gauge couplings, see [405] and App. B.3 for the explicit definition and derivation of the corresponding running. This fiducial SM develops a meta-stability scale at $\Lambda_{\text{meta}}^{(\text{SM})} = 2.54 \times 10^9$ GeV. The following consideration is independent of the exact location of the subplanckian metastability scale. In combination with the EFT cutoff scale, it defines the scale at which new physics is expected, i.e.,

$$\Lambda_{\text{new-phys}}^{(\text{SM})} = \text{Min}\left(\Lambda_{\text{meta}}^{(\text{SM})}, \Lambda_{\text{EFT}}^{(\text{SM})}\right) . \tag{3.10}$$

If the metastability scale actually exists, it is desireable to find new-physics models, for instance for dark matter, which stabilize the Higgs potential. It is well-established that an additional scalar field, accounting for dark matter via a thermal freezeout [412, 421–424], can also shift the metastability scale to higher energies via its Higgs-portal coupling [411–414, 417, 422].

Fermionic dark matter can stabilize the Higgs potential. As can be seen in Eq. (3.7), fermionic dark matter has the right structure to similarly delay the onset of metastability. While it is well-known that marginal Yukawa couplings to fermions destabilize the corresponding scalar quartic coupling, the same does not hold for the higher-order portal coupling $\lambda_{h\psi}$. In the threshold regime at scales $k \approx \bar{m}_\psi$, i.e., for $m_\psi = \bar{m}_\psi/k < 1/3$, the contributions of $\lambda_{h\psi}$ are positive, cf. Eq. (3.7). Hence, they can stabilize the quartic coupling. The different effect of marginal Yukawa-type fluctuations compared to perturbatively non-renormalizable portal-type fluctuations can be attributed to their distinct symmetry structure. While Yukawa interactions break the discrete scalar symmetry $\phi \to -\phi$, portal interactions do not. The extensive functional RG study in [4], see also App. B, confirms the following simple intuition:

- Decoupling: $\bar{m}_\psi \gg \Lambda_{\text{meta}}^{(\text{SM})}$. If the fermionic dark matter is too heavy, it has already decoupled and cannot affect the metastability scale.
- Destabilizing: $\bar{m}_\psi \approx \Lambda_{\text{meta}}^{(\text{SM})}$. If the dark fermion's mass is close to the metastability scale, it destabilizes the scalar potential further.
- Stabilizing: $\bar{m}_\psi \ll \Lambda_{\text{meta}}^{(\text{SM})}$. Fermionic Higgs-portal dark matter with a mass below the metastability scale can stabilize the Higgs-potential.

While the stabilizing effect is very desirable, the non-perturbative nature of the portal coupling $\bar{\lambda}_{h\psi}$ can quickly overstabilize the scalar potential. Its dimensionless counterpart $\lambda_{h\psi}$ grows with a power-law behavior towards larger energies. As it outgrows $\mathcal{O}(1)$ values, it generates a novel Landau-pole like divergence in the scalar potential. The non-perturbative analysis in [4] confirms that portal couplings $\bar{\lambda}_{h\psi} > 1/\Lambda_{\text{meta}}^{(\text{SM})}$ lead to a scalar Landau pole below the former metastability scale such that the overall regime of validity of the EFT cannot be extended.

A numerical investigation of how far the EFT-regime can be extended due to fermionic portal dark-matter with mass $\bar{m}_\psi$ and portal coupling $\lambda_{h\psi}$ is presented in Fig. 6. It confirms that fermionic dark matter with a mass $\bar{m}_\psi \approx \Lambda_{\text{meta}}^{(\text{SM})} = 2.54 \times 10^9$ GeV destabilizes the Higgs-potential further (red region). The upper-right gray-shaded triangle lies outside of the EFT bound $\bar{\lambda}_{h\psi}\, \bar{m}_\psi < 4\pi$. In the left-hand gray-shaded triangle, fermionic dark matter is coupled too strongly to the scalar sector and causes a new Landau-pole like divergence. Correspondingly, the

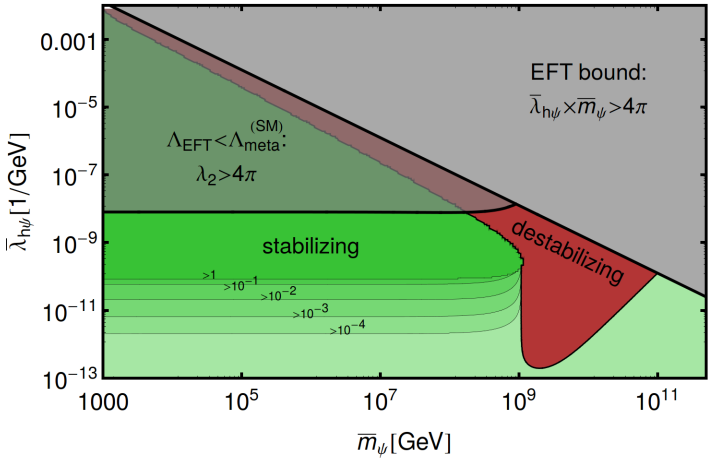

Figure 6: Regions in the parameter space of dark matter mass $\bar{m}_\psi$ and portal coupling $\bar{\lambda}_{h\psi}$, in which the Higgs potential is (de)stabilized. In the green (red) region the Higgs stability-bound is shifted to larger (smaller) values. The thin contours show the relative increase of the metastability scale, i.e., $(\Lambda_{\rm meta}^{\rm (fdmSM)}-\Lambda_{\rm meta}^{\rm (SM)})/\Lambda_{\rm meta}^{\rm (SM)}$. The shaded regions indicate where a perturbative EFT description, either in the fermionic sector or in the scalar sector breaks down.

EFT breaks down below the SM metastability scale, i.e., $\Lambda_{\rm EFT}^{\rm (fdmSM)} < \Lambda_{\rm meta}^{\rm (SM)}$. In all these three regions, either strong dynamics or additional new physics is required to extend the Standard Model beyond $\Lambda_{\rm meta}^{\rm (SM)}$. Only comparatively light, i.e., $\bar{m}_\psi \ll \Lambda_{\rm meta}^{\rm (SM)}$, and weakly coupled, i.e., $\bar{\lambda}_{h\psi} > 1/\Lambda_{\rm meta}^{\rm (SM)}$, fermionic dark matter (green region in Fig. 6) can slightly increase the metastability scale without introducing new divergences. Even in the latter case, similar to higher-order couplings in the scalar potential itself [403, 405, 406, 408, 425–429], the fermionic Higgs-portal coupling can only delay the onset of the metastability scale by one or two orders of magnitude.

Relic-density constraints. Assuming that the fermionic dark matter is produced by a thermal freeze-out after inflation, its Higgs-portal coupling connects to its relic abundance. The larger the portal coupling $\bar{\lambda}_{h\psi}$, the more dark matter decays into visible matter and vice versa. A very small portal coupling thus leads to an overabundance of dark matter in the early universe and prohibits a viable cosmological evolution. Perturbative studies place this relic-density bound for fermionic Higgs-portal dark matter at $\bar{\lambda}_{h\psi} < 10^{-3}$ GeV^{-1}, see, e.g., [430]. Under the assumption that non-perturbative effects do not qualitatively alter this conclusion, the relic-density bound is in stark conflict with the present study of Higgs stability. On its own, fermionic dark matter coupled via a Higgs-portal would either overclose the universe or destabilize the Standard Model at energies far below the Planck scale and even below a possible metastability scale.
This conclusion persists even if the SM itself does not develop a subplanckian metastability scale. It exemplifies that the validity of the SM up to the Planck scale is a very subtle balance. Demanding that this balance is not broken by new physics, i.e., that new degrees of freedom preserve the possibility of a transplanckian cutoff scale, severely constrains the admissible form of new degrees of freedom. In the present example, fermionic dark matter has to either develop a strongly coupled fixed point as tentatively suggested by the functional RG study in Sec. 3.1.1, or inevitably requires a larger subplanckian dark sector.

3.2 Asymptotic safety at a large number of degrees of freedom

In this section, we investigate the only known perturbative example of four-dimensional asymptotic safety without gravity. The corresponding Litim-Sannino fixed point [309] in gauge-Yukawa theories at a large number of fermions and gauge bosons has been introduced in Sec. 2.3 as an example for scale invariance due to a balance of different perturbative loop orders. Its possible phenomenological consequences have been studied in [431, 432][51]. Here, we emphasize two crucial points. Firstly, we investigate if Litim-Sannino fixed points can persist in the presence of gravitational contributions, see Sec. 3.2.1. Secondly, we will explore these fixed points as possible intermediate fixed points which might dominate the running between the Planck and the electroweak scale in Sec. 3.2.2. This example will also further elucidate the concept of effective asymptotic safety.

3.2.1 Litim-Sannino fixed points and gravitational corrections

The Litim-Sannino fixed points of an $SU(N_C)$ gauge-Yukawa theory are perturbatively controlled by an arbitrarily small parameter $\epsilon = N_F/N_C - 11/2$ (Veneziano limit [320]) where N_F is the number of vector-like fermions, cf. [309]. For the rescaled gauge and Yukawa coupling $\tilde{\alpha}_g = \frac{N_C\, g^2}{(4\pi)^2}$ and $\tilde{\alpha}_y = \frac{N_C\, g^2}{(4\pi)^2}$ a fixed point is achieved by a balance of different loop-orders, cf. Sec. 2.3.3 for a detailed explanation of the fixed point mechanism[52]. Working at next-to-leading order, the pure gauge-Yukawa fixed point arises at $\tilde{\alpha}_{g\,*} = \mathcal{O}(\epsilon)$ and $\tilde{\alpha}_{y\,*} = \mathcal{O}(\epsilon)$ with one IR-attractive direction with critical exponent $\theta_1 = \mathcal{O}(\epsilon)$ and one UV-attractive direction with critical exponent $\theta_2 = \mathcal{O}(\epsilon^2)$. It can thus be expected that any additional $\mathcal{O}(\epsilon)$ contribution potentially alters the corresponding fixed-point structure. Here, we will investigate under which conditions such a fixed point persists under the inclusion of subplanckian gravitational contibutions, cf. [10]. This will allow to estimate the highest scale $k < M_{\text{Planck}}$ at which it is still viable to neglect gravitational fluctuations.

Below M_{Planck}, we can approximate the leading-order gravitational contributions to be proportional to the Newton coupling $\overline{G}$, while all other gravitational couplings are approximated to vanish. In the classical regime, the dimensionful $\overline{G}$ is still constant. Hence, the dimensionless Newton coupling runs quadratically with energy scale k, i.e.,

$$G = \overline{G}\, k^2 = \frac{k^2}{8\pi\, M_{\text{Planck}}^2}\,. \tag{3.11}$$

Including the respective gravitational contributions $\tilde{\alpha}_g\, f_g(G)$ and $\tilde{\alpha}_y\, f_y(G)$ to the running of $\tilde{\alpha}_g$

[51] The relation to possible large-N_F fixed-points at a finite number of gauge bosons, cf. [327] for a recent review, remains uncertain. Given the phenomenological interest [433–440], one should keep in mind that such fixed points arise very close to a pole in the $1/N_F$ expansion (where N_F is the number of fermions). This entails huge anomalous dimensions and even though couplings might remain arbitrarily small, the huge shift towards relevance in the critical exponents signals an extremely large degree of non-perturbativity. This casts doubt on the stability of such fixed points under possible additional poles at higher-order in $1/N_F$, cf. also [441–443]. For a recent summary see also the respective sections in [444].

[52] We do not discuss the respective extension of this fixed point to the scalar quartic couplings, cf. Sec. [309], as the main fixed-point mechanism resides in the gauge-Yukawa sector. While scalar quartic couplings and their stability are crucial for phenomenological viability, the question whether the fixed point persists under gravitational fluctuations remains unaltered.

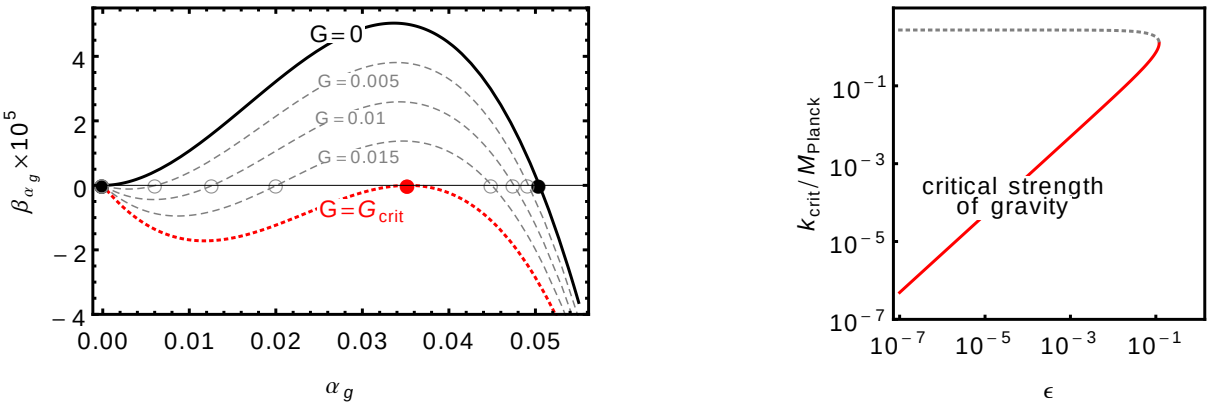

Figure 7: Left-hand panel: β-function and fixed points of the Litim-Sannino gauge coupling $\tilde{\alpha}_g$ for $\epsilon = 0.1$ and different values of the dimensionless Newton coupling G. Right-hand panel: critical scale $k_{\rm crit}/M_{\rm Planck}$ above which the Litim-Sannino fixed point annihilates due to gravitational fluctuations (red line). Its reappearance above the gray dashed line is considered an artifact of the truncation, see main text.

and $\tilde{\alpha}_y$ in [309], we find

$$\beta_{\tilde{\alpha}_g} = \tilde{\alpha}_g \left[C\tilde{\alpha}_g^2 + B\tilde{\alpha}_g - f_g(G) \right] \quad \text{with} \quad C = \left(25 + \frac{26}{3}\epsilon\right), \quad B = \frac{4}{3}\epsilon - 2\left(\frac{11}{2} + \epsilon\right)^2 \tilde{\alpha}_y \,, \tag{3.12}$$

$$\beta_{\tilde{\alpha}_y} = \tilde{\alpha}_y \left[E\tilde{\alpha}_y - F\tilde{\alpha}_g - f_y(G) \right] \quad \text{with} \quad E = (13 + 2\epsilon) \,, \quad F = 6 \,. \tag{3.13}$$

The gravitational contributions are not suppressed by the limit of large N_C and N_F because they act like an anomalous dimension[53]. We determine the contributions $f_g(G)$ and $f_y(G)$ within a functional RG scheme specified in Sec. 4 and App. C[54]. The explicit contributions read

$$f_g(G) = \frac{G}{2\pi} \,, \qquad f_y(G) = -\frac{17\,G}{10\pi} \,. \tag{3.14}$$

Anticipating results in Sec. 4, we note that an $\mathcal{O}(1)$ cosmological constant can potentially flip the sign of $f_y(G)$. The cosmological constant evolves like k^4 in the subplanckian regime, cf. Sec. 2.4.2. It can thus safely be neglected in the regime of interest, i.e., for $k < M_{\rm Planck}$.
As long as $\tilde{\alpha}_{g\,*} > f_y/F$ holds, the Yukawa coupling $\tilde{\alpha}_y$ will always have a positive fixed point. We verify this assumption a posteriori in the following results. Inserting the solution back into $\beta_{\tilde{\alpha}_g}$ in Eq. (3.12), we find that in the perturbative regime of interest, i.e., for $0 < \epsilon < 1$ and $0 < G < 1$, the coefficients of $\tilde{\alpha}_g$, $\tilde{\alpha}_g^2$, and $\tilde{\alpha}_g^3$ are always negative, positive, and negative respectively. Without gravity the gauge coupling exhibits a Gaußian IR-attractive fixed point at $\tilde{\alpha}_{g\,*}^{\rm GFP} = 0$ and the UV-attractive Litim-Sannino fixed point at $\tilde{\alpha}_{g\,*}^{\rm LS} \neq 0$ (cf., black-filled circles in the left-hand panel of Fig. 7). The gravitational contributions split the former into a non-vanishing IR-attractive fixed point at $\tilde{\alpha}_{g\,*}^{\rm sGFP}$ and a – now UV-attractive – Gaußian fixed point $\tilde{\alpha}_{g\,*}^{\rm GFP} = 0$ (cf., gray-empty circles in the left-hand panel of Fig. 7). For $\epsilon \lesssim 0.12$, the two fixed points $\tilde{\alpha}_{g\,*}^{\rm sGFP}$ and $\tilde{\alpha}_{g\,*}^{\rm LS} \neq 0$ approach each other, cf. Fig. 7, and annihilate at a critical $G_{\rm crit}(\epsilon)$ (cf., red-filled circle in the left-hand panel of Fig. 7). At even larger $G \sim \mathcal{O}(1)$, the two fixed points reappear. Such values of G lie close to the Planck scale where it becomes questionable whether backreaction and high-order couplings can still be neglected. The reappearance might thus be an artifact of the present

[53] Rescaling $\alpha \to \alpha \times \text{const}$ in $k\,\partial_k \alpha_i = \beta_{\alpha_i} = \alpha\, f_i + \ldots$ only affects terms which scale non-linearly in α.

[54] Scheme dependence and the relation to perturbative schemes is explicitly discussed in Sec. 4.5.4. For definiteness, we work with a gravitational de-Donder type gauge fixing with $\beta = 1$ and $\alpha \to 0$, cf. [10, App.A] for the gauge-dependent contributions.

approximation[55].
Using Eq. (3.11) to convert the critical value of G into a scale, we infer that the regime in which gravitational fluctuations can safely be neglected when analyzing Litim-Sannino fixed points extends to scales

$$k_{\text{crit}} \approx \frac{M_{\text{Planck}}}{8\pi}\,\epsilon\,. \tag{3.15}$$

The right-hand panel of Fig. 7 confirms this approximation in the full result. The smaller ϵ, i.e., the more perturbative the Litim-Sannino fixed-point structure is, the more sensitively it reacts to gravitational corrections. To conclude, Litim-Sannino type fixed-points should be regarded as realizing effective asymptotic safety at subplanckian scales. In the following section, we will investigate the remaining effective predictive power of the Litim-Sannino scenario.

3.2.2 Effective asymptotic safety and predictivity for Litim-Sannino models

The analysis of the last section demonstrates that it is questionable to interpret any form of asymptotic safety which does not encompass gravitational degrees of freedom as fundamental. The phenomenology of such asymptotically safe extensions of the Standard Model should thus be discussed in the framework of effective field theory (EFT) below a high energy cutoff $\Lambda_{\text{EFT}} < M_{\text{Planck}}$. This correctly captures our ignorance of UV-physics above that scale[56].
Effective asymptotic safety can still retain a significant amount of predictivity along its IR-attractive directions, cf. Sec. 3.1.1. Along the latter, the RG flow can focus a large range of coupling values in the UV to a much smaller range in the IR. The amount of predictivity depends on (i) how strongly the IR-attractive directions are pulled towards the fixed point, i.e., how large the negative critical exponents are, and on (ii) over how many scales the flow remains in the vicinity of the fixed point. The latter depends on the number of scales over which the EFT is valid. This includes how strongly the fixed point repels the IR-repulsive directions[57].

Predictivity of Litim-Sannino models. Turning to the Litim-Sannino models of the previous section, cf. Eqs. (3.12)-(3.13), we evolve the flow over 17 orders of magnitude to represent the running from the Planck down to the electroweak scale. The flow of $\tilde{\alpha}_g$ and $\tilde{\alpha}_y$ is initialized at arbitrary points in an ellipse with major axes $[0, 2\,\tilde{\alpha}_{g\,*}]$ and $[0, 2\,\tilde{\alpha}_{y\,*}]$ and are (de-) focused along the IR-attractive (IR-repulsive) direction. The four right-hand panels in Fig. 34 visualize explicit examples of this (de-) focusing for different values of ϵ. The black diagonal marks the linearized critical hypersurface. All points are attracted to this surface towards the IR. At the same time, each point is repelled by the fixed point along the direction within the critical hypersurface. The relative size of the final area, in comparison to the initial area, provides a measure for the predictivity of the Litim-Sannino fixed point. The overall area shrinks as long as the

[55] For $\epsilon \gtrsim 0.12$, no annihilation takes place and no bound can be inferred. On the other hand, it is unclear whether at these values (i) the Litim-Sannino fixed point is still perturbatively controlled, and (ii) backreaction effects of the gravity-matter system can be neglected, cf. Sec. 4. Certainly, the present analysis is insufficient to conclude anything about this regime.

[56] Even when gravitational degrees of freedom are included, this EFT view on non-perturbative fixed points remains the most conservative notion of asymptotic safety. We will come back to this in Sec. 5.

[57] Without knowledge of the underlying UV physics, it is, of course, hard to assume anything about how initial conditions should be distributed around the fixed point. It might well be that unknown microscopic physics places the effective theory very close to the fixed point in all IR-repulsive directions, in which case the flow remains close to the fixed point and predictivity is maximal. Statements about predictivity thus always remain relative statements.

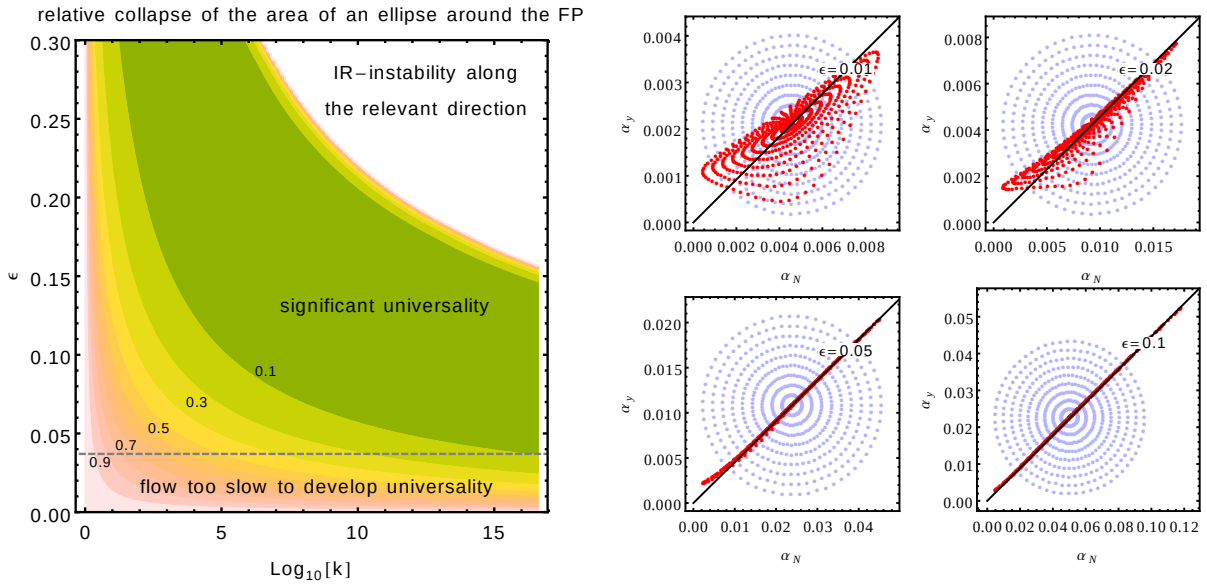

Figure 8: Left-hand panel: Degree of universality imprinted by the asymptotically safe fixed point of simple gauge-Yukawa models, cf. Eqs. (3.12)-(3.13) (measured by the relative collapse of the area of an ellipse around the fixed point) when flowing towards the IR over k scales.
Right-hand panel: Examples of collapsed shells from some UV-scale (light blue) to some IR-scale 17 orders of magnitude lower (dark red) for four different values of ϵ.

flow along the IR-attractive with critical exponent $\theta_1 = \mathcal{O}(\epsilon)$ is stronger than the one along the IR-repulsive direction with critical exponent $\theta_2 = \mathcal{O}(\epsilon^2)$. The left-hand panel in Fig. 34 depicts how the degree of predictivity depends on both the perturbative control parameter ϵ and the orders of magnitude over which the asymptotically safe fixed point dominates the EFT. If ϵ is too small, the flow is not strong enough to develop a significant degree of universality during the finite separation of scales. If ϵ is too large, the flow develops an IR instability along the IR-repulsive direction.

Simple Litim-Sannino-type extensions of the Standard Model. We further investigate the predictivity of effective asymptotic safety for phenomenologically relevant Litim-Sannino extensions of the Standard Model gauge group. We restrict the study to cases in which the gauge sector of the Standard Model is not modified. Following [431], we couple $i = 1, \ldots, N_f$ additional vector-like fermions ψ_i transforming in the representation R_2 under the Standard Model SU(2) gauge group to facilitate an asymptotically safe fixed point. To demonstrate our point, it is sufficient to focus on those cases in which the ψ's are colorless (i.e., do not transform nuder the SU(3)) and uncharged under the $U(1)$. Further, an uncharged complex scalar field allows for BSM Yukawa couplings

$$\mathcal{L}_{\text{BSM}} = -y \,\text{tr}\left[\bar{\psi}_L \, S \, \psi_R + \bar{\psi}_R \, S^\dagger \, \psi_L\right] . \tag{3.16}$$

The respective β-functions are given in [431, 445]. In [445], a systematic search for N_f copies of R_2 representations reveals four cases which are perturbatively well-controlled:

$$\begin{aligned} &\text{Model A:} \quad (N_f, R_2) = (1,3) , && \text{Model B:} \quad (N_f, R_2) = (1,2) , \\ &\text{Model C:} \quad (N_f, R_2) = (2,2) , && \text{Model D:} \quad (N_f, R_2) = (3,2) , \end{aligned} \tag{3.17}$$

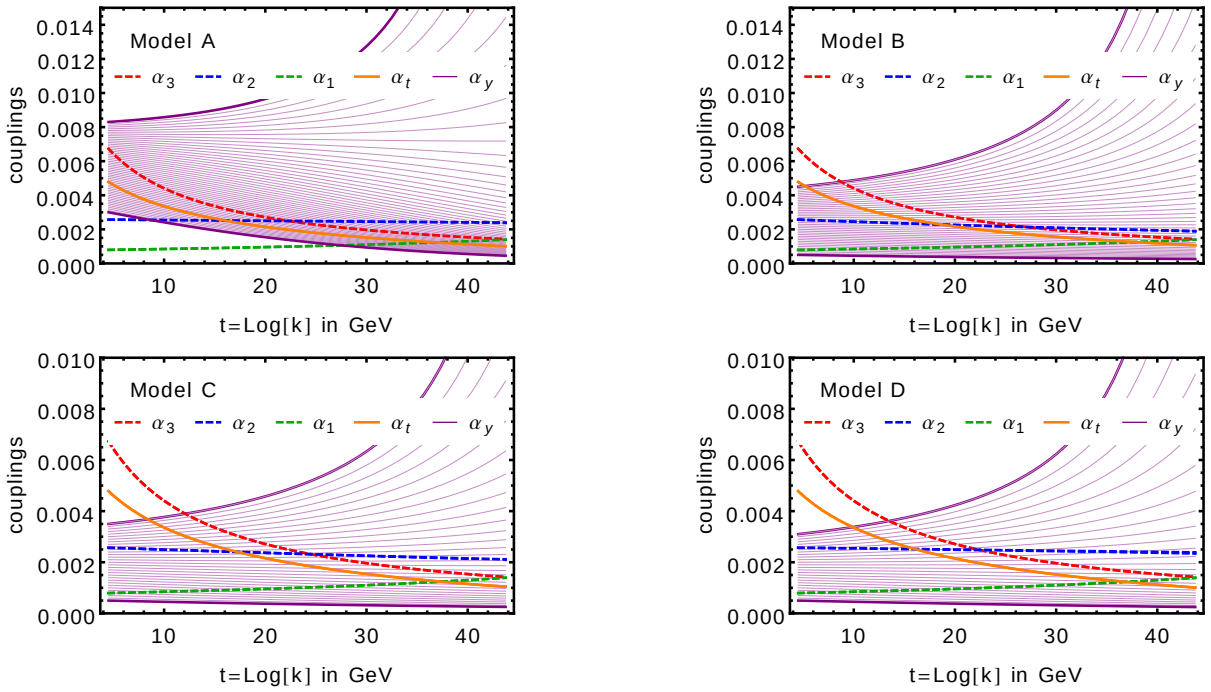

Figure 9: Running of the SM couplings $(\alpha_3, \alpha_2, \alpha_1, \alpha_t)$ supplemented by the BSM Yukawa coupling α_y. The four SM couplings are initialized at their measured low-energy values $(0.000795, 0.00257, 0.00673, 0.00478)$ at the matching scale of 91 GeV, while the BSM Yukawa coupling is varied over a wide range of UV-values. Like the Standard Model, all four identified BSM models can be extended up to M_{Planck} and hence serve as effective field theories. The asymptotically safe fixed point significantly focusses the BSM coupling and predicts its value to lie within the indicated (purple) regime of trajectories.

cf. Tab. IV in [445]. The authors of [445] discard all four of these because the U(1) Landau-pole cannot be cured. While this conclusion is correct concerning fundamental asymptotic safety, the Landau pole remains safely beyond the Planck scale and can thus be considered as outside of the regime of validity of the EFT anyhow. Instead, one should consider these fixed points as examples of effective asymptotic safety. Fig. 9 clearly shows that in all four cases the Landau pole is merely a theoretical issue and not of any relevance for effective asymptotic safety below the Planck scale. Moreover, the BSM Yukawa coupling α_y is significantly focused from the full perturbative regime to a smaller window in the IR. This focusing can be considered as an effective prediction by the respective Litim-Sannino type fixed point. The IR window can thereby guide experimental searches for the Yukawa coupling of this particular BSM model.

Conclusion

New physics which is added to the SM can introduce new divergences which can only be cured by strong dynamics, cf. Sec. 3.1.1. Extensions which remain within the realm of perturbativity typically cannot cure fundamental inconsistencies like the Landau pole but can still exhibit effective asymptotic safety. The Planck scale remains as the implied scale of new physics.

At Planckian scales, quantum gravity impacts quantum matter and vice versa. The structure of joint gravity-matter fixed points derives from global symmetries. This chapter highlights and evaluates two resulting bounds on asymptotically safe gravity arising from the existence (weak-gravity bound) and the viability (viability bound) of the fixed point in the matter sector. Reviewing how matter fluctuations impact on gravity we delineate a weak-gravity mechanism which is crucial to realize the viability bound for Yukawa couplings. If a weak-gravity mechanism can be realized, asymptotically safe gravity could UV-complete the Standard Model. The latter imposes upper bounds on the Abelian gauge coupling and Yukawa couplings which lie in the vicinity of the observed values.

4 Matter in asymptotically safe gravity: structure and symmetry

The discovery of the Higgs mass [199, 200] completes the SM up to the Planck scale, cf. Sec. 1. It falls into a narrow window of values in which the Higgs potential gives a strong hint for scale invariance at the Planck scale. We aim to extend this novel scale symmetry beyond the Planck scale and expand it to other sectors of the SM. The natural candidate to achieve this is a scale-invariant quantum-gravity model, cf. Sec. 2. This section closely examines the fixed-point structure of scale-invariant gravity-matter systems which follows from the global symmetry structure, cf. Sec. 4.1. It scrutinizes constraints arising from the existence (Sec. 4.2) and phenomenological viability (Sec. 4.3) of gravity-matter fixed points and discusses how fermions might induce a weak-gravity mechanism which could allow to UV-complete the Standard Model (SM), cf. Sec. 4.5.

4.1 Maximally symmetric asymtotic safety

All matter gravitates. Its propagation follows geodesics in spacetime. Whenever spacetime is curved, the particle's motion is influenced by this curvature. This also includes massless particles defying the Newtonian intuition that a particle's mass causes its gravitational motion. Indeed, also light rays get bent by curvature which causes astrophysical lensing effects, cf. Sec. 7. As in classical GR, particles also gravitate in quantum spacetime. Hence, whenever spacetime fluctuates due to quantum interactions, the particles in that spacetime will also necessarily interact via quantum fluctuations. This is the mechanism of quantum-gravity induced matter interactions [9, 446–453][58].

Thus, asymptotic safety in gravity-matter systems necessarily requires asymptotically safe (not free) matter theories. Put differently, a non-vanishing fixed point for gravity also induces a non-vanishing fixed point for a minimal set of matter couplings. This set of interactions is distinguished by enhanced global symmetries.

Every dynamical field couples to gravity via its kinetic term. Assuming that asymptotically safe quantum gravity does not break global symmetries[59] – for which there is no evidence in any

[58] The induction of matter interactions is not unique to gravity. Also, non-Abelian and Abelian gauge theories induce higher-order matter interactions. Non-Abelian gauge theories might even induce gravity [454–458].

[59] Semi-classical arguments indicate that any global symmetry is broken by quantum gravity. These are related to information loss and Hawking radiation in black-hole spacetimes. Such arguments might be circumvented by the existence of Planck-size black-hole remnants and their properties as the final state of Hawking evaporation. Remnants naturally arise in most singularity-resolving quantum-gravity theories. In asymptotic safety, RG-improved black-hole spacetimes indicate the existence of remnants, see Sec. 7 for an in-depth discussion of RG-improved spacetimes. In any case, global-symmetry violations are not necessarily a generic feature of gravitational quantum effects but might distinguish between different quantum-gravity models.

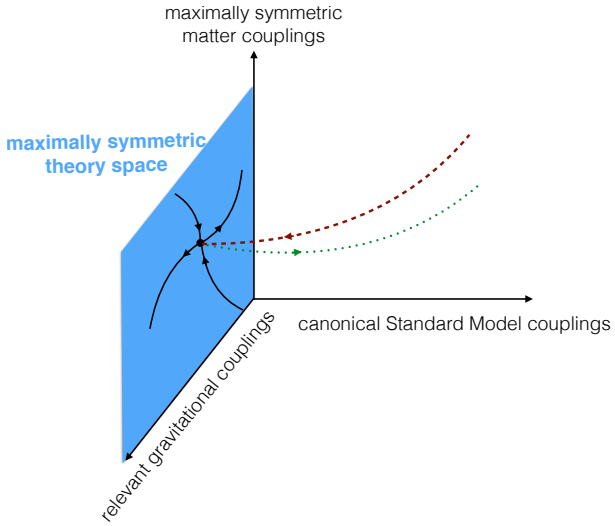

Figure 10: Sketch of the RG flow of gravity-matter systems. The fixed point of maximally-symmetric asymptotic safety (MSAS) lies within the theory space preserving the maximal global symmetries (cyan plane). Gravitational interactions necessarily induce non-vanishing higher-order interactions within the symmetry-protected maximally-symmetric sector of the matter theory. All SM couplings break the maximal global symmetry and thus vanish at the MSAS. For viable IR-physics to emerge (indicated by the green dotted trajectory) towards the IR, the SM directions have to be UV-attractive.

truncation of the functional RG[60] – the set of induced couplings is distinguished by invariance of the corresponding operators under the global symmetries of the kinetic terms. We refer to this minimally coupled version as *maximally-symmetric asymptotic safety* (MSAS). Since all classically marginal SM couplings break at least parts of this maximal global symmetry, cf., Tab. 4, the former are not induced and thus vanish at the MSAS fixed point. We will give explicit examples in a moment. Of course, the existence of alternative fixed points with reduced global symmetry is not excluded, cf. Sec. 4.4 and Sec. 4.5.
The induction of matter interactions leads to a bound on gravitational theory space. If gravitational fluctuations are too strong, matter self-interactions cannot compensate any longer and scale-invariance in the matter sector is lost. Since gravity has to remain sufficiently weak, we refer to this as the *weak-gravity bound*, cf. Sec. 4.2.

An intriguing picture emerges if MSAS is connected to low-energy physics by the RG flow, cf. Fig. 10. On the one hand, IR physics is dominated by the Gaußian fixed point (GFP) at which gravitational interactions (almost) vanish. A special set of matter interactions associated with the GFP – the marginal SM couplings – determines the low-energy physics. On the other hand, there is the less familiar but nevertheless scale-invariant regime. It is dominated by a non-Gaußian fixed point (MSAS) at which gravitational interactions are non-vanishing. Again, there is a special set of interactions: the gravitationally induced couplings. As a consequence of global symmetries, the set of marginal couplings and the set of induced couplings do not overlap. We will explicitly demonstrate this for scalars, fermions and gauge fields in a moment.

Since all gravitationally induced couplings are higher-order couplings, cf. Tab. 3, they are all quickly (i.e., with power-law running) driven to zero in the vicinity of the GFP. If any significantly non-zero matter interactions are to emerge towards low energies, some of the classically marginal couplings have to overlap with IR-repulsive directions of MSAS. More specifically, a trajectory that connects MSAS to viable IR physics, requires that a minimal set of classically marginal couplings, sufficient to break the global symmetries of MSAS to those of the IR theory, aligns or at least overlaps with IR-repulsive directions at the MSAS, cf. Fig. 10. This puts a second constraint on gravitational theory space – the *viability bound*, cf. Sec. 4.3.

[60] Most functional RG calculations have been performed in a Euclidean setting and thus do not sum over black-hole spacetimes.

fields	gravity-induced operators	maximal global symmetry	marginal ops	reduced symm
gauge field A	$\left(F^2\big\vert_{\text{Abelian}}\right)^{n\geqslant 2}$	$\mathbb{Z}_2^A:\quad A_\mu \to -A_\mu$	$AAAA$ $(\partial[AAA])$	$\mathbb{Z}_2^A$ $(-)$
scalar ϕ	$(\partial\phi\,\partial\phi)^{n\geqslant 2}$	$\mathbb{Z}_2^\phi:\ \phi\to-\phi$ $T^\phi_{\text{shift}}:\ \phi\to\phi+\alpha$	ϕ^4	$\mathbb{Z}_2^\phi$
fermion ψ	$(V\pm A)^{n\geqslant 2}$	$\text{U}(1):\ \psi\to e^{i\alpha}\psi$ $\text{U}(1)_{\text{chiral}}:\ \psi\to e^{i\gamma_5\alpha}\psi$	–	–
gauge-scalar	$(\partial\phi\,\partial\phi)^{n\geqslant 1}\left(F^2\big\vert_{\text{Abelian}}\right)^{m\geqslant 1}$	$\mathbb{Z}_2^A\otimes\mathbb{Z}_2^\phi\otimes T_{\text{shift}}$	$\phi\phi AA$ $(\partial[\phi\phi A])$	$\mathbb{Z}_2^A\otimes\mathbb{Z}_2^\phi$ $(\mathbb{Z}_2^\phi)$
gauge-fermion	$(V\pm A)^{n\geqslant 1}\left(F^2\big\vert_{\text{Abelian}}\right)^{m\geqslant 1}$	$\mathbb{Z}_2^A\otimes\text{U}(1)\otimes\text{U}(1)_{\text{chiral}}$	$\bar\psi \not{A}\psi$	
scalar-fermion	$(\partial\phi\,\partial\phi)^{n\geqslant 1}(V\pm A)^{m\geqslant 1}$	$\mathbb{Z}_2^\phi\otimes T_{\text{shift}}\otimes\text{U}(1)\otimes\text{U}(1)_{\text{chiral}}$	$\phi\,\bar\psi\psi$	$\phi\to-\phi$ $\psi\to e^{i\gamma_5\pi/2}\psi$

Table 3: Table of global symmetry structures in induced and marginal matter interactions. We ommit index structure which potentially admits for several induced operators (second column) at each level. F denotes the (non-) Abelian field-strength tensor and $V\pm A$ are vector and axial fermion bilinears, see, e.g., [459, App.A].

We now scrutinize the disjoint sets of marginal and induced interactions for scalars, fermions and gauge fields, cf. Tab. 3 for a summarizing table. Kinetic terms for gauge fields (Abelian and non-Abelian) are $\mathbb{Z}_2$-reflection symmetric, $A^a_\mu\to -A^a_\mu$ and obey a shift symmetry $A^a_\mu\to A^a_\mu$+const. Interactions with an uneven number of gauge fields break the global $\mathbb{Z}_2$ symmetry. Moreover, interactions without a sufficient number of derivative break shift symmetry. This excludes the marginal non-Abelian self-interactions[61], as well as any non-minimal couplings to fermions and scalars[62]. MSAS requires all marginal interactions to vanish and hence "Abelianizes" non-Abelian gauge theories[63].

For scalars ϕ, the kinetic term is $\mathbb{Z}_2$-symmetric under $\phi\to-\phi$ and shift-symmetric under transformations taking $\phi\to\phi+\text{const}$. Maintaining $\mathbb{Z}_2$ symmetry requires even powers of ϕ. Shift-symmetry is preserved by derivatives[64] acting on each ϕ. This excludes scalar potentials and Yukawa interactions, as they do not contain derivatives.

Kinetic terms for Dirac fermions, ψ, are invariant under a global U(1) phase $\psi\to e^{i\alpha}\psi$ and a chiral phase $\psi\to e^{i\gamma_5\alpha}\psi$. Equivalently, this corresponds to separate global symmetries for the two left- and right-handed Weyl fermions. Yukawa interactions partially break the global symmetries of fermion and scalar kinetic term to a discrete chiral symmetry under which $\phi\to-\phi$ and $\psi\to e^{i\gamma_5\pi/2}\psi$.

We conclude that MSAS could induce asymptotic freedom for the marginal SM couplings if a suitable set of marginal couplings overlaps with IR-repulsive directions (viability bound). At the same time, it will induce a different set of higher-order interactions present in the UV. These can only have a fixed point if gravity is sufficiently weak (weak-gravity bound).

[61] Marginal interactions with three non-Abelian gauge fields, i.e., $g\,f^{abc}(\partial_\mu A^a_\nu)A^{\mu b}A^{\nu c}$ break $\mathbb{Z}_2$-reflection symmetry (and shift symmetry). Marginal non-Abelian gauge interactions with four gauge fields, i.e., $g^2(f^{eab}A^a_\mu A^b_\nu)(f^{ecd}A^c_\mu A^d_\nu)$ break the shift symmetry because of the lack of derivatives.

[62] The gauge-fermion interaction $g\,A^a_\mu\bar\psi\gamma^\mu T^a\psi$ and gauge-scalar interaction $g\,(\partial^\mu\phi)T^a A^a_\mu A^b_\nu A^{\nu b}$ break $\mathbb{Z}_2$-reflection symmetry of the gauge field (and shift symmetry). The gauge-scalar interaction $\phi\phi A^a_\mu A^{\mu a}$ breaks the global shift symmetry of both the scalar and the gauge field.

[63] The structure of the induced interactions might still differ for Abelian and non-Abelian gauge theories.

[64] Some derivatives may be shifted from one scalar field to another through partial integration. But, for instance, for vertices involving 4 scalar fields, all the shift-symmetric invariants involve 4 derivatives, cf. [448]

4.1.1 Matter fluctuations and the potential loss of asymptotic safety of gravity

Minimal couplings to matter – in quantum gravity as in every usual gauge theory – lead to contributions of matter loops to the anomalous dimension of the gauge coupling [343]. In gauge theories, scalars and fermions lead to screening contributions[65]. For an Abelian gauge theory without gauge-boson self-interactions, this leads to a Landau pole [202], cf. Sec. 1.2.2. For non-Abelian gauge theories in four dimensions, the antiscreening self-interactions of the gauge bosons can induce asymptotic freedom. This holds up to a critical number of matter degrees of freedom, at which asymptotic freedom is lost and Landau-pole like behavior is restored.
Above four dimensions, i.e., for $D = 4 + \epsilon$, perturbative ϵ-expansions suggest that asymptotic freedom of Yang-Mills theory without matter is replaced by asymptotic safety[66]. This mechanism resembles precisely the asymptotic-safety mechanism for gravity in $D = 2 + \epsilon$. If one adds matter fluctuations, asymptotic safety in $D = 4 + \epsilon$ (or $D = 2 + \epsilon$ for gravity) is lost as soon as asymptotic freedom is lost in $D = 4$ (or $D = 2$ for gravity). The resemblance strongly suggests an equivalent loss of asymptotically safe gravity under the impact of too much matter[67], at least for $\epsilon \ll 1$. Whether it extends to $\epsilon = 2$ was first investigated with the functional RG in [343]. We briefly review the results since they are the basis for the subsequently explored weak-gravity mechanism in Sec. 4.1.2 and the thereby suggested gravitationally induced UV-completion for the SM, cf. Sec. 4.5.

Schematic β-functions encompassing the results from [343], see also Eq. (2.33), were expanded to perturbative order in Sec. 2.4.2. We recall β_G for the dimensionless Newton coupling G and its fixed points,

$$\beta_G = 2\,G + \mathcal{A}(\Lambda)\,G^2 \qquad \text{with} \quad G_{*\,\mathrm{GFP}} = 0, \quad G_{*\,\mathrm{NGFP}} = -\frac{2}{\mathcal{A}(\Lambda)}\,. \tag{4.1}$$

Perturbative ϵ-expansions [242, 340, 341] (which neglect the Λ-dependence in $\mathcal{A}(\Lambda)$), background-field approximations, as well as fluctuation-field expansions of the functional RG [338, 343, 351–357][68] agree that, just like for ordinary gauge theories: fermions and scalars screen (positive sign) the gravitational Newton coupling G, while Abelian and non-Abelian gauge-fields as well as gravitational self-interactions antiscreen (negative sign) the running of G. In [343], the authors find for the perturbative approximation, cf. Eq. (2.34),

$$\mathcal{A}|_{\mathrm{perturbative}} = \frac{1}{6\pi}(N_S + N_W - 4\,N_V - 46)\,, \tag{4.2}$$

with N_S, N_W, and N_V the number of scalars, fermions and gauge bosons, respectively, cf. [465] for spin-3/2 fields. Since the Newton coupling cannot cross $G = 0$ due to the IR-attractive Gaußian fixed point, any viable UV fixed-point has to lie at $G_{*\,\mathrm{NGFP}} \geqslant 0$. Without matter $G_{*\,\mathrm{NGFP}} = 6\pi/23$ and is viable. As more screening (i.e., scalar and fermionic) matter contributions are added, the fixed point moves to larger and larger values. At $\mathcal{A}_{\mathrm{crit}} = 0$, it escapes to $G_{*\,\mathrm{NGFP}} \to \infty^+$, i.e., towards positive values. Beyond the pole, where screening contributions dominate, it reappears at negative $G_{*\,\mathrm{NGFP}} < 0$ and is no longer viable – just like asymptotic freedom, asymptotic safety is lost because of a too large matter content.

[65] This holds for the universal 1-loop contributions of arbitrary scalar and fermionic representations, cf. [306, Eq. (6.1)], wherein Dynkin indices are always positive.

[66] A functional RG study in [460] as well as a 4th-order ϵ-expansion [461] find an upper critical dimension $5 < D_c < 6$. Lattice studies [462, 463], see [464] for a recent review, have not yet confirmed this result.

[67] The argument assumes that the asymptotically safe fixed point in $D = 2 + \epsilon$ can be continuously connected to the one in $D = 4$.

[68] See [444] for a summary of available approximations.

4.1.2 A weak-gravity mechanism: The propagator of gravitational fluctuations

Aside from the question of how matter fluctuations influence the gravitational fixed point, we are most interested in determining the influence of gravitational interactions on the marginal pure-matter interactions of the SM, since these are the couplings which can eventually be compared to experiment once we follow the RG-flow down to the electroweak scale.
The divergent behavior of the gravitational fixed point for $G_{*\,\mathrm{NGFP}} \to \infty$ close to the critical matter content of the theory, i.e., for $\mathcal{A} \to \mathcal{A}_{\mathrm{crit}}$, naïvely suggests that before the viable fixed point disappears, gravitational interactions grow stronger. But, gravitational dynamics is more intricate. At the heart of a more proper understanding lies the cosmological constant.

The propagator of metric fluctuations and a mass-like suppression mechanism. Pure-matter interactions and the running of the corresponding couplings by definition do not involve external curvature fluctuations. These pure-matter couplings will be at the center of the following discussion. We work with a linear split[69] for the metric, i.e.,

$$g_{\mu\nu} = \bar{g}_{\mu\nu} + h_{\mu\nu} \,. \tag{4.3}$$

Regarding matter interactions without external curvature fluctuations $h_{\mu\nu}$, the choice of background $\bar{g}_{\mu\nu}$ is completely arbitrary and drops out of all final results. Without loss of generality, we make the convenient choice of a flat background, i.e., $\bar{g}_{\mu\nu} = \delta_{\mu\nu}$. Due to the 1-loop structure of the flow equation, we can moreover already conclude that only terms with at most two powers of $h_{\mu\nu}$, i.e., only the propagator of metric fluctuations will directly influence pure-matter interactions[70].
To determine the propagator of metric fluctuations, we start from the gauge-fixed gravitational action, including a complete set of those curvature invariants which can contribute to the flat-space propagator of metric fluctuations up to sixth order in derivatives [466], i.e.,

$$\begin{aligned}\Gamma_{k\,\mathrm{grav}} =& \frac{Z_h}{16\pi\bar{G}} \int d^4x \sqrt{g} \left(R - 2\bar{\Lambda}\right) + S_{\text{gauge-fixing}} \\ &+ \frac{Z_h}{16\pi\bar{G}} \int d^4x \sqrt{g} \left(\bar{a}R^2 + \bar{b}R_{\mu\nu}R^{\mu\nu} + \bar{c}R\Box R + \bar{d}R_{\mu\nu}\Box R^{\mu\nu} + \mathcal{O}(p^8)\right) \,.\end{aligned} \tag{4.4}$$

Throughout the following calculations we employ a standard background (de-Donder) gauge-fixing $S_{\text{gauge-fixing}}$ specified in Sec. 4.5.4 where we also discuss gauge dependence[71]. We transition to dimensionless couplings and introduce the gravitational anomalous dimension (wave-function renormalization) η_h, i.e.,

$$G = \bar{G}k^2, \quad \Lambda = \bar{\Lambda}k^{-2}, \quad a = \bar{a}k^2, \quad b = \bar{b}k^2, \quad c = \bar{c}k^4, \quad d = \bar{d}k^4, \quad \eta_h = -\partial_t \log(Z_h). \tag{4.5}$$

Varying the gravitational action in Eq. (4.4) twice with respect to the metric fluctuation $h_{\mu\nu}$ yields the two-point function $\Gamma^{(2)}_{k\,\mathrm{grav}}$, where $^{(2)}$ indicates the second variation. The tensorial

[69] See Sec. 2.5 for a discussion and references regarding different metric splits.

[70] Assume that a vertex with more than two internal curvature fluctuations $h_{\mu\nu}$ would contribute. Because we are only interested in pure matter interactions without external curvature fluctuations, all three of these legs would have to end in another vertex. This automatically generates a 1PI-irreducible diagram with at least two loops. This is in contradiction to the manifest 1-loop structure of the flow equation, cf. Eq. (2.5).

[71] The above truncation of higher-order curvature invariants to finite order will result in potential unitarity violations, cf. Sec. 1.3.1. We refer the reader to Sec. 4.3.1 for a discussion of such truncation ghosts and the question of unitarity violations. Further, we point out that we have pulled out a factor of $1/\bar{G}$ for all higher-order interactions, which renders them dimensionful as opposed to the quadratic gravity couplings in Sec. 1.3.1.

structure of the regulator is chosen to be spectrally adjusted [308], i.e.,

$$R_{k\,\mu\nu\kappa\lambda} = \left(\Gamma^{(2)}_{k\,\mu\nu\kappa\lambda}(k^2) - \Gamma^{(2)}_{k\,\mu\nu\kappa\lambda}(p^2)\right) r_k(p^2)\,, \tag{4.6}$$

where $r_k(p^2)$ is the scalar shape function. For the results presented in the main text, we use the Litim shape function [371], which simplifies the integration of the loop-momentum in the flow equation. For this choice of regulator one can conveniently replace

$$\Gamma^{(2)}_{k\,\mu\nu\kappa\lambda}(p^2) + R_{k\,\mu\nu\kappa\lambda} \quad \longrightarrow \quad \Gamma^{(2)}_{k\,\mu\nu\kappa\lambda}(k^2)\,, \tag{4.7}$$

such that no dependence on the external momentum p remains in the denominator. Inversion of the resulting $\Gamma^{(2)}_{k\,\mathrm{grav}}(k^2)$ by use of some appropriate projection basis [218, 467], yields the regularized propagator, see, e.g., [347] for details.

The resulting York-decomposition [467] propagates (i) a gauge-independent transverse traceless spin-2 mode $h^{\mathrm{TT}}_{\mu\nu}$, such that $\partial^\mu h^{\mathrm{TT}}_{\mu\nu} = 0$ and $h^{\mu\ \mathrm{TT}}_{\mu} = 0$, (ii) a pure-gauge vector mode, and (iii) a two-component scalar sector containing one physical and one additional gauge degree of freedom. The pure-gauge vector mode can be removed by fixing one gauge parameter $\alpha = 0$. This choice is also favored as a fixed point of the gauge-parameter flow [468, 469]. The second gauge parameter β rotates the second gauge mode in the scalar sector. In the following, we choose $\beta = 0$, such that the physical mode fully aligns with the trace mode $h = h^\mu_\mu$. We will recover and discuss the full gauge-dependence in Sec. 4.5.4, but for now (and whenever we fix the gauge) we choose $\beta = 0$ and subsequently $\alpha \to 0$. In this case, the two remaining physical modes are given by

$$\left(\Gamma^{(2)}_{k,\,\mathrm{TT}}(p^2)\right)^{-1} = \frac{32\pi\bar{G}}{p^2 - 2\bar{\Lambda} + \bar{b}p^4 - \bar{d}p^6} P^{\mathrm{TT}}_{\mu\nu\kappa\lambda}(p)\,, \tag{4.8}$$

$$\left(\Gamma^{(2)}_{k\,h}(p^2)\right)^{-1} = -\frac{256\pi\bar{G}}{3p^2 - 4\bar{\Lambda} - 6p^4(3\bar{a} + \bar{b}) + 6p^6(3\bar{c} + \bar{d})}\,. \tag{4.9}$$

The TT-projector $P^{\mathrm{TT}}_{\mu\nu\kappa\lambda}(p)$ is specified in [470, Eq. (B8)].
Returning to the contributions to pure-matter interactions, we observe that the effective strength of gravitational fluctuations is not solely determined by the Newton coupling $\bar{G}$, but by the magnitude of the above propagators, or their generalization to infinite order in momentum. In both modes, the cosmological constant (and all higher-order interactions) appear as mass-like terms in the denominators. Not only can they damp the effective strength of gravitational fluctuations in matter diagrams, but they can potentially even lead to sign changes by changing the relative magnitude of the contributions of different diagrams. This is crucial, as the signs correspond to the screening or antiscreening nature of gravitational contributions which in turn determine whether a UV-complete matter sector with non-trivial IR structure is possible or not.

The cosmological constant as an effective mass term. For now, we focus on the cosmological constant and work in the Einstein-Hilbert truncations, i.e., neglect the influence of higher-curvature terms in Eqs. (4.8)-(4.9). The running and the fixed point of the cosmological constant, as determined from truncations identifying background and fluctuation fields to close the flow equation [343], is given by

$$\beta_\Lambda = -2\Lambda + \mathcal{A}(\Lambda)\, G_N\, \Lambda + \mathcal{B}(\Lambda) G_N\,, \qquad \Lambda_{*\mathrm{NGFP}} = -\frac{\mathcal{B}(\Lambda_{*\mathrm{NGFP}})}{2\,\mathcal{A}(\Lambda_{*\mathrm{NGFP}})}\,, \tag{4.10}$$

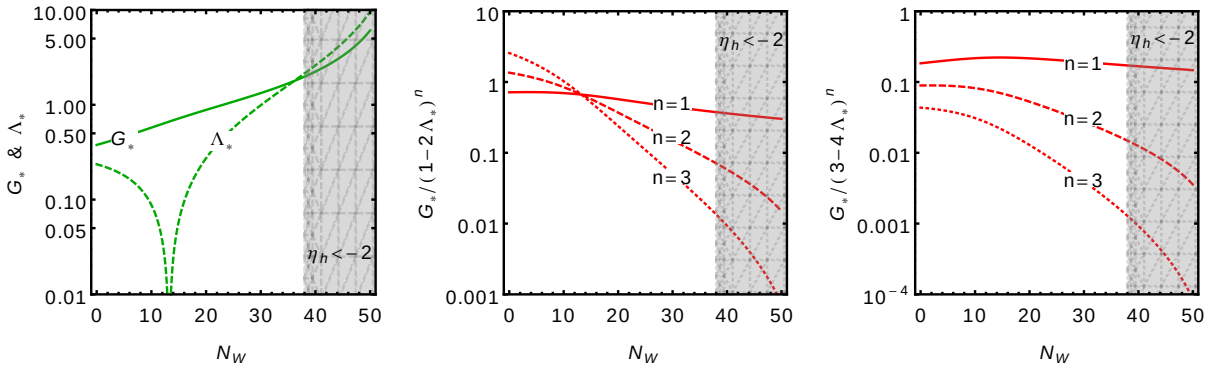

Figure 11: Left-hand panel: Gravitational fixed point values from [343] for $\alpha = \beta = 0$ and SM matter $N_S = 4$, $N_V = 12$, as a function of N_W ($N_W = 45$ for the SM). Middle panel: effective TT-mode strength (otherwise same as left-hand panel). Right-hand panel: effective Tr-mode strength (otherwise same as left-hand panel). We also mark the region (gray-shaded) in which $\eta_h < -2$, i.e., signalling a possible breakdown of the truncation. Compare to Fig. 13 in [452] for qualitatively similar results in a fluctuation-field calculation.

where, we have already plugged in the fixed point Eq. (4.1) for G. The full threshold functions $\mathcal{A}(\Lambda)$ and $\mathcal{B}(\Lambda)$ can be inferred from [343]. In the perturbative approximation, i.e., expanding $\mathcal{A}(\Lambda)$ to zeroth and $\mathcal{B}(\Lambda)$ to first order in Λ one finds

$$\Lambda_{*\mathrm{NGFP}} \approx \frac{3}{4} \times \frac{2 + N_S + 2\,N_V - 2\,N_W}{31 + 4\,N_V - N_S - N_W} \,. \tag{4.11}$$

This simplified equation already reveals the main mechanism. The numerator changes sign with N_W much quicker than both denominators of $\Lambda_{*\mathrm{NGFP}}$ (Eq. (4.11)) and $G_{*\mathrm{NGFP}}$ (Eq. (4.1)). This causes an effective weakening of gravitational contributions to all matter couplings with growing fermion number. The weakening persists until the truncation breaks down. The latter is signalled by the gravitational anomalous dimension growing large and exceeding the bound of $|\eta_h| > 2$ [352][72].

Beyond the background-field approximation. The impact of the propagator of metric fluctuations depends on the fluctuation couplings associated with the fluctuating metric $h_{\mu\nu}$ and not the background couplings associated with the background metric $\bar{g}_{\mu\nu}$. The above weak-gravity mechanism was presented in approximations which identify background and fluctuations. While the dynamical mechanism for a weak propagator of metric fluctuations is modified in momentum-dependent fluctuation-field approximations [352, 356, 357, 384–386, 471], the suppression of the effective strength of gravitational modes persists and even is amplified, cf. Fig. 13 in [452]

4.1.3 The scalar-fermion sector of MSAS

To give an explicit example, we investigate the effect of asymptotically safe quantum gravity on a simple model containing a single real scalar field ϕ and a Dirac fermion ψ. In the present truncation, gravitational couplings only enter via the propagator of metric fluctuations discussed in the previous Sec. 4.1.2 where we treat them as external parameters. The model will be used to demonstrate the weak-gravity bound, cf. Sec. 4.2, and the viability bound 4.3.

[72] For $\eta_h < 2$, the regulator limits demanded below Eq. (2.4) are inverted. In particular, the regulator vanishes in the UV and does not properly integrate out modes any longer, see [352, Sec.III.D]

We systematically truncate the maximally-symmetric theory space using a mixed derivative-operator expansion, cf. Sec. 2.2.1. At each order in canonical dimension, one constructs a complete basis of maximally symmetric interactions invariant under the global symmetries of the kinetic terms, cf. Tab. 3. The resulting truncation up to order 8 reads

$$\begin{aligned}\Gamma_{k,\mathrm{MSAS}} =& \frac{Z_\phi}{2}\int d^4x\sqrt{g}\,(g^{\mu\nu}\partial_\mu\phi\partial_\nu\phi) + iZ_\psi\int d^4x\sqrt{g}\bar\psi\not\nabla\psi \\ &+\frac{1}{2}\int d^4x\sqrt{g}\Big[\bar\lambda_A\,(i\bar\psi\gamma_\mu\gamma_5\psi)(i\bar\psi\gamma^\mu\gamma_5\psi)+\bar\lambda_V\,(\bar\psi\gamma_\mu\psi)(\bar\psi\gamma^\mu\psi)\Big] \\ &+\int d^4x\sqrt{g}\Big[i\bar\chi_1\left(\bar\psi\gamma^\mu\nabla_\nu\psi-(\nabla_\nu\bar\psi)\gamma^\mu\psi\right)(\partial_\mu\phi\partial^\nu\phi) \\ &\qquad + i\bar\chi_2\left(\bar\psi\gamma^\mu\nabla_\mu\psi-(\nabla_\mu\bar\psi)\gamma^\mu\psi\right)(\partial_\nu\phi\partial^\nu\phi)\Big]\,.\end{aligned}$$

The kinetic terms for the scalar and fermion in the first line include wave-function renormalizations Z_ϕ and Z_ψ, respectively. The two invariants and respective four-fermion couplings $\bar\lambda_A$ and $\bar\lambda_V$ span a full basis of maximally-symmetric couplings at order 6 [448, 472]. There are no such invariants at order 8. The third line shows the two lowest-order (i.e., order-8) independent mixed fermion-scalar interactions [449] which are invariant under the full global symmetry. We neglect order-8 pure-scalar invariants which also exist in the maximally-symmetric theory space [448, 473].

Beyond the maximally-symmetric theory space, we are interested in bounds on gravitational parameter space arising from the requirement of non-vanishing marginal couplings, i.e., whether the flow towards the IR can depart from the maximally-symmetric hypersurface, cf. Fig. 10. Hence, we also include a set of interactions which breaks the maximal global symmetry, i.e.,

$$\Gamma_{k\,\mathrm{marginal}} = \int d^4x\sqrt{g}\left(i\,y\,\phi\bar\psi\psi+\bar\lambda_S(\bar\psi\psi)(\bar\psi\psi)\right). \tag{4.12}$$

This includes a marginal Yukawa coupling y. Any non-vanishing y explicitly breaks the maximal global symmetry to a remaining discrete chiral symmetry[73], cf. Tab. 3. We also include the additional four-fermion interaction $\bar\lambda_S$ to investigate its interplay with the Yukawa coupling[74]. As for the pure-gravity couplings, we transition to renormalized dimensionless couplings and introduce anomalous dimensions, i.e.,

$$\lambda_X = \frac{\bar\lambda_X}{Z_\psi^2}k^2\,,\quad \chi_i = \frac{\bar\chi_i}{Z_\psi\,Z_\phi}k^4\,,\qquad \eta_\phi = -\partial_t\ln Z_\phi\,,\quad \eta_\psi = -\partial_t\ln Z_\psi\,. \tag{4.13}$$

Given the overall truncation $\Gamma_k = \Gamma_{k\,\mathrm{grav}} + \Gamma_{k,\mathrm{MSAS}} + \Gamma_{k\,\mathrm{marginal}}$, the flow equation (2.5) can be expanded in terms of external fields, cf. Sec. 2.1 for an introduction to this expansion and App. C.1 for the explicit application to the present truncation where the representation in terms of diagrams is shown in Fig. 36. The resulting set of β-functions for the dimensionless matter

[73] A quartic scalar self-inteaction would further break the global symmetry, cf. Tab 3.

[74] Together, λ_A, λ_V, and λ_S form a Fierz-complete basis under the discrete chiral symmetry of the Yukawa term.

couplings and anomalous dimensions reads

$$\beta_{\chi_1} = \chi_1\left(\eta_\psi + \eta_\phi + 4\right) + \mathcal{M}_{\chi_1}^{\chi^2} + G^2\mathcal{I}_{\chi_1} + G\mathcal{D}_{\chi_1} \tag{4.14}$$

$$\beta_{\chi_2} = \chi_2\left(\eta_\psi + \eta_\phi + 4\right) + \mathcal{M}_{\chi_2}^{\chi^2} + G^2\mathcal{I}_{\chi_2} + G\mathcal{D}_{\chi_2}\,, \tag{4.15}$$

$$\begin{aligned}\beta_{\lambda_A} = {}& 2\lambda_A\left(\eta_\psi + 1\right) + \frac{4}{3}\left(\lambda_A - \lambda_V\right)y^2\,\mathcal{M}_\lambda^{\lambda y^2} + \left(\lambda_A^2 - \lambda_A\left(3\lambda_S + 2\lambda_V\right) + 3\lambda_V\left(\lambda_S - \lambda_V\right)\right)\mathcal{M}_\lambda^\lambda \\ & + G^2\,\mathcal{I}_\lambda + G\lambda_A\,\mathcal{D}_\lambda\,,\end{aligned} \tag{4.16}$$

$$\begin{aligned}\beta_{\lambda_V} = {}& 2\lambda_V\left(\eta_\psi + 1\right) + 2\left(\lambda_A - 2\lambda_V\right)y^2\,\mathcal{M}_\lambda^{\lambda y^2} - 2\left(\lambda_A\left(\lambda_S + 2\lambda_V\right) + 2\lambda_V\left(\lambda_V - \lambda_S\right)\right)\mathcal{M}_\lambda^\lambda \\ & + G\lambda_V\,\mathcal{D}_\lambda\,,\end{aligned} \tag{4.17}$$

$$\beta_y = y\left(\eta_\psi + \frac{\eta_\phi}{2}\right) + y^3\,\mathcal{M}_y^{y^3} - y\left(4\lambda_A - 3\lambda_S + 4\lambda_V\right)\mathcal{M}_y^{\lambda y} + Gy\,\mathcal{D}_y \tag{4.18}$$

$$\begin{aligned}\beta_{\lambda_S} = {}& 2\lambda_S\left(\eta_\psi + 1\right) + \lambda_S\left(-6\lambda_A + \lambda_S + 2\lambda_V\right)\mathcal{M}_\lambda^\lambda + 2\left(2\lambda_A + \lambda_S - 6\lambda_V\right)y^2\,\mathcal{M}_\lambda^{\lambda y^2} \\ & + G\lambda_S\,\mathcal{D}_\lambda + Gy^2\,\mathcal{C}_\lambda^{Gy^2}\,,\end{aligned} \tag{4.19}$$

$$\eta_\phi = G\,\mathcal{D}_{\eta_\phi} + \mathcal{M}_{\eta_\phi}^{\chi} + y^2\mathcal{M}_{\eta_\phi}^{y^2}\,, \tag{4.20}$$

$$\eta_\psi = G\,\mathcal{D}_{\eta_\psi} + \mathcal{M}_{\eta_\psi}^{\chi} + y^2\mathcal{M}_{\eta_\psi}^{y^2}\,. \tag{4.21}$$

The above notation makes all powers of the gravitational Newton coupling G and the matter couplings y, λ_A, λ_V, and λ_S explicit[75]. The threshold integrals $\mathcal{I}_i$, $\mathcal{D}_i$, and $\mathcal{C}_i^j$ only depend on the set of gravitational couplings Λ, a, b, c, and d and on the anomalous dimensions η_i. The $\mathcal{M}_i^j$ denote pure-matter contributions. All the thresholds depend on the choice of regulator shape function and are given in App. C.2. Gravitationally induced terms, denoted by $\mathcal{I}_i$, only occur for the set of maximally symmetric couplings χ_1, χ_2, λ_A. To the contrary, all matter interactions, including the global-symmetry reducing y and λ_S, receive gravitational corrections linear in the respective matter coupling itself, i.e., $\mathcal{D}_i$. Together with gravitational contributions in the matter anomalous dimensions, they lead to terms which mimic an increase or decrease in the effective spacetime dimension that the matter field probes, cf. Sec. 5. These contributions are of crucial phenomenological importance in Sec. 4.4 and 4.5. Further, β_{λ_S} also contains a term $\mathcal{C}_i^j$ which describes gravity contributions mediated by another matter coupling, in this case by y. This exemplifies that once the global symmetries are broken (here, once $y \neq 0$) a new set of secondarily induced couplings (here λ_S) invariant under the reduced symmetry is necessarily present as well.

The following two sections discuss the bounds on the propagator of metric fluctuations that arise due to the above symmetry considerations. We conjecture the existence of such bounds to be generic for *any* gravity-matter system in which gravitational fluctuations do not violate global symmetries. Indeed, the weak-gravity bound has also been explicitly verified in [9, 449–453]. The viability bound has recently been explored in [474] for unimodular asymptotically safety [475–477].

[75] Too shorten notation, we make an exception for χ_1 and χ_2 because the two mix. Factors of χ_i are contained in $\mathcal{M}_{\chi_i}^{\chi^2}$, and $\mathcal{D}_{\chi_i}$, cf. App. C.2.

4.2 Weak-gravity bound: gravitationally induced matter interactions

The β-functions in Eqs. (4.14)-(4.16) explicitly show that gravitational fluctuations will induce the respective couplings[76], i.e., χ_1, χ_2 and λ_A. Non-vanishing $G \neq 0$ results in a non-vanishing contribution $\sim \mathcal{I}$ in each of those β-functions, even if $\chi_1 \equiv 0$, $\chi_2 \equiv 0$, and $\lambda_A \equiv 0$, respectively. Hence, these couplings are inevitably generated. Based on global-symmetry considerations, this applies to all maximally-symmetric couplings, i.e., those associated with operators which are invariant under the global symmetries of the kinetic terms of all matter fields, cf. Tab. 3. All maximally-symmetric operators involve an even number $2n$ of each type of matter fields. Collectively denoting these couplings by $\bar{\lambda}_{2n}$, their dimensionless counterparts $\lambda_{2n} = \bar{\lambda}_{2n} k^{-d_{\bar{\lambda}_{2n}}}$ run according to

$$\beta_{\lambda_{2n}} = \left(-d_{\bar{\lambda}_{2n}} + \mathcal{D}_{\lambda_{2n}} G\right) \lambda_{2n} + \mathcal{M}_{\lambda_{2n}} \lambda_{2n}^2 + \mathcal{C}_{\lambda_{2n}} + \mathcal{I}_{\lambda_{2n}} G^n \,, \tag{4.22}$$

where, $d_{\bar{\lambda}_{2n}}$ is the canonical dimension of the associate operator. $\mathcal{I}_{\lambda_{2n}}$ and $\mathcal{D}_{\lambda_{2n}}$ denote terms which depend on the gravitational couplings alone. Further, $\mathcal{C}_{\lambda_{2n}}$ collectively denotes possible mixed contribution involving gravitational couplings and $\lambda_{2(m\neq n)}$. Finally, $\mathcal{M}_{\lambda_{2n}}$ denotes self-interactions and does not depend on other couplings. None of the above depend on λ_{2n} itself. Crucially, $\mathcal{M}_{\lambda_{2n}}$ vanishes for $n > 2$ due to the 1-loop nature of the flow equation[77]. Hence, their β-functions are linear in λ_{2n} itself, with a single fixed point at

$$\lambda_{2n\,*} = \frac{\mathcal{I}_{\lambda_{2n}} G^n + \mathcal{C}_{\lambda_{2n}}}{\mathcal{D}_{\lambda_{2n}} G - d_{\bar{\lambda}_{2n}}} \qquad \forall\ n > 2 \,. \tag{4.23}$$

We can explicitly observe gravitational induction: the free fixed point $\lambda_{2n\,*}(G = 0) = 0$ (note that $\mathcal{C}_{\lambda_{2n}}$ vanishes if all λ_{2n} vanish) will be shifted to non-vanishing values by $G \neq 0$.
In contrast, the lowest-order induced couplings λ_4 have a special structure. They receive quadratic contributions and hence have fixed points at

$$\lambda_{4\,*} = \frac{1}{2\,\mathcal{M}_{\lambda_4}} \left[d_{\bar{\lambda}_4} - \mathcal{D}_{\lambda_4} G \pm \sqrt{\left(d_{\bar{\lambda}_4} - \mathcal{D}_{\lambda_4} G\right)^2 - 4\,\mathcal{M}_{\lambda_4} \left(\mathcal{I}_{\lambda_4} G^2 + \mathcal{C}_{\lambda_4}\right)} \right] . \tag{4.24}$$

The respective free fixed points $\lambda_{4\,*} \equiv 0$ are shifted away from zero as soon as $G \neq 0$. Moreover, if $\mathcal{M}_{\lambda_4}$ and $\mathcal{I}_{\lambda_4}$ have the same sign, there exists a critical $G_{\rm crit}$, at which the two fixed points collide. Beyond the collision, i.e., for $G > G_{\rm crit}$ and beyond the weak-gravity bound, no real fixed point remains. This causes novel divergences which are no longer tamed by any fixed point. Hence, asymptotic safety is lost.
The weak-gravity bound can be observed for the lowest-order pure-scalar [448], the pure-gauge [450, 453], and mixed scalar-fermion [9, 449] maximally-symmetric couplings[78]. While higher-order λ_{2n} can lead to shifts of $G_{\rm crit}$, they will not generate further bounds. The induced term

[76] The three four-fermion interactions $\lambda_S(\bar{\psi}\psi)(\bar{\psi}\psi)$, $\lambda_A\,(i\bar{\psi}\gamma_\mu\gamma_5\psi)(i\bar{\psi}\gamma^\mu\gamma_5\psi)$, and $\bar{\lambda}_V\,(\bar{\psi}\gamma_\mu\psi)(\bar{\psi}\gamma^\mu\psi)$ form a Fierz-complete basis invariant under the reduced symmetry at non-vanishing Yukawa coupling y. Moreover the bilinears associated with λ_A and λ_V are both invariant under the larger global $U(1)_{\rm chiral}$ symmetry of the kinetic terms. It is puzzling that only λ_A but not λ_V is induced by gravitational fluctuations. Indeed, gauge-interactions induce both λ_A and λ_V, see [478–480]. At the technical level, this results from a different type of diagram and therefore vertex structure in gauge as compared to gravitational induction, cf. [447].

[77] In a 1-loop diagram, there can only be two internal lines at each vertex. Hence, a 1-loop diagram containing (more than) 2 vertices with $2n$ legs each must have (more than) $4(n-1)$ external legs. We are interested in self-contributions of such diagrams, i.e., in cases with $2n$ external legs. This leads to the condition $4(n-1) = 2n$, which holds for $n = 2$, but not for any $n > 2$.

[78] Four-fermion interacions [9, 447, 472] do not exhibit a weak-gravity bound as $G_{\rm crit} < 0$ because $\mathcal{M}_{\lambda_4}$ and $\mathcal{I}_{\lambda_4}$ have opposite sign due to an relative sign in the fermionic loop.

couplings	$\mathbb{Z}_2^A: \ A_\mu \to -A_\mu$	$T^\phi_{\text{shift}}: \ \phi \to \phi + \text{const.}$	$U(1)_{\text{chiral}}: \ \psi \to e^{i\gamma_5\alpha}$
$g \neq 0$	✗	✗	✓
$y \neq 0$	✓	✗	✗
$\lambda_4 \neq 0$	✓	✗	✓

Table 4: Global symmetry structure of a U(1) gauge theory with a charged Dirac fermion and a charged scalar and its reduction by the marginal couplings α (gauge), y (Yukawa), and λ_4 (scalar quartic). ✓ (✗) indicates that the symmetry is preserved (broken) by a non-vanishing value of the respective coupling.

$\sim \mathcal{I}_{\lambda_4} G^2$ also depends on all higher-order gravitational couplings which enter the propagator of metric fluctuations, cf. Eqs. (4.8)-(4.9). Hence, the weak gravity bound is an interdependent constraint on all directions in gravitational parameter space, see Sec. 4.3.1. In general, this also includes non-minimal matter-gravity couplings, cf. [354, 451, 452, 481, 482].

4.3 Viability bound: emergence of a non-trivial low-energy sector

The marginal SM couplings are *not* maximally symmetric because they break part of the global symmetry of the matter kinetic terms, cf. Tab. 3. Hence, they vanish at the maximally-symmetric fixed point. In order to still allow SM structure in the IR, they have to either overlap with a UV-attractive direction or be induced by other SM couplings which do so. In the SM, this includes three types of marginal couplings: (i) the gauge couplings, (ii) the Yukawa couplings, and (iii) the scalar quartic coupling. We will delineate the global symmetry structure for a U(1)-gauge theory with a complex scalar ϕ and a Dirac fermion ψ, but similar global-symmetry arguments hold for the SM as well. The respective Lagrangian reads

$$\begin{aligned}\mathcal{L} =& \frac{1}{4}\left(\partial_\mu A_\nu - \partial_\nu A_\nu\right)^2 \ + \partial_\mu\phi^\dagger\,\partial^\mu\phi \ + i\,\bar\psi_L\,\partial\!\!\!/\,\psi_L \ + i\,\bar\psi_R\,\gamma_5\partial\!\!\!/\,\psi_R \\ &+ i\,g\,A_\mu\bar\psi_L\gamma^\mu\psi_L \ + i\,g\,A_\mu\bar\psi_R\gamma_5\gamma^\mu\psi_R \ - g^2\,A_\mu\phi^\dagger A^\mu\phi \ + y\left(\bar\psi_R\,\phi\,\psi_L - \bar\psi_L\,\phi^\dagger\,\psi_R\right) \ + \lambda_4\left(\phi^\dagger\phi\right)^2\end{aligned} \tag{4.25}$$

To make the global symmetry structure most apparent, we have decomposed the Dirac fermion into left and right Weyl components and expanded the gauge-covariant derivatives. The full Lagrangian is invariant under the gauge symmetry $U(1)_A$ under which $A_\mu \to A_\mu - \frac{1}{g}\partial_\mu\alpha(x)$, $\psi \to e^{i\,\alpha(x)}\psi$, and $\phi \to e^{i\,\alpha(x)}\phi$. For $y = 0$, $\lambda_4 = 0$, and vanishing gauge coupling $\alpha = 0$, the Lagrangian is moreover invariant under the global symmetries

$$U(1)_{\text{chiral}} \otimes \mathbb{Z}_2^A \otimes T^\phi_{\text{shift}} \ , \tag{4.26}$$

where $U(1)_{\text{chiral}}$ denotes the additional global chiral symmetry of the fermion kinetic term, T^ϕ_{shift} the shift symmetry of the scalar kinetic term, and $\mathbb{Z}_2^A$ the global reflection symmetry of the gauge fields, cf. Tab. 4 for the transformations. A non-vanishing gauge coupling $g \neq 0$ preserves the $U(1)_{\text{chiral}}$ but breaks the $\mathbb{Z}_2^A \otimes T^\phi_{\text{shift}}$ symmetry because of the minimal coupling to the scalar. A non-vanishing Yukawa coupling $y \neq 0$ preserves the $\mathbb{Z}_2^A$ but breaks the $U(1)_{\text{chiral}} \otimes T^\phi_{\text{shift}}$ symmetry. A non-vanishing quartic coupling only breaks T^ϕ_{shift}. The global-symmetry structure is summarized in Tab. 4. Both $\alpha \neq 0$ and $y \neq 0$ already break T^ϕ_{shift}, i.e., the only global symmetry that protects λ_4. Hence, a non-vanishing gauge or Yukawa coupling will automatically induce a non-vanishing quartic coupling.

We conclude: A minimal subset of marginal couplings which fully breaks the global symmetries of MSAS to those of the IR theory has to overlap with UV-attractive directions at the

maximally-symmetric fixed point. Otherwise, no RG-flow can connect MSAS to this IR theory. Concerning the SM, this requires that gauge and Yukawa couplings overlap with UV-attractive directions. The quartic coupling is exempt from this demand because it does not further break a global symmetry[79]. It will be generated by the gauge-Yukawa sector anyways.

Gauge-viability bound. Gravitational contributions to gauge couplings have been calculated both in perturbation theory [483–495] and with the functional RG [356, 450, 496–500]. The perturbative literature features a long-standing discussion whether the results are arbitrary in view of scheme-dependence. We divert this question to a separate discussion in Sec. 4.5.4. The functional RG finds that any non-vanishing gravitational contribution to gauge couplings is antiscreening [450, 496, 498–500]. In particular, this holds for the gauge-invariant contribution from the traceless-transverse gravitational mode. These can be taken as strong indications that asymptotically safe gravity obeys the gauge-viability bound.

Yukawa-viability bound. The viability bound of the Yukawa coupling is more intricate and not straightforwardly fulfilled. Therefore, we will now take a closer look at the critical exponent of the Yukawa coupling which can be derived from Eq. (4.18) as

$$\theta_y = \left[-\partial_y \beta_y\right]_{\text{MSAS}} = -\left(\eta_\psi + \frac{\eta_\phi}{2}\right) - \mathcal{D}_y\, G + 4\,\lambda_{A\,*}\,\mathcal{M}_y^{\lambda\, y}\,. \tag{4.27}$$

It depends on the gravitational couplings: directly via traceless-transverse (TT) and trace-mode contribtions in $\mathcal{D}_y$, via TT- and trace-mode contributions in the anomalous dimensions η_ψ and η_ϕ, and indirectly via the induced MSAS couplings, i.e., via λ_A as well as via χ_1- and χ_2-contribtions in the fermion and scalar anomalous dimensions. Given the 1-loop structure of the flow equation (2.5) and for MSAS, there do not exist any further contributions. Still, as for every truncation, higher-order couplings can indirectly contribute by shifting the above contributions. Note that we focus on the MSAS here, so gauge contributions vanish.
Plugging in the expressions in App. C.2, Eqs. (C.3)-(C.17), neglegting the contributions from induced couplings, and setting the loop-anomalous dimensions to zero, we can reorder the TT- and trace-mode contributions in $\mathcal{D}_y$, η_ψ, and η_ϕ to approximate the critical exponent, i.e.,

$$\theta_{y,\,\text{approx}} = \underbrace{-\frac{15\,G}{16\,\pi\,(1-2\Lambda)^2}}_{=:\,\theta_{y,\,\text{TT}}} \quad \underbrace{-\frac{7\,G}{16\,\pi\,(3-4\,\Lambda)^2} + \frac{7\,G}{24\,\pi\,(3-4\,\Lambda)}}_{=:\,\theta_{y,\,\text{Tr}}}\,. \tag{4.28}$$

Negative fixed-point values for G as well as values of the cosmological constant beyond the pole of the TT mode ($1/(1-2\Lambda)$) cannot be continuously connected to the Gaußian fixed-point, cf. Sec. 2.4.2. Hence, we focus on $\Lambda < 1/2$ and $G > 0$. Therefore, in the TT-approximation (and without the influence of higher-order curvature couplings) MSAS does not pass the Yukawa-viability bound. Hence, it fails to connect to any IR theory with non-vanishing Yukawas, in particular, with the SM.
On the other hand, the trace-mode contributions $\theta_{y,\,\text{Tr}}$ can change sign, cf. Eq. 4.28. The decisive sign-change arises from diagrams in η_ψ and $\mathcal{D}_y$ which contain internal fermion propagators. Whenever those are regulated one picks up a relative sign. It is vital that these diagrams contain only a single unregulated propagator of metric fluctuations and therefore only a single

[79] The scalar mass-term has the same global-symmetry structure as the quartic coupling. It will also be generated by gauge and Yukawa interactions and we accept the corresponding fine-tuning, cf. Sec. 1.

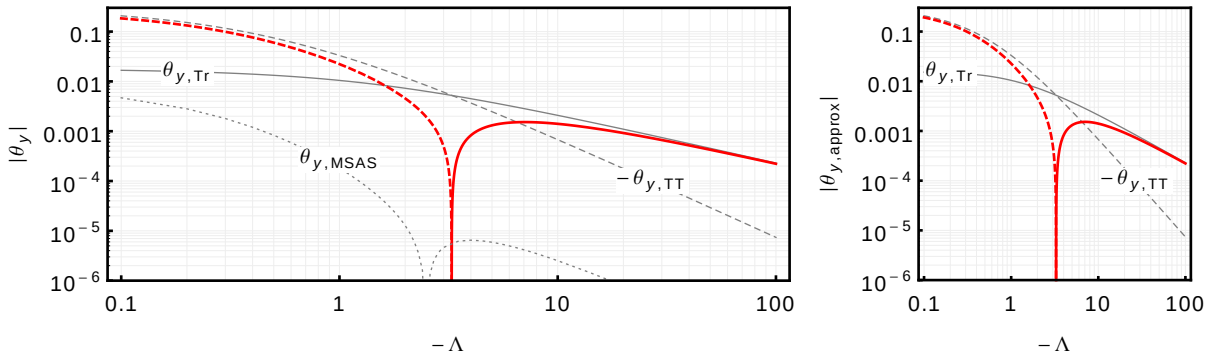

Figure 12: Critical exponent of the Yukawa coupling θ_y with growing negative Λ. The thin gray lines show the individual contributions from the trace mode (solid), the traceless-transverse mode (dashed), and via induced interactions (dotted). The thick red line shows the additive full result. For $\Lambda > \Lambda_{\mathrm{crit}} \approx -3$, $\theta_y < 0$ (thick red-dashed line) and fails the viability bound. For $\Lambda < \Lambda_{\mathrm{crit}}$, $\theta_y < 0$ (thick red-solid line) and the viability bound is passed. The approximated result (right-hand panel), cf. Eq. 4.28, and the full result (left-hand panel) are practically indistinguishable because induced contributions $\theta_{y,\,\mathrm{MSAS}}$ are subleading.

power of Λ in the denominator, cf. last term in Eq. 4.28. To the contrary, all diagrams in which non-fermionic propagators are regulated contain multiple powers of the propagator of metric fluctuations.
In combination with the cosmological constant acting as an effective mass-term for gravitational fluctuations, see Sec. 4.1.2, this completes the following crucial mechanism: With growing $-\Lambda$, all gravitational contributions become weak (weak-gravity mechanism), cf. Fig. 11. The higher the power of contributing gravitational modes in a diagram, the stronger the suppression. Hence, diagrams with a single power of the propagator of metric fluctuations, i.e., those with the benign sign, dominate. Thereby, growing $-\Lambda$ can flip the sign of $\theta_{y,\,\mathrm{approx}}$ at $\Lambda_{\mathrm{crit}} \approx -3$ which enables the possibility of non-zero Yukawa couplings in the IR. We depict this mechanism in Fig. 12 where we also show the full result to verify that the above approximation is indeed very good. For a discussion of the subleading back-coupling of induced couplings see [9] and App. C.4.

4.3.1 Constraints on higher-order gravitational parameter space

The weak-gravity bound and the viability bound are both actually bounds on the full propagator of metric fluctuations. Here, we have used the Einstein-Hilbert truncation, see Sec. 2.4.2, and have converted those bounds into bounds on the fixed-point values of G and Λ. But the action of asymptotically safe gravity is expected to contain an infinite sum of higher-derivative terms which contribute to the propagating gravitational modes at all orders, cf. Eqs. (4.8) and (4.9). An extended discussion of the weak-gravity and the viability bound including higher-order operators is delegated to App. C.3. Finite truncations of higher-order gravitational couplings will automatically introduce truncation ghosts, i.e., higher-order propagating modes with wrong-sign kinetic terms. Therefore, any physics associated with higher-order gravitational couplings should make sure that physical effects are not due to truncation ghosts. This can be inferred by validating that the truncated theory remains a proper EFT in the whole energy regime of physical interest, i.e., that all physical scales remain below the truncation-EFT cutoff implied by unitarity, cf. Sec. 1.2.2.

4.4 The fixed-point structure of marginal Standard-Model couplings

4.4.1 Gravitationally induced anomalous dimensions

Whenever MSAS obeys the viability bound such that a global-symmetry reducing coupling becomes UV-attractive a new asymptotically safe and symmetry-reduced fixed point becomes available. This is apparent when returning to the structure of the respective β-functions, for instance, for the Yukawa coupling, cf. Eq. 4.18,

$$\beta_y = \mathcal{M}_y^{y^3}\, y^3 - f_y\, y\,. \tag{4.29}$$

Here, we have summarized all contributions linear in y itself into f_y and chosen the sign such that positive f_y obeys the viability bound. It exhibits a free (○) and an interacting fixed point (●) with corresponding critical exponents, i.e.,

$$y^2_{*\,\bigcirc} = 0\,, \quad \text{with} \quad \theta_i = f_y \qquad \text{and} \qquad y^2_{*\,\bullet} = \frac{f_y}{\mathcal{M}_y^{y^3}}\,, \quad \text{with} \quad \theta_i = -f_y\,. \tag{4.30}$$

For positive f_y, the interacting $y_{*\,\bullet}$ lies at positive real values and is IR-attractive. The free (MSAS) fixed point is UV-attractive and allows for a non-vanishing Yukawa coupling to emanate towards the IR, cf. Sec. 4.3[80]. The viability bound and the existence of a real-valued interacting fixed point are thus equivalent.
Indeed, all this structure depends linearly on f_y. Therefore, conclusions about the suppression of matter-mediated effects from Sec. 4.3 carry over to the interacting fixed-point structure. These corrections are small and only modify f_y at the 1%-level, in particular, cf. the discussion around Fig. 12. It is thus consistent to neglect matter-mediated effects in the following discussion and only consider the direct gravitational contribution, i.e.,

$$f_y \approx -G\,\mathcal{D}_y - \eta_\psi - \frac{\eta_\phi}{2}\,. \tag{4.31}$$

As soon as $y_* \neq 0$, the maximally-symmetric sector and the marginal sector couple back into each other. As long as y_* remains perturbatively small, the same holds for the back-coupling, cf. [9].

4.4.2 Upper bound structures for global-symmetry reducing couplings

The fixed-point structure in Eq. 4.30 is depicted in Fig. 13. For now, we focus on the trans-planckian regime above M_{Planck} where $f_y \approx$ const. For coupling values above $y^2_{*\bullet}$, the screening contribution $\mathcal{M}_y^{y^3}\, y^3$ dominates and the Yukawa coupling y is driven to lower values towards the IR. Towards the UV such trajectories will remain divergent and are thus *not* UV-complete. For coupling values below $y^2_{*\bullet}$, the running is dominated by the antiscreening gravitational contribution f_y and y increases towards the IR. Such trajectories are asymptotically free and thus UV-complete. Indeed, they emanate from the free fixed point and correspond to MSAS. The critical trajectory realizes symmetry-reduced asymptotic safety by dynamically balancing the screening and antiscreening contributions. If fundamental asymptotic safety at $y^2_{*\bullet}$ is realized, this fixes the Yukawa coupling at all scales. At the same time, the asymptotically safe trajectory constitutes an upper bound on all UV-complete trajectories, cf. Fig. 13.

[80] For negative f_y, the interacting fixed point $y_{*\,\bullet}$ lies at complex values for the Yukawa coupling and is thus unphysical. The free (MSAS) fixed point at $y_{*\,\bigcirc} \equiv 0$ is IR-attractive and violates the viability bound, cf. Sec. 4.3.

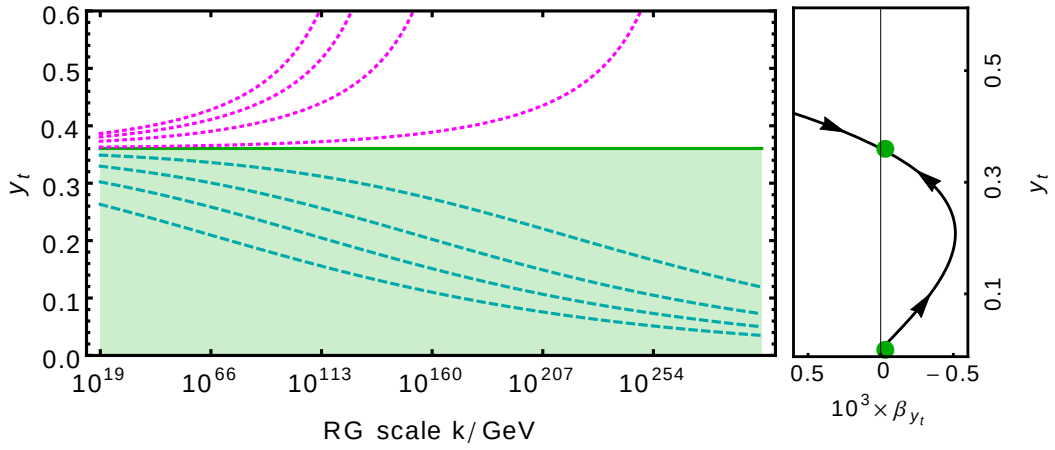

Figure 13: Left-hand panel: Transplanckian running of y_t. The asymptotically safe trajectory (solid green line) $y^2_{t\,*\bullet}$ sets an upper bound. For IR values below the upper bound (turqoise dashed lines), the trajectories are asymptotically free and emanate from $y^2_{t\,*\bigcirc}$. IR values above the upper bound (pink dotted lines) remain divergent and do not correspond to UV-complete trajectories. Right-hand panel: Flipped plot of β_{y_t} to indicate how the running in the left-hand panel results from the two corresponding fixed points (green dots). Flow lines point from the UV to the IR. Both plots are obtained with values of the following Section 4.5.

4.5 Towards an asymptotically safe UV completion for the Standard Model

Having discussed how (i) fermionic fluctuations can lead to perturbatively small gravitational propagators, cf. Sec. 4.1.2, (ii) the same regime allows for the emergence of non-trivial IR structure in global-symmetry-reducing marginal couplings, cf. Sec. 4.3, and (iii) the emergent fixed-point structure of the Yukawa coupling sets an upper bound on the Yukawa coupling, cf. Sec. 4.4, it is exciting to analyze this bound in the context of the SM.
In the following, we focus on the heavy SM sector[81], i.e., on the Abelian, weak, and strong gauge-couplings $g_Y = \sqrt{3/5}g_1$, g_2, and g_3, respectively, the top- and bottom Yukawa coupling y_t and y_b, as well as the Higgs-quartic coupling λ_H. We will discuss the full SM in Sec. 5. The heavy SM 1-loop running is given by, see, e.g., [26],

$$\beta^{(1)}_{g_i} = \frac{b_i\, g_i^3}{16\pi^2} - g_i\, f_g\,, \qquad \text{where} \quad b_Y = \frac{41}{6}\,, \quad b_2 = -\frac{19}{6}\,, \quad b_3 = -7\,, \tag{4.32}$$

$$\beta^{(1)}_{y_{t\,(b)}} = \frac{y_{t\,(b)}}{16\pi^2}\left[\frac{9}{2}y^2_{t\,(b)} + \frac{3}{2}y^2_{b\,(t)} - 3(Y_Q^2 + Y^2_{t\,(b)}) - \frac{9}{4}g_2^2 - 8g_3^2\right] - y_{t\,(b)}\, f_y\,, \tag{4.33}$$

$$\beta^{(1)}_{\lambda_H} = \frac{1}{16\pi^2}\left[\lambda\left(24\lambda + 12(y_t^2 + y_b^2) - 9g_2^2 - 3g_Y^2\right) - 6(y_t^4 + y_b^4) + \frac{9g_2^4}{8} + \frac{27g_Y^4}{72} + \frac{9g_Y^2 g_2^2}{12}\right] + \lambda_H\, f_\lambda\,, \tag{4.34}$$

[81] All the remaining Yukawa couplings are smaller than y_b and much smaller than y_t. Hence, they can consistently be neglected. Still, we include the corresponding degrees of freedom which contribute to the gauge running, that is we take lower generation quarks as well as leptons into account but approximate them as fully massless. The inclusion of sterile right-handed neutrinos will not influence the subplanckian running of the heavy SM at all because sterile neutrinos are uncharged under all the gauge groups.

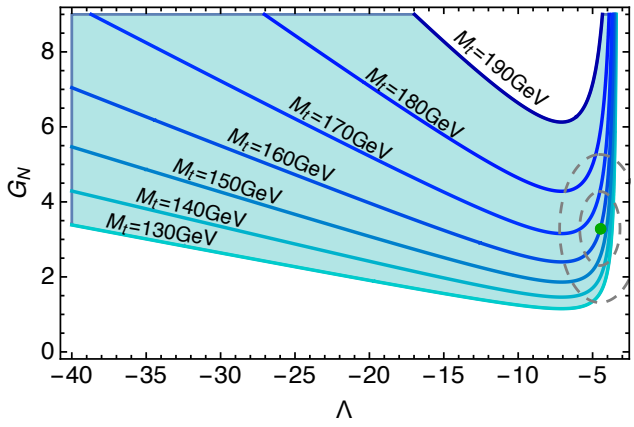

Figure 14: Contours of different top mass values at $k = 173\,\mathrm{GeV}$ (running mass) in microscopic gravitational parameter space. The green dot and gray dashed curves indicate the approximated location of gravitational couplings $G_N \equiv G$ (Newton coupling) and Λ (microscopic cosmological constant), see Eq. (4.39) and discussion in the main text.

where $Y_t = 2/3$, $Y_b = -1/3$, and $Y_Q = 1/6$ are the SM hypercharges of the right-handed top, the right-handed bottom and the left-handed quark doublet respectively. Here, we have included the dominant linear gravitational contributions f_i. They are universal to all gauge couplings f_g, all Yukawa couplings f_y, and all Higgs quartics f_λ. The f_i depend on the Newton coupling G, the cosmological constant Λ, and in principle on the infinite tower of higher-order gravitational interactions. Neglecting the influence of higher-order couplings, they read

$$f_g(G,\Lambda) = G\frac{5(1-4\Lambda)}{18\pi^2(1-2\Lambda)^2}\,, \tag{4.35}$$

$$f_y(G,\Lambda) = -G\frac{96+\Lambda(-235+\Lambda(103+56\Lambda))}{12\pi^2(3+2\Lambda(-5+4\Lambda))^2}\,, \tag{4.36}$$

$$f_\lambda(G,\Lambda) = G\frac{165-8\Lambda\,(61+\Lambda(-49+4\Lambda))}{6\pi^2\,(3+2\Lambda(-5+4\Lambda))^2}\,. \tag{4.37}$$

All these contributions are calculated in the functional RG scheme with a spectrally adjusted [308] sharp cutoff [371] and in the gravitational Landau-gauge limit. The f_y is obtained from the calculation in [9, 449], see Sec. 4.1 and App. C for the details of this derivation. It has also been calculated in [501–503][82]. Further, f_g has been obtained in [450, 496, 498–500] and f_λ can be inferred, e.g., from [107, 353, 448, 481, 501, 502, 504–506]. Scheme- and residual gauge-dependence will be explicitly discussed in Sec. 4.5.4 to infer a minimal systematic error.

4.5.1 Yukawa couplings and a viable phenomenology

Emergence of SM-like IR structure, i.e., $g_Y \neq 0$, $y \neq 0$, and $\lambda_H \neq 0$ requires $f_g >$ and $f_y >$, i.e., the respective viability bounds to be fulfilled, see Sec. 4.3. Note that $f_\lambda < 0$ is *not* required because λ_H does not further break the global symmetry structure. From the location of sign changes in the numerators in Eqs. (4.35) and (4.36) we infer that this happens at $\Lambda < 1/4$ for the gauge and at $\Lambda \lesssim -3.3$ for the Yukawa coupling. We have carefully analyzed the underlying reason for the Yukawa bound in Sec. 4.3. It remains as a crucial open question to understand whether this mechanism persists in extended truncations and whether the gravitational couplings indeed converge in this regime. In Fig. 14 we show contours of different running top-mass values in the Λ–G-plane for the Einstein-Hilbert truncation, i.e., at vanishing higher-derivative couplings

[82] In [501] trace diagrams are not included which causes for a structurally different result.

(left-hand panel)[83]. To demonstrate that non-vanishing higher-order couplings indeed influence the result, we additionally show a slice in the Λ–b plane (at $G_* = -4.51$, see Eq. (4.39) below), cf. App. C.3. Indeed it is very hard to estimate the truncation error arising due to neglected higher-derivative couplings. It is, therefore, crucial to extend truncations incorporating the full SM matter content to include higher-order interactions in the future.

4.5.2 Upper bound for the top mass from asymptotic safety

Existing gravitational truncations fulfill the gauge-viability bound [500], but most of them violate the Yukawa-viability bound, see Tab. I in [9]. Crucially, the addition of SM matter – fermionic degrees of freedom in particular – are indicated to lead to an effective mass term which suppresses propagating gravitational modes, see Sec. 4.1.2, as well as [343, 452], and thus might allow for structure to emerge. Since matter fluctuations seem to be crucial, we will use results from [343] but adjusted to the Landau gauge limit, see [482] for the corresponding gravitational contributions. For completeness, we quote the running here,

$$\beta_G = 2\,G - G^2\,f_G(\Lambda), \qquad \beta_\Lambda = -2\,\Lambda - \frac{G}{2\pi}\,f_\Lambda(\Lambda) - G\,\Lambda\,f_G(\Lambda), \tag{4.38}$$

$$\text{with} \qquad f_G(\Lambda) = \frac{5}{6\pi(1-2\Lambda)} + \frac{5}{3\pi(1-2\Lambda)^2} - \frac{1}{2\pi(3-4\Lambda)} + \frac{11+32\ln(3/2)}{12\pi} - \frac{N_W+N_S-4N_V}{6\pi}\,,$$
$$f_\Lambda(\Lambda) = 7 - \frac{3}{2(3-4\Lambda)} + \frac{2N_W-N_S-2N_V}{2} - \frac{5}{2(1-2\Lambda)} - 8\ln(3/2)\,,$$

where N_S, N_V, and N_W denote the number of real scalars, gauge bosons, and Weyl fermions, respectively ($N_S = 4$, $N_V = 12$, and $N_W = 45$ for the SM; $N_W = 48$ if right-handed sterile neutrinos are included). As we have anticipated in Sec. 4.1.2 and 4.3 the gravitational fixed point in presence of all SM degrees of freedom, i.e.,

$$G_* \approx 3.29\,, \qquad \Lambda_* \approx -4.51\,, \tag{4.39}$$

results in perturbatively small f_i and fulfils both viability bounds.

A top mass that saturates the upper bound. The combined RG equations allow to evolve the upper-bound structure presented in Fig. 13 down to the top-mass scale at $k_{\rm IR} = 173$ GeV. To do so, we initialize the combined running of heavy SM and gravitational couplings in the IR. The Newton coupling G and the cosmological constant Λ are fixed by the respective experimental values $G(k_{\rm IR}) \approx 10^{-38}{\rm GeV}^{-2} \times k_{\rm IR}^2$ and $\Lambda(k_{\rm IR}) \approx 10^{-120}{\rm GeV}^2/k_{\rm IR}^2$. The value of $G(k_{\rm IR})$ determines the Planck scale at which gravitational couplings transition to classical scaling and vanish rapidly, see Fig. 16. The precise IR-value of the cosmological constant does not influence the conclusions. For the SM couplings, we use the NNLO values from Tab. 3 in [31]. This running is also used to map the fixed-point values used to obtain the contours in Fig. 14 to values for the running top mass M_t. In Fig. 13 on the other hand, we sample different values for the top-Yukawa coupling to obtain the different trajectories. We find the predictive upper-bound

[83] The contours in Fig 14 are obtained at the fixed-point, that is each contour in M_t is mapped to a specific fixed-point value of the Yukawa coupling, for which the contour is generated. For this mapping we use the evolution of the gravitational couplings corresponding to Eqs. (4.38) below with modified matter content such that they realize the respective gravitational coupling values. We explicitly check that in all cases the gravitational running approximates closely a θ-function, but indeed subleading threshold effects remain. We use the same mapping to obtain the Λ–b contours as well, although thresholds in extended truncations might differ.

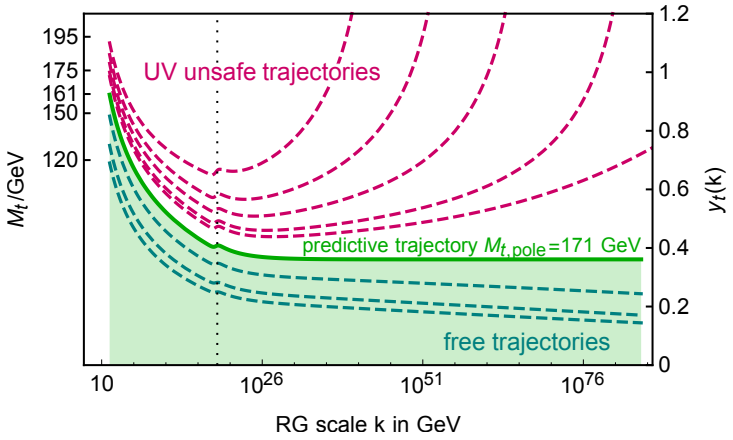

Figure 15: Upper bound on the running top mass: A larger top mass leads to UV unsafe trajectories. From the upper bound, an asymptotically safe UV regime is reached. Below the upper bound, the Yukawa coupling becomes asymptotically free. At the Planck scale (dotted vertical line) the y_t smoothly transitions from transplanckian to Standard-Model running, cf. Fig. 16 for a zoomed-in plot of the transition region.

trajectory (green line in Fig 13), which corresponds to a UV-completion at the asymptotically safe top-Yukawa fixed point, to result in a running mass of M_t = 161 GeV. Converting this particular value for running mass to the pole mass [31, 507] the present truncation obtains a value of $M_{\mathrm{t,\,pole}}$ = 171 GeV. Since this result is in striking agreement with the experimental value [27, 28], two cautious comments should be added.

Firstly, the SM itself is dominated by a partial IR-fixed point in the ratio of the top-Yukawa and the strong gauge coupling [300–303]. This fixed-point acts as an attractor towards the IR and focuses a comparatively large range of Planck-scale values to the vicinity of $M_{\mathrm{t,\,pole}}$, cf. Fig. 13. Once a weak-gravity mechanism, see Sec. 4.1.2, that obeys the Yukawa-viability bound, see Sec. 4.3, is realized, a broad range of gravitational fixed-point values will thus approximately agree with the measured top-mass value, cf. Fig. 14.
Secondly, both the gravitational contributions to the matter sector, as well as the gravitational truncation itself, are subject to several systematic errors which we will further discuss in Sec. 4.5.4:

(i) unknown systematic errors since the gravitational truncation is not yet converged,

(ii) scheme-dependence of contributions from dimensionful gravitational couplings,

(iii) residual gauge-dependence since the regulator breaks gauge invariance,

(iv) the regulator choice itself introduces a systematic error.

Given that (i) and (ii) are hard to estimate without access to extended truncations, the upper-bound structure close to SM values should be regarded as a tentative mechanism that encourages further studies. That said, the minimal systematic error which can be estimated is dominated by changes arising from varying the regulator. This shifts the gravitational fixed-point values roughly by 60%, cf. [8] and references therein. In Fig. 14 we display a corresponding ellipsis of 60% overall spread and another with 60% spread in each direction. As a result one can infer error estimates of $M_{\mathrm{t,\,pole}} = 171^{+30}_{-171}$ GeV. In particular, a violation of the Yukawa structure-bound which would predict a vanishing top-mass remains within the systematic uncertainty. This reflects that it is of great importance to put further theoretical effort into determining whether

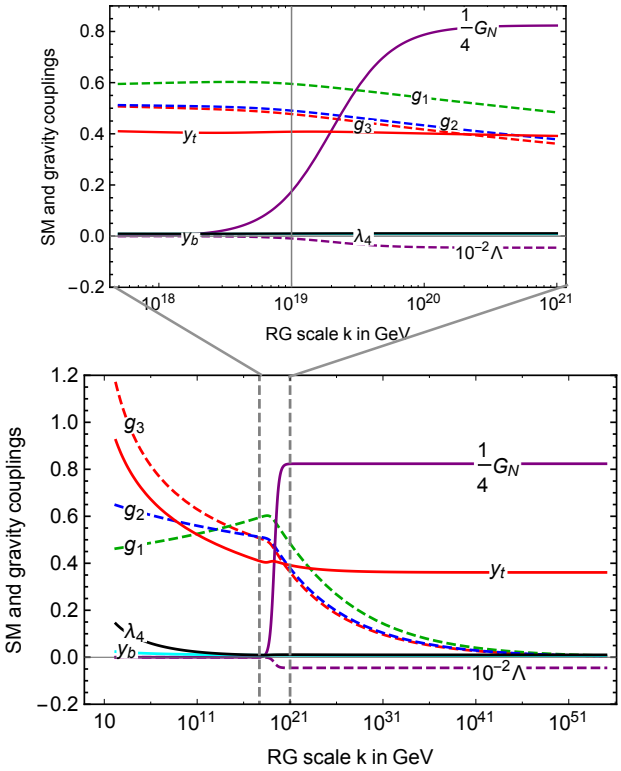

Figure 16: Running of the couplings of the SM as well as the Newton coupling G and the cosmological constant Λ with Renormalization Group scale k. Above the Planck scale, the theory approaches a scale-invariant asymptotically safe regime. Below the Planck scale, matter couplings run as in the pure SM. The zoomed-in region (upper panel) around the Planck scale shows that all couplings smoothly transition from asymptotically safe running above to pure SM running below the Planck scale. In this threshold regime, the gravitational couplings quickly transition from asymptotically safe to classical scaling.

a convergent weak-gravity mechanism can be established in asymptotically safe gravity-matter systems.

4.5.3 First trajectories of an asymptotically safe Standard Model

Under the assumption that convergence of the weak-gravity mechanism can be established, asymptotically safe quantum gravity could UV-complete the SM, cf. Fig. 16. Above the Planck scale the IR-attractive couplings are initialized at their constant fixed-point values, cf. Eq. (4.39). The deviation from scale invariance in all the IR-repulsive directions is fixed by experimental values. At the Planck scale, the gravitational couplings quickly transition to approximately vanishing values, see Fig. 16. This threshold regime only extends over roughly 2 orders of magnitude, below which gravitational fluctuations have effectively turned off and the 1-loop SM running takes over. Taking the present truncation at face value suggests that this UV-completion emanates from an asymptotically safe fixed point at

$$y_b^* = 0\,, \quad y_t^* = 0.36\,, \quad \lambda_4^* = 0.01\,, \quad g_i^* = 0\,. \tag{4.40}$$

It realizes an asymptotically safe fixed point for the top-Yukawa coupling. Hence, the top mass corresponds to an IR-attractive direction and is thus fixed by quantum scale-symmetry of the UV-completion. It is "retrodicted" at $M_t = 161\,\text{GeV}$ running mass, i.e., $M_{\text{t, pole}} = 171\,\text{GeV}$ pole mass, in agreement with observation. Motivated by this intriguing result, we systematically explore the maximal possible enhancement of predictive power for perturbative asymptotically safe UV-completions of the SM in Sec. 5.

Here, all the gauge couplings, as well as all other Yukawa couplings are asymptotically free, cf. Fig. 16, and thus remain as free parameters. The Higgs-quartic coupling is the only other IR-attractive and hence predicted direction. Its finite fixed-point value automatically follows

from the finite top-Yukawa fixed point, cf. Eq. 4.34. Since the scalar quartic coupling is not protected by an additional global symmetry, it has to be non-vanishing once the top-Yukawa coupling is finite. The positive fixed-point value for λ_H results in a Higgs mass of 131 GeV and it remains as an open question for now whether induced or higher-order interactions can reconcile stability with a consistent IR value. We also stress that the electroweak scale is *not* predicted but an input of our calculation and we accept the associated fine-tuned initial condition as one free parameter of the theory.
A UV-completion remains accessible even if the value of f_y should increase in convergent truncations. In that case, the full SM would become asymptotically free. The Yukawa coupling would then realize one of the turquoise-dashed lines in Fig. 13. As long as $f_\lambda > 0$, the scalar quartic coupling remains a prediction. In fact, the predicted IR-value for λ_H decreases if the Yukawa coupling becomes asymptotically free and is further lowered, the faster the transplanckian running of the Yukawa coupling, i.e., the larger f_y. Eventually, the presented weak-gravity mechanism explicitly realizes the scenario proposed in [34]. We already pointed out, that the present analysis implies that fulfilling the Yukawa structure-bound requires a weak-gravity mechanism. Hence, a large f_y necessary to realize the Higgs-mass prediction in [34] could be problematic.
Finally, the presented mechanism is very sensitive to extra degrees of freedom since the latter influence the gravitational fixed-point values, cf. Eq. (4.1). For instance, the inclusion of three right-handed neutrinos shifts the top pole-mass to 182 GeV. This reflects the intuitive notion that scale-invariance is a non-local (in energy scale) property of a quantum field theory. Once established, degrees of freedom at arbitrary scales will modify and possibly spoil it.

4.5.4 Systematic errors and convergence

Convergence and backreaction. The presented weak-gravity mechanism and, in particular, the obtained top-mass value in the IR are subject to unknown systematic errors because the gravitational truncation is not yet converged. This concerns extensions to higher-order gravitational operators [348, 360–366, 368–370, 372–376] which have to be reassessed in the presence of SM matter, the effect of non-minimal couplings [354, 451, 452, 481, 482], and the backreaction of induced matter couplings. We have verified that contributions from induced pure-matter couplings are negligibly small, cf. App. C.4. Understanding the remaining systematic errors amounts to establishing whether asymptotically safe gravity persists and converges to realize a weak-gravity mechanism in the presence of Standard-Model matter. This remains as an outstanding task for future research on asymptotically safe gravity-matter systems.

Scheme-dependence. For all QFTs, the coefficients in β-functions beyond two-loop order depend on the RG scheme [18]. Only one-loop (two-loop) contributions from marginal couplings are universal to all (massless) RG-schemes. The present analysis combines the 1-loop SM running of a perturbative RG scheme with gravitational contributions obtained in a functional RG scheme. The 1-loop β-functions of the SM are universal to all RG-schemes since they only comprise marginal couplings. In particular, the same contributions result from functional RG calculations. Hence, the presented RG flows correspond to a consistent functional RG-scheme. But, the NNLO matching combines two inequivalent RG-schemes which introduces an error. The same holds for repeating the analysis with higher-order perturbative SM β-functions. Instead, it is very desirable to evolve the full SM down to the electroweak scale purely within the functional RG scheme. At the respective top-mass scale one could then infer the respective freezeout value. While the coefficients of β-functions remain scheme dependent, physical quantities such as the freezeout value of the top mass are not.

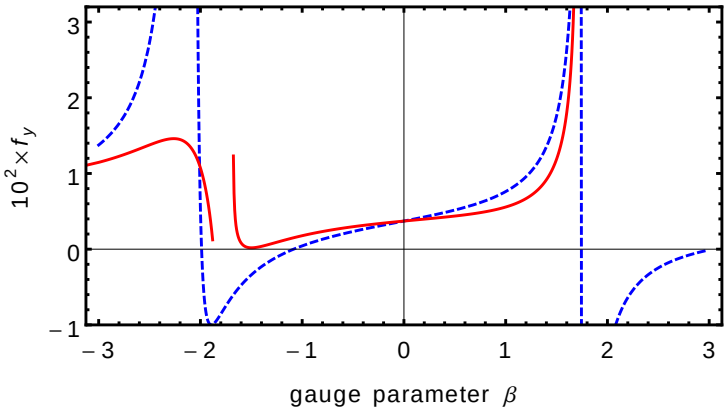

Figure 17: Dependence of the gravitationally induced contribution to Yukawa couplings f_y on the gravitational gauge parameter β: in comparison to the direct gauge dependence of f_y (blue-dashed line), taking also the gauge-dependence of gravitational fixed-point values into account (solid-red line) softens the overall dependence on β.

Gauge-dependence. In all calculations of this section, we have employed a de-Donder type gauge fixing for the metric fluctuations by adding a gauge fixing term

$$S_{\text{gauge-fixing}} = \frac{1}{16\pi \overline{G}} \frac{1}{2\alpha} \int d^4x \sqrt{\overline{g}}\, \overline{g}^{\mu\nu} F_\mu F_\nu \qquad \text{with} \quad F_\mu = \left[\delta^\rho_\mu \overline{D}^\sigma - \frac{1+\beta}{d} \overline{g}^{\sigma\rho} \overline{D}_\mu\right] g_{\rho\sigma} \,, \quad (4.41)$$

where g is the full metric and $\overline{g}$ the background metric which we choose to be flat. Also, $\overline{D}$ denotes the covariant derivative for the background metric. The gauge fixing depends on two parameters α and β. Since the choice of background and the mass-like regulator break gauge invariance, its dependence on the gauge parameters α and β does not fully drop out in the final results. See, e.g., [508–515] for efforts to derive a gauge-invariant formulation of the functional RG. Here, we will analyze how large the regulator-induced gauge-dependence is.
Throughout this section we have chosen $\alpha = 0$ and $\beta = 0$. The former is theoretically favorable, as it strictly implements the gauge-fixing condition and moreover corresponds to an attractor of the flow [468, 469]. There are no strong arguments for a favorable choice of β, see [347] for an analysis concerning the principle of minimum sensitivity.
Regulator-induced gauge-dependence occurs whenever the propagator of metric fluctuations enters the calculation. Hence, there are two sources of gauge dependence in the gravitational contribution[84] to Yukawa couplings f_y. A direct gauge-dependence arises from gravitational fluctuations contributing to the running of the Yukawa coupling. Additionally, also the gravitational fixed-point values themselves pick up a regulator-induced gauge-dependence. This feeds back into the value of f_y and contributes an indirect gauge-dependence. In Fig. 17 we compare the purely direct gauge-dependence (blue dashed line) with the combined direct and indirect one (solid red line). It is encouraging that the overall gauge-dependence seems to be attenuated as compared to the direct one alone. This might be taken as an indication that in a converged truncation gauge-dependence cancels out entirely. In particular, $f_y > 0$ holds apart from very confined regions close to poles where very likely the truncation breaks down. For $\beta \gtrsim 1.8$, the gravitational fixed point does not exist and we cannot obtain a combined gauge-dependence any longer.

[84] Here, we only consider direct gravitational contributions to f_y, neglect the subleading feedback of induced couplings, and approximate the loop-anomalous dimensions to be vanishing, see Sec. 4.3.

Sec. 4 indicates that leading-order asymptotically safe gravitational fluctuations at and beyond the Planck scale result in constant and perturbatively small anomalous dimensions for all matter couplings. Without further assumptions, we investigate the available fixed-point structure for the Standard Model within the perturbative regime. Because gravitational contributions are universal to all gauge couplings and all Yukawa couplings (as well as to all quartic couplings), respectively, this introduces only two (three) free parameters. Quantum scale symmetry could enhance the predictive power of the Standard Model by placing upper bounds on all Yukawa couplings, Abelian gauge couplings, and the quartic coupling. The number of predicted relations can thus outweigh the two (three) free parameters. We thereby uncover a mechanism which links the mass difference of top and bottom quark to their charge ratio, present a dynamical mechanism which favors small Dirac neutrino-mass, and successfully extend the UV-completion to the CKM-Yukawa sector.

5 The asymptotically safe Standard Model (ASSM)

The three open riddles of modern physics (i) dark matter, (ii) the baryon asymmetry of the universe, and (iii) neutrino masses all permit explanations that leave the Standard-Model running of couplings untouched, see Sec. 1. Moreover, the Standard Model[85] (SM) is consistent up to the Planck scale, see Sec. 1.2, with the Higgs-potential providing a strong hint for Planckian scale invariance. The only actual inconsistency in the SM (or νSM, cf. Sec. 1) are the transplanckian Landau poles. At the same time, an effective-field-theory (EFT) treatment of quantum corrections to gravity inevitably predicts a new-physics scale, more precisely, a strong-coupling scale: the Planck scale M_{Planck}. Consequently, the present thesis explores a radical change of paradigm: instead of electroweak-scale model building, it attributes *all* new physics to scale invariance and Planckian energy scales.
A mechanism and first quantitative indications for a weak-gravity regime of asymptotic safety in which perturbatively small gravitational contributions could UV-complete the SM was uncovered in Sec. 4. The suggested mechanism hinges on a large and negative fixed-point value for the cosmological constant driven by fluctuations of the comparatively large number of SM fermions.
This serves as a strong motivation to independently explore the minimal perturbative modifications required to UV-complete the SM. While keeping the quantum gravitational motivation in mind, the following results can also be viewed as a minimal parameterization of any scale-invariant new physics that resolves the Landau-pole problems and therefore UV-completes the SM.

5.1 Standard-Model UV-completion from dimensional reduction

The lack of antiscreening self-interactions leads to a fundamental inconsistency in the SM: given its measured value, the U(1)-hypercharge coupling develops a Landau pole at $\approx 10^{41}$ GeV, see Sec. 1.2.2. In this context, it is insightful to recall the discussion of the ϵ-expansion and asymptotic-safety mechanisms in Sec. 2.3: A QFT with screening self-interactions in its critical dimension D_c develops both an asymptotically free and an IR-attractive asymptotically safe fixed point below its critical dimension, i.e., for $D = D_c - \epsilon$. Reduction of the spacetime dimension turns the marginal coupling in D_c into a relevant coupling in $D_c - \epsilon$. For the SM U(1) gauge

[85] The same arguments also hold for the minimally extended Standard Model (νSM), see Sec. 1.1.1, since the additional sterile neutrinos do not alter the running.

coupling g_Y, $D_c = 4$. In $D = 4 - \epsilon$ the 1-loop running reads

$$\beta_{g_i} = \frac{b_i\, g_i^3}{16\pi^2} - \frac{\epsilon}{2}\, g_i \,. \tag{5.1}$$

Since there are no self-interactions, the screening matter fluctuations dominate, i.e., $b_Y = 41/6$. In $D = 4$, this makes the Landau-pole problem evident. But, in $D = 4 - \epsilon$, i.e., $\epsilon > 0$, dimensional reduction adds an effective antiscreening contribution. The β-function, cf. Eq. (5.1), now allows for both an asymptotically free and an asymptotically safe fixed point, cf. Sec. 4.3, and the Landau pole is avoided.
The same argument of the antiscreening effect of dimensional reduction also holds in the Higgs-Yukawa sector. Indeed, if spacetime is dimensionally reduced above some new-physics scale $M_{\rm NP}$ to, for instance, $D = 3$, i.e., $\epsilon = 1$, this removes all Landau poles and UV-completes the entire SM.

In the "top-down" picture of Sec. 4, the structure of a linear antiscreening contribution resembles the effect of gravitational contributions to non-maximally symmetric couplings required for infrared structure, cf. Sec. 4. Here, we have now argued for the same – antiscreening and linear – contributions by demanding minimal new physics contributions which remove the Landau poles of the SM. Together this motivates the following simple assumptions:

- We assume no additional degrees of freedom which modify the SM running below the new-physics scale $M_{\rm NP}$.
- We assume a constant new-physics contribution

$$f_i = \begin{cases} 0, & k < M_{\rm NP} \\ \text{const}, & k \geq M_{\rm NP}, \end{cases} \tag{5.2}$$

  which contributes (at least to leading order) linearly in the respective SM couplings. Resembling gravity, we allow for different contributions to the different type of SM couplings, i.e., for a contribution f_g, universal to all gauge couplings, a contribution f_y, universal to all Yukawa couplings, and a contribution f_λ for the Higgs-quartic coupling.
- Finally, we will only explore the perturbative regime which we identify with $f_i \ll 1$. This allows us to self-consistently use the perturbative 1-loop (and for validation also the 2-loop) β-functions.

In this very simple setup, we explore the available fixed-point structure, with a particular focus on maximally enhanced predictivity. Indeed, we will rediscover the same mechanisms as in Sec. 4, but from a minimal "bottom-up" perspective. Interpreting the new-physics contribution as arising from the sharp transition into an asymptotically safe gravitational scaling regime, see Sec. 2.4.2, and identifying $M_{\rm NP} = M_{\rm Planck}$ with the Planck scale, recovers the effect of asymptotically safe quantum gravity. In this context, it is very suggestive, that completely unrelated arguments for an effective dimensional reduction of spacetime arise in many different quantum-gravity models, i.e., in string theory [516], in dynamical triangulations [517], in loop quantum gravity [518], from the Wheeler-DeWitt equation [519], in causal sets [520, 521], and in asymptotic safety [522–524], cf. [525] for a recent review.

The β-functions of any gauge-Yukawa theory, in particular, the SM, exhibit a loop-level hierarchy: The 1-loop running of all of the gauge couplings is not influenced by any of the other

fixed point	$g^2_{Y,*}$	$g^2_{2,*}$	$g^2_{3,*}$	viable for	critical exponents
$\mathrm{FP}^{g_Y g_2 g_3}_{\bigcirc\bigcirc\bigcirc}$	0	0	0	$f_g > \frac{41}{6}\frac{g^2_Y(k=M_{\rm NP})}{16\pi^2}$	$(f_g,\, f_g,\, f_g)$
$\mathrm{FP}^{g_Y g_2 g_3}_{\bullet\bigcirc\bigcirc}$	$16\pi^2\frac{6\,f_g}{41}$	0	0	$f_g = \frac{41}{6}\frac{g^2_Y(k=M_{\rm NP})}{16\pi^2}$	$(-f_g,\, f_g,\, f_g)$

Table 5: List of fixed points which can UV-complete the SM gauge-sector (g^2_Y, g^2_2, g^2_3). The naming convention indicates which of the gauge-couplings vanishes (white circle) or not (black circle) value.

couplings. Yukawa (quartic) couplings only contribute at 2-loop (3-loop). The Yukawa couplings do depend on the gauge couplings at 1-loop but are not influenced by the scalar quartic couplings which only contribute at 2-loop. This allows to first discuss the gauge-coupling fixed points in terms f_g, separately; then discuss the Yukawa coupling fixed points in terms of f_y; and finally the available fixed points for the quartic coupling in terms of f_λ.

5.2 Gauge couplings and upper bounds from asymptotic safety

The above ordering allows discussing the fixed-point structure for gauge couplings independently. In the case of an Abelian gauge-group, for which there are only screening contributions from matter fluctuations[86], the fixed-point and the emerging upper-bound have the same structure as for the Yukawa coupling in Sec. 4.4, cf. also [500] for an analysis along the lines of Sec. 4.5. Using the same notation as for the Yukawa coupling in Eq. 4.30, the fixed points are summarized in Tab. 5. For an antiscreening new-physics contribution, i.e., $f_g > 0$, the free fixed point is UV-attractive and trajectories can emanate from it. At the same time, the interacting fixed point becomes physical. Since it is IR-attractive, it focuses all trajectories emanating from the free FP and sets an upper bound for any emergent IR physics, cf. Fig. 13 in Sec. 4.4. Hence, there is a critical strength of the antiscreening new-physics contribution, i.e., $f_g = f_{g,\rm crit} \approx 9.7\times10^{-3}$, for which it becomes possible to accommodate the Abelian gauge coupling of the SM. For all values $f_g > f_{g,\rm crit}$, the Abelian SM gauge-coupling value is accommodated on an asymptotically free trajectory [500]. More generally, the phenomenological scale-dependent coupling value $g_i(k)$ of any screening gauge-group sets a critical $f_{g,\rm crit} = \frac{g_i^2(k=M_{\rm NP})}{16\pi^2}\, b_Y$ required to accomodate its RG trajectory. Regarding the antiscreening non-Abelian gauge-couplings, i.e., $b_i < 0$, there are no phenomenological constraints on f_g at all[87].

5.3 Single-generation Yukawa fixed-points

To remain as instructive as possible, we will first restrict the discussion to an analysis of the fixed-point structure of the 3rd generation of SM fermions including a right-handed neutrino. Besides the Abelian, weak, and strong gauge couplings g_Y, g_2, and g_3, this includes the top (y_t), bottom (y_b), tau (y_τ) and a possible tau-neutrino (y_{ν_τ}) Yukawa coupling[88]. We do however include the correct number of fluctuating fields in the gauge-coupling evolution. Multiple generations and mixing will be discussed in Sec. 5.4.

[86] The same applies for non-Abelian gauge groups for which the screening fermionic contributions dominate.

[87] For $f_g > 0$, the free fixed point is UV-attractive. Trajectories emanating from it can reach all IR values. The interacting fixed point is unphysical since it lies at negative $g^2_{i,*}$. For $f_g < 0$, on the other hand, the free fixed point is IR-attractive, but now the interacting fixed point lies at positive values. Again, there exists a UV-attractive fixed point at positive $g^2_{i,*}$ from which all IR-values can be reached.

[88] We refrain from also analyzing the Higgs-quartic coupling λ_H in this section.

fixed point	$y^2_{t,*}$	$y^2_{b,*}$	θ_1	θ_2
$\mathrm{FP}^{g_Y y_t y_b}_{\bullet\circ\circ}$	0	0	$\frac{5f_g}{82}+f_y$	$\frac{17f_g}{82}+f_y$
$\mathrm{FP}^{g_Y y_t y_b}_{\bullet\bullet\circ}$	$\frac{16\pi^2}{369}(17f_g+82f_y)$	0	$-\frac{f_g}{123}+\frac{2f_y}{3}$	$-\frac{17f_g}{82}-f_y$
$\mathrm{FP}^{g_Y y_t y_b}_{\bullet\circ\bullet}$	0	$\frac{16\pi^2}{369}(5f_g+82f_y)$	$-\frac{5f_g}{82}-f_y$	$\frac{23f_g}{123}+\frac{2f_y}{3}$
$\mathrm{FP}^{g_Y y_t y_b}_{\bullet\bullet\bullet}$	$\frac{4\pi^2}{123}(23f_g+82f_y)$	$-\frac{4\pi^2}{123}(f_g-82f_y)$	$\frac{-33f_g-246f_y-\#}{328}$	$\frac{-33f_g-246f_y+\#}{328}$

Table 6: List of fixed points which can UV-complete the 3rd-generation quark-Yukawa sector. We name the FPs according to which of the gauge- and Yukawa-couplings $(g_Y^2,\, y_t^2,\, y_b^2)$ take vanishing ($\circ$) or non-vanishing ($\bullet$) values. The non-Abelian gauge couplings are asymptotically free, i.e., vanish as well. Also, we have fixed the SM charges $Y_Q \to \frac{1}{6}$, $Y_u \to \frac{2}{3}$ and $Y_d \to -\frac{1}{3}$, and use the shorthand notation $\# = \sqrt{1273 f_g^2 + 1804 f_g f_y + 6724 f_y^2}$.

The set of 1-loop Yukawa β-functions, including the aforementioned linear new-physics contributions f_y, are given by

$$\beta^{(1)}_{y_{t\,(b)}} = \frac{y_{t\,(b)}}{16\pi^2}\left[\frac{9}{2}y^2_{t\,(b)} + \frac{3}{2}y^2_{b\,(t)} + y^2_\tau + y^2_{\nu_\tau} - 3\big(Y_Q^2 + Y^2_{t\,(b)}\big)\, g_Y^2 - \frac{9}{4}g_2^2 - 8g_3^2\right] - y_{t\,(b)}\, f_y\,, \tag{5.3}$$

$$\beta^{(1)}_{y_{\tau\,(\nu_\tau)}} = \frac{y_{t\,(b)}}{16\pi^2}\left[\frac{5}{2}y^2_{\tau\,(\nu_\tau)} + \frac{1}{2}y^2_{\nu_\tau\,(\tau)} + 3y_t^2 + 3y_b^2 - 3\big(Y_L^2 + Y^2_{\tau\,(\nu)}\big)\, g_Y^2 - \frac{9}{4}g_2^2\right] - y_{\tau\,(\nu_\tau)}\, f_y\,. \tag{5.4}$$

They agree with the full νSM 1-loop β-functions in the respective limit of vanishing lower-generation Yukawas, cf., e.g., [26, 526]. The SM hypercharge assignments $Y_{t/b/\tau/\nu_\tau}$ and $Q_{L/B}$ can be found in Tab. 1. The choice of adding a right-handed neutrino to the SM is only important for the results in Sec. 5.3.2.

Given the gauge contributions in Eqs. (5.3) and (5.4), the set of fixed points in the heavy-generation Yukawa sector will depend on the fixed-point value of gauge couplings. Aiming for maximal predictivity, we focus on the more predictive gauge-coupling fixed point with non-vanishing $g_{Y\,*}$, for which the experimental value already fixes the new-physics contribution to $f_g \approx 9.7 \times 10^{-3}$.

5.3.1 Mass-difference for charged quarks from asymptotic safety

Focussing on the 3rd-generation quark-Yukawa couplings y_t and y_b, i.e., setting $y_\tau = y_{\nu_\tau} = 0$, the β-function in Eq. (5.3) is exchange symmetric under $t \leftrightarrow b$ symmetry – except for the U(1) contribution $\sim Y^2_{t\,(b)}\, g_Y^2$. The latter distinguishes top and bottom quark in the SM by their distinct right-handed hypercharges $Y_t = 2/3$ but $Y_b = -1/3$.
While the Yukawa fixed-point structure at vanishing gauge coupling is $(t \leftrightarrow b)$-symmetric as well[89], the four available top-bottom fixed points, cf. Tab. 6 for non-vanishing gauge couplings are not. We focus on the most predictive fixed point $\mathrm{FP}^{g_Y g_2 g_3}_{\bullet\bullet\bullet}$. Specifying to SM charges, solving the three fixed-point equations to eliminate f_g and f_y reveals the key scale-symmetry relation

$$y^2_{t\,*} - y^2_{b\,*} = \frac{1}{3}g^2_{Y\,*}\,. \tag{5.5}$$

[89] In this case, $f_y > 0$ is necessary to accommodate non-vanishing Yukawa couplings, see Sec. 4.

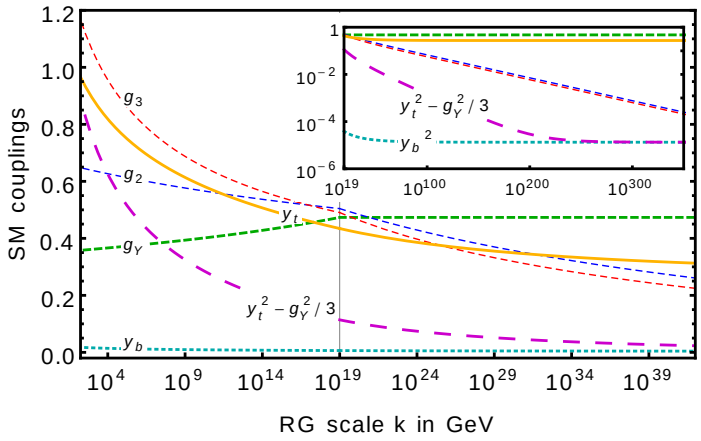

Figure 18: Running of SM couplings for $f_g = 9.7 \times 10^{-3}$ and $f_y = 1.188 \times 10^{-4}$, realizing $g(k_{\rm IR}) = 0.358$, $y_t(k_{\rm IR}) = 0.965$, and $y_b(k_{\rm IR}) = 0.018$ in the IR, i.e., at $k_{\rm IR} = 173\,{\rm GeV}$. The pink wide-dashed line evolves the scale-symmetry relation $y_t^2 - g_Y^2/3$, cf. Eq. (5.5), which approaches y_{b*}^2 (dotted line) in the far UV.

This relation is a consequence of the predictive power of asymptotic safety – there are three predicted couplings (g_{Y*}, y_{t*}, y_{b*}) – outgrowing the number of free parameters (f_g, f_y). Most excitingly, even without precise knowledge of f_g and f_y, FP$^{g_Y g_2 g_3}_{\bullet\bullet\bullet}$ makes an exact prediction.
As for the 1-dimensional case, cf. Sec. 2.2.2 and Sec. 4.3, the maximally predictive fixed-point bounds trajectories emanating from less-predictive fixed points. It distinguishes the unique UV-complete theory with the largest distance in theory space from the maximally-symmetric fixed point at the origin. Critical trajectories between FP$^{g_Y g_2 g_3}_{\bullet\bullet\bullet}$ and less predictive fixed points such as FP$^{g_Y y_t y_b}_{\bullet\bullet\circ}$ or FP$^{g_Y y_t y_b}_{\bullet\circ\bullet}$ trace the boundaries of this region.

Enhanced predictive power. This maximally predictive form of scale symmetry can be compared to observations by evolving the RG-flow from FP$^{g_Y y_t y_b}_{\bullet\bullet\bullet}$ down to the electroweak scale, more precisely, down to $k_{\rm IR} = 173\,{\rm GeV}$, cf. Fig. 18. This requires to also evolve the non-Abelian gauge couplings such that they match with observation. Since they remain asymptotically free, they correspond to two UV-attractive directions. Towards the IR, their departure from scale symmetry has to be fixed by the two corresponding experimental values, i.e., $g_2(k_{\rm IR}) = 0.64779$ and $g_3(k_{\rm IR}) = 1.1666$, see, e.g., [31]. We stress that the only further two free parameters are f_g and f_y: $f_g = 9.7 \times 10^{-3}$ is fixed by $g_Y(k_{\rm IR} = 173\,{\rm GeV}) = 0.358$; further, we choose $f_y = 1.188 \cdot 10^{-4}$. Quite surprisingly, this choice realizes IR values for the top and bottom Yukawa couplings, i.e., $y_t(k_{\rm IR}) = 0.965$ and $y_b(k_{\rm IR}) = 0.018$, in close vicinity of the experimental values[90].
Put differently, the maximally-predictive fixed point constitutes evidence for a fundamental scale symmetry. At low energies, this symmetry is hidden. It is revealed by a minimal Planck-scale UV-completion, i.e., adding f_g and f_y, and evolving the SM running couplings towards the UV. The dynamical emergence of the associated scale-symmetry relation, cf. Eq. (5.5), can be observed in Fig. 18.

[90] The top-Yukawa value is actually a bit too large. It corresponds to $y_t(k = 168\,{\rm GeV}) = 0.967$ and thus to a top pole mass [527] of $M_t = 178\,{\rm GeV}$. This discrepancy can be attributed to threshold effects which are neglected here. If asymptotically safe gravity generates f_g and f_y, the transition is not sharp, as in Eq. (5.2). Instead, they continuously transition to zero over roughly two orders of magnitude, cf. Fig. 16. From the explicit gravitational running in Sec. 4.5, we infer that this results in an error of 1-5%. Indeed, Fig. 16 also suggests, that these threshold corrections would indeed result in a lower M_t.

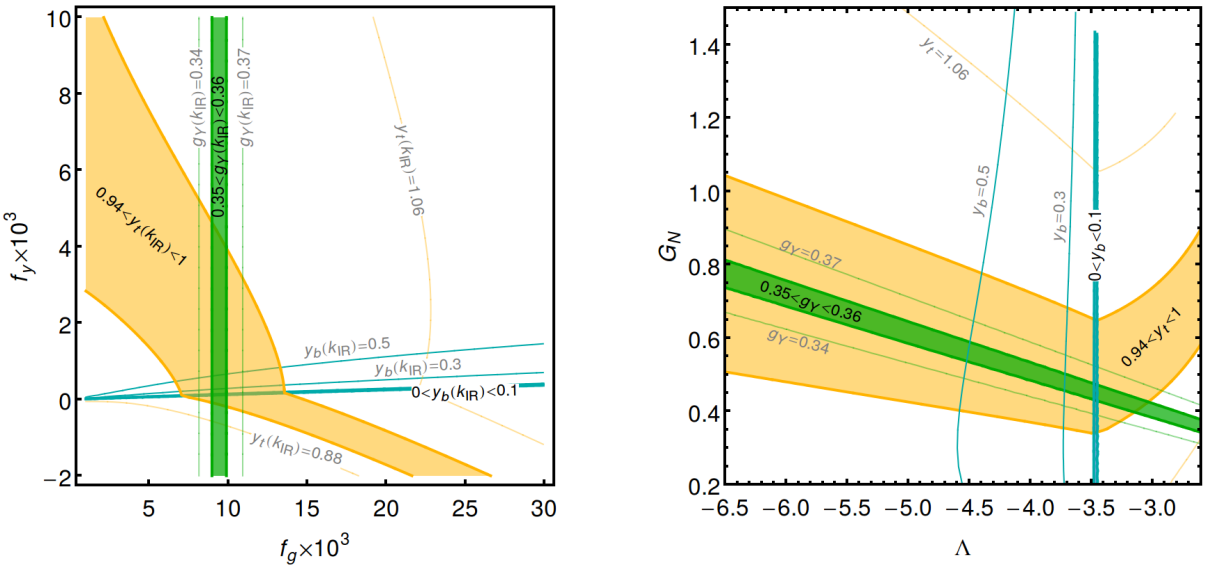

Figure 19: Left panel: Bands of IR values of the couplings $g_{Y,\mathrm{IR}}$, $y_{t,\mathrm{IR}}$ and $y_{b,\mathrm{IR}}$ at the top-mass scale $k_{\mathrm{IR}} = 173\,\mathrm{GeV}$, as a function of asymptotically safe gravity contributions f_g and f_y, see also [5]. Right panel: The same bands in the plane spanned by the dimensionless Newton coupling $G \equiv G_N$ and the dimensionless cosmological constant Λ, cf. [8, 500].

Gravitational parameter space. Here, we examine the antiscreening new-physics contributions f_g and f_y away from their experimentally favored values to scrutinize how non-trivial the uncovered scale-symmetry relation in Eq. (5.5) is. To do so, we sample the RG evolution for a grid of different values of f_g and f_y. Modifying the latter results in modified $g(k_{\mathrm{IR}})$, $y_t(k_{\mathrm{IR}})$, and $y_b(k_{\mathrm{IR}})$ in the IR. In the left panel of Fig. 19 we present the resulting contours and highlight regions in the vicinity of the observed values. This visualizes that the scale-symmetry relation between the IR coupling values is non-trivial. To give an example, a larger gauge coupling $g_Y(k_{\mathrm{IR}}) > 0.37$, a smaller Yukawa coupling $y_t(k_{\mathrm{IR}}) < 0.88$, or both at the same time, appear to be incompatible with a non-vanishing $y_b(k_{\mathrm{IR}}) > 0$. Moreover, we use the approximate gravitational contributions in Sec. 4, cf. Eqs. (4.35)-(4.36), to also obtain the contours in gravitational coupling space. The right-hand panel in Fig. 19 shows the resulting slice through theory space spanned by the Newton coupling G and the cosmological constant Λ assuming vanishing higher-order gravitational couplings. We conclude by emphasizing that a realization of this maximally predictive UV-completion in asymptotically safe gravity requires that the gravity-matter fixed point converges to realize a weak-gravity mechanism, cf. Sec. 4.

Mass difference from charge difference. The $(t \leftrightarrow b)$ exchange symmetry is broken only by the respective U(1) contributions $\sim Y^2_{t(b)}\, g^2_Y$, cf. Eq. (5.3). For equal right-handed hypercharges, i.e., $Y_t = Y_b$, the maximally predictive fixed would thus predict $y_{t*} = y_{b*}$. This suggests that the generated mass ratio is tied to the quark charges. Keeping the charges arbitrary, the scale-symmetry relation in Eq. 5.5 reads

$$y^2_{b*} = y^2_{t*} - (Q^2_t - Q^2_b) g^2_{Y*}\,, \tag{5.6}$$

where $Q_{t(b)} = Y_{t(b)}$ are the electric charges of the top and bottom quark. The latter equate to the hypercharges, because the right-handed quarks transform as singlets under the weak gauge symmetry. Furthermore, $Q_b = Q_t - 1$ and $Y_Q = Q_t - 1/2$ have to hold to ensure equal electric

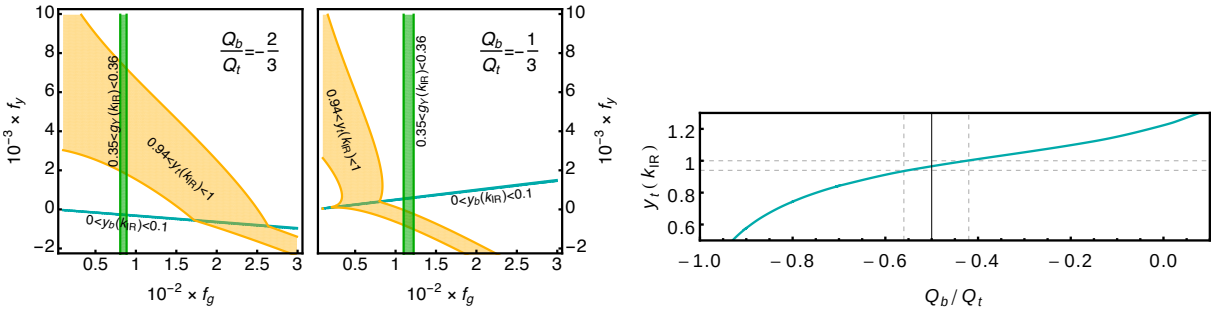

Figure 20: Left-hand panel: For charge ratios Q_b/Q_t deviating from the SM value, the same observational contours as in Fig. 19 do not overlap. Right-hand panel: Top-Yukawa coupling $y_t(k_{\rm IR})$ at $k_{\rm IR} = 173\,\text{GeV}$ with varying charge ratio Q_b/Q_t at fixed $g_Y(k_{\rm IR}) = 0.358$ and $M_b = 4.9\,\text{GeV}$.

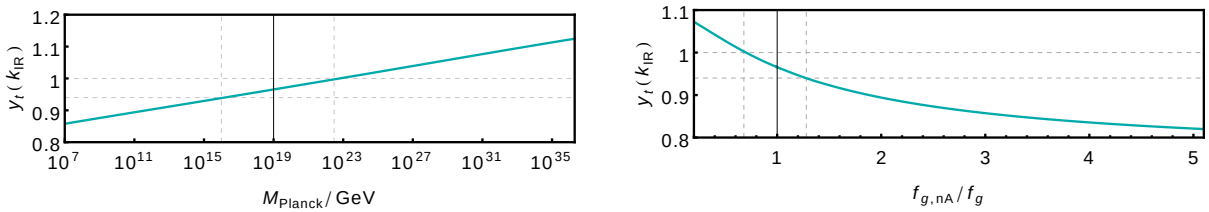

Figure 21: Left-hand panel: Top-Yukawa coupling $y_t(k_{\rm IR})$ at $k_{\rm IR} = 173\,\text{GeV}$ with varying new-physics scale $M_{\rm NP}$. Right-hand panel: Top-Yukawa coupling $y_t(k_{\rm IR})$ at $k_{\rm IR} = 173\,\text{GeV}$ with varying non-universal new-physics contribution $f_{g,\rm nA}/f_g$. In all cases we fix $g_Y(k_{\rm IR}) = 0.358$ and $M_b = 4.9\,\text{GeV}$.

charges for the left- and right handed top and bottom quark.
Repeating the above analysis for other choices of hypercharges demonstrates that the enhanced predictive power of the uncovered UV-completion uniquely ties the experimentally observed mass difference of top and bottom quark to their SM charge ratio $Q_b/Q_t = -1/2$, cf. right-hand panel in Fig. 20. For other charge ratios, the experimental contours do not overlap, cf. two right-hand panels in Fig. 20.

Is this a signature of quantum gravity? Finally, we observe that the uncovered scale-symmetry relation in Eq. (5.5) points to the prototypical properties of quantum gravity. Two key features of quantum gravity are (i) its intrinsic scale – the Planck scale – and (ii) that its contributions are blind to the internal symmetries of matter fields. Varying the scale of new physics, the left-hand panel in Fig. 21 reveals that the mechanism favors the Planck scale. The universality of gravitational contributions to gauge fields can, for instance, be broken by allowing for a distinct $f_{g,\rm nA}$ to replace f_g in the running of g_2 and g_3. As displayed in the right-hand panel in Fig. 21, the mechanism also favors universal contributions to all gauge fields.

5.3.2 Dynamically vanishing Dirac-neutrino masses from scale-invariance

Extending the analysis to the 3rd-generation lepton sector (including a right-handed neutrino such as to allow for a neutrino-Yukawa coupling), we will focus on the maximally predictive fixed point both in the gauge as well as in the heavy-generation quark sector, i.e., we extend the fixed point $\text{FP}^{g_Y y_t y_b}_{\bullet\bullet\bullet}$ of the last Sec. 5.3.1. In Tab. 7, we list the three available extensions of this fixed into the 3rd-generation lepton sector.
One might wonder, why there are only three fixed points and, in particular, why the fully interacting fixed-point is absent. This is a result of leptons and quarks coupling to the same

	IR-physics	$\frac{y_{t,*}^2}{16\pi^2}$	$\frac{y_{b,*}^2}{16\pi^2}$	$\frac{y_{\tau,*}^2}{16\pi^2}$	$\frac{y_{\nu_\tau,*}^2}{16\pi^2}$	$\theta_{t/b}$	θ_τ	θ_{ν_τ}
$\mathrm{FP}^{y_t y_b y_\tau y_{\nu_\tau}}_{\bullet\bullet\circ\circ}$	massless neutrino	$\frac{23f_g}{492}+\frac{f_y}{6}$	$\frac{f_y}{6}-\frac{f_g}{492}$	0	0	$\frac{(-33f_g-246f_y\pm A)}{328}$	$\frac{17f_g}{41}$	$-\frac{f_g}{41}$
$\mathrm{FP}^{y_t y_b y_\tau y_{\nu_\tau}}_{\bullet\bullet\bullet\circ}$	tau heavier than top	$\frac{f_g}{1476}+\frac{f_y}{6}$	$\frac{f_y}{6}-\frac{71f_g}{1476}$	$\frac{34f_g}{123}$	0	-	-	-
$\mathrm{FP}^{y_t y_b y_\tau y_{\nu_\tau}}_{\bullet\bullet\circ\bullet}$	complex couplings	$\frac{73f_g}{1476}+\frac{f_y}{6}$	$\frac{f_g}{1476}+\frac{f_y}{6}$	0	$-\frac{2f_g}{123}$	-	-	-

Table 7: We list all fixed points of the set of Eqs. (5.3)-(5.4) at which both y_t and y_b are non-vanishing. $A=\sqrt{1804f_gf_y+1273f_g^2+6724f_y^2}$ and we have specified to SM charges, i.e., $Y_L=1/2$, $Y_\tau=-1$, and $Y_{\nu_\tau}=0$. We also list the corresponding critical exponents for the vanishing-neutrino-mass fixed point. While the couplings are only approximately aligned with the corresponding eigendirections, y_τ (y_{ν_τ}) only overlaps with the eigendirection of θ_τ (θ_{ν_τ}) The critical exponents for the other two non-viable fixed points (2nd and 3rd line) are roots of fourth-order polynomials which cannot be brought to a particularly simple form, but are straightforward to obtain from Eqs. (5.3)-(5.4). Note that the limit $f_g\to 0$ does *not* continuously deform to the fixed-point structure at vanishing $g_{Y\,*}$.

SM-Higgs. To elucidate this further, we introduce a continuous parameter ϵ in the corresponding contributions to the quark and lepton β-functions in Eqs. (5.3) and (5.4), i.e., in those contributions arising from a mediating joint Higgs particle. Specifically, we replace $(y_\tau^2+y_{\nu_\tau}^2)\to\epsilon(y_\tau^2+y_{\nu_\tau}^2)$ in $\beta_{y_{t(b)}}$ and $(3y_t^2+3y_b^2)\to\epsilon(3y_t^2+3y_b^2)$ in $\beta_{y_{\tau(\nu_\tau)}}$. For $\epsilon\to 0$, the quarks and the lepton do not couple via a joint Higgs, for $\epsilon\to 1$ we recover the SM case with Higgs-mediated contributions. General ϵ permits for a fully interacting fixed point at which

$$y_{\nu_\tau\,*}^2=\frac{192\pi^2(\epsilon-1)f_y+((11-12\epsilon)\epsilon-15)g_{Y\,*}^2}{24\,(\epsilon^2-1)}\,, \tag{5.7}$$

where we have specified to SM charges. The other non-vanishing fixed-point values have a similar structure, i.e., $y_{t\,*}^2\sim 1/\left(\epsilon^2-1\right)$, $y_{b\,*}^2\sim 1/\left(\epsilon^2-1\right)$, and $y_{\tau\,*}^2\sim 1/\left(\epsilon^2-1\right)$. In the joint-Higgs limit, i.e., for $\epsilon\to 0$, the fully interacting fixed point escapes to ∞.

At all of the remaining three maximally-predictive fixed points, $\frac{g_{Y,*}^2}{16\pi^2}=\frac{6}{41}f_g$ (and $g_{2,*}^2=g_{3,*}^2=0$), which we use to eliminate $g_{Y,*}^2$ in favor of f_g. The third fixed point in Tab. 7 can be excluded because either the neutrino-Yukawa or the U(1) gauge coupling has to be complex-valued. The second one is not viable because it would predict a very heavy τ-lepton, in particular, heavier than the top-quark. Such a UV-completion is in stark contradiction with observation.

All of the above statements are independent of the value of f_y. We conclude that the only viable fixed point is $\mathrm{FP}^{y_t y_b y_\tau y_{\nu_\tau}}_{\bullet\bullet\circ\circ}$, i.e.,

$$\begin{aligned}&\frac{y_{t,*}^2}{16\pi^2}=\frac{23f_g}{24Y_{\rm tot}}+\frac{f_y}{6}\,,\quad \frac{y_{b,*}^2}{16\pi^2}=\frac{f_y}{6}-\frac{f_g}{24Y_{\rm tot}}\,,\quad y_{\tau,*}^2=y_{\nu_\tau,*}^2=0\,,\\ &\theta_{t/b}=\frac{-33f_g-12f_yY_{\rm tot}\pm A}{16Y_{\rm tot}}\,,\quad \theta_\tau=\frac{f_g\left(36Y_L^2+36Y_\tau^2-11\right)}{4Y_{\rm tot}}\,,\quad \theta_{\nu_\tau}=\frac{f_g\left(36Y_L^2+36Y_{\nu_\tau}^2-11\right)}{4Y_{\rm tot}}\,,\end{aligned} \tag{5.8}$$

where $A=\sqrt{88f_gf_yY_{\rm tot}+1273f_g^2+16f_y^2Y_{\rm tot}^2}$ and $Y_{\rm tot}=6Y_L^2+6Y_{\nu_\tau}^2+6Y_\tau^2+13$. This fixed point exhibits three IR-attractive directions along which g_Y, y_t, and y_b follow as predictions. As has been explicitly discussed in Sec. 5.3.1, this not only fixes the two new-physics parameters f_g and f_y but also ties the mass-difference of charged quarks to their charge difference.

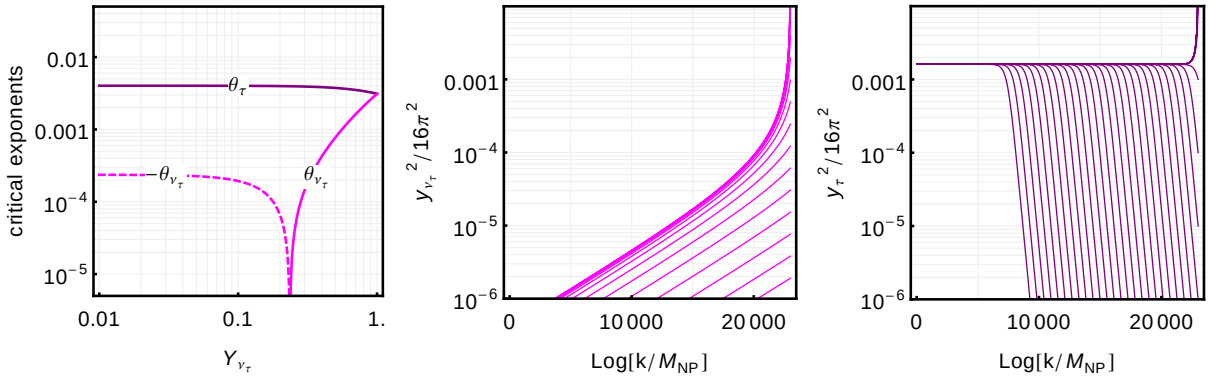

Figure 22: Left-hand panel: θ_τ (upper line) and θ_{ν_τ} (lower line) as a function of the neutrino hypercharge Y_{ν_τ} with dashed (continuous) lines indicating negative (positive) θ_i. For a sterile right-handed neutrino, i.e., $Y_{\nu_\tau} = 0$, $\theta_{\nu_\tau} < 0$. Middle panel: Scaling of y_{ν_τ} above $M_{\rm NP}$, while all other couplings are set to their fixed-point values. Right-hand panel: Scaling of y_τ above $M_{\rm NP}$, while all other couplings are set to their fixed-point values.

Notice again, that the critical exponents in the lepton sector are independent of the specific value of f_y. Their signs are determined purely by the corresponding charges. In particular, specifying to SM charges, i.e., $Y_L = 1/2$, $Y_\tau = -1$, and $Y_{\nu_\tau} = 0$, leads to one IR-attractive and one IR-repulsive direction in the leptonic sector. While the eigendirection of the critical exponents in the quark sector are slightly misaligned with the couplings, this is not the case in the lepton sector. The IR-attractive (IR-repulsive) critical exponent θ_{ν_τ} (θ_τ) has no overlap with y_{ν_τ} (y_τ). The IR-repulsive direction thus allows for an asymptotically free and non-vanishing y_τ to emerge from the UV-completion even though $y_{\tau,*} = 0$ at the fixed point. In particular, the IR-value of the SM can be reached. To the contrary, y_{ν_τ} only overlaps with the IR-attractive eigendirection corresponding to θ_{ν_τ}. Hence, the neutrino Yukawa is dynamically driven to $y_{\nu_\tau,*} = 0$. Consequentially, the Dirac mass of the τ-neutrino is predicted to be vanishing.

In the left-hand panel of Fig. 22, we present the dependence of the critical exponents on Y_{ν_τ} to explicitly show that $\theta_{\nu_\tau} < 0$, and hence the vanishing neutrino Yukawa coupling, can be attributed to its vanishing charge $Y_{\nu_\tau} = 0$. Fundamental asymptotic safety at this fixed point thus predicts an exactly vanishing Dirac-neutrino mass. Having both a vanishing Dirac and a vanishing Majorana mass is in contradiction to observed neutrino oscillations, cf. Sec. 1.1.1 and fundamental asymptotic safety at $\mathrm{FP}^{y_t y_b y_\tau y_{\nu_\tau}}_{\bullet\bullet\circ\bullet}$ would be excluded. Of course, additional right-handed Majorana mass terms are possible. We caution that this might also alter the fixed-point structure, cf. [528].

In the effective-asymptotic-safety interpretation (see Sec. 3), i.e., assuming that some more fundamental theory reduces to a QFT in the vicinity of $\mathrm{FP}^{y_t y_b y_\tau y_{\nu_\tau}}_{\bullet\bullet\circ\bullet}$, a small Dirac neutrino mass would still be favored. This could provide a dynamical alternative to the see-saw mechanism. The middle and right-hand panel of Fig. 22 present such an explicit mapping of UV- to IR-windows in the vicinity of the fixed point. This demonstrates that a (small) non-vanishing y_τ can be reached, while y_{ν_τ} and hence the neutrino Dirac-mass is dynamically driven to zero. However, the phenomenologically excluded heavy-τ fixed point $\mathrm{FP}^{y_t y_b y_\tau y_{\nu_\tau}}_{\bullet\bullet\bullet\circ}$ features a large IR-attractive critical exponent than $\mathrm{FP}^{y_t y_b y_\tau y_{\nu_\tau}}_{\bullet\bullet\circ\bullet}$. As a consequence, the basin of attraction of the phenomenologically interesting fixed point $\mathrm{FP}^{y_t y_b y_\tau y_{\nu_\tau}}_{\bullet\bullet\circ\bullet}$ is very narrow in the τ-direction. Nevertheless, the mechanism of dynamically vanishing neutrino mass deserves future attention.

In particular, it would be important to understand whether it occurs for any combination of quark and lepton representations that couple to a joint Higgs. If so, it might be possible to construct BSM models in which the heavy-lepton fixed point $\mathrm{FP}^{y_t y_b y_\tau y_{\nu_\tau}}_{\bullet\bullet\circ\bullet}$ does not exhibit a large IR-attractive direction. The latter would make a dynamically small Dirac-neutrino mass the generic prediction of such a model.

5.4 Fixed-point structure in multiple generations

The three generations of SM quarks ${u^i}_{L/R} = (t_{L/R}, c_{L/R}, u_{L/R})$ and ${d^i}_{L/R} = (b_{L/R}, s_{L/R}, d_{L/R})$ couple to the SM gauge group[91]. In particular, the left-handed components couple to the $W^\pm$ weak gauge-bosons via

$$\mathcal{L}_{\text{flavor}} \quad \sim \quad W^+_\mu \, \bar{u}^i_L \, \gamma^\mu \, d^i_L + W^-_\mu \, \bar{d}^i_L \, \gamma^\mu \, u^i_L \, . \tag{5.9}$$

These – and all other SM-gauge – interactions are invariant under global $U(1)^6_L$ and $U(1)^6_R$ (or equivalently $U(1)^6_{\text{axial}}$ and $U(1)^6_{\text{chiral}}$) rotations, *separately*, that is, the gauge interactions do not mix left- with right-handed quarks. Contrarily, the Yukawa couplings to the Higgs-doublet H mix left- and right-handed components

$$\mathcal{L}_{\text{mass}} \quad \sim \quad -Q^i_L \, H \, Y^{ij}_D \, d^j_R - Q^i_L \, \widetilde{H} \, Y^{ij}_U \, u^j_R \, , \tag{5.10}$$

where $Q^i_L = (u^i_L, d^i_L)$, $\widetilde{H} = i\sigma_2 \, H^*$, and $Y_{U/D}$ are the matrix Yukawa-couplings. Diagonal Yukawa matrices preserve the global $U(1)^6_{\text{axial}}$ but break the $U(1)^6_{\text{chiral}}$[92]. As we will see, the Yukawa matrices need not be diagonal.

For general non-diagonal $Y_{U/D}$, these can be diagonalized by complex unitary matrices U and D such that $\mathrm{diag}(y_u^2, y_c^2, y_t^2) = U \, M_U \, U^\dagger$ and $\mathrm{diag}(y_d^2, y_s^2, y_b^2) = D \, M_D \, D^\dagger$, which defines,

$$V = U \, D^\dagger = \begin{bmatrix} V_{ud} & V_{us} & V_{ub} \\ V_{cd} & V_{cs} & V_{cb} \\ V_{td} & V_{ts} & V_{tb} \end{bmatrix} , \tag{5.11}$$

the CKM-matrix. It accounts for the fact that the quarks need not be diagonalized simultaneously for the weak interactions (flavor basis) and the Yukawa interactions (mass basis). For the special case in which they can, no CKM matrix is necessary. Generalizing to N_g generations, the 1-loop running for the Yukawa couplings [529], cf. [526] for 2-loop results, in the flavor basis and supplemented by the flavor-universal new-physics contribution f_y reads

$$\beta_{y_i} = \frac{y_i}{16\pi^2} \left[3 \sum_{j=1}^{N_g} y_j^2 + 3 \sum_{\rho=1}^{N_g} y_\rho^2 - \left(\frac{17}{12} g_Y^2 + \frac{9}{4} g_2^2 + 8 g_3^2 \right) + \frac{3}{2} y_i^2 - \frac{3}{2} \sum_{\rho=1}^{N_g} y_\rho^2 |V_{i\rho}|^2 \right] - f_y \, y_i, \tag{5.12}$$

$$\beta_{y_\rho} = \frac{y_\rho}{16\pi^2} \left[3 \sum_{i=1}^{N_g} y_i^2 + 3 \sum_{\sigma=1}^{N_g} y_\sigma^2 - \left(\frac{5}{12} g_Y^2 + \frac{9}{4} g_2^2 + 8 g_3^2 \right) + \frac{3}{2} y_\rho^2 - \frac{3}{2} \sum_{i=1}^{N_g} y_i^2 |V_{i\rho}|^2 \right] - f_y \, y_\rho, \tag{5.13}$$

[91] Interactions with the U(1), SU(3) and the neutral SU(2) gauge bosons are omitted. They are not of importance for the following since they mix neither up- and down-type quarks nor left- and right-handed components.

[92] This generalizes the global symmetry and the resulting fixed-point structure in Sec. 4 to multiple generations. In particular, each diagonal Yukawa coupling breaks an additional global $U(1)_{\text{axial}}$ symmetry. Under the influence of antiscreening gravitational contributions, there will thus be 2^6 fixed points including all combinations of $y_{i*} = 0$ and $y_{i*} \neq 0$. The choice of fixed point, i.e., which y_{i*} vanish or not, determines which part of the $U(1)^6_{\text{chiral}}$ is already broken in the UV.

The running for the squared CKM matrix elements [530–533] reads

$$\beta_{|V_{i\rho}|^2} = -\frac{3}{2}\left[\sum_{\sigma,j\neq i}\frac{y_i^2+y_j^2}{y_i^2-y_j^2}y_\sigma^2\left(V_{i\sigma}V_{j\sigma}^*V_{j\rho}V_{i\rho}^*+\text{c.c.}\right)+\sum_{j,\sigma\neq\rho}\frac{y_\rho^2+y_\sigma^2}{y_\rho^2-y_\sigma^2}y_j^2\left(V_{j\sigma}^*V_{j\rho}V_{i\sigma}V_{i\rho}^*+\text{c.c.}\right)\right]. \quad (5.14)$$

As a consequence of its flavor universality, the new-physics contribution f_y drops out of the running of the CKM elements. Moreover, the CKM-running exhibits poles whenever two up-type or two down-type Yukawa couplings are equal. This is a result of unitarity which is explicitly used in the derivation. As a consequence, the special surfaces in theory space, defined by pairs of non-vanishing and degenerate Yukawa couplings, are dynamically disconnected from the rest of theory space, i.e., unitary RG-flows cannot cross from one side of the CKM-poles to the other. The only exception are vanishing degenerate Yukawas $y_i = y_j = 0$. These special points can be dynamically approached from both within the non-degenerate theory space or from within connected degenerate surfaces. Moreover, for the SM quark hierarchy and a dominating top-Yukawa coupling a diagonal (non-mixing) CKM matrix corresponds to an IR-attractive fixed point, see [300]. We will see in the following that interesting Yukawa hierarchies can be obtained from RG-flows transitioning between different non-mixing fixed points (crossover).

5.4.1 Analytical results and mechanisms for two generations

Because the phenomenologically interesting case of 3 generations cannot be solved analytically, we will use the 2-generation case as an instructive example. Unitarity of the CKM-matrix implies a single independent mixing parameter only, i.e.,

$$|V_{ij}|^2 = \begin{bmatrix} W & 1-W \\ 1-W & W \end{bmatrix}. \quad (5.15)$$

Interpreting the two generations as the second and third SM generation identifies W with the respective SM mixing angle $W = \cos(\theta_{23})^2$, cf. Tab. 9 in App. A. The explicit β-functions follow from Eqs. (5.12)-(5.14), i.e.,

$$\beta_W = \frac{3}{16\pi^2}W(W-1)\left[(y_t^2+y_c^2)\frac{y_b^2-y_s^2}{y_t^2-y_c^2}+(y_b^2+y_s^2)\frac{y_t^2-y_c^2}{y_b^2-y_s^2}\right]. \quad (5.16)$$

As for the one-generation case in Sec. 5.3.1, we assume the most-predictive gauge-coupling fixed point $\text{FP}^{g_Y g_2 g_3}_{\bullet\circ\circ}$, cf. Sec. 5.2.

UV fixed-points. Besides the fully Gaußian Yukawa fixed-point[93], there are 24 fixed points[94] which can be grouped into 6 classes of 4 fixed points related by the permutation symmetries

[93] The fully Gaußian Yukawa fixed-point is absent in the given parameterization because it corresponds to a trivial CKM matrix. It nevertheless exists and can be approached by a continuous RG-flow initiated at non-diagonal CKM-matrix.

[94] At 1-loop level, these appear to be 20 fixed points and two lines of solutions. The two lines can be associated with two (to the best of our knowledge accidental) 1-loop scale-invariant quantities, cf. also [534, 535],

$$I_{(1)} = \frac{\text{Tr}(M_U M_D)}{(\det(M_U M_D))^{1/N_g}}, \quad I_{(2)} = \text{Tr}((M_U M_D)^{-1})(\det(M_U M_D))^{1/N_g}, \quad (5.17)$$

where $M_U \equiv Y_U Y_U^\dagger$. We observe that this (accidental) scale-invariance is broken at 2-loop level, cf. also [536]. Together with the arguments from permutation symmetry, cf. discussion around Tab. 8, this leads us to conclude that these lines physically correspond to four fixed points at higher-loop level.

	y_{t*}^2/π^2	y_{b*}^2/π^2	y_{c*}^2/π^2	y_{s*}^2/π^2	W_*	viable for
$\mathrm{FP}^{y_t y_b y_c y_s W}_{\bullet\bullet\circ\circ\circ}$	$\frac{16(f_g+2f_y)}{15}$	$\frac{16(-19f_g+82f_y)}{615}$	0	0	0	$f_y \geq \frac{19f_g}{82}$
$\mathrm{FP}^{y_t y_b y_c y_s W}_{\bullet\bullet\circ\circ\bullet}$	$\frac{4(23f_g+82f_y)}{123}$	$\frac{4(-f_g+82f_y)}{123}$	0	0	1	–
$\mathrm{FP}^{y_t y_b y_c y_s W}_{\bullet\bullet\bullet\circ\bullet}$	$\frac{4(11f_g+82f_y)}{123}$	$\frac{4(-13f_g+82f_y)}{123}$	$\frac{32f_g}{41}$	0	1	–
$\mathrm{FP}^{y_t y_b y_c y_s W}_{\bullet\bullet\circ\bullet\bullet}$	$\frac{4(35f_g+82f_y)}{123}$	$\frac{4(11f_g+82f_y)}{123}$	0	$-\frac{32f_g}{41}$	1	–
$\widetilde{\mathrm{FP}}^{y_t y_b y_c y_s W}_{\bullet\bullet\circ\bullet\bullet}$	$\frac{16(65f_g+82f_y)}{1107}$	$\frac{8(-21f_g+246f_y-r)}{1107}$	0	$\frac{8(-21f_g+246f_y+r)}{1107}$	$\frac{1}{2}+\frac{r}{2(65f_g+82f_y)}$	–
$\widetilde{\mathrm{FP}}^{y_t y_b y_c y_s W}_{\bullet\bullet\bullet\circ\bullet}$	$\frac{8(87f_g+246f_y-s)}{1107}$	$\frac{16(-43f_g+82f_y)}{1107}$	$\frac{8(87f_g+246f_y+s)}{1107}$	0	$\frac{1}{2}-\frac{s}{2(43f_g-82f_y)}$	–

Table 8: Representatives of the 6 non-vanishing fixed-point classes of the two-generation system where $r = \sqrt{3(7f_g - 82f_y)(65f_g + 82f_y)}$ and $s = \sqrt{3(43f_g - 82f_y)(29f_g + 82f_y)}$. The remaining 18 fixed points can be generated by exchanging $(t \leftrightarrow b)$ and/or $(b \leftrightarrow s)$, cf. main text. Each ● (○) is accompanied by an IR-attractive (UV-attractive) direction.

$(t \leftrightarrow b)$ and $(b \leftrightarrow s)$, cf. Tab. 8. For the 4 classes at which $W_* = 1$ or $W_* = 0$, each permutation has to be accompanied by a flip $(W_* = 1) \leftrightarrow (W_* = 0)$. For the other two classes, W_* is permutation invariant. The number of UV-attractive (IR-attractive) directions can be inferred from the number of non-vanishing (vanishing) couplings, i.e., the number of ● (○), respectively[95]. Here, we identify the two-generation system with the 2nd and 3rd SM generation. In this case, the only class of interacting fixed points which supports a viable RG trajectory, i.e., can be connected to SM coupling values by a continuous RG flow, is the one in the first line of Tab. 8.

Crossover RG flows. Fixed points at which $W_* = 1$ are phenomenologically excluded since at such fixed points W corresponds to an IR-attractive direction[96] and thus cannot flow to different values towards the IR. This contradicts $W = \cos(\theta_{23})^2 \neq 1$ at the electroweak scale, cf. Tab. 9 in App. A. Any viable flow therefore transitions from a fixed point at $W_* = 0$ towards a fixed point at $W_* = 1$ (crossover), cf. left-hand panel in Fig. 23. Further, at any viable fixed point the SM hierarchy has to hold $y_{t*} \geqslant y_{c*}$ and $y_{b*} \geqslant y_{s*}$ since the RG flow cannot cross the CKM-poles, i.e., the hierarchy is preserved at all scales. Consequentially, the flow has to transition from

$$\mathrm{FP}^{y_t y_b y_c y_s W}_{\bullet\bullet\circ\circ\circ} \quad \xrightarrow[(y_b \leftrightarrow y_s)]{\text{UV to IR}} \quad \mathrm{FP}^{y_t y_b y_c y_s W}_{\bullet\circ\circ\bullet\bullet}\,, \tag{5.18}$$

at some intermediate crossover scale k_W. At the UV-fixed point, y_t and y_b are predicted by scale symmetry (by the same mechanism as in the one-generation case[97], cf. Sec. 5.3.1). The approximate IR fixed-point, however, attracts y_s instead of y_b because the CKM element has transitioned. Since both fixed points belong to the same class, i.e., are related by $(y_b \leftrightarrow y_s)$ exchange, the fixed point values y_{b*}^2 at the UV fixed point $\mathrm{FP}^{y_t y_b y_c y_s W}_{\bullet\bullet\circ\circ\circ}$ and y_{s*}^2 at the IR fixed point $\mathrm{FP}^{y_t y_b y_c y_s W}_{\bullet\circ\circ\bullet\bullet}$ are equal. We will denote the common value by $y_{b/s*}^2$ As a consequence of the CKM pole structure, $y_s^2(k) < y_{b/s*}^2$ at all scales k.

[95] The question of whether the respective coupling can flow to different values towards the IR depends on whether the respective fixed-point value enhances a global symmetry of the IR theory (here, the SM). If so, the coupling is *not* generated by an IR-directed flow in other UV-attractive directions, cf. Sec. 4.3

[96] Moreover, $W \neq 0$ is not generated by other UV-attractive directions because it enhances a global symmetry of the SM, cf. Sec. 4.3

[97] While the mechansim is precisely the same, the fixed-point relation (and the corresponding f_y), cf. Eq. (5.5), changes to $y_{t*}^2 - y_{b*}^2 = \frac{2}{3} g_{Y*}^2$

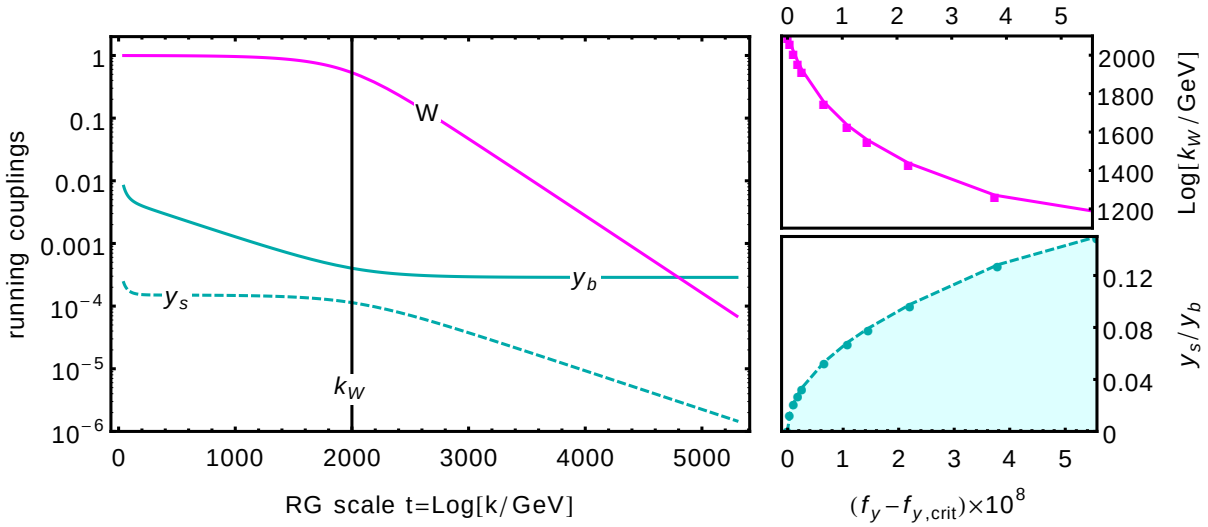

Figure 23: Left-hand panel: RG flow for a specific $f_y = f_{y,\mathrm{crit}} + 4\times10^{-9}$ and $M_{\mathrm{NP}} = M_{\mathrm{Planck}}$, emanating from $\mathrm{FP}^{y_t y_b y_c y_s W}_{\bullet\bullet\circ\circ\circ}$ passing close to $\mathrm{FP}^{y_t y_b y_c y_s W}_{\bullet\circ\circ\bullet\bullet}$ towards the IR. The three free parameters (UV-attractive directions of $\mathrm{FP}^{y_t y_b y_c y_s W}_{\bullet\bullet\circ\circ\circ}$) are chosen such that all Yukawas approach SM IR-values within ~ 10% error at the electroweak scale. This results in a transition scale of $Log(k_W/\mathrm{GeV}) \approx 2000$. Right-hand panels: At fixed f_y, approximate matching of the IR-values of y_t, y_b, y_c, and W fixes the transition scale k_W (upper panel) and can only be achieve up to an upper bound on the IR-ratio y_s/y_b (here shown as a function of f_y).

Whether the crossover implies a large hierarchy at the electroweak scale k_{ew}, i.e., if $y_s^2(k_{\mathrm{ew}}) \ll y_b^2(k_{\mathrm{ew}})$, depends on the crossover scale k_W which in turn depends on the precise value of f_y, cf. right-hand panel in Fig. 23. The closer f_y to the critical $f_{y,\mathrm{crit}} = 19/82\, f_g$, cf. first line in Tab. 8, the higher the viable crossover scale k_W.
Above k_W, y_b is fixed to remain (approximately) scale invariant while y_s scales with its UV-attractive critical exponent $\theta > 0$, i.e., $y_s^2(k > k_W) \sim k^{-\theta}$. Below k_W, y_s becomes (approximately) scale invariant[98] and now y_b scales with the same UV-attractive critical exponent, i.e., $y_b^2(k < k_W) \sim k^{-\theta}$. This can also be observed in the left-hand panel of Fig. 23 where θ corresponds to the slope of y_s (y_b) above (below) the transition scale k_W. Thus, the higher k_W, the longer the RG-time during which $y_b^2(k)$ scales to larger values while $y_s^2 \approx y_{b/s\,*}^2$ remains fixed. Hence, the larger the hierarchy at low scales.

While the presented mechanism crucially relies on scale-invariant new-physics contributions $f_{g/y}$, the associated new-physics scale need not be the Planck scale. Indeed, the hierarchy is set by the crossover scale k_W and not the new-physics scale M_{NP}. The mechanism to generate hierarchies via CKM crossovers could thus be at work in any scale-invariant UV-completion of the SM, as long as it obeys the conditions stated in Sec. 5.1.

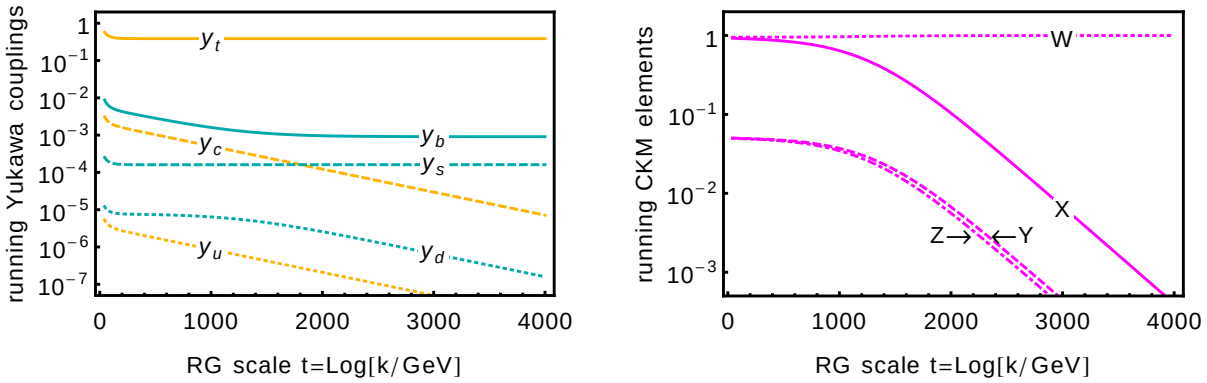

Figure 24: RG flow of Standar-Model quark Yukawa couplings (left-hand panel) and CKM-elements (right-hand panel) above the new physics scale $M_{\rm NP}$ for $f_y = 2.2476 \times 10^{-3}$, see main text.

5.4.2 Three-generation CKM-mixing angles and scale-invariance

For the case of three generations, the CKM matrix can be parameterized by 4 physical parameters, $X = |V_{ud}|^2$, $Y = |V_{us}|^2$, $Z = |V_{cd}|^2$, and $W = |V_{cs}|^2$, for which it reads

$$|V_{ij}|^2 = \begin{bmatrix} X & Y & 1-X-Y \\ Z & W & 1-Z-W \\ 1-X-Z & 1-Y-W & X+Y+Z+W-1 \end{bmatrix} . \tag{5.19}$$

For the respective β-functions, see, e.g., [532], as well as App. D. Unfortunately, the three-generation fixed-point structure cannot be fully solved analytically. However, the non-mixing fixed points, i.e., the three-generation equivalent of the first four lines in Tab. 8, can be obtained by the following observation. Whenever $|V_{ij}|^2$ corresponds to one of the following non-mixing matrices

$$M_{123} = \begin{bmatrix} 1 & 0 & 0 \\ 0 & 1 & 0 \\ 0 & 0 & 1 \end{bmatrix} , \quad M_{132} = \begin{bmatrix} 1 & 0 & 0 \\ 0 & 0 & 1 \\ 0 & 1 & 0 \end{bmatrix} , \quad M_{321} = \begin{bmatrix} 0 & 0 & 1 \\ 0 & 1 & 0 \\ 1 & 0 & 0 \end{bmatrix} ,$$
$$M_{213} = \begin{bmatrix} 0 & 1 & 0 \\ 1 & 0 & 0 \\ 0 & 0 & 1 \end{bmatrix} , \quad M_{312} = \begin{bmatrix} 0 & 0 & 1 \\ 1 & 0 & 0 \\ 0 & 1 & 0 \end{bmatrix} , \quad M_{231} = \begin{bmatrix} 0 & 1 & 0 \\ 0 & 0 & 1 \\ 1 & 0 & 0 \end{bmatrix} , \tag{5.20}$$

the RG-flow of the CKM matrix vanishes – independently of the values of the Yukawa couplings. These cases are all referred to as non-mixing because they simply correspond to redefenitions of which down-type quark is paired with which up-type quark to form a family. The three-generation extension of the crossover in the two-generation case, cf. Eq. (5.18) and Fig. 23, is given by the crossover $M_{321} \to M_{123}$ or in the above notation by

$$\text{FP}^{y_t\, y_b\, y_c y_s y_u y_d X\, Y\, Z\, W}_{\bullet\bullet\circ\circ\circ\circ\circ\circ\circ\bullet} \xrightarrow[(y_b \leftrightarrow y_d)]{\text{UV to IR}} \text{FP}^{y_t\, y_b\, y_c y_s y_u y_d X\, Y\, Z\, W}_{\bullet\circ\circ\circ\circ\bullet\bullet\circ\circ\bullet} . \tag{5.21}$$

The two fixed points involved in the crossover are related by a permutation symmetry $(y_b \leftrightarrow y_d)$ which takes the associated CKM element from $X_* = 0$ in the UV to $X_* = 1$ in the IR.

[98] This only occurs if y_s approximately saturates the upper bound which is *not* required for the transition of the CKM element from $W \approx 0$ to $W \approx 1$.

Identifying $M_{\rm NP} = M_{\rm Planck}$ and for $f_y = 2.2476 \times 10^{-3}$, the UV initial conditions corresponding to UV-attractive directions of the UV fixed-point can be chosen such that all $y_{i\neq t}$, X, Y, Z, and W match to the tree-level matched experimental values (cf. Tab. 9) at $k = 173\,\text{GeV}$ within a 1% error. The top-Yukawa coupling is about 10-15% too heavy. The latter is a consequence of $X_* = 0$ at the UV fixed point. Hence, the latter does not correspond to the fixed-point class extending the single-generation fixed point explored in Sec. 5.3.1 but to a different one. We can distinguish the two fixed point classes by the implied relations for the non-vanishing gauge- and Yukawa-couplings, i.e.,

$$(X_* = 1)\ \text{class:}\quad y_{t*}^2 - y_{b*}^2 = \frac{1}{3} g_{Y*}^2\,, \qquad (X_* = 0)\ \text{class:}\quad y_{t*}^2 - y_{b*}^2 = \frac{2}{3} g_{Y*}^2\,. \tag{5.22}$$

If y_{b*}^2 is negligibly small, i.e., a large hierarchy is realized and given the SM RG-trajectory of g_Y, $y_{t*}^2 = 2/3\, g_{Y*}^2$ implies a significantly too heavy top quark. Crossover RG-flows between other UV-fixed points to the SM fixed-point in the IR could be possible as well and it is not guaranteed that we have found all fixed points of the three-generation system. Certainly, the fully Gaußian Yukawa fixed point is accessible as a UV-completion.

5.5 Effective asymptotic safety of quantum gravity

We have advocated that any fixed point of a non-gravitational beyond SM theory should be analyzed within the concept of effective asymptotic safety, Sec. 3. As such, an asymptotically safe fixed point can still imprint a significant degree of predictivity on the respective effective field theory (EFT) by mapping a large range of values at the EFT cutoff scale to a much smaller range of values at lower scales.
It is certainly most conservative to regard any form of asymptotic safety – including gravity – as effective. This simply allows for the possibility that new physics might occur despite any fundamental theoretical demand. Here, we therefore broaden our view and re-examine asymptotically safe gravity as an effective theory.

The scales of effective asymptotic safety. For now, assume the fixed point features only a single UV-attractive (or equivalently IR-repulsive) direction, tentatively called G. Effective asymptotic safety is then determined by two scales: (i) the scale $k_{\rm fund}$ at which the QFT is replaced by a more fundamental theory and (ii) the scale $k_{\rm tr}$ at which G deviates $\mathcal{O}(1)$ from the fixed point. Whether and to what degree effective asymptotic safety is realized depends on the separation of scales between $k_{\rm tr}$ and $k_{\rm fund}$. This in turn depends on the relevant critical exponent θ_G and the unknown initial value $G(k_{\rm fund})$ of the UV-attractive coupling at $k_{\rm fund}$. The orders of magnitude in scales for which effective asymptotic safety is realized is then given by

$$\log(k_{\rm fund}/k_{\rm tr}) = \frac{\log\left(|G(k_{\rm fund}) - G_*|\right)}{\theta_G}\,. \tag{5.23}$$

In case of multiple UV-attractive directions this generalizes to the minimum of all the respective RHS terms. Eq. (5.23) demonstrates that the realization of effective asymptotic safety requires one finely tuned initial value at $k_{\rm fund}$ for each UV-attractive direction[99].

[99] In this context, the Gaußian fixed point (GFP) of the SM is no different. In this case, the transition scale is set by the electroweak scale, i.e., $k_{\rm tr} = k_{\rm ew}$. The squared Higgs mass m^2 corresponds to an IR-repulsive direction with critical exponent $\theta_{m^2} = 2$. A more fundamental theory at $k_{\rm fund} \gg k_{\rm ew}$ either accepts a finely tuned free parameter or has to explain the smallness of $m^2(k_{\rm fund}) = (k_{\rm fund}/k_{\rm tr})^2$.

Global constraints from asymptotically safe fixed points. Fixed points impose global conditions on RG flows. One example is the Gaußian fixed point (GFP) for the Newton coupling G. Being IR-attractive, its value $G_{*\,\mathrm{GFP}} = 0$ cannot be crossed by any IR-directed RG flow. We have measured a positive Newton coupling at IR scales. Therefore, any UV theory which predicts a negative Newton coupling at UV-scales is already experimentally ruled out.
If an asymptotically safe gravitational fixed point is present, it also imposes such a global constraint. We recall the perturbative approximation of the running dimensionless Newton coupling in Eq. (4.1) which exhibits (aside from the GFP) an asymptotically safe fixed point at

$$G_{*\,\mathrm{NGFP}} = \frac{12\pi}{46 + 4\,N_V - N_S - N_W}\,, \tag{5.24}$$

where N_S, N_W, and N_V count the scalar, Weyl, and vector matter degrees of freedom. Also, recall that at the asymptotically safe fixed point the Newton coupling G corresponds to an IR-repulsive direction. If present, its value cannot be crossed by any RG flow either and thus shields the GFP. All $G > G_{*\,\mathrm{NGFP}}$ are thus phenomenologically excluded as well. We can conclude that for any phenomenologically viable theory

$$G_{*\,\mathrm{GFP}} < G(k) < G_{*\,\mathrm{NGFP}} \qquad \text{at all } k\,. \tag{5.25}$$

For pure gravity ($N_S = N_W = N_V = 0$), the asymptotically safe fixed point is $\mathcal{O}(1)$ and thus only constrains the Newton coupling to lie within the perturbative regime. For $4\,N_V - N_S - N_W < 46$, the asymptotically safe fixed point lies at $G_{*\,\mathrm{NGFP}} < 0$ and thus has no implication for theories dominated by many fermions and many scalars. But for $4\,N_V - N_S - N_W \gg 46$, i.e., for theories dominated by many vector degrees of freedom, it constrains the admissible values for $G(k)$ to a smaller and smaller window.
We emphasize that the above argument assumes that the fixed point exists, in particular, if many vector degrees of freedom are included. The behavior $G_{*\,\mathrm{NGFP}} \overset{N_V\to\infty}{\longrightarrow} 0$ is supported by an increasingly perturbative value for $G_{*\,\mathrm{NGFP}}$ any by all functional RG studies to date, cf. in particular [343, Fig.10] and [356, Fig.9]. Further, it might be possible to circumvent the bound along other coupling directions in the full gravitational theory space.

Effective asymptotic safety constraint on string compactifications. String theory compactifications typically feature very many matter degrees of freedom. If the asymptotically safe fixed point in the large-N_V limit can be established, this implies: Any string-theory compactification in which the matter sector is dominanted by many vector degrees of freedom but for which $G \sim \mathcal{O}(1)$ at the string scale lies in the swampland, i.e., could be phenomenologically excluded.

The parametric investigation of quantum scale symmetry in the Standard Model can be generalized to grand unification. These are particularly appealing since their fixed-point structure could fix all marginal couplings if a sufficient number of matter degrees of freedom is added. If such a grand-unified extension of the asymptotically safe Reuter fixed-point for quantum gravity exists, scale-symmetry might fix all the marginal couplings in terms of asymptotically safe gravity contributions and the group-theoretic structure. We initiate a program to explore whether one such fully-predictive model can reproduce the Standard Model.

6 Unified asymptotic safety

The last two sections 4 and 5 were focused on gravitationally induced UV-completions of the Standard Model (SM) without any intermediate new physics. But, the parametric investigation of fixed points in the ASSM, cf. Sec. 5.1, extends to other beyond SM scenarios which are consistent up to M_{Planck}. Here, we will consider grand unified theories (GUTs).
GUTs pose a non-gravitational possibility to cure the $U(1)_Y$ Landau-pole problem. To do so, the Abelian $U(1)_Y$ has to be embedded in a larger non-Abelian gauge group. Typical GUTs break the enlarged gauge group by a successive chain of Higgs-mechanisms with different scalar VEVs oriented in specific directions of a large scalar potential. In this context, the electroweak phase-transition, during which $SU(2)_L \otimes U(1)_Y$ breaks to $U(1)_{\text{em}}$ is only the last step of a successive chain of symmetry breaking steps.
Removal of the $U(1)_Y$ Landau pole only requires to unify the hypercharge into a non-Abelian gauge group. This can already be achieved by a single unification step into a Pati-Salam model with gauge group $SU(4) \otimes SU(2)_L \otimes SU(2)_R$, cf. [537] and Sec. 6.1. In that sense, a Pati-Salam GUT poses the most minimalistic GUT to avoid the Landau-pole and reproduce the SM in the IR. Going beyond Pati-Salam, one can unify all gauge interactions into a simple[100] non-Abelian gauge group such as $SU(5)$ or $SO(10)$. Evidence for the latter is provided by the approximate crossing of all the three gauge couplings of the SM in the high-energy range of $10^{-14} - 10^{-17}$ GeV, see far-left panel in Fig. 1 in Sec. 6.1.2[101]. The second major reason is simplicity. For instance, an entire generation of SM fermions neatly fits into a single representation of $SO(10)$. The latter only contains a single additional Weyl fermion which comes with just the right charges (after symmetry breaking to the SM) to be identified with the right-handed neutrino. This gives a third reason to favor simple GUTs since, thereby, grand unification naturally accounts for the only BSM field already required by experimental data, cf. Sec. 1.1.1. We will discuss these embeddings more explicitly in Sec. 6.13.

Increasingly stringent experimental bounds on proton decay have pushed M_{GUT} to the vicinity of the Planck scale M_{Planck}. For this and other reasons, simple GUT breaking-chains are already experimentally ruled out, see Sec. 6.2. The remaining minimal and viable GUTs (both non-SUSY [545–558] and SUSY [559–570]), have more free parameters than the SM. This creates a predictivity problem for grand unification which defies the original idea of simplicity. Most of the parameters are hidden in an intricate Higgs-Yukawa sector which is fitted to give the correct fermion-mass spectrum and a scalar potential to generate the breaking chain.

[100] A simple group can be defined as not containing any subgroups but itself and the trivial group. Examples of such are the Lie groups $SU(N)$ and $SO(N)$. See, e.g., [538, 539].

[101] The crossing of SM gauge-couplings is realized at the 1-loop level within theoretical uncertainty. At higher-loop order, exact gauge-unification requires either new degrees of freedom, see, e.g., [398, Ch. 16], or several breaking steps [540–544].

The vicinity of the GUT and the Planck scale and the enhanced predictivity of the asymptotically safe Standard Model, see Sec. 5, motivates us to reconsider the predictivity of GUTs in the presence of gravitational fluctuations, see Sec. 6.3 and 6.4. Before turning to predictivity in asymptotically safe unification, we review grand unification in Sec. 6.1 and discuss the current minimal non-SUSY GUTs in Sec. 6.2. The knowledgeable reader may skip these sections. Group-theoretic language is explained or avoided as far as possible. Where nevertheless confused, the reader is referred, e.g., to [538, 539]

6.1 Motivation: why unify?

The SM can be summarized by specifying its gauge group, fermionic matter content, and scalar representations, i.e., $\left(\mathcal{G}_{\rm SM}, \mathcal{F}^{(i)}_{\rm SM}, \mathcal{S}_{\rm SM}\right)$, cf. Eqs. (1.6), (1.7), and (1.8), respectively. The couplings of all possible renormalizable operators comprise its set of free parameters. The fermionic matter content comes in three families of irreducible representations, that is $i = \{1, 2, 3\}$. One fermionic generation is spread out over five different representations. Moreover, the inclusion of a right-handed neutrino singlet is implied by neutrino oscillations (νSM, see Sec. 1.1.1). The gauge group, as well as the fermionic matter content, remain unexplained and somewhat arbitrary.

6.1.1 Unification of quarks and leptons and charge quantization

There are two main routes to unification: the $SU(5)$ Georgi-Glashow model [571]; and $SU(4) \otimes SU(2) \otimes SU(2)$ Pati-Salam models [537]. The following section demonstrates how the fermion content of the SM (or νSM) can be embedded into representations of these unifying groups, and further into a single representation of SO(10)[572].
The quarks and leptons of the SM can be written in an $SU(2)_L$ vector-like notation as

$$Q = \begin{pmatrix} u_1 & u_2 & u_3 \\ d_1 & d_2 & d_3 \end{pmatrix}, \quad L = \begin{pmatrix} \nu \\ e \end{pmatrix}, \quad \begin{matrix} u^c = (u^c_1 & u^c_2 & u^c_3) \\ d^c = (d^c_1 & d^c_2 & d^c_3) \end{matrix}, \quad \begin{matrix} e^c \\ \nu^c \end{matrix}, \tag{6.1}$$

where the conjugate Weyl-fermions denote right-handed chirality fields. Here, we have already included a right-handed neutrino ν^c singlet, see Sec. 1.1.1. Unifying the right-handed singlets u^c with d^c and e^c with ν^c into a right-handed $\mathrm{SU}(2)_R$ doublet suggests an enlargement of the SM gauge[102] group $SU(3) \otimes SU(2)_L \otimes U(1)_Y$ to $SU(3) \otimes SU(2)_L \otimes SU(2)_R \otimes U(1)_{B-L}$, in which leptons ($L$ and L^c below) and quarks (Q and Q^c below) are merely distinguished by their $B-L$ charges[103], i.e.,

$$Q = \begin{pmatrix} u_1 & u_2 & u_3 \\ d_1 & d_2 & d_3 \end{pmatrix}, \quad L = \begin{pmatrix} \nu \\ e \end{pmatrix}, \quad Q^c = \begin{pmatrix} d^c_1 & d^c_2 & d^c_3 \\ -u^c_1 & -u^c_2 & -u^c_3 \end{pmatrix}, \quad L^c = \begin{pmatrix} e^c \\ -\nu^c \end{pmatrix}. \tag{6.2}$$

The gauge boson of the additional $U(1)_{B-L}$ gauge symmetry mediates a new force between leptons and baryons. Written in the above form, it becomes quite suggestive to interpret "Lepton number as the Fourth Color"[537], simply writing

$$\underbrace{\widetilde{Q} = \begin{pmatrix} u_1 & u_2 & u_3 & \nu \\ d_1 & d_2 & d_3 & e \end{pmatrix}}_{(4,2,1)}, \quad \underbrace{\widetilde{Q}^c = \begin{pmatrix} d^c_1 & d^c_2 & d^c_3 & e^c \\ -u^c_1 & -u^c_2 & -u^c_3 & -\nu^c \end{pmatrix}}_{(4,1,2)}, \tag{6.3}$$

[102] Of course, an enlarged global symmetry need not be gauged. But, since we attempt to unify the SM gauge group into a larger simple group anyways, we follow the principle of gauging every new symmetry.
[103] For a connection of $U(1)_{B-L}$ symmetry to baryon and lepton-number conservation/violation see Sec. 1.1.1.

where $(4,2,1)$ and $(4,1,2)$ already denoted the fields as representation of the unified Pati-Salam gauge group $SU(4)\otimes SU(2)_L\otimes SU(2)_R$[537]. Although this path is very suggestive, it is not the minimal possible way to go: already in the first step, we have enlarged the rank 4 SM gauge group to a rank 5 gauge group[104]. This gives the additional freedom to embed the right-handed neutrino. But, how far can we unify without a right-handed neutrino and without rank-enlargement?

Georgi and Glashow [571] argued that amongst all rank-4 Lie groups only SU(5) contains an SU(3) subgroup, allows for complex representations as required by chiral fermions, and admits for quarks and leptons with SM hypercharges[105]. The 24 gauge bosons of the adjoint representation of $SU(5)$ are given as traceless generators T_{ab}, naturally represented by 5×5 complex and traceless matrices. The correct embedding of the SM gauge bosons can be observed from the corresponding decomposition under $SU(5)\to\mathcal{G}_{\rm SM}$[106]

$$\mathbf{24} = \underbrace{(\mathbf{8},\mathbf{1})_0}_{\text{gluons } G^{ij}} + \underbrace{(\mathbf{1},\mathbf{3})_0}_{\text{weak boson } W^{\pm,0}} + \underbrace{(\mathbf{1},\mathbf{1})_0}_{\text{hypercharge boson } B} + \underbrace{(\mathbf{3},\overline{\mathbf{2}})_{-5/6}}_{\text{new heavy bosons } X} + \underbrace{(\overline{\mathbf{3}},\mathbf{2})_{+5/6}}_{\text{new heavy bosons } Y} . \quad (6.4)$$

The two lowest-dimensional representations $\overline{\mathbf{5}}_F$ and $\mathbf{10}_F$ decompose under $SU(5)\to\mathcal{G}_{\rm SM}$ according to[107]

$$\overline{\mathbf{5}}_F \to (\overline{\mathbf{3}},\mathbf{1})_{(1/3)}\oplus(\mathbf{1},\mathbf{2})_{(-1/2)}) \qquad \text{and} \qquad \mathbf{10}_F \to (\overline{\mathbf{3}},\mathbf{1})_{(-2/3)}\oplus(\mathbf{3},\mathbf{2})_{(1/6)}\oplus(\mathbf{1},\mathbf{1})_{(1)} .$$

Comparing to Eq. (1.7), we observe that a SM family of fermions fit perfectly[108] into a $\overline{\mathbf{5}}_F$ and $\mathbf{10}_F$ representation of the SU(5). Moreover, the hypercharges of each individual representation must sum to zero since the hypercharge generator, as part of the traceless $SU(5)$, must be traceless as well. This explains that the electric charges of quarks and leptons (and thus of proton and electron) are related – grand unification implies charge quantization.

[104] The rank of a Lie group is defined by the dimension of its Cartan subalgebra, i.e., the maximal subalgebra of simultaneously diagonalizable generators. For $SU(N)$, rank$[SU(N)] = N-1$. For $SO(2N)$, rank$[SO(2N)] = N$. See, e.g., [538, 539]. A given gauge group can only be embedded in another of equal or larger rank.

[105] Besides SU(5), $\mathrm{SU(3)}^2 = \mathrm{SU(3)}\otimes\mathrm{SU(3)}$ also contains an SU(3) and allows for chiral fermions. Trying to embed the SM into $\mathrm{SU(3)}^2$ demands that $\mathrm{SU(2)}\otimes\mathrm{U(1)}$ be embedded into the second SU(3). As part of SU(3) which is by definition traceless, the SM $U(1)$ generating electric charge must be traceless as well. Its action on every single representation of the $\mathrm{SU(3)}^2$ must vanish, i.e., the hypercharges must sum to zero. But, quarks and leptons transform differently (as triplets and singlets, respectively) under the SM SU(3). Hence, they cannot be part of the same $\mathrm{SU(3)}^2$-representation. Thus, $\mathrm{SU(3)}^2$ requires that the quark (and lepton) charges of one SM generation sum to zero individually. We conclude that without additional fermions, $\mathrm{SU(3)}^2$-unification of the SM cannot be realized and SU(5) remains as the only minimal rank-4 Lie group which can contain the SM [571]. Adding additional (as of yet unobserved) fermions could remove the demand for chirality as well as the problem of hypercharges of quarks (and leptons) not summing to zero, individually.

[106] More explicitly, one can identify the SM $SU(3)$ generators with the left-upper 3×3 submatrix, the $SU(2)_L$ generators with the right-lower submatrix, and the $U(1)_Y$ with the remaining generator diag$(-2/3, -2/3, -2/3, 1, 1)$.

[107] And, since the $\overline{\mathbf{5}}_F$ is a complex representations also the corresponding $\mathbf{5}_F$.

[108] An explicit embedding is given by

$$\overline{\mathbf{5}}_F = \begin{pmatrix} d_1^c \\ d_2^c \\ d_3^c \\ e \\ -\nu \end{pmatrix}, \qquad \mathbf{10}_F = \begin{pmatrix} 0 & u_3^c & -u_2^c & u_1 & d_1 \\ -u_3^c & 0 & u_1^c & u_2 & d_2 \\ u_2^c & -u_1^c & 0 & u_3 & d_3 \\ -u_1 & -u_2 & -u_3 & 0 & e^c \\ -d_1 & -d_2 & -d_3 & -e^c & 0 \end{pmatrix} . \quad (6.5)$$

We have seen that leptons can be viewed as the fourth color in a unifying rank-5 Pati-Salam gauge group $SU(4) \otimes SU(2)_L \otimes SU(2)_R$. Demanding minimal rank (and under the assumption of no additional fermions) uniquely leads to the unifying Georgi-Glashow gauge group $SU(5)$. It turns out that both of these unification paths lead to the unique simple rank 5 group which contains one SM generation in a single fermionic representation: SO(10) with the corresponding $\mathbf{16}_F$ representation [572]. This can most easily be seen by the branching rules, see, e.g., [539, 573], into both, the Georgi-Glashow and the Pati-Salam GUT, i.e.,

$$\begin{aligned} SO(10) &\to SU(5) \times U(1)_X : && \mathbf{16} = \mathbf{10}_{-5} + \overline{\mathbf{5}}_3 + \mathbf{1}_{-1} \,, \\ SO(10) &\to SU(4) \times SU(2)_L \times SU(2)_R : && \mathbf{16} = (\mathbf{4}, \mathbf{2}, \mathbf{1}) + (\overline{\mathbf{4}}, \mathbf{1}, \mathbf{2}) \,. \end{aligned} \tag{6.6}$$

The additional $U(1)_X$ along the Georgi-Glashow path is a remnant of the higher rank 5 of $SO(10)$ compared to the rank 4 of $SU(5)$. Its charge is given by a combination of hypercharge and $B-L$ charge, i.e., $X = 2Y - 5(B-L)$. In Eq. 6.6, one identifies the intermediate fermionic representations of SU(5) and Pati-Salam, cf. Eq. (6.5) and (6.3), respectively. These decompose further into the SM representations. These are the two main routes of spontaneous symmetry breaking from $SO(10)$ to the SM, cf. Fig. 25.
Regarding anomalies and charge conservation, $SO(10)$ is an anomaly-free group [574][109]. This manifests in the otherwise non-trivial anomaly cancellations of the SM and in the resulting charge quantization, cf. Sec. 1.1.1.

6.1.2 Gauge unification, proton decay and $SO(10)$ breaking chains

Fig. 25 summarizes all group-theoretically admissible breaking chains from $SO(10)$ to the SM[110]. Along the arrows in Fig. 25, we list the scalar representations which can account for the respective breaking step[111]. Intermediate breaking steps can be collapsed. The scalar representation of the second step is sufficient to realize the entire collapsed breaking step since it can develop a VEV which is invariant under the target symmetry group. We will refer to models with n intermediate symmetry groups as $(n+1)$-step models. This construction does not specify how to construct the corresponding scalar potential to realize the suitable global (or at least sufficiently stable) minimum in the scalar potential[112].

[109] This follows from the antisymmetric nature of its generators $T_{ij} = -T_{ji}$. Being a tensor invariant, the anomaly $\mathrm{tr}(\{T_{ij}, T_{kl}\}T_{mn})$ must be a general combination of Kronecker δ's. Obviously, the whole object must be symmetric under pair-exchange of $ij \leftrightarrow kl$, $ij \leftrightarrow mn$, and $kl \leftrightarrow mn$. At the same time, the antisymmetry of the generators implies it must be antisymmetric under exchange of $i \leftrightarrow j$, $k \leftrightarrow l$, and $m \leftrightarrow n$. These two demands contradict each other unless the anomaly vanishes, $\mathrm{tr}(\{T_{ij}, T_{kl}\}T_{mn}) = 0$.

[110] One can generate these by listing all possible maximal subgroups $\mathcal{G}_1 \subset \mathcal{G}_{\mathrm{GUT}}$ of $\mathcal{G}_{\mathrm{GUT}} = SO(10)$, and then the maximal subgroups $\mathcal{G}_2 \subset \mathcal{G}_1$ of those, and so on [539, 573]. Finally, one picks out those chains which end up at the SM $\mathcal{G}_{\mathrm{SM}}$.

[111] This assumes nothing about how the breaking steps are realized. From hereon, we assume that the breaking is achieved by a VEV in the potential of one or multiple scalar GUT representations. This requires to understand which scalar representations can acquire a VEV which leaves the desired subgroup invariant. It has been conjectured [539, 575], based on a proof for the specific case of real and irreducible scalar representations [575–577], that this can be read off from the branching rules of the scalar representation of $\mathcal{G}_1$ into the scalar representations of $\mathcal{G}_2$. If those contain a singlet under $\mathcal{G}_2$, the corresponding scalar representation can break $\mathcal{G}_1 \to \mathcal{G}_2$. It is quite intuitive that the singlet which transforms trivially under $\mathcal{G}_2$ can leave precisely this subgroup unbroken. We emphasize that this remains a (although by now well-tested) conjecture.

[112] To check for such explicit potentials one (i) constructs the most general (perturbatively renormalizable) Higgs-potential with associated couplings, (ii) minimizes the potential in dependence on those couplings, (iii) determines coupling ranges for which a specific minimum that leaves a specific subgroup invariant is realized. This has first been done for irreducible (fundamental) representation of $SU(N)$ and $SO(N)$ [578] and subsequently extended to adjoint representations in [579] and other specific cases of $SO(10)$ [580–589].

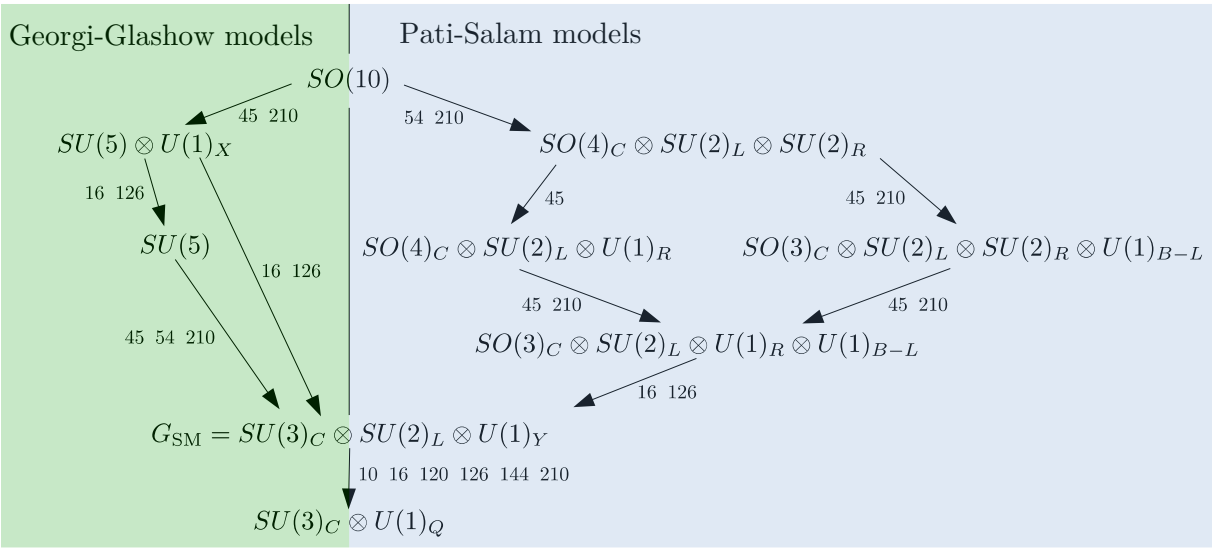

Figure 25: SO(10) breaking chains with possible breaking representations with dimensions 210 or less. For realistic Yukawa sectors at least a $\mathbf{126}_H$ and either one or both of the other possible Higgs-representation participating in Yukawa-interactions, i.e., $\mathbf{10}_H$, $\mathbf{120}_H$, have to be involved in the breaking [554, 568]. D-parity models have been neglected. Effective one-, two- or three-scale models can be obtained by identifying two breaking steps.

It is quite obvious from Fig. 25 that there is a plethora of other possible breaking chains. What is worse, the complexity of the scalar potential, i.e., the number of renormalizable couplings, grows rapidly with the size and number of scalar representations. As we shall see below, experimental bounds on proton decay can by now exclude the simplest breaking chains. Therefore, the increase in predictivity which is gained from unifying the representations and couplings of the SM is lost again due to the arbitrariness of a large scalar GUT potential.

Proton decay. The universal prediction of all GUTs is a finite lifetime of baryons and the proton in particular. This experimentally constrains the unification scale $M_{\rm GUT}$, at which quarks and leptons are not split in distinct representations anymore. At $M_{\rm GUT}$, the heavy gauge bosons associated with the additional symmetry generators (in the explicit $SU(5)$ embedding in Eq. (6.4) denoted by X and Y) of mass $M_X \sim M_Y \sim M_{\rm GUT}$ start mediating interactions between quarks and leptons. Thereby, one quark q inside a baryon B can "oscillate" into a lepton and thereby the baryon decays into a meson M and a lepton ℓ. Schematically, $B = qqq \to qq\ell = M + \ell$. Since this decay is mediated by a gauge boson propagator $\sim 1/M^2_{\rm GUT}$ (i.e., by two fermion-fermion-gauge vertices with coupling $\sqrt{\alpha_{\rm GUT}}$), the corresponding amplitude $\mathcal{A}_{B\to M+\ell}$ has to scale with $\alpha_{\rm GUT}$ and with $1/M^2_{\rm GUT}$. This results in a proton lifetime $\tau_{\rm proton}$ or inverse decay width $\Gamma_{\rm proton}$ of

$$\tau_{\rm proton} = \frac{1}{\Gamma_{\rm proton}} \sim \frac{1}{\alpha^2_{\rm GUT}} \frac{M^4_{\rm GUT}}{m^5_{\rm proton}} \,. \tag{6.7}$$

Here, we have used dimensional analysis to determine the power with which the only other mass scale $m_{\rm proton}$ has to enter the expression. We assume $\alpha \sim 1/40$ and the proton mass is given by 938 MeV [12]. Current lower bounds on the proton lifetime of $\tau_{\rm proton} \gtrsim 10^{34}\, y \approx 3.1 \times 10^{41}\, s \approx$

$4.8 \times 10^{65}\,\mathrm{GeV}^{-1}$ [590] lead to an approximate lower bound on the unification scale,

$$M_{\mathrm{GUT}} \gtrsim 3.8 \times 10^{15}\,\mathrm{GeV}\,. \tag{6.8}$$

More rigorous derivations depend on the specific GUT model but the order of magnitude is well estimated in the above approximation. By now, this constraint has become tight enough to rule out simple single-step GUT breaking chains, see below.

One- and multi-step models. GUT-breaking to the SM can be achieved in a single step[113]

$$SU(5) \xrightarrow{24} \mathcal{G}_{\mathrm{SM}} \qquad \text{or} \qquad SO(10) \xrightarrow{144} \mathcal{G}_{\mathrm{SM}}\,. \tag{6.9}$$

In any case, we know from Sec. 1.1.1 that without additional degrees of freedom at intermediate scales the gauge couplings of the SM do not unify at a common scale, cf. left-hand panel in Fig. 1 or left-hand panel in [398, Fig.15.1] for 2-loop runnning.
TeV-scale supersymmetry (SUSY) can resolve this issue [591, 592] because the SUSY-partners alter the running of gauge couplings above the TeV-scale, cf. right-hand panel in [398, Fig.15.1]. Demanding exact SUSY-unification fixes both the SUSY and the GUT-scale (up to threshold effects). The latter has been found [593] to violate proton-decay bounds, cf. Eq. (6.8)[114]. Moreover, SUSY introduces a second scale M_{SUSY} and thereby a new parameter in addition to M_{GUT}. SUSY one-step breaking chains are thus equivalent to non-SUSY breaking chains with one intermediate step[115], such as

$$SO(10) \to SU(3)_C \times SU(2)_L \times SU(2)_R \times U(1)_X \to \mathcal{G}_{\mathrm{SM}}\,. \tag{6.10}$$

Non-SUSY three-step models have been analyzed at two-loop level in [543, 544], where it has been shown that even the most minimal models – both in terms of the dimension of the scalar representation as well as in terms of the number of free parameters in the Higgs potential – remain viable. Obviously, this extends to breaking chains with multiple intermediate scales.

6.1.3 Fermion masses in $SO(10)$ unification

GUTs in general, and the $SO(10)$ in particular, not only predict the unification of gauge-couplings but also (partially) unify and therefore predict relations among the Yukawa couplings. All fermions of one SM family unify into a single $\mathbf{16}_F$ representation of $SO(10)$. The only renormalizable Yukawa-type invariants can be formed with either **10**, **120** or $\overline{\mathbf{126}}$ scalar representations because the $\mathbf{16}_F$ fermion bilinear decomposes as, cf. [594],

$$\mathbf{16}_F \otimes \mathbf{16}_F = \mathbf{10}_S \oplus \mathbf{120}_A \oplus \overline{\mathbf{126}}_S\,, \tag{6.11}$$

[113] For $SU(5)$ this can be achieved via a **24** scalar representation. For $SO(10)$ one requires a **144** scalar representation. Alternatively, one can use multiple representations, i.e., one representation of each of the sets {**16**, **126**} and {**45**, **54**, **210**} and break at the same scale. While one of the **16** or **126** representations is needed to reduce the rank of $SO(10)$, one of the **45**, **54**, or **210** representations is required to admit for a maximal little group different from $SU(5) \times U(1)$. The latter can then yield the SM when intersected with $SU(5)$ itself.
[114] [593] indeed fixes the mass of the colored Higgs-Triplett by demanding sufficiently large threshold effects to achieve exact unification given lower-limits on the SUSY scale from collider physics. Proton decay bounds can then exclude this Higgs-Triplet mass scale.
[115] It remains non-trivial that a consistent choice places $M_{\mathrm{SUSY}} \sim$ TeV.

where S and A denote symmetric and anti-symmetric representations in generation space. Other Higgs-sectors will not couple to the fermionic sector by marginal invariants and therefore there are three independent Yukawa couplings (matrices in generation space), i.e.,

$$\mathcal{L}_Y = \mathbf{16}_F \left(Y_{10}\, \mathbf{10}_S + Y_{120}\, \mathbf{120}_A + Y_{126}\, \overline{\mathbf{126}}_S \right) \mathbf{16}_F + \text{h.c.} \,. \tag{6.12}$$

When the Higgs potential is broken and acquires a vacuum expectation value $\mathcal{V}$, the mass matrices (in family space) – M_u, M_d, M_D, M_l, M_r and M_L for up-type quark, down-type quark, Dirac neutrino, charged lepton, right-handed (seesaw type-1) and left-handed (seesaw type-2) Majorana-neutrino – are determined by the corresponding $\mathcal{V}$-components and the three Yukawa-matrices Y_{10}, Y_{120} and Y_{126}[595], i.e.,

$$\begin{aligned}
M_u &= \mathcal{V}^u_{10} Y_{10} + \mathcal{V}^u_{120} Y_{120} + \mathcal{V}^u_{126} Y_{126} \,, & M_d &= \mathcal{V}^d_{10} Y_{10} + \mathcal{V}^d_{120} Y_{120} + \mathcal{V}^d_{126} Y_{126} \,, \\
M_D &= \mathcal{V}^u_{10} Y_{10} + \mathcal{V}^D_{120} Y_{120} - 3\mathcal{V}^u_{126} Y_{126} \,, & M_l &= \mathcal{V}^d_{10} Y_{10} + \mathcal{V}^l_{120} Y_{120} - 3\mathcal{V}^d_{126} Y_{126} \,, \\
M_R &= \mathcal{V}^R_{126} Y_{126} \,, & M_L &= \mathcal{V}^L_{126} Y_{126} \,.
\end{aligned} \tag{6.13}$$

With a dominating Y_{10} contribution in the heaviest family this implies $M_b \simeq M_\tau$, while a dominating Y_{126} contribution in the second family favors $M_\mu \simeq 3M_s$, i.e., the 3rd-generation relations predicted by unification [596]. These relations hold at the GUT scale and have to be RG-evolved down to the electroweak scale to compare to the observed mass spectra. Therefore, they depend on the specifics of the model.
While cancellations of different $\mathcal{V}_i$ for quarks and leptons allow for small Yukawa couplings – accepting significant fine tuning, see Sec. 1.1.1 – this cannot be achieved for the Majorana neutrino masses. This is another very intriguing group-theoretic consequence: A typically large $\mathcal{V}_{126} \sim 10^{10-16}$ GeV VEV results in very heavy Majorana neutrino masses and thereby naturally realizes a see-saw mechanism, cf. Sec. 1.1.1.

6.1.4 Unification and asymptotic freedom

In the context of this thesis, the most crucial feature of grand unification is the possible removal of the U(1) and Higgs-Yukawa Landau poles, see Sec. 1.1.1. The U(1) Landau-pole is obviously cured as soon as the Abelian gauge group is unified into a non-Abelian one[116]. Since gauge unification only recasts Yukawa couplings into other Yukawa couplings and, cf. Sec. 6.1.2, introduces many more scalar quartic couplings, Landau poles in the Higgs-Yukawa sector seem to persist. One might expect that if all gauge couplings vanish towards asymptotic freedom, all antiscreening contributions in the Higgs-Yukawa sector vanish as well and only the screening matter self-interactions remain. While this is true in principle, one has to take the respective limits more carefully. This has first been noticed already in the 70s [529], along with the first discussions of asymptotic freedom [202, 304, 597–600]. Non-Abelian gauge theories including Yukawa and quartic couplings can still feature complete asymptotic freedom (CAF) [529], provided that specific ratios of gauge and matter couplings remain large enough [601–604]. See [605] and [606] for the first explicit SU(5) and Pati-Salam constructions, respectively. Such constructions have recently regained attention under the names of total asymptotic freedom (TAF) [607] and stable asymptotically free extensions (SAFEs) [608], but the concept remains the same, see [609–611] for functional RG studies. For a single gauge coupling $\alpha_g = \frac{g^2}{4\pi}$ and Yukawa coupling $\alpha_y = \frac{y^2}{4\pi}$,

[116] At least as long as the screening contributions of too many matter fields do not overpower antiscreening from non-Abelian self-interactions.

with respective β-functions $\beta_g \sim -B\,\alpha_g^2$ (cf. Eq. (2.25)) and $\beta_y \sim E\,\alpha_y^2 - F\,\alpha_g\alpha_y$ (cf. Eq. (2.27)), the CAF conditions [607] are

$$B > 0 \qquad \& \qquad F > B \qquad \& \qquad \frac{\alpha_y(k_0)}{\alpha_g(k_0)} \leqslant \frac{F-B}{2\,E}\,. \tag{6.14}$$

Here, k_0 is some initial RG scale above which the theory is (or is not) completely asymptotically free. Such conditions generalize to semi-simple gauge groups, an arbitrary number of Yukawa couplings, and can include quartic couplings [607]. Therefore, GUTs which obey the CAF-conditions and break to the SM can offer UV-completions even in the absence of gravity[117]

6.2 Minimal GUTs and a lack of predictivity

A grand unified theory is defined by its group-theoretic data, i.e., by its gauge group $\mathcal{G}_{\rm GUT}$ and its fermionic, $\mathcal{F}_{\rm GUT}$, as well as scalar, $\mathcal{S}_{\rm GUT}$, matter content. As for the SM, its perturbative Lagrangian in four dimensions follows by introducing couplings to *all* marginal (perturbatively renormalizable) interaction terms allowed by the symmetry $\mathcal{G}_{\rm GUT}$. A viable GUT has to (at least) fulfill the following demands:

(i) $\mathcal{G}_{\rm GUT}$ has to contain the SM and the fermionic GUT representations $\mathcal{F}_{\rm GUT}$ have to contain the SM fermions, cf. Sec. 6.1.1.

(ii) Gauge couplings have to unify and the scale at which leptons and baryons are unified has to evade constraints from the non-observation of proton decay, cf. Sec. 6.1.2.

(iii) A set of scalar representations $\mathcal{S}_{\rm Yukawa}$ coupling to $\mathcal{F}_{\rm GUT}$ via marginal Yukawa couplings has to reproduce the fermionic mass spectrum of the SM, cf. Sec. 6.1.3.

(iv) A set of scalar representations $\mathcal{S}_{\rm breaking}$ and its scalar potential has to develop suitable VEVs to break $\mathcal{G}_{\rm GUT}$ to the SM, cf. Fig. 25.

In the absence of gravity contributions, one might add the demand for CAF. Including gravity, this translates into the weaker constraint of the absence of subplanckian Landau poles. We will discuss this demand with and without gravity in Sec 6.3.2, respectively. In the following, we will focus on non-SUSY models only.

Minimal non-SUSY SU(5): a predictive but non-viable GUT As we have discussed in Sec. 6.1, the only rank-4 simple group which can break to the SM is $SU(5)$. In that respect, it is the ultimate minimal GUT. The quarks and leptons (without right-handed neutrinos) fit neatly into the complex $\bar{\mathbf{5}}_F$ and $\mathbf{10}_F$ fermionic representation of $SU(5)$, cf. Eqs. (6.5). The SM Higgs can be embedded into a complex scalar $\mathbf{5}$ representation of $SU(5)$. Finally, GUT-symmetry breaking can be achieved via a fundamental scalar $\mathbf{24}$ representation. We can summarize the model as

$$(\mathcal{G}_{\rm GUT},\, \mathcal{F}_{\rm GUT},\, \mathcal{S}_{\rm GUT}) = (SU(5),\, \bar{\mathbf{5}}_F + \mathbf{10}_F,\, \mathbf{5} + \mathbf{24}) \tag{6.15}$$

[117] See [222, 223, 458, 612], as well as Sec. 1.3.1 for asymptotically free quadratic gravity and [229] for other scenarios in which gravity weakens towards larger scales. In those scenarios GUTs and CAF-conditions become particularly important, because the gauge-matter sector has to be UV-complete on its own.

with a breaking chain of

$$\mathcal{G}_{\rm GUT} \xrightarrow{\mathbf{24}} \mathcal{G}_{\rm SM} \xrightarrow{\mathbf{5}} SU(3)_C \times U(1)_{\rm em} \,. \tag{6.16}$$

This minimal model is much more predictive than the SM but also turns out to be excluded for several reasons. Firstly, we have already seen that gauge coupling unification is not exact. Further, also the Yukawa sector is highly predictive, but turns out to give wrong predictions [613, 614][118]. Finally, this GUT model does not account for a right-handed neutrino. Of course, one can simply add more scalar representations to account for more free parameters to fit the SM Yukawas. But, since there is no possibility of multi-step breaking of $\mathcal{G}_{\rm GUT} \to \mathcal{G}_{\rm SM}$ there is no (non-SUSY) way to resolve the non-unification of gauge couplings. Nevertheless, we will come back to this model in Sec. 6.3 as it constitutes a comparatively simple and instructive example.

Minimal non-SUSY $SO(10)$: a viable but non-predictive GUT We also present the minimal viable non-SUSY $SO(10)$ GUT. It is non-predictive, that is, it has more free parameters than the SM. Gauge unification and proton-decay bounds, cf. Sec. 6.1.2, require (at least) a two-step breaking chain, with one of each of the two sets of scalar representations $\{\mathbf{16}, \mathbf{126}\}$ and $\{\mathbf{45}, \mathbf{54}, \mathbf{210}\}$, respectively. The fermions of the νSM, including the right-handed neutrino, neatly fit into a single $\mathbf{16}_F$ representation of $SO(10)$. The SM Higgs can fit into many different scalar representations, but the minimal choice is certainly the fundamental **10**. A viable Yukawa sector, cf. Sec. 6.1.3, requires the presence of at least two different of the three scalar representations (**10**, **120**, **126**) which admit Yukawa couplings to the $\mathbf{16}_F$. Comparison of the resulting mass relations, cf. Eqs. (6.13), to experiment excludes the possibility of just one of these representations, as well as the possibility of two equal copies [566–568]. This requires at least one comparatively large scalar representation – either the **120** or the **126**. While all three options to combine two distinct ones of these representations remain viable, the **10** is required to contain the SM Higgs anyways. The **126** is the other minimal choice as it can also be used to realize the rank-reducing breaking step[119]. A viable Yukawa sector also requires to complexify

[118] The most general renormalizable Yukawa Lagrangian for the above field content $\mathcal{F}_{\rm GUT}$ and $\mathcal{S}_{\rm GUT}$, in $SU(3) \times SU(2)$ decomposed schematic notation reads

$$\overline{\mathbf{5}}_F = \begin{pmatrix} d^c \\ \epsilon_2 L \end{pmatrix} , \qquad \mathbf{10}_F = \begin{pmatrix} \epsilon_3 u^c & Q \\ -Q^T & \epsilon_2 e^c \end{pmatrix} , \qquad \mathbf{5} = \begin{pmatrix} T \\ H \end{pmatrix} . \tag{6.17}$$

In this notation, u^c, d^c and e^c denote the right-handed up-type, down-type and lepton singlets, Q and L the left-handed quark and lepton doublet, H the SM Higgs doublet, and T the remaining heavy triplet in the **5** of $SU(5)$ connected to doublet-triplet fine-tuning. With those definition, the Yukawa Lagragian reads

$$\mathcal{L}_Y\,(\mathcal{F}_{\rm GUT}, \mathcal{S}_{\rm GUT}) = \overline{\mathbf{5}}_F\, \mathcal{Y}_5\, \mathbf{10}_F\, \mathbf{5}^* + \frac{\epsilon_5}{8} \mathbf{10}_F\, \mathcal{Y}_{10}\, \mathbf{10}_F\, \mathbf{5} \,, \tag{6.18}$$

where ϵ_n denote n-dimensional Levi-Cevita symbols. Neglecting terms involving the Higgs-triplet T, we find

$$\mathcal{L}_Y\,(\mathcal{F}_{\rm GUT}, \mathcal{S}_{\rm GUT}) \supset d^c\, \mathcal{Y}_5\, Q\, H^* + L\, \mathcal{Y}_5\, e^c\, H^* + \frac{1}{2}\, u^c (\mathcal{Y}_{10} + \mathcal{Y}_{10}^T) Q\, H \,. \tag{6.19}$$

Comparing with the SM Lagrangian this implies

$$\mathcal{Y}_d = \mathcal{Y}_e^T \qquad \left(\text{and} \quad \mathcal{Y}_u = \mathcal{Y}_u^T \right) . \tag{6.20}$$

Modulo minor modifications that arise because those relations hold at $M_{\rm GUT}$ and have to be RG-evolved down to the electroweak scale, the non-trivial relation implies $M_b \approx M_\tau$, $M_s \approx M_\mu$, and $M_d \approx M_e$. While the first relation is not too far off, the latter two are in stark conflict with observation, cf. Tab. 9 in App. A.

[119] Further, only this scalar representation naturally realizes a seesaw mechanism, see Sec. 6.1.3.

the a priori real **10** representation. An additional Pecci-Quinn $U(1)$ symmetry [615] can then reduce the number of additional parameters [546, 549, 566]. Overall, the minimal model can be summarized as

$$(\mathcal{G}_{\rm GUT}, \mathcal{F}_{\rm GUT}, \mathcal{S}_{\rm GUT}) = (SO(10), \mathbf{16}_F, \mathbf{10} + \mathbf{45} + \mathbf{126}) \tag{6.21}$$

with a breaking chain of

$$\mathcal{G}_{\rm GUT} \xrightarrow{\mathbf{45}} \left\{ \begin{array}{c} SU(3)_3 \times SU(2)_L \times SU(2)_R \times U(1)_{(B-L)/2} \\ SU(3)_3 \times SU(2)_L \times U(1)_R \times U(1)_{(B-L)/2} \\ SU(3)_4 \times SU(2)_L \times U(1)_R \end{array} \right\} \xrightarrow{\mathbf{126}} \mathcal{G}_{\rm SM} \xrightarrow{\mathbf{10}} SU(3)_C \times U(1)_{\rm em} \,, \tag{6.22}$$

where any of the intermediate three groups can be chosen, cf. [543, 544]. Such models can realize seesaw type I and II mechanisms to generate neutrino masses [558]. The large Higgs-Yukawa sector already suggests many free parameters. In the case of type-I seesaw only, there is the single gauge coupling, 15 free parameters in the Yukawa sector, 4 parameters in the scalar VEVs, and, although consistent with $\lambda(M_{\rm GUT}) = 0$, the SM Higgs quartic couplings [558]. This makes for 21 free parameters. This does not include the many free renormalizable parameters in the scalar GUT potential. Different choices can lead to non-viable breaking chains, potentially not realizing the SM. The above counting simply assumes that the scalar potential can be constructed to realize the required VEVs. The model could be viable but is certainly not predictive anymore. This is the main hurdle that current GUT scenarios face. In the following Sec. 6.3 and Sec. 6.4 we discuss that an embedding into a gravitationally induced UV-completion can potentially restore predictivity and offers a new paradigm for GUT model building.

6.3 Losing asymptotically freedom and gaining asymptotic safety

In the following, we will look at a single gauge, $\alpha_g = g^2/(4\pi)$, and Yukawa coupling, $\alpha_y = y^2/(4\pi)$, at order $\mathcal{O}(\alpha_i^2)$. At this order, we can neglect contributions from quartic couplings, cf. Sec. 5, which we will return to in Sec. 6.4. The gauge and Yukawa couplings can be thought of as the single, fully unified GUT gauge coupling and a respective Yukawa coupling. Cases with multiple Yukawa couplings remain to be explored in future studies. As for the SM, cf. Sec. 5, we add linear, antiscreening, and scale-invariant gravitational contributions f_g and f_y to gauge and Yukawa couplings, respectively. For a discussion, we refer to Sec. 5, and simply recall that antiscreening $f_g \geqslant 0$ is generically found in all functional RG truncations. Moreover, antiscreening $f_y > 0$ could be realized by sufficient fermionic matter and a corresponding weak-gravity mechanism, cf. 4. We will restrict to these regimes in the following discussion. Interpreting (f_g, f_y) as unknown but perturbatively small parameters ensures well-controlled perturbative asymptotically safe fixed points, cf. Sec. 5. Matching with IR values, i.e., $\alpha_g \sim 1/40$ suggests that phenomenologically most interesting cases are well within this perturbative regime. At order $\mathcal{O}(\alpha_i^2)$ the respective β-functions are given by

$$\beta_{\alpha_g} = -f_g\,\alpha_g + (\mathcal{N} - \mathcal{N}_c)\,\frac{\alpha_g^2}{4\pi} + \mathcal{O}(\alpha_i^3)\,, \tag{6.23}$$

$$\beta_{\alpha_y} = -\left(f_y + F\,\alpha_g\right)\,\alpha_y + E\,\frac{\alpha_y^2}{4\pi} + \mathcal{O}(\alpha_i^3)\,. \tag{6.24}$$

Here, $(\mathcal{N} - \mathcal{N}_c)$ parameterizes gauge and matter fluctuations which impact the GUT-gauge coupling. We define $\mathcal{N}_c$ to contain the fluctuations from gauge-bosons and from the minimal

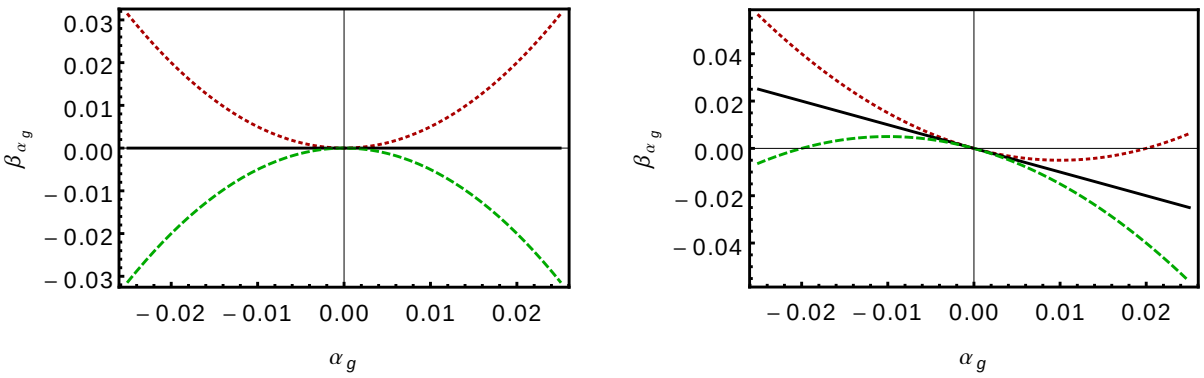

Figure 26: Gauge coupling β-function, cf. Eq. (6.23) for $\mathcal{N} > \mathcal{N}_c$ (red dotted), $\mathcal{N} = \mathcal{N}_c$ (black), and $\mathcal{N} < \mathcal{N}_c$ (green dashed). Positive values of the couplings run towards asymptotc freedom whenever the β-function is negative. The left-hand panel shows the well-known case without gravity. The right-hand side shows the case including an anticreening gravitational contribution.

set of matter interactions that recovers the SM. Then, $\mathcal{N}$ parameterizes all additional (scalar) representations, e.g., the ones required to realize the chain of symmetry breaking (see Sec. 6.1.2) or a realistic Yuakwa sector (see Sec. 6.1.3). Alternatively, one can view $(\mathcal{N} - \mathcal{N}_c)$ as a single parameter which contains all fluctuations. Similarly, E parameterizes Yukawa self-interactions and F the gauge contributions to Yukawa couplings[120]. Both, $E > 0$ and $F > 0$ for all gauge groups and all matter representations [529].

6.3.1 Complete asymptotic freedom in the presence of gravity

We start by looking at the gauge coupling α_g which to order $\mathcal{O}(\alpha_i^3)$ is independent of α_y. Explicit values for $(\mathcal{N} - \mathcal{N}_c)$ can be obtained from the group theoretic Casimir invariants and Dynkin indices, see, e.g., [544]. In case of $SU(5)$, $\mathcal{N}_c = 85/3$ which includes three generations of $\mathbf{5}_F$ and $\mathbf{10}_F$ representations to host the SM fermions and a scalar $\mathbf{5}$ to host the SM Higgs. Similarly, for $SO(10)$ the critical $\mathcal{N}_c = 50$ contains three generations of the fermionic $\mathbf{16}_F$ as well as a scalar $\mathbf{10}$ for the Higgs. For N_i additional scalar representations of dimension $\mathbf{i}$ one finds[121]

$$SU(5): \quad \mathcal{N} = \frac{1}{3}\left(N_5 + 3N_{10} + 7N_{15} + 5N_{24} + 28N_{35} + 22N_{40} + 24N_{45} + 35N_{50} + 49N_{70}\right), \tag{6.25}$$

$$SO(10): \quad \mathcal{N} = \frac{1}{3}\left(N_{10} + 4N_{16} + 8N_{45} + 12N_{54} + 28N_{120} + 70N_{126} + 68N_{144} + 56N_{210}\right). \tag{6.26}$$

As long as $\mathcal{N} < \mathcal{N}_c$, the gauge coupling is asymptotically free, even without gravitational fluctuations ($f_g = 0$). Asymptotic freedom is signalled by a negative β-function, cf. Fig. 26. For $\mathcal{N} > \mathcal{N}_c$, asymptotic freedom without gravity is lost. This simply corresponds to the critical matter content at which screening matter fluctuations overpower antiscreening gauge self-interactions and is a rephrasing of the non-gravitational CAF condition.
Theories obeying the non-gravitating CAF conditions, i.e., $\mathcal{N} < \mathcal{N}_c$, remain asymptotically free under the influence of gravitational fluctuations, i.e., for $f_g > 0$. But, now also theories with $\mathcal{N} > \mathcal{N}_c$ can be asymptotically free if the value of the coupling does not exceed a critical value.

[120] We have chosen our notation to align with GUT-conventions and with [1, 7] (where $f_g = -\eta_g$). This means that with respect to conventions in Sec. 2 and Sec. 3 there appear factors of (4π).
[121] The counting already takes into account whenever representations are required to be complex.

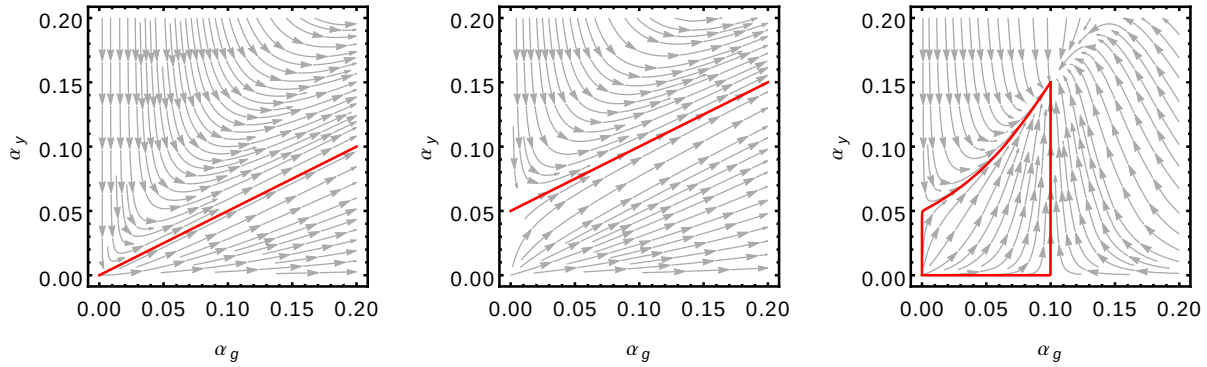

Figure 27: Streamplots of running of gauge and Yukawa coupling (arrows point towards the IR) for three different cases: The left panel shows the case without gravitational contributions and for antiscreening $\mathcal{N} - \mathcal{N}_c = -B = -1$. The middle panel shows a case with gravitational contributions $f_g = f_y = 1/10$, still with antiscreening $\mathcal{N} - \mathcal{N}_c = -1$. The right panel shows again $f_g = f_y = 1/10$, but now with screening $\mathcal{N} - \mathcal{N}_c = 1$. In all cases, $F = 2$ and $E = 1$ were chosen. In the left and middle panel the region below the red line indicates CAF theories. In the right hand panel the red line bounds the now finite region of CAF theories.

In the right-hand panel of Fig. 26, this value corresponds to the value of α_g at which β_{α_g} turns back to positive values. The gravitational CAF conditions for the gauge coupling thus read

$$\mathcal{N} < \mathcal{N}_c\,, \qquad \text{or} \qquad \mathcal{N} > \mathcal{N}_c \quad \text{with} \quad \alpha_g < \frac{4\pi\, f_g}{\mathcal{N} - \mathcal{N}_c}\,. \tag{6.27}$$

We conclude that the window of asymptotically free gauge theories is enlarged by gravitational fluctuations.

For the mixed gauge-Yukawa system the situation is more intricate. We recall the case without gravity: Besides $\mathcal{N} - \mathcal{N}_c = -4\pi\, B < 0$, there is a fixed ratio $\alpha_y/\alpha_g < (F + (\mathcal{N} - \mathcal{N}_c))/(8\pi\, E)$, cf. Eq. (6.14), that bounds the slice of non-gravitating completely asymptotically free theories in theory space. This can also be seen in the left panel of Fig. 27. For gauge theories which are asymptotically free on their own, i.e., $\mathcal{N} < \mathcal{N}_c$, the CAF conditions without gravity, cf. Eq. (6.14) are only slightly modified to read

$$F > B > 0 \qquad \& \qquad \alpha_y \leqslant \frac{F + (\mathcal{N} - \mathcal{N}_c)}{8\pi\, E}\, \frac{2\, f_y}{f_g + f_y}\, \alpha_g + \frac{f_y}{F}\,. \tag{6.28}$$

In the limit $f_y \to 0$ and at constant f_g the CAF window closes completely.
For gauge theories in which asymptotic freedom is lost on their own due to $\mathcal{N} > \mathcal{N}_c$ gravitational contributions restore a finite window of CAF theories, both in α and α_y, cf. right-hand panel of Fig. 27. While a general analytic expression for the running can be obtained, a closed analytic expression for the CAF conditions, in this case, is too complicated to reasonably present. For the resulting window, see right-hand panel of Fig. 27.

6.3.2 Asymptotic safety at the boundary of complete asymptotic freedom

Looking at the flow lines (which point towards the IR) in Fig. 27, it strikes the eye that the boundaries of CAF are IR attractive. This is a consequence of a second asymptotically safe

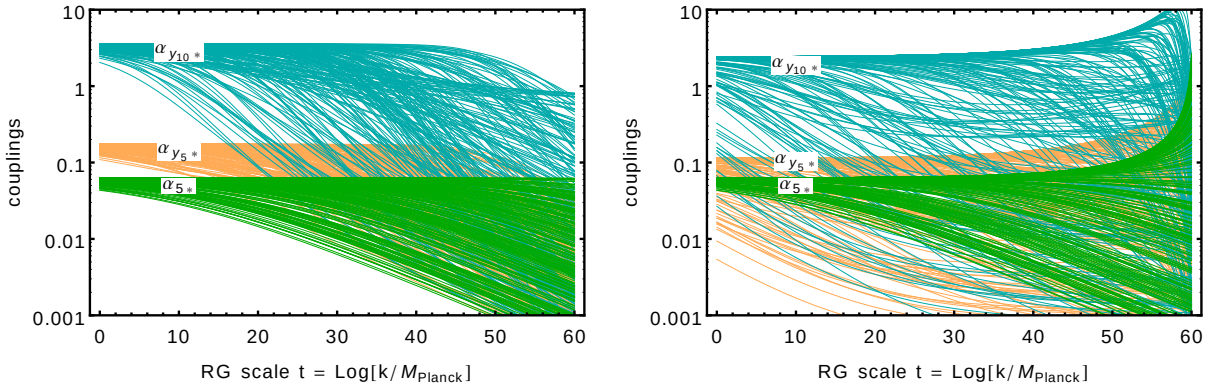

Figure 28: Effective asymptotic safety for the gauge-Yukawa sector of the minimal SU(5) GUT with 4 additional scalar **50** representations. Left panel: $f_g = f_y = 0.1$; asymptotically free trajectories with random intial values, see main text. Right panel: $f_g = 0.1$, $f_y = 0$; non asymptotically-free trajectories with random intial values, see main text.

UV-completion with enhanced predictivity[122], i.e.,

$$\alpha_{g*} = \frac{4\pi\, f_g}{\mathcal{N} - \mathcal{N}_c}\,, \tag{6.29}$$

associated with an IR-attractive direction and critical exponent $\theta = -f_g$.
Similarly, the combined gauge-Yukawa system exhibits four fixed points. These constitute the four corners of the respective CAF window in the right-hand panel of Fig. 27. As for the SM, cf. Sec. 5, each asymptotically safe coupling corresponds to an additional IR-attractive direction at the corresponding fixed point. The most predictive fixed point is the completely asymptotically safe one. Taking asymptotic safety as fundamental, each such gauge and Yukawa coupling is fixed at all scales. Its value is fully determined by the group-theoretic GUT content, i.e., $(\mathcal{G}_{\text{GUT}}, \mathcal{F}_{\text{GUT}}, \mathcal{S}_{\text{GUT}})$ and the asymptotically safe gravitational contribution $f_{g/y}$. Similar conclusions apply to the scalar GUT potential, see the following Sec. 6.4. Complete asymptotic safety (CAS) in the presence of gravitational contributions could thus fix *all* perturbatively renormalizable couplings of a given GUT.
Even for effective asymptotic safety, cf. Sec. 3.2.2 and Sec. 5.5, the fully non-Gaußian fixed point remains present and attracts trajectories towards the IR. In particular, also CAF trajectories cross over to the CAS fixed point. The larger the gravitational contributions, the quicker this cross-over is. This is simply because the critical exponents grow with $f_{g/y}$. For large enough $f_{g/y}$, the IR-physics of CAF and CAS is essentially indistinguishable.

6.3.3 Asymptotically safe gauge-Yukawa sector of minimal SU(5)

We use the minimal SU(5) GUT with fermionic $\mathbf{5}_F$ and $\mathbf{10}_F$, as well as scalar **5** and **24**, cf. Sec. 6.2 to exemplify the predictivity of effective asymptotic safety. The model is already phenomenologically excluded but nevertheless instructive. The running of the Yukawa couplings,

[122] Corrections from the next (two-loop) order do not change this conclusion, as long as α_{g*} stays perturbatively small. This can be achieved by either a perturbatively small f_g, or by a large $\mathcal{N} - \mathcal{N}_c$. Two-loop contributions scale with $\alpha^3\mathcal{N}'$, where $\mathcal{N}'$ depends linearly on the number of scalar representations, i.e., $\mathcal{N}' \sim \mathcal{O}(\mathcal{N} - \mathcal{N}_c)$. The terms are thus suppressed by an additional factor of α in comparison to the one-loop contribution.

as defined in Eq. (6.18), expressed as $\alpha_{y_i} = y_i^2/(4\pi)$, reads[123]

$$\beta_{\alpha_{y_5}} = \frac{1}{4\pi}\left(28\alpha_{y_5}^2 - \frac{3}{8}\alpha_{y_{10}}\alpha_{y_5} - 45\alpha_5\alpha_{y_5}\right) - f_y\,\alpha_{y_5}\ , \tag{6.30}$$

$$\beta_{\alpha_{y_{10}}} = \frac{1}{4\pi}\left(\frac{3}{2}\alpha_{y_{10}}^2 - \frac{1}{2}\alpha_{y_5}\alpha_{y_{10}} - \frac{216}{5}\alpha_5\alpha_{y_{10}}\right) - f_y\,\alpha_{y_{10}}\ . \tag{6.31}$$

The gauge running is given by the general Eq. (6.23). With the above matter content, i.e., $(\mathcal{N} - \mathcal{N}_c) = -\frac{80}{3}$, the gauge coupling is still asymptotically free. Since we want to present an example of CAS, we add 4 additional scalar **50** representations which cause for a loss of asymptotic freedom, i.e., $(\mathcal{N} - \mathcal{N}_c) = 20$, but do not participate in the Yukawa sector. Provided sufficiently antiscreening gravitational fluctuations, the theory is asymptotically safe.
Fig. 28 shows trajectories with different initial conditions sampled from an exponentiated random distribution in the deep UV at $\log[k/M_{\rm Planck}] = 60$. The left-hand panel shows asymptotically free trajectories for the case of $f_g = f_y = 0.1$. We initialize at different points in the interval $[e^{-8}, \alpha_{i*}]$, where α_{i*} is the fixed-point value at which only the respective coupling is safe and all others are free. While this need not be the combined boundary of UV-complete theories, it ensures that all initialized trajectories are CAF. In the right-hand panel, $f_g = 0.1$ but $f_y = 0$. Hence, no asymptotically free trajectories can exist, cf. discussion around Eq. (6.28). Since the gauge coupling runs to asymptotic freedom with a power law, Landau poles in the Yukawa sector will eventually occur for all trajectories but the CAS one[124]. We initialize in the window $[e^{-8}, e^{1}]$. In both cases, the imprint of the fully IR attractive CAS fixed point is clearly visible. It attracts all initial conditions and effective asymptotic safety determines most of the IR physics below $M_{\rm Planck}$.

6.4 Restoring predictivity for GUTs: asymptotically safe potentials

We have discussed that not only the SM, cf. Sec. 5, but general gauge-Yukawa theories can exhibit complete asymptotic safety (CAS) under the influence of gravitational fluctuations. Large regions of their theory space are dominated by the corresponding CAS fixed-point, cf. Fig. 28 which could vastly enhance the predictive power of grand unification. Without gravitational fluctuations, the greatest arbitrariness in grand unification originates from the undetermined grand unified scalar potential, cf. Sec. 6.1. In the SM, theory and experiment indicate that the Planckian scalar potential could be largely determined by scale symmetry, cf. [29, 34, 35]. Here, we investigate whether this can extend to GUT potentials and can thereby result in fully-predictive GUT models without any renormalizable free parameters.

6.4.1 Planck-induced GUT-symmetry breaking: a simple toy model

We start by investigating a simple U(1) toy-model for which it is straightforward to obtain the full non-perturbative RG-flow from the flow equation (2.5)[125]. Containing a charged complex

[123] The β-functions have been checked using the pyr@te package [26, 616].

[124] Perturbativity of the CAS fixed point in case of multiple Yukawa couplings may require a fine-tuning of the gravitational contributions f_y close to non-zero values. This is because hierarchies in the Yukawa sector can lead to some Yukawas with non-perturbatively large fixed-point values. These could give significant contributions at higher-loop order which might invalidate perturbation theory. It can even occur that one Yukawa coupling cannot be tuned to small values if one requires all other Yukawa couplings to remain with real CAS fixed points.

[125] Calculating the functional RG equations for scalar potentials with multiple invariants and gauge-Yukawa contributions can become quite involved, see, e.g., [611] for a Yukawa-QCD model, and remains of great interest for future research.

scalar field singlet ϕ and a neutral Dirac fermion ψ, its classical action reads

$$S_{\mathrm{U}(1)} = \int d^4x\,\sqrt{g}\left[\frac{1}{4}F^{\mu\nu}F_{\mu\nu} + (D^\mu\phi^*)(D_\mu\phi) + i\,\bar\psi\not{D}\psi + y\,(\bar\psi_R\phi^*\psi_L - \bar\psi_L\phi\,\psi_R) + U(\phi)\right], \quad (6.32)$$

where $U(\phi)$ denotes the scalar potential of interest. Including the anomalous dimension η_ϕ from wave-function renormalizations and introducing the dimensionless field variable $\rho = \phi * \phi/k^2$, the RG flow of the dimensionless scalar potential $u = U/k^4$ is given by

$$\begin{aligned} k\,\partial_k\,u(\rho) \;=\; & -4\,u(\rho) + (2+\eta_\phi)\rho\,u'(\rho) \;+\frac{1}{32\pi^2}\left(\frac{1}{1+u'(\rho)+2\rho u''(\rho)} + \frac{1}{1+u'(\rho)}\right) \\ & + \underbrace{\frac{3}{32\pi^2(1+4\pi\,\alpha_g\rho)}}_{\text{gauge}} \;\underbrace{-\frac{1}{8\pi^2(1+4\pi\,\alpha_y\rho)}}_{\text{Yukawa}} \;+\underbrace{\frac{5}{24\pi^2\left(1-\frac{2u(\rho)}{\tilde M_P^2}\right)} + \frac{1}{24\pi^2\left(1-\frac{u(\rho)}{2\tilde M_P^2}\right)}}_{\text{gravity}}, \end{aligned} \quad (6.33)$$

where primes denote derivatives with respect to ρ and we have neglected measure contributions as well as mixing of the complex scalar and the scalar gravitational mode, cf. App. E for the full expression[126]. We have also neglected the non-minimal scalar-curvature coupling. The first line in Eq. (E.2) denotes the contributions from scalar self-interactions. The gauge contributions depend on $\alpha_g \equiv g^2/(4\pi)$ and the Yukawa contributions on $\alpha_y \equiv y^2/(4\pi)$. The gravitational contributions depend on the running dimensionless Planck mass $\tilde M_P^2(k) = 1/(8\pi\,G(k))$, cf. (2.34) in Sec. 2 for the running of the dimensionless Newton coupling G.

Taylor-expanding the scalar potential around $\rho = 0$, as in Sec. 3.1.1, identifying the scalar mass $m = u'(\rho)|_{\rho=0}$ and quartic coupling $\lambda = u''(\rho)|_{\rho=0}$, and neglecting all higher-order terms as well as η_ϕ, one finds

$$\begin{aligned} \beta_{m^2} &= k\partial_k u'|_{\rho=0} = (A-2)m^2 - \frac{3}{8\pi}\,\alpha_g + \frac{1}{2\pi}\alpha_y + \mathcal{O}(\lambda)\,. \\ \beta_\lambda &= k\partial_k u''|_{\rho=0} = A\,\lambda + 3\,\alpha_g^2 - 4\,\alpha_y^2 + \mathcal{O}(\lambda^2)\,. \end{aligned} \quad (6.34)$$

To give a simple intuition, we have moreover assumed small m^2 to be negligible, i.e., $m^2 \ll 1$ in β_{m^2} and $m^2 \to 0$ in β_λ. The validity of this approximation is confirmed by the full numerical study leading to Fig. 29. While the anomalous scaling contributions can be assumed to be dominated by gravitational contributions, i.e., $A \approx f_\lambda$ in Sec. 4.5, it also receives (subleading) contributions $\sim \alpha_i\,\lambda$ from the gauge-Yukawa sector. As a result, we find fixed points at

$$\lambda_* = \frac{4\,\alpha_y^2 - 3\,\alpha_g^2}{A}, \qquad\qquad m_*^2 = \frac{1}{8\pi} \times \frac{4\,\alpha_y - 3\,\alpha_g}{2-A}\,. \quad (6.35)$$

Noting that $\alpha_i > 0$ are physical, we can conclude with four qualitatively different cases:

(i) For weak gravity, i.e., $A < 2$, and Yukawa dominance, i.e., $\alpha_y > \alpha_g$, the potential is stable around the origin ($m_* > 0$ and $\lambda_* > 0$), the quartic coupling is predicted but the mass remains a free parameter.

[126] The gauge and Yukawa contributions agree with [264, 317, 617], where also contributions to the scalar anomalous dimension η_ϕ are given explicitly. To reproduce the universal one-loop β-functions without gravity, it is sufficient to use the standard perturbative one-loop expressions for η_ϕ.

(ii) For weak gravity, i.e., $A < 2$, and gauge dominance, i.e., $\alpha_g > \alpha_y$, the potential is unstable around the origin ($m_* < 0$ and $\lambda_* < 0$). Again, the quartic coupling is predicted and the mass remains a free parameter.

(iii) For strong gravity, i.e., $A > 2$, and Yukawa dominance, i.e., $\alpha_g > \alpha_y$, the local potential is symmetry-broken but stable at quartic order ($m_* < 0$ and $\lambda_* > 0$) and both the quartic coupling and the mass are predicted.

(iv) For strong gravity, i.e., $A > 2$, and gauge dominance, i.e., $\alpha_g < \alpha_y$, the potential is stable around the origin but develops a quartic instability ($m_* > 0$ and $\lambda_* < 0$) where again both the quartic coupling and the mass are predicted.

The respective behavior is confirmed to high order in the local expansion around $\rho = 0$ and without the approximations in Eq. (6.34). It holds, at least for sufficiently small $\alpha_i \ll A$. Cases (iii) and (iv) are particularly interesting because the entire scalar potential is predicted. However, conclusive statements about global stability require to go beyond local expansions and use, for instance, pseudospectral methods [618]. Conjecturing that if such cases are globally stable, then the GUT symmetry-breaking scale is predicted to lie close to the Planck scale, we defer this case to future studies. Instead, we focus on the weak-gravity cases (i) and (ii) in the following.

Evolution of the fixed-point potential. Focusing on the Yukawa-dominated weak-gravity case (i), i.e., $\alpha_g < \alpha_y \ll A \ll 2$, the stable fixed-point potential $u_*(\rho)$ converges rapidly for a local expansion up to order $\sim \rho^{12}$, cf. solid-green line in Fig. 29 for order $n = 12$. Approximating $\alpha_i(k) \approx$ const., and for running dimensionless Planck mass $M^2_{\text{Planck}}(k) = 1/(8\pi\, G(k)) = M^2_{\text{Planck}\,*} + \bar{M}^2_{\text{Planck}}/k^2$ we can evolve the order $n = 12$ fixed-point potential towards the IR. At the gravitational transition scale $k_t \equiv \bar{M}_{\text{Planck}}/M_{\text{Planck}\,*}$, the Newton coupling transitions from fixed-point scaling to classical scaling, cf. Eq. (7.2) which causes a quick suppression of gravitational contributions. Consequently, the Yukawa coupling dominates the RG-flow of m^2. Towards the IR, its screening contribution quickly drives the mass to negative values, cf. Fig. 29 for an explicit example. The potential quickly develops a minimum and a vacuum expectation value right below the Planck scale.
The above holds, as long as contributions of the mass term itself are subleading, i.e., deviations of the relevant Newton coupling and not those of a relevant mass term cause the trajectory to depart from the fixed point. This need not be the case as the mass term corresponds to a UV-attractive direction. Indeed, its value can be chosen (fine-tuned) such as to avoid (or arbitrarily delay) the scale of symmetry breaking. This arbitrariness is absent in the fully predictive case.

6.4.2 Quartic couplings and the direction of symmetry breaking

More realistic scalar potentials have multiple quartic invariants and can thus develop different VEVs. The specific VEV decides to which subgroup the associated GUT breaks. Since the transplanckian quartic couplings are fixed by scale symmetry, the direction of symmetry breaking can be predicted, possibly depending on the relevant mass scales. The generalization of Eq. (6.34) to general quartic scalar potentials $U(\mathbf{\Phi}) = \frac{1}{4!}\lambda_{abcd}\mathbf{\Phi}_a\mathbf{\Phi}_b\mathbf{\Phi}_c\mathbf{\Phi}_d$ is given by, cf. [619],

$$k\partial_k\lambda_{abcd} = \beta_{\lambda_{abcd}} = \frac{1}{16\pi^2}\left(\mathbf{\Lambda}^2_{abcd} + \mathbf{S}^{(\text{eff})}_{2\,ae}(\eta_\lambda, \alpha_g, \mathbf{Y})\,\lambda_{ebcd} + \mathbf{A}^{(\text{eff})}_{abcd}(\alpha_g, \mathbf{Y})\right) + f_\lambda\,\lambda_{abcd}\,, \tag{6.36}$$

where $\mathbf{\Lambda}^2_{abcd} = \lambda_{abef}\lambda_{efcd} + \lambda_{acef}\lambda_{efbd} + \lambda_{adef}\lambda_{efbc}$ and $f_\lambda\,\lambda_{abcd}$ parameterizes the gravitational contribution, universal to all quartic couplings λ_{abcd}. $\mathbf{S}_{2\,ae}$ and $\mathbf{A}^{(\text{eff})}_{abcd}$ depend on the gauge coupling α_g and the generalized Yukawa couplings defined by $\mathcal{L}_Y = -\left(Y^a_{ij}\bar{\psi}_i\mathbf{\Phi}_a\psi_j + \text{h.c.}\right)$ where $\zeta = 1$

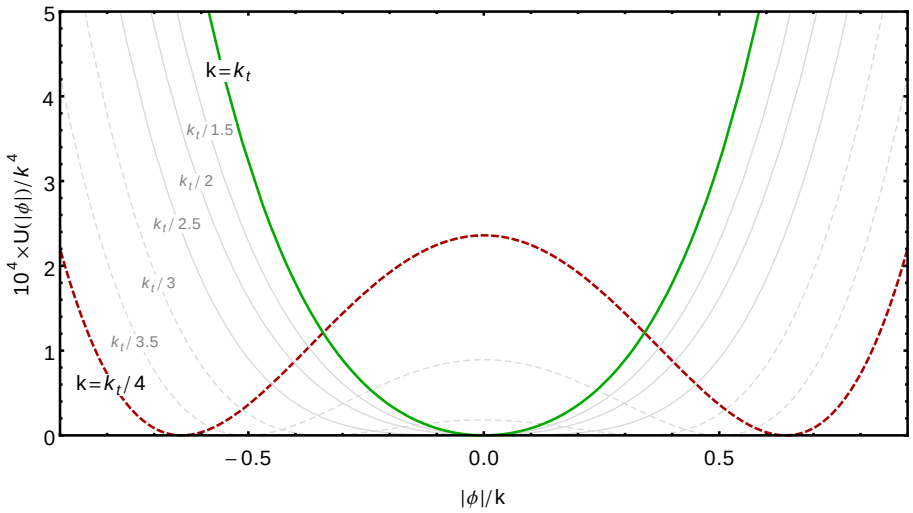

Figure 29: Numerical evolution of the scalar potential, starting from the initial condition $U/k^4 = u_*$ at $k = k_t$ (green continuous line). Thin (dashed) lines depict the evolution before (and after) symmetry breaking. The latter occurs at $k/k_t \approx 1/2.5$. At $k/k_t \approx 1/4$ (red-dashed line) a non-trivial minimum has clearly developed. The gravitational, gauge and Yukawa contributions are chosen as $A = 1/10$, $\alpha_g = 0$ and $\alpha_y = 1/100$.

($\zeta = 1/2$) for Dirac (Weyl) fermions, cf. [619] for explicit expressions.

Minimal SO(10): a promising candidate. A stable fixed-point potential requires Yukawa dominance (at least for weak-gravity). Without additional BSM fermions, this requires scalar representations that admit Yukawa couplings to the $\mathbf{16}_F$ of SO(10) which contains one complete generation of SM fermions, i.e., the **10**, **120**, or **126**. Scalar representations which, such as **45**, **54**, or **210**, do not couple to the $\mathbf{16}_F$ are automatically gauge-dominated. Ignoring the possible issue of global stability, the latter representations might already be broken at $\sim M_{\text{Planck}}$. To that end, it is quite suggestive that scalar representations from the gauge-dominated and from the Yukawa-dominated set are responsible for the first and subsequent breaking steps, respectively, cf. Fig. 25.
Focusing on the direction of the second breaking step of the minimal SO(10) model with scalar representations $\mathcal{S}_{\text{GUT}} = (\mathbf{10} + \mathbf{45} + \mathbf{126})$, cf. Sec. 6.2, the general quartic scalar potential can be found in [552]. Whenever all four quartic couplings $\lambda_i^{(126)} > 0$ of the **126** are positive, the second breaking step is realized along the phenomenologically viable $SU(5)$ direction [587]. It can be shown from Eq. (6.36) and under the assumption of $\alpha_g < Y_{ij}^a \ll A \ll 2$ that $\lambda_i^{(126)} > 0$ is indeed predicted by transplanckian scale symmetry. This strongly encourages a future study of the full fixed-point potential of the minimal SO(10) GUT.

Part III

New horizons: Black-hole physics as a potential window into quantum gravity

Quantum-gravity effects could create a repulsive force to resolve the spacetime singularities inside black holes. Many different quantum-gravity models result in similar quantum-improved and singularity-free black-hole spacetimes. With a minimal set of assumptions, this chapter explores the impact of singularity-resolving physics on black-hole shadows. While the effect is hugely suppressed if singularity resolution is tied to Planckian physics, the ground-breaking observations of the EHT are not able to exclude horizonless objects within our parameterization. This leaves open a wide parameter space of unexpected but admissible modified gravitational dynamics to resolve the singularity.

7 Shadows without singularities

Gravitational-wave signatures, as well as the direct image of the shadow of a galaxy's central object, verify that these behave like – or at least approximate very closely – black holes with an event horizon. Nevertheless, these extremely compact objects *cannot* be exactly described by the black holes of GR, simply because the latter are unphysical objects, cf. Sec. 1.2.1. Spacetime singularities at their center, at which all physical quantities diverge, signal the breakdown of GR. Some form of new gravitational physics – quantum gravity is the prime candidate – has to resolve the singularity. In the following we review singularity resolution by quantum-gravitational effects in Sec. 7.1, in particular in the context of asymptotic safety, and study its generic effect on black-hole shadows in Sec. 7.2 and 7.3.

7.1 Singularity resolution in quantum gravity

A simple argument by which quantum effects resolve singularities is provided by Renormalization-Group improvement. The classical Coulomb potential of electrodynamics serves as an instructive example. Just as the Schwarzschild spacetime, or the Newtonian potential, it exhibits a central singularity. Quantum-field theoretic (1-loop) effects lead to the modified Uehling potential [620] and contribute a measurable effect to the Lamb-shift [621]. These can be obtained by direct calculation. Another way to determine the quantum-improved potential is to (i) upgrade the classical coupling constant to a scale-dependent coupling which "runs" due to effects of quantum renormalization (cf. Part I and II) and (ii) identify this RG scale $k = 1/d$ with a physical scale, i.e., the radial distance d to the central charge. For the highly symmetric Coulomb potential, the choice of scale identification is unique. Since the background spacetime, with respect to which the distance is measured, remains fixed, the result is self-consistent. As a consequence, the resulting RG-improved potential precisely matches the Uehling potential.

7.1.1 Renormalization-Group improved black holes

The concept of RG improvement can also be applied to black-hole spacetimes [622, 623]. For spherically symmetric Schwarzschild black holes, i.e.,

$$ds^2 = -f_{\text{class}}(r)dt^2 + f_{\text{class}}(r)^{-1}dr^2 + r^2 d\Omega^2, \qquad \text{with} \qquad f_{\text{class}}(r) = 1 - \frac{2\,M\,\bar{G}_0}{r}\,, \tag{7.1}$$

Newton's constant $\bar{G}_0$ is upgraded to a running coupling $\bar{G}(k)$. For asymptotically safe gravity, cf. Sec. 2.4.2, the running Newton coupling, i.e.,

$$\bar{G}(k) = \frac{\bar{G}_0}{1 + \gamma\,\bar{G}_0 k^2}\,, \tag{7.2}$$

simply interpolates between a classical regime for $k \to 0$ for which $\bar{G} = \bar{G}_0$ takes its constant classical value $\bar{G}_0$ and a quantum regime for $k \to \infty$ in which $\bar{G} \sim 1/(\gamma\, k^2)$ weakens quadratically with growing scales k. Here, $\gamma = 1/G_*$ corresponds to the inverse dimensionless fixed-point value of the Newton coupling, cf. Sec. 2.4.2.
Further, RG improvement requires to identify the RG scale k with a physical scale of the system. The radial coordinate r is not an option because it is not a coordinate-invariant and thus not a physical quantity. Coordinate-invariant quantities in Schwarzschild spacetime are, for instance, the proper distance, see [623], or curvature invariants which will be used in the following. Since Schwarzschild spacetime is a vacuum solution, the Ricci scalar and Ricci tensor vanish at every point. Instead, we will identify scales with (one of) the next higher-order curvature invariants – the Kretschmann scalar $K = R_{\mu\nu\rho\sigma}R^{\mu\nu\rho\sigma}$. For classical Schwarzschild spacetime, it evaluates to

$$K_{\text{class}} = \frac{48\,\bar{G}_0^2\,M^2}{r^6}\,. \tag{7.3}$$

Given that the Kretschmann scalar is of mass-dimension four, one identifies $k^2 \sim K_{\text{class}}^{1/2} \sim (\bar{G}_0^2\,M^2)/r^3$. The same proportionality is also obtained from scale identification with the proper distance along a lightlike radial ray or the proper distance of an infalling observer to the center of the black hole [623]. It leads to a regular RG-improved Schwarzschild metric of Hayward type [624][127], i.e., with

$$f_{\text{improved}}(r) = 1 - \frac{2\,M\,\bar{G}\,(k\,(K_{\text{class}}(r)))}{r} = 1 - \frac{2\,r^2/r_g^2}{r^3/r_g^3 + \tilde{\gamma}}\,. \tag{7.4}$$

In the second step we have introduced natural units, i.e., $\bar{G}_0 = 1/M_{\text{Planck}}^2$ and $r_g = M/M_{\text{Planck}}^2$, and a rescaled $\tilde{\gamma} = \gamma \times M_{\text{Planck}}^2/M^2$. In this way, all the dependence on the comparison between the black-hole mass and the Planck mass is absorbed into $\tilde{\gamma}$ alone. The corresponding RG-improved spacetime is regular. This can be observed via the RG-improved Kretschmann scalar

$$K_{\text{improved}} = \frac{48\left(2\tilde{\gamma}^4 - \frac{4r^9\tilde{\gamma}}{r_g^9} + \frac{18r^6\tilde{\gamma}^2}{r_g^6} - \frac{2r^3\tilde{\gamma}^3}{r_g^3} + \frac{r^{12}}{r_g^{12}}\right)}{r_g^4\left(\tilde{\gamma} + \frac{r^3}{r_g^3}\right)^6} \quad \xrightarrow{r\to 0} \quad \frac{96}{r_g^4\,\tilde{\gamma}^2} = \frac{96\,M_{\text{Planck}}^4}{\gamma}\,. \tag{7.5}$$

The curvature of the center is Planckian but now finite due to the quantum effects. The quantum-repulsive force also modifies the final stages of Hawking radiation and suggests a Planck-size black-hole remnant [623, 626–628], cf. Sec. 1.1.3 for such Planckian remnants in the context of dark matter.
RG improved black-hole spacetimes have been investigated extensively, including studies of dynamical collapse [629–632], in higher dimensions [633], including quadratic-gravity couplings [634], as well as in the presence of a cosmological constant [635–640]. See also [641] for a functional truncation of asymptotic safety and the resulting quantum-improved Newtonian potential. Quasi-normal modes and axial-symmetric cases have been discussed in [642] and [3, 633, 639, 643, 644], respectively.

Keeping in mind that RG improvement is by no means a full quantum-gravity calculation, we emphasize a degree of arbitrariness for the black-hole case in comparison to the former example

[127] Hayward simply postulated this metric as an example for a regular spacetime which matches Schwarzschild at asymptotically large radii and features a regular core, also see [625] for an earlier suggestion.

of RG-improving the classical Coulomb potential. Firstly, the RG-improved solution is *not* self-consistent since the background metric has been modified. In particular, a scale identification $k^2 \sim K^{1/2}_{\text{improved}}$ re-establishes the singularity. In [645], the RG-improvement has been iterated to obtain a converged and self-consistent solution. This procedure again recovers a regular metric, the Dymnikova solution [646, 647].
Secondly, the full quantum theory can be expected to receive contributions from the cosmological constant and higher-order operators. We caution that this leads to spacetimes with multiple physical scales. A simple scale identification will thus not necessarily give physically meaningful results. Indeed, it has been shown in [640] that, for a single-scale RG-improvement of Schwarzschild-de-Sitter spacetime, singularity-resolution requires the cosmological constant to approach an asymptotically free fixed point with a critical exponent $\theta \geqslant 2$.

7.1.2 Singularity resolution from other quantum-gravity models

The singularity-resolving effect of quantum fluctuations, as suggested by RG improvement in the previous section can be attributed to the antiscreening character of gravitational quantum fluctuations. The same repulsive nature of gravitational quantum fluctuations has been observed in many different quantum-gravity approaches. In Loop Quantum Gravity the fundamental discreteness of spacetime also leads to an effective repulsive force, see, e.g., [648]. The resulting regular black-hole spacetimes [649–652] are also of Hayward type. Moreover, a non-commutative structure of spacetime [653] as well as stringy corrections [654] motivate a similar repulsive character of quantum gravity. Even the very basic application of an uncertainty principle for spacetime points motivates regular black-hole solutions [655].

The requirement of a repulsive force to resolve a classical singularity can be extended into a very general argument. This force need not be provided by quantum effects. Any modification of gravity which vanishes at large distances such that the Schwarzschild metric is reproduced and resolves the curvature singularities such that a regular and hence physical spacetime is obtained has to be a repulsive force. If, in favor of simplicity, its repulsive character does not change at intermediate scales, one can generally conclude that it will weaken the gravitational force generically. As a result, any modifying repulsive force that leads to singularity resolution will generically lead to a more compact horizon as in [624, 646, 647, 656].

7.2 Spherically-symmetric and singularity-free shadows

Given the first observation of a black-hole shadow [109–114], it is crucial to understand how singularity-resolving physics qualitatively modifies such images [3], see also [657–659]. Even without calculation, it is intuitive that a repulsive force will lead to a weakening of gravity, hence a more compact object with a smaller horizon, and thus also to a smaller shadow image.

For massless particles (photons) in a general static and spherically symmetric metric $ds^2 = -f(r)\,dt^2 + h(r)\,dr^2 + r^2 d\Omega^2$ there exist multiple distinct critical surfaces. For obvious symmetry reasons, all of these are exactly circular. An event horizon is defined as the surface which cannot be crossed by *any* (in particular not by radial) geodesics. This corresponds to the radial distance at which the g_{rr} component of the metric diverges, i.e.,

$$1/h(r_{\text{horizon}}) = 0\,. \tag{7.6}$$

For Schwarzschild spacetime one recovers $r_{\text{horizon}} = 2r_g$.
Outside of the horizon, radial geodesics all escape to infinity. This is not true however for non-radial photons. The larger the angular momentum of a photon (and hence the smaller its radial component), the further outside it can still be captured by the black hole. At a particular radial distance from the horizon photons with purely angular momentum can circle the central object on an unstable orbit – the photon sphere. Marginally inside this object and they will fall towards the event horizon, marginally outside this object and they will escape to infinity[128]. To determine the location of the photon sphere, i.e., the critical lightlike geodesic, we have to solve the geodesic equation $g_{\mu\nu}\dot{x}^\mu\dot{x}^\nu = 0$ within the respective spacetime. The two constants of motion, i.e., energy E and angular momentum L_z, and their respective Euler-Lagrange equations

$$\dot{t} = \frac{E}{f(r)} \qquad \text{and} \qquad \dot{\phi} = \frac{L_z}{r^2} \tag{7.7}$$

can be used to reduce the geodesic motion to a purely radial equation, see, e.g., [660],

$$\dot{r} = \frac{1}{h(r)}\left(\frac{E^2}{A(r)} - \frac{L_z^2}{r^2}\right) . \tag{7.8}$$

The critical trajectory is defined by $\dot{r} = 0$ and $\partial_r\dot{r} = 0$, from which one finds the condition

$$2\,f(r_{\gamma\text{-sphere}}) - r_{\gamma\text{-sphere}}\,f'(r_{\gamma\text{-sphere}}) = 0 , \tag{7.9}$$

In case of multiple horizons, there also exist multiple photon spheres.
Taking an image of a black hole from asymptotic infinity, all lightlike geodesics will already be attracted towards the black hole as they approach the photon sphere. Hence, the shadow in the image plane will appear larger than the photon sphere. It is determined by the critical impact parameter

$$\lambda_{\text{crit}}(r_{\gamma\text{-sphere}}) \equiv \left.\frac{L_z}{E}\right|_{r_{\gamma\text{-sphere}}} = \frac{r_{\gamma\text{-sphere}}}{\sqrt{f(r_{\gamma\text{-sphere}})}} . \tag{7.10}$$

For Schwarzschild spacetime, one finds $\lambda_{\text{crit}} = 3\sqrt{3}\,r_g$. For the outermost horizon, it always holds that $\lambda_{\text{crit}} > r_{\gamma\text{-sphere}} > r_{\text{horizon}}$.

Turning to the quantum-improved metric in Eq. (7.4), we only consider solutions of the horizon, photon-sphere and shadow conditions which are positive and real, i.e., physical, for at least some range of the new-physics parameter $\tilde{\gamma}$. The quantum-improved horizon which continuously deforms into the Schwarzschild horizon lies at

$$r_H = \frac{r_g}{6}\left[4 + 8\times 2^{1/3}\,\zeta^{-1} + 2^{2/3}\zeta\right], \qquad \text{with} \qquad \zeta = \left(16 - 27\tilde{\gamma} + 3\sqrt{3\tilde{\gamma}^2(-32+27\tilde{\gamma})}\right)^{1/3} . \tag{7.11}$$

Because the quantum-improved solution has a regular de-Sitter core instead of a singularity at $r = 0$, another interior horizon emerges from $r = 0$ with growing $\tilde{\gamma}$, cf. red-dashed line in Fig. 30. With growing $\tilde{\gamma}$ the outer horizon shrinks while the inner one grows. At a critical $\tilde{\gamma}_{\text{crit},1} = 35/27$, the repulsive force grows so strong that the two horizons collide and a horizonless compact object remains. The same structure of real solutions is found for the photon sphere, cf. green-dotted

[128] For any massive particles there exists a stable circular orbit outside of the photon sphere: the innermost stable circular orbit (ISCO).

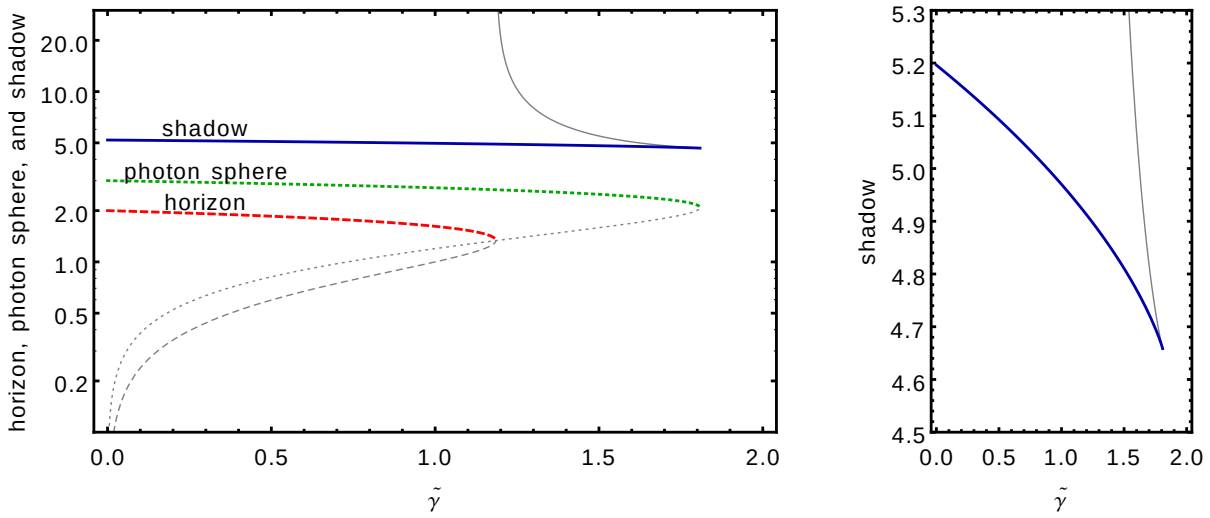

Figure 30: Left-hand panel: Horizon (red-dashed line), photon sphere (green-dotted line), and shadow (blue-solid line) for a regular black hole with $\tilde{\gamma}$ parameterizing the relative strength of singularity-resolving physics. Thin dashed, dotted, and solid gray lines mark the respective location of the inner horizon, the inner photon sphere, and the image of the latter. Right-hand panel: Zoom-in plot of the shadow boundary in the image plane at infinite radial distance.

line in Fig. 30. However, the photon sphere disappears at a larger $\tilde{\gamma}_{\mathrm{crit},2} = 1.81 > \tilde{\gamma}_{\mathrm{crit},1}$. Since the outer shadow is algebraically determined from the outer photon sphere, it also persists up to $\tilde{\gamma}_{\mathrm{crit},2}$. The inner shadow, however, remains complex as long as the inner photon sphere lies within the outer horizon, i.e., until $\tilde{\gamma}_{\mathrm{crit},1}$ is reached. Physically this can be understood since the image plane and the inner photon sphere are separated by an event horizon and hence cannot be in causal contact. Contrarily, in the horizonless spacetime, i.e., for $\tilde{\gamma} > \tilde{\gamma}_{\mathrm{crit},1}$, the two can be in causal contact. Therefore, the inner photon sphere formally results in an additional critical impact parameter connecting points in the image plane to the inner photon sphere. This image of the inner photon sphere moves inwards from infinite radial distance, cf. Fig. 30. At $\tilde{\gamma}_{\mathrm{crit},2}$ the two critical impact parameters collide and vanish into the complex plane.
It should be emphasized that for $\tilde{\gamma} > \tilde{\gamma}_{\mathrm{crit},1}$, no spacetime point is causally disconnected from the image plane. The appearance of the remaining horizonless compact object in the image plane and whether it can be distinguished from a black-hole shadow crucially depends on whether it still captures photons inside the outer photon sphere or possibly even emits radiation from its surface. This can only be answered in more realistic general-relativistic-magnetohydrodynamic (GRMHD) simulations [661] which can determine the matter distribution and its emissivity within the horizonless spacetime. Therefore, the highly relevant question of whether horizonless objects resulting from new singularity-resolving physics can mimic a black-hole shadow has to be deferred to future research. In the following, we focus on values $\tilde{\gamma} < \tilde{\gamma}_{\mathrm{crit},1}$ for which the horizon still exists.

Degeneracy of singular and non-singular shadows. For any new repulsive gravitational force, the size of the black-hole shadow in the image plane shrinks, cf. Fig. 30. Due to spherical symmetry, the singularity-free shadow boundary is degenerate to a Schwarzschild shadow of lower mass. In particular, the RG-improved metric can be rewritten as a Schwarzschild metric

with an effective mass

$$M_{\rm eff}(r) = \frac{M}{1+\tilde{\gamma}\,(r_g/r)^3}\,. \tag{7.12}$$

For each $\tilde{\gamma} < \tilde{\gamma}_{\rm crit,1}$, one can find a classical mass $M' = M_{\rm eff}(r_{\rm horizon})$. The shadow of the classical black hole of mass M' and that of the regular black hole of mass M will appear degenerate. To distinguish the two cases, one requires a second mass measurement at different radial distance. This can, for instance, be extracted from the measurement of orbital periods of stars at distances $\gtrsim 10^3\, r_g$. Since the modifications fall of with r^{-3}, any influence of $\tilde{\gamma} < \mathcal{O}(1)$ is tiny at orbital scales and the orbital mass $M'' \approx M$ to very good degree. Hence, the two mass measurements M' and M'' allow to infer

$$\tilde{\gamma} = \left(\frac{M''}{M'} - 1\right) \frac{r_g}{r_{\rm horizon}}\,. \tag{7.13}$$

For the case of M87*, M' is measured by the EHT collaboration [114] with an accuracy of 14% and M'' is measured by stellar dynamics [662] with an accuracy of 10%. Within 1σ standard deviation of each measurement, $M''/M' \approx 0.54^{+0.25}_{-0.16}$. Within 2σ of each other, the measurements agree. Despite the 1σ disagreement, we only emphasize that a horizonless object with $\tilde{\gamma} > \tilde{\gamma}_{\rm crit,1} \approx 1.3$ *cannot* be excluded by current data.

7.3 A dent in singularity-free Kerr spacetime

Astrophysical black holes (or their singularity-free counterparts) are assumed to rotate. In classical GR, rotating black holes of mass M and angular momentum J can be described by the Kerr metric in Boyer-Lindquist coordinates [663], i.e.,

$$\begin{aligned} ds^2 = &-\left(1 - \frac{2\bar{G}_0 M\, r}{\Sigma}\right) dt^2 - \frac{4\,a\,\bar{G}_0 M\, r\, \sin(\theta)^2}{\Sigma}\, dt\, d\phi + \frac{\Sigma}{\Delta} dr^2 + \Sigma\, d\theta^2 \\ &+ \left(r^2 + a^2 + \frac{2\,a^2\,\bar{G}_0 M\, r\, \sin(\theta)^2}{\Sigma}\right) \sin(\theta)^2\, d\phi^2\,, \end{aligned} \tag{7.14}$$

where $a = J/M$ is the spin parameter, $\Sigma = r^2 + a^2\cos(\theta)^2$ and $\Delta = r^2 - 2\,M\,r + a^2$. For the Kerr metric, one distinguishes between a divergent radial metric component $1/g_{rr} = 0$ which defines horizons, and a vanishing temporal component of the metric $g_{tt} = 0$ which defines ergospheres. For the spherically-symmetric case these two surfaces agree. For the Kerr metric one finds

$$r^{\pm}_{\rm horizon} = M \pm \sqrt{M^2 - a^2}\,, \qquad r^{\pm}_{\rm ergo} = M \pm \sqrt{M^2 - a^2\,\cos(\theta)^2}\,, \tag{7.15}$$

see dashed lines in Fig. 31. For spins $a > M$, the horizon would vanish leading to a naked singularity. Hence, such a are considered as unphysical within GR. For singularity-free spacetimes, in principle, no such restriction is required.

Note that the horizon remains spherical. This is a manifestation of a hidden constant of motion – the so-called Carter constant [664]. The latter allows separating the radial and the angular dynamics of the motion of a light-like test particle within Kerr spacetime. This also applies for generalizations to arbitrary $M \to M(r)$. Making use of this constant of motion, one can find an analytic expression for the shadow boundary within the image plane, see, e.g., [660, 665, 666]. For growing spin-parameter and within the equatorial plane, the shadow moves within the image

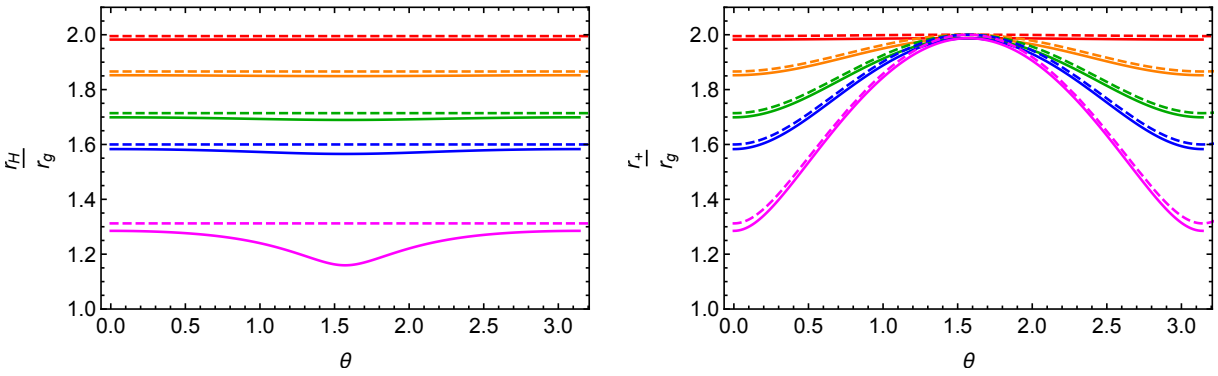

Figure 31: Left panel: Classical (dashed lines) and quantum-improved ($\tilde{\gamma} = 0.05$, continuous lines) outer horizon r^+_{horizon}. From top to bottom we show cases for $a = 0.\,r_g$ (red), $a = 0.5\,r_g$ (orange), $a = 0.7\,r_g$ (green), $a = 0.8\,r_g$ (blue) and $a = 0.95\,r_g$ (magenta). Right panel: Outer boundary of the ergosphere r^+_{ergo} in the same cases.

plane in the direction of the black-holes spin. More interestingly, it is also deformed. With growing a it flattens on the prograde side of the image (the side at which the rotation of the black hole points out of the image plane), see thin green lines in the right-hand panel Fig. 32. As the horizon remains spherical, this effect arises solely due to frame dragging within the ergosphere of the spinning black hole. Co-rotating light rays on the prograde side can approach the horizon much closer than those in retrograde (moving against the black-holes spin) motion. Withing the equatorial plane two – a prograde and a retrograde – photon sphere can be distinguished [667], i.e.,

$$r^{\pm}_{\gamma\text{-sphere}} = 2M\left[1+\cos\left(\frac{2}{3}\arccos\left(\mp\frac{|a|}{M}\right)\right)\right], \qquad \begin{cases} r^+_{\gamma\text{-sphere}}: & \text{prograde} \\ r^-_{\gamma\text{-sphere}}: & \text{retrograde} \end{cases}. \tag{7.16}$$

Outside the equatorial plane, no circular photon orbits are possible. For extremal Kerr black holes, i.e., for $a = M$, the photon sphere and the horizon coincide. Fascinatingly, prograde light rays winding around near-extremal black holes can probe the black-hole spacetime arbitrarily close to the horizon. This makes them a unique candidate for probing new physics at horizon scales.

Regarding RG-improvement, we would like to identify the RG-scale k with local curvature scales, as we did for spherically-symmetric spacetimes. For constant mass M (classical Kerr case), the Kretschmann curvature is given by

$$K(r,\theta,a) = \frac{48G_0^2M^2}{(r^2+a^2\cos(\theta)^2)^6}\Big(r^6 - 15r^4a^2\cos(\theta)^2 + 15r^2a^4\cos(\theta)^4 - a^6\cos(\theta)^6\Big). \tag{7.17}$$

For large enough a, one finds regions of negative curvature, even outside of the horizon. Therefore, identifying $k^2 \sim K(r,\theta,a)^{1/2}$ is problematic as it would lead to complex-valued regions of spacetime. Similarly, $k^2 \sim |K(r,\theta,a)|^{1/2}$ would lead to singular surfaces.
One alternative is to simply drop all angular θ-dependence of the curvature [633, 639, 643, 644]. This corresponds to using simply the spherically-symmetric RG-improvement which we have expressed as a radial-distance dependent effective mass, cf. in Eq. (7.12). In this case, the geodesic motion of a test particle is still separable (i.e., the Carter constant is still conserved) and the

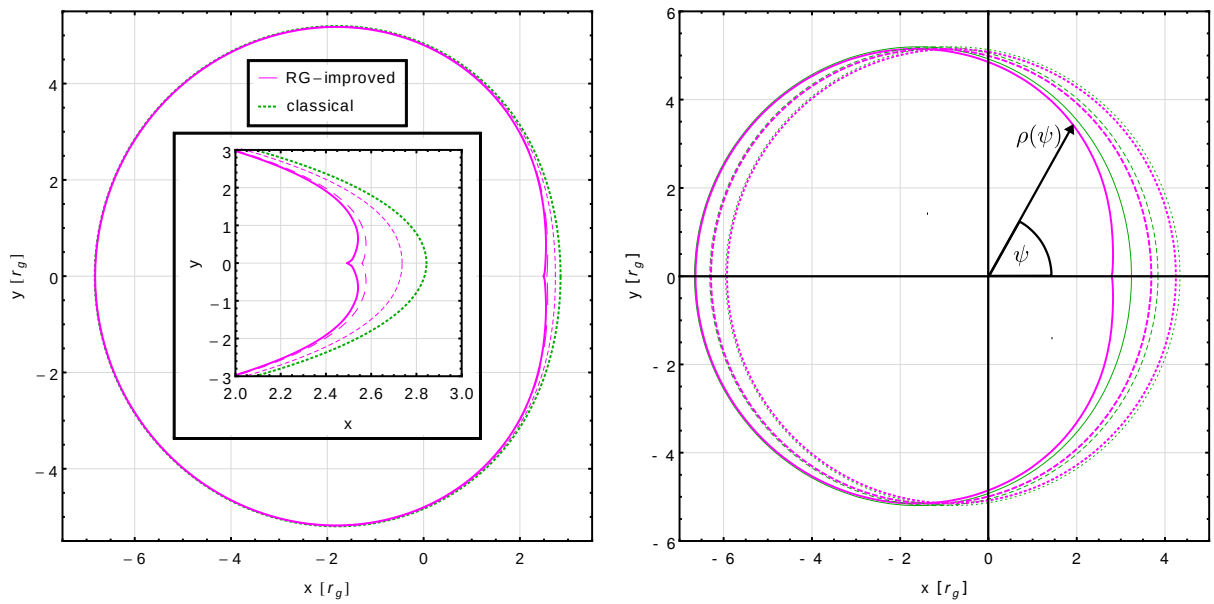

Figure 32: Left-hand panel: Classical (green dotted) and RG-improved (magenta) shadow for fixed spin parameter $a = 0.9\,r_g$. Shadows with growing $\tilde{\gamma} = (0.05, 0.1, 0.11)$ are marked by (narrow-dashed, wide-dashed and continuous) lines, respectively. Right-hand panel: Classical (thin green) and RG-improved (thick magenta) shadows at fixed $\tilde{\gamma} = 0.25$ for various spin-parameters $a = 0.4\,r_g$ (dotted), $a = 0.6\,r_g$ (dashed), and $a = 0.8\,r_g$ (continuous). In all cases the origin of the image plane lies within the equatorial plane.

RG-improved shadow boundary can be analytically obtained[129]. As an artifact of neglecting all θ-dependence, the shadow boundary is again exactly degenerate with a lower-mass classical black hole, as for the Schwarzschild case, see discussion in Sec. 7.2.

Physically, we expect that only the magnitude of local curvature sets the scale. This motivates an RG-improvement with the enveloping function of the Kretschmann scalar, i.e.,

$$k^2 = \frac{\bar{G}_0 M\, r^3}{(r^2 + a^2\cos(\theta)^2)^3}\,. \tag{7.18}$$

That is, we neglect[130] the a-dependent polynomial substructure in $K(r,\theta,a)$. This corresponds to an effective mass which now depends on both r and θ, i.e.,

$$M_{\rm eff}(r,\theta) = M\left(1 + \tilde{\gamma}\,\frac{r^3/r_g^3}{\left[r^2/r_g^2 + a^2/r_g^2\,\cos(\theta)^2\right]^3}\right)^{-1}\,. \tag{7.19}$$

As a consequence of the θ-dependence, the horizon is no longer spherical for $\tilde{\gamma} \neq 0$, cf. continuous lines in Fig. 31, and the Carter constant is no longer conserved, i.e., the radial and angular motion no longer separable. To obtain the shadow boundary, we have to thus resort to numerical methods. It can already be anticipated that the non-spherical horizon will now deform not just the size but also the shape of the shadow boundary in comparison to the classical one.

[129] See [659] for a derivation using the Newman-Janis algorithm [668]. The Newman-Janis algorithm preserves the Carter constant and only generates specific rotating solutions of the form Eq. (7.14).

[130] We checked that the RG-improvement obtained from a scale identification with the proper distance along the path of an infalling observer [643] results in a qualitatively similar deformation of the horizon.

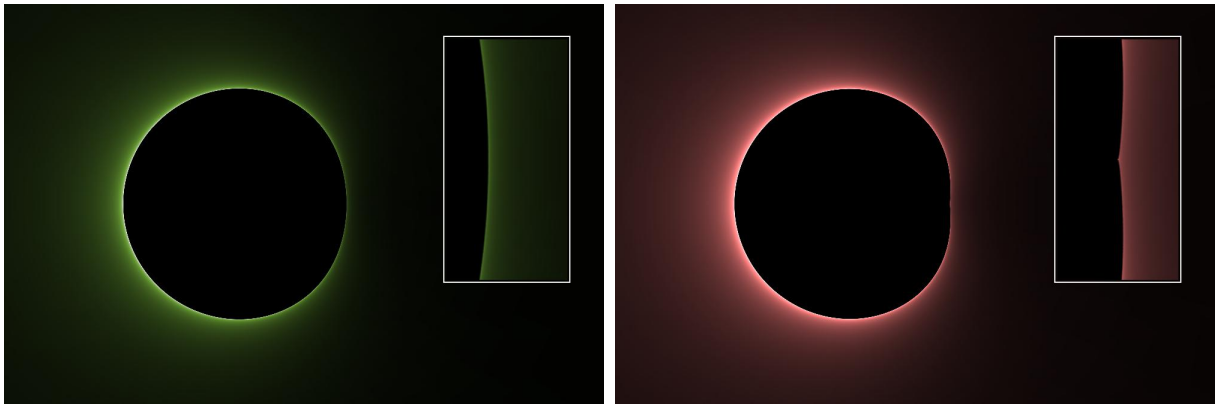

Figure 33: Image intensity extracted in the affine-parameter-emissivity approximation, see App. F for details. Left-hand and right-hand panel show the classical and singularity-free (for $\tilde{\gamma} = 0.11$) shadows, respectively. In both cases the spin-parameter is chosen at $a = 0.9\, r_g$. The insets zoom into the prograde (right) side of the image to reveal a close-up of the characteristic dent that results from singularity resolving physics.

Numerical shadow boundary. To obtain the shadow boundary, we numerically evolve the null geodesic equation to obtain light rays that we initialize perpendicularly to the observer screen. We distinguish two classes of light rays: (i) those that cross the black-hole horizon and (ii) those that escape to radial infinity. Within the screen, we parameterize the shadow boundary by its radial distance $\rho(\psi)$ to an origin of choice within the shadow, see right-hand panel in Fig. 32. The shadow boundary corresponds to the critical $\rho(\psi)$ that separates the classes (i) and (ii). For each boundary angle ψ, $\rho(\psi)$ can be approximated by a nested bisection, choosing the smaller or greater next-step interval whenever the respective light ray in the middle of the previous interval escapes (ii) or falls into the horizon (i). See, e.g., [660, Fig. 3.5] for a sketch of the geometrical setup and further description of the numerical ray tracing algorithm.
Fig. 32 compares the RG-improved to the classical shadow boundary for fixed a and varying $\tilde{\gamma}$ in the left-hand panel, and varying a but fixed $\tilde{\gamma}$ in the right-hand panel. Both growing a and growing $\tilde{\gamma}$ can lead to horizonless objects. Since the spacetime is singularity-free, these are no longer necessarily unphysical. Nevertheless, a meaningful discussion of the horizonless cases requires a model of the matter within the spacetime and will thus be subject of future GRMHD investigations. For near-extremal cases, i.e., close to the disappearance of the horizon at $\tilde{\gamma}_{\text{crit}}(a)$, the shadow develops a distinct feature on its prograde side, cf. Fig. 32. The shadow boundary develops a dent because rays which approach the prograde photon sphere can probe the θ-dependence of the singularity-free horizon. Additional subleading features which might be an artifact of our approximation of the Kretschmann scalar during the RG improvement are presented in App. F.2.

Conclusion

Black-hole shadows enable two novel probes of singularity-resolving physics if the latter is (i) caused by a repulsive force and (ii) grows with the absolute value of local curvature scales. For non-spinning black holes, we find that the most sensitive measurement is a comparison of a mass measurement at the photon-sphere via a black-hole shadow with a different mass measurement, e.g., from the orbital motion of stars, at a much larger distance to the black hole. Spherical shadows do not permit to test physics directly at the horizon ($r_{\text{horizon}} = 2M$) but are only sensitive to modifications of the spacetime outside the photon sphere ($r_{\gamma\text{-sphere}} = 3M$).

Excitingly, the shadows of spinning black holes can probe physics even closer to the horizon. As the black-hole spin grows towards extremality, light rays marginally outside the prograde photon sphere can, in principle, test physics arbitrarily close to the horizon. In those extreme cases, new singularity-resolving physics which obeys (i) and (ii) generically causes a characteristic dent-like feature in the shadow image, cf. Fig. 33 and 32.
We caution that we find the features of Planck-scale singularity resolution to be suppressed by $(M_{\text{Planck}}/M)^3$. For any astrophysically relevant black hole, effects from Planckian singularity resolution will not be detectable in practice.
Finally, experimental precision is not sufficient to exclude singularity-free horizonless compact objects within our model of new physics. This strongly motivates future research in this direction.

Closing matter

Conclusions

The effective field theory of General Relativity perturbatively breaks down and requires some type of new physics at the Planck scale $M_{\rm Planck}$. At the same time, experimental probes of the electroweak scale $M_{\rm ew}$ face a persistent absence of new physics. Reassessing the Standard Model of particle physics from the implied but somewhat unusual viewpoint of associating any new physics with $M_{\rm Planck}$ instead of with $M_{\rm ew}$, reveals hints for a new type of symmetry hidden within the Standard-Model parameters, cf. Sec. 1. Firstly, the Standard Model is perfectly consistent up to the Planck scale. Secondly, its measured coupling values delicately balance such that the Higgs potential is compatible with flatness, i.e., scale-invariance, at $M_{\rm Planck}$. To conclude, the measured values of Standard-Model couplings seem to point towards Planckian scale symmetry.
Concurrently, non-perturbative access to fixed points of the Renormalization Group flow has provided a large body of evidence for the Reuter universality class of Euclidean quantum gravity. Instead of breaking down at $M_{\rm Planck}$, General Relativity could become asymptotically safe, cf. Sec. 2. Above $M_{\rm Planck}$, the resulting joint theory of quantum gravity and matter could be dominated by the scaling exponents of the Reuter fixed-point. We have explored the predictive power of quantum scale symmetry and investigated the resulting phenomenology of a potential combined UV-completion of the Standard Model (Part II) and General Relativity (Part III).

We have investigated [10] and constructed [6] four-dimensional field theories which could exhibit asymptotic safety without the presence of quantum gravity in Sec. 3. All known examples fail to incorporate an Abelian gauge group and thus cannot contain the Standard Model unless it unifies into a purely non-Abelian gauge theory. Moreover, we advocate that such non-gravitational fixed points should be regarded as realizing effective asymptotic safety with a Planckian cutoff scale. Nevertheless, the predictivity of effective asymptotic safety might help guide model-building efforts and experimental dark-matter searches. In the absence of strongly interacting asymptotic safety, fermionic Higgs-portal models either over-stabilize the Higgs-potential or overclose the universe [4]. If on the other hand, the uncovered tentative mechanism [6] for asymptotic safety in scalar-fermion portal models persists in phenomenologically relevant extensions, the former could predict a relation between the Higgs-portal coupling to fermionic dark matter and the associated dark-fermion mass. Due to their non-perturbative RG flow, such models remain highly predictive even in effective asymptotic safety. We have also investigated the effective degree of predictivity for Litim-Sannino models for which we explicitly demonstrate that gravitational fluctuations can probably not just be ignored [10].

Turning to the interplay of asymptotically safe quantum gravity and matter in Sec. 4, we have scrutinized how global symmetries determine the available fixed-point structure of the matter theory. We have uncovered how two crucial constraints on asymptotically safe gravity could arise from demanding the existence (weak-gravity bound) and the viability (viability bound) of a fixed point in the matter sector [9]. We delineated a potential weak-gravity mechanism, driven by the presence of many fermionic degrees of freedom. This mechanism is crucial for asymptotically safe gravity-matter systems to evade the viability bound for Yukawa couplings: the present truncations suggest that without realizing a weak-gravity mechanism, asymptotic safety cannot be connected to IR-theories with non-vanishing Yukawa interactions.
Strikingly, present truncations indicate that the Standard Model contains enough fermionic degrees of freedom to realize the weak-gravity mechanism such that non-vanishing Yukawa in-

teractions can be accommodated. The resulting interacting fixed point is more predictive than the remaining free fixed point. It thus places an upper bound on all admissible RG trajectories. Assuming that the joint gravity-matter fixed point converges such as to realize a weak-gravity regime, the most predictive version of asymptotically safe gravity could UV-complete the Standard Model and predict a top mass within the vicinity of the observed value [8].

The weak-gravity mechanism suggests that gravitational fluctuations at and beyond the Planck scale manifest in scale-invariant, i.e., constant, antiscreening, and perturbatively small anomalous dimensions for gauge and Yukawa couplings, respectively. These contributions correspond to an effective reduction of the spacetime dimension. Without further assumptions, this defines a perturbative framework to investigate Planckian quantum scale symmetry. We apply the latter to the Standard Model. Focusing on the most predictive fixed points for the heavy quark generation, we have uncovered indications that scale symmetry links the mass ratio of top and bottom quark to their electric charges [5]. Moreover, upon including a right-handed neutrino, scale-invariance could dynamically drive the neutrino Yukawa coupling and hence its Dirac mass to small values.
We have successfully extended the heavy-quark-generation fixed-point structure to multiple generations. The scale-invariant contributions which are universal to all Yukawas cannot contribute to the running of the CKM parameters which mix multiple generations. Nevertheless, transitions between different non-mixing fixed points entail an interesting phenomenological structure. Unitarity of the CKM matrix results in poles in the CKM-sector of theory space which cannot be crossed by any continuous RG flow. Possible resulting hierarchies between quarks of different generations depend on the CKM transition scale rather than the Planck scale.
In view of effective asymptotic safety, the quantum-gravity fixed point could also result in global constraints on the RG flow. Consequentially, its potential existence has implications for any other fundamental theory of quantum gravity as well. To give an example, we delineated that an asymptotically safe fixed point could entail new swampland constraints on phenomenologically viable String compactifications in which vector bosons dominate the particle spectrum.

The predictive power of quantum scale symmetry can be extended to grand unified theories [7], cf. Sec. 6. Similar to the Standard-Model, a transplanckian scaling regime could place upper bounds on admissible gauge and Yukawa couplings. We have thereby generalized the concept of complete asymptotic freedom to complete asymptotic safety in gauge-Yukawa theories.
Moreover, we have pointed out that an asymptotically safe grand unified theory could remain without any free marginal couplings [1]. In particular, this includes the multi-dimensional scalar potentials which are responsible for spontaneous symmetry breaking of the unified gauge group to the Standard Model. Thereby, scale symmetry could restore the predictive power of grand unification. It can fix all quartic couplings of the unified scalar potential and thus could determine the direction of symmetry breaking. We have outlined how to exploit this predictive power for minimal non-supersymmetric SO(10) models.

Finally, an asymptotically safe scaling regime might not just resolve the singularities of the Standard Model but also curvature singularities in General Relativity. For the first time, we determine the impact of singularity-resolving physics on both non-spinning and spinning black-hole shadows [3], cf. Sec. 7. Different quantum-gravity models motivate structurally similar singularity-free black-hole spacetimes. Singularity resolution tied to local curvature scales tends to shrink the shadow size and could imprint characteristic features on the shadow-shape of spin-

ning black holes. On the one hand, the magnitude of such features in the shadow boundary is tied to the Planck scale and therefore suppressed. On the other hand, we find that the groundbreaking observations of the Event Horizon Telescope are not yet able to exclude horizonless objects. This allows to speculate about unexpected but experimentally not yet excluded modified gravitational dynamics to resolve the singularity.

We conclude with the exciting possibility of an asymptotically safe Standard Model (ASSM). Quantum scale-symmetry could manifest itself in upper bounds on sufficiently screened gauge couplings as well as on all Yukawa couplings. We have thereby uncovered intriguing hints that the predictive power of the ASSM potentially enhances the predictivity of the Standard Model.

Outlook

On the basis of this PhD thesis, we identify three potential points of contact between quantum gravity and observation on which we give a short outlook below: (i) marginal couplings in particle physics; (ii) global properties of Renormalization Group flows and their significance for cosmological evolution; and (iii) black-hole dynamics and stability in the strong-gravity regime.

(i) Quantum scale symmetry: beyond the Standard Model.
The most obvious continuation of the research efforts in this thesis is to extend the fixed-point analysis in the asymptotically safe Standard Model, cf. Sec. 5 to include the PMNS mixing matrix for three leptonic generations. Moreover, the Higgs potential poses a crucial open question. At fixed points with non-vanishing gauge and Yukawa interactions, the Higgs-potential will be non-vanishing, in general. A study of its stability and a potential connection to the observed IR value depends decisively on its non-minimal coupling to gravity and remains a pivotal question for future research.
The investigated paradigm of Planckian quantum scale symmetry generalizes to any beyond Standard-Model theory which is consistent up to the Planck scale. We have already delineated such efforts for grand unified models. The determination of the full quartic scalar potential of the minimal SO(10) model is certainly an outstanding future task. Such efforts would gain particular relevance once predictive fixed-points of the Standard Model could potentially be excluded. We emphasize that studies along the line of Sec. 5 do not necessarily require a non-perturbative calculation. We eventually envision that particle physics software such as SARAH [669] or Pyr@te [670] can be extended to generate the asymptotically safe fixed-point structure for any such new physics model.

(ii) Global properties of the RG flow and cosmology.
Several instances within this thesis exemplify that the presence of fixed points and the separatrices between them – assumed here as unequivocally established – affects the global properties of RG flows. One example are the eigenvectors of one fixed point (e.g., the Gaußian one) which do depend on the existence and location of other fixed points (e.g., an asymptotically safe one), cf. Fig. 3 in Sec. 2.4.2. While a proper understanding of such global properties requires a sufficiently converged truncation of the RG-flow, the result could be of crucial phenomenological significance. Regarding quantum gravity and except for the marginal couplings in (i), most properties of the asymptotically safe fixed point will always be Planck-scale suppressed. In contrast, the eigenvectors of the Gaußian fixed point determine physics in the vicinity of experimentally accessible scales. If these depend on the presence of the asymptotically safe fixed point, the

latter could become testable. In the context of cosmology, the freezeout of the cosmological constant in the vicinity of the Gaußian fixed point occurs at CMB scales, cf. last paragraph in Sec. 2.4.2. Therefore, its eigenvectors could be accessible by current CMB experiments.

(iii) Black-hole dynamics: from quantum to strong-field gravity.
This thesis exploits the logarithmic running of marginal matter couplings. Under the assumption that all intermediate physics is known, this provides a unique theoretical connection to potentially test Planck-scale physics. It also applies to the marginal pure-gravity couplings at the quadratic curvature level. The latter are thus unsuppressed below the Planck scale and current weak-field measurements leave them basically unconstrained, i.e., they could be as large as 10^{60}. A comparison of curvature scales in the solar system to those at the surface of black holes reveals that constraints can be dramatically improved by advances of theory and experiment into the strong-field regime. The black-hole dynamics of the effective theory of quadratic gravity not only provides one of the most extreme tests of General Relativity but might also result in implications for quantum-gravity theories at its origin.
Before being able to perform full binary-merger simulations in quadratic gravity, the physical stability of black-hole solutions should be established. Stability of the Schwarzschild solution against spherically-symmetric perturbations has already been performed in [671]. Testing stability against arbitrary perturbations requires a numerical analysis and thus a well-posed initial value problem. While the existence of the latter has been proven [672], the proof is not constructive and a derivation of the corresponding evolution equations remains as a first future task to tackle this exciting question. If black-hole solutions turn out to be stable, this could open up future research to constrain quadratic gravity via binary mergers. If the former are unstable, however, this would imply that the leading-order quantum corrections in a local-operator expansion are not sufficient to obtain viable IR dynamics.

Arguably, the above three promising research avenues resulting from this thesis warrant further investigation. We hope that this thesis exemplifies that quantum gravity is an experimentally driven research field. Despite the enormity of the Planck scale, "making quantum gravity observable" is not a hopeless effort – and the most exciting low-energy phenomenology of quantum gravity remains to be explored in the future.

Appendix

coupling	1-loop scheme at $k = 173$ GeV	parameter	measured value
g_Y	0.35	α_{EM}	7.2973525698(24) [673]
g_2	0.65	M_W	80.385 ± 0.015 [674]
g_3	1.17	M_Z	91.1876 ± 0.002 [674]
y_t	0.94	M_t	163 ± 3 GeV [27, 28] (running mass)
y_b	24×10^{-3}	M_b	4.18 ± 0.03 GeV ($\overline{MS}$ value) [398]
y_c	73×10^{-4}	M_c	1.275 ± 0.025 GeV [398]
y_s	5×10^{-4}	M_s	95 ± 5 MeV [398]
y_u	1×10^{-5}	M_u	$2.3^{+0.7}_{-0.5}$ MeV [398]
y_d	2×10^{-5}	M_d	$4.8^{+0.7}_{-0.3}$ MeV [398]
X	0.949	$\lvert V_{ud}\rvert$	0.97425(22) [398]
Y	0.05	$\lvert V_{us}\rvert$	0.2252(9) [398]
Z	0.05	$\lvert V_{cd}\rvert$	0.230(11) [398]
W	1	$\lvert V_{cs}\rvert$	1.006(23) [398]
y_τ	102×10^{-4}	M_τ	1776.82 ± 0.16 MeV [398]
y_μ	6×10^{-4}	M_μ	105.6583715(35) MeV [398]
y_e	2.87×10^{-4}	M_e	0.510998928(11) MeV [398]
θ_{QCD}	~ 0	—	—
vev/GeV	246 GeV	G_F	1.1663787(6) GeV [673]
λ_H	0.1	M_H	125.15 ± 0.24 GeV [398]

Table 9: Tree-level matching values of the Standard-Model couplings at a common RG-scale of $k = 173$ GeV. In all cases, the last digit shown is significant (some values might be known more precisely). We also state the experimentally measured parameters used to determine the coupling values. For explicit β-functions and relations between experimental parameters and couplings please refer to [26].

A Standard-Model parameters and couplings

Tab. 9 provides reference values for measured Standard-Model parameters and tree-level matching to running couplings. Unless specified otherwise, these are used to initialize 1-loop perturbative RG flows within this thesis.

B Fermionic Higgs-portal model: Supplementary material

B.1 β-functions for the fermionic Higgs-portal model

Here, we present supplementary information on the derivation of the β-functions for the $O(N)$-scalar ϕ coupled to a dark fermion ψ, cf. Sec. 3. In view of Sec. 3.1.2 where also a toy-SM is coupled, we also include a generalized Yukawa coupling term to a *different* fermion denoted by $\bar{t}$. Therefore the truncation of the effective action reads

$$\Gamma_k = \int d^dx \left[\frac{Z_\phi}{2}\partial_\mu\phi\partial^\mu\phi + \bar{U}(\rho) + Z_\mathrm{t}\,\bar{t}\mathrm{i}\partial\!\!\!/ t + \frac{\mathrm{i}}{\sqrt{2}}\bar{H}(\rho)\phi\,\bar{t}t + Z_\psi\,\bar{\psi}\mathrm{i}\partial\!\!\!/\psi + \mathrm{i}\bar{V}(\rho)\bar{\psi}\psi \right]. \tag{B.1}$$

We emphasize the different global symmetry structure: The generalized Yukawa-coupling term is invariant under a discrete chiral symmetry under which $\phi \to -\phi$, $t \to \mathrm{e}^{\mathrm{i}\frac{\pi}{2}\gamma_5}t$, and $\bar{t} \to \bar{t}\,\mathrm{e}^{\mathrm{i}\frac{\pi}{2}\gamma_5}$. The generalized dark-matter portal term is invariant under a continuous U(1) symmetry under which $\psi \to \mathrm{e}^{\mathrm{i}\alpha}\psi$ and $\bar{\psi} \to \mathrm{e}^{-\mathrm{i}\alpha}\bar{\psi}$.
To derive the flow of the scalar potential $\bar{U}(\rho)$ and the scalar functions $\bar{H}(\rho)$ and $\bar{V}(\rho)$, we expand the flow equation (2.5) in terms of the fermionic fields but we keep the scalar potentials generic. More specifically, we can split the two-point function $\Gamma_k^{(2)} + R_k$ into

$$\Gamma_k^{(2)} + R_k = \mathcal{P}_k + \mathcal{F}_k\,, \tag{B.2}$$

where $\mathcal{P}_k = \left(\Gamma_k^{(2)} + R_k\right)\big|_{\psi=\bar{\psi}=t=\bar{t}=0}$ and $\mathcal{F}_k = (\Gamma_k^{(2)} + R_k) - \mathcal{P}_k$ is the remaining part. This admits the so-called $\mathcal{P}$–$\mathcal{F}$ expansion [459], i.e.,

$$\partial_t\Gamma_k = \frac{1}{2}\mathrm{Tr}\,\tilde{\partial}_t\,\mathcal{P}_k^{-1} + \frac{1}{2}\sum_n \frac{(-1)^{n-1}}{n}\mathrm{STr}\tilde{\partial}_t\left(\mathcal{P}_k^{-1}\mathcal{F}\right)^n\,, \tag{B.3}$$

where $\tilde{\partial}_t$ denotes a scale-derivative which *only* acts on regulators R_k. Calculating the matrix multiplications and traces in Eq. (B.3) to sufficiently high order and projecting on the corresponding field monomial obtains the RG-flow of $\bar{U}(\rho)$, $\bar{H}(\rho)$, and $\bar{V}(\rho)$. Transitioning to renormalized and dimensionless quantities, i.e.,

$$\begin{aligned} \rho &= Z_\phi k^{d-2}\tilde{\rho}\,, & U &= k^{-d}\bar{U}\,,\\ H &= Z_\phi^{-\frac{1}{2}}Z_\psi^{-1}k^{\frac{4-d}{2}}\bar{H}\,, & V &= Z_\psi^{-1}k^{-1}\bar{V}\,, \end{aligned} \tag{B.4}$$

the running of the potential functions reads

$$\begin{aligned} \partial_t U(\tilde{\rho}) &= -d\,U + \left(d-2+\eta_\phi\right)\tilde{\rho}U'\\ &\quad + 2v_d\left[l_0^{(B)d}(\omega_\phi;\eta_\phi) - d_\gamma\,l_0^{(\mathrm{F})d}(\omega_\mathrm{t};\eta_\mathrm{t}) - d_\gamma N_\mathrm{f}\,l_0^{(\mathrm{F})d}(\omega_\psi;\eta_\psi)\right], \end{aligned} \tag{B.5}$$

$$\begin{aligned} \partial_t h_\mathrm{t}(\tilde{\rho}) &= \frac{1}{2}(d-4+\eta_\phi+2\eta_\mathrm{t})h_\mathrm{t} + (d-2+\eta_\phi)\tilde{\rho}h_\mathrm{t}'\\ &\quad + 2v_d\,h_\mathrm{t}(h_\mathrm{t}+2\tilde{\rho}h_\mathrm{t}')^2\,l_{1,1}^{(\mathrm{BF})d}(\omega_\phi,\omega_\mathrm{t};\eta_\phi,\eta_\mathrm{t}) - 2v_d\,(3h_\mathrm{t}'+2\tilde{\rho}h_\mathrm{t}'')\,l_1^{(\mathrm{B})d}(\omega_\phi;\eta_\phi), \end{aligned} \tag{B.6}$$

$$\begin{aligned} \partial_t h_\psi(\tilde{\rho}) &= (-1+\eta_\psi)h_\psi + (d-2+\eta_\phi)\tilde{\rho}h_\psi'\\ &\quad + 8v_d\,\tilde{\rho}\,h_\psi h_\psi'^2\,l_{1,1}^{(\mathrm{BF})d}(\omega_\phi,\omega_\psi;\eta_\phi,\eta_\psi) - 2v_d\,(h_\psi'+2\tilde{\rho}\,h_\psi'')\,l_1^{(\mathrm{B})d}(\omega_\phi;\eta_\phi)\,, \end{aligned} \tag{B.7}$$

where we have defined the generalized mass thresholds $\omega_\phi = U' + 2\tilde{\rho}U''$, $\omega_\mathrm{t} = \tilde{\rho}h_\mathrm{t}^2$, and $\omega_\psi = h_\psi^2$, primes denote derivatives with respect to the dimensionless field invariant $\tilde{\rho}$, d denotes the

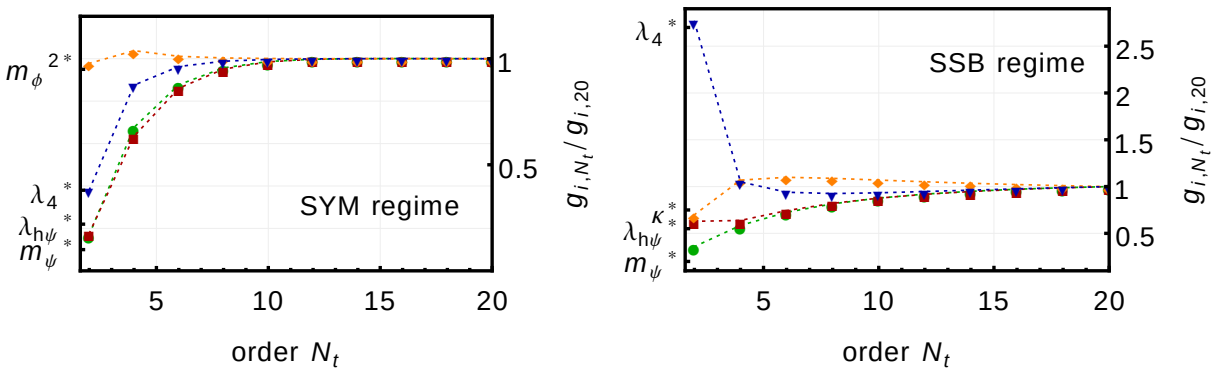

Figure 34: Left-hand panel: Fixed-point values in the symmetric regime with increasing truncation order $N_t = N_U$, keeping $N_V = 1$ at the first non-trivial order. Right-hand panel: Same as the left-hand panel but now in the symmetry-broken regime, including anomalous dimension (referred to as $\mathrm{LPA}'_{\mathrm{N_V}}$ in the literature). The fixed-point values are normalized to their highest-order values.

spacetime dimension, d_γ is the dimension of the Clifford algebra, and $v_d^{-1} = 2^{d+1}\pi^{\frac{d}{2}}\Gamma(d/2)$. Further, the running of the anomalous dimensions $\eta_{\phi/\mathrm{t}/\psi} = -\partial_t \ln Z_{\phi/\mathrm{t}/\psi}$ encodes the running of wave-function renormalizations. Their flow can be obtained by appropriate momentum-dependent projections of the 1st order of Eq. (B.3) and reads

$$\eta_\phi = \frac{4v_d}{d}\Big\{2\kappa\big(3U'' + 2\kappa U'''\big)^2 m_2^{(\mathrm{B})d}(\omega_\phi;\eta_\phi) \quad + d_\gamma(h_\mathrm{t} + 2\kappa h_\mathrm{t}')^2\Big[m_4^{(\mathrm{F})d}(\omega_\mathrm{t};\eta_\mathrm{t}) - \kappa h_\mathrm{t}^2 m_2^{(\mathrm{F})d}(\omega_\mathrm{t};\eta_\mathrm{t})\Big]$$
$$+ 4d_\gamma\kappa h_\psi'\Big[m_4^{(\mathrm{F})d}(\omega_\psi;\eta_\psi) - h_\psi^2 m_2^{(\mathrm{F})d}(\omega_\psi;\eta_\psi)\Big]\Big\}_{\tilde\rho=\kappa}, \tag{B.8}$$

$$\eta_\mathrm{t} = \frac{4v_d}{d}(h_\mathrm{t} + 2\kappa h_\mathrm{t}')^2 m_{1,2}^{(\mathrm{FB})d}(\omega_\mathrm{t},\omega_\phi;\eta_\mathrm{t},\eta_\phi)\Big|_{\tilde\rho=\kappa}, \tag{B.9}$$

$$\eta_\psi = \frac{16v_d}{d}\kappa\, h_\psi'^2\, m_{1,2}^{(\mathrm{FB})d}(\omega_\psi,\omega_\phi;\eta_\psi,\eta_\phi)\Big|_{\tilde\rho=\kappa}, \tag{B.10}$$

evaluated at the VEV $\tilde\rho = \kappa$. Note that we drop the $\sim$ in the main text.
To evaluate the threshold functions l and m the choice of regulator has to be specified. We use a spectrally adjusted [308] Litim-type [675], i.e.,

$$R_k^B = Z_B\left(k^2 - p^2\right)\theta\left(k^2 - p^2\right), \qquad R_k^F = Z_F\not{p}\left(\sqrt{k^2/p^2} - 1\right)\theta\left(k^2 - p^2\right), \tag{B.11}$$

for bosonic and fermionic modes, respectively. For this regulator choice, the threshold functions are given in [406, App.A].

The β-functions can be expanded in terms of symmetric (SYM) or symmetry-broken (SSB) potentials, i.e.,

$$U_{\mathrm{SYM}}(\tilde\rho) = \sum_{n=1}^{N_U}\frac{\lambda_{2n}}{n!}\tilde\rho^n, \qquad H_{\mathrm{SYM}}(\tilde\rho) = \sum_{n=0}^{N_H}\frac{y_n}{n!}\tilde\rho^n, \qquad V_{\mathrm{SYM}}(\tilde\rho) = \sum_{n=0}^{N_V}\frac{\lambda_{2n}^{(V)}}{n!}\tilde\rho^n, \tag{B.12}$$

$$U_{\mathrm{SSB}}(\tilde\rho) = \sum_{n=1}^{N_U}\frac{\lambda_{2n}}{n!}(\tilde\rho-\kappa)^n, \quad H_{\mathrm{SSB}}(\tilde\rho) = \sum_{n=0}^{N_H}\frac{y_n}{n!}(\tilde\rho-\kappa)^n, \quad V_{\mathrm{SSB}}(\tilde\rho) = \sum_{n=0}^{N_V}\frac{\lambda_{2n}^{(V)}}{n!}(\tilde\rho-\kappa)^n, \tag{B.13}$$

Identifying $m_\phi = \lambda_2$, $m_\psi = \lambda_0^{(\mathrm{V})}$, λ_4, and $\lambda_{h\psi} = \lambda_2^{(\mathrm{V})}$ in the symmetric phase, neglecting the generalized Yukawa coupling $H(\tilde\rho)$ as well as anomalous dimensions $\eta_\phi = \eta_\psi = 0$, and setting all

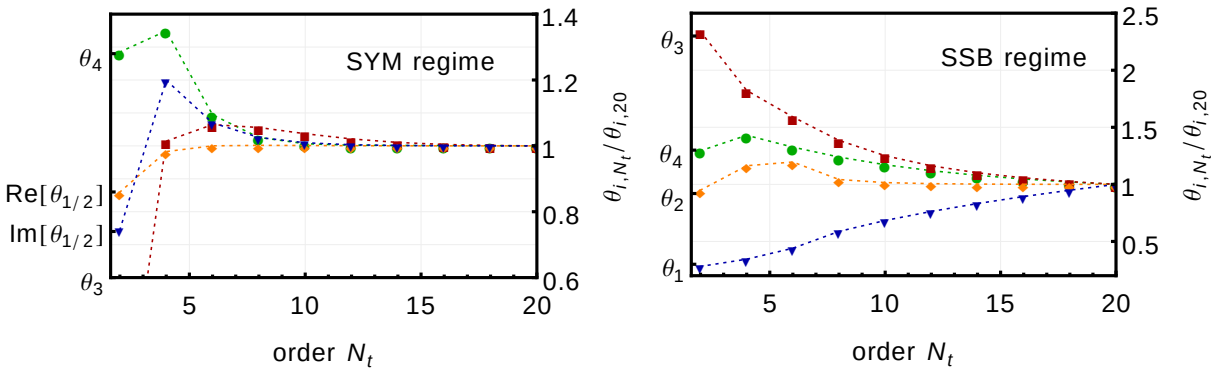

Figure 35: Critical exponents with increasing order $N_t = N_V$ in the symmetric (left-hand panel) and spontaneously broken (right-hand panel) regime. The latter includes anomalous dimensions (LPA'_{N_V}). All critical exponents are normalized to the highest-order values.

higher-order couplings to zero, reproduces the simple truncation in Eqs. (3.6)-(3.9) in the main text.

B.2 Convergence properties of the asymptotically safe fixed point

In Fig. 34 and Fig. 35 we show the convergence of fixed-point values and critical exponents with high order in the truncated scalar potential $U(\rho)$, respectively. Despite the non-vanishing vacuum expectation value, cf. 2 in Sec. 3 of the main text, the convergence is faster in the symmetric expansion. We have explored a simultaneous expansion of both the scalar potential $U(\rho)$ and the generalized Higgs-portal function $V(\rho)$ which does not significantly improve the convergence properties in the SSB expansion. In the future, we want to test whether an expansion including higher-order four-fermion interactions improves the convergence.

B.3 Fiducial Standard-Model to mimic the Higgs potential

To infer the (de-)stabilizing effect of the fermionic dark-matter model on a possible SM metastability scale (experimental values are consistent with a metastable, instable or fully stable Higgs potential, see discussion in Sec. 3.1 as well as Sec. 1.1 of the main text), we mimic the effect of marginal Standard-Model gauge and Yukawa couplings in the toy model following [405]. To that end, we modify the truncated effective action in Eq. (B.1) to include an $SU(N_C)$ gauge group under which we charge n_f fermions, all but $i = t$ with negligibly small Yukawa couplings to the scalar (Higgs), i.e.,

$$\Gamma_k = \int d^d x \Bigg[\frac{Z_G}{4} F^a_{\mu\nu} F^{a\,\mu\nu} + \frac{Z_\phi}{2} \partial_\mu \phi \partial^\mu \phi + \sum_i^{n_f} Z_i \, \bar{q}_i \mathrm{i} \not{D} q_i + Z_\psi \, \bar{\psi} \mathrm{i} \not{\partial} \psi + \bar{U}(\rho) + \frac{\mathrm{i}}{\sqrt{2}} \bar{H}(\rho) \phi \, \bar{q}_t q_t + \mathrm{i} V(\rho) \bar{\psi} \psi \Bigg]. \tag{B.14}$$

The scalar (Higgs) is uncharged under the $SU(N_C)$. Instead of also adding the actual electroweak sector of the SM under which the Higgs is charged, we include a fiducial gauge contribution g_F

to mimic the electroweak sector, by which we amend Eqs. (B.5)-(B.7), i.e.,

$$\partial_t u(\tilde{\rho})\Big|_{\text{fid-SM}} = \partial_t u(\tilde{\rho}) + \frac{4v_d}{d}\frac{c_u}{1+\frac{\tilde{\rho}\, g_F^2}{2}}, \tag{B.15}$$

$$\partial_t h_{\mathrm{t}}(\tilde{\rho})\Big|_{\text{fid-SM}} = \partial_t h_{\mathrm{t}}(\tilde{\rho}) + 2\, v_d\, c_{\mathrm{t}}\, g_F^2 h_{\mathrm{t}} - 4\, v_d \frac{N_c^2-1}{2N_c} g_s^2\, h_{\mathrm{t}}(3-\xi)\, l_{1,1}^{(\mathrm{BF})d}(0,\omega_{\mathrm{t}};\eta_G,\eta_{\mathrm{t}})\,, \tag{B.16}$$

where g_s denotes the $SU(N_C)$ gauge coupling. It has been confirmed in [405] that for $N_C = 3$ and $n_f = 6$, this fiducial SM successfully captures the running Higgs-potential for scales sufficiently high above the electroweak scale.

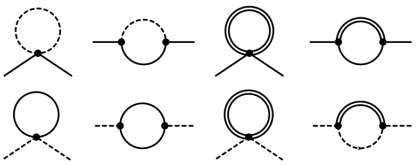

(a) Contributions to η_ψ (upper row) and η_ϕ (lower row), cf. Eq. (4.21)) and (cf. Eq. (4.20)), respectively: Diagrams from left to right: χ-, Yukawa- and two gravitational contributions.

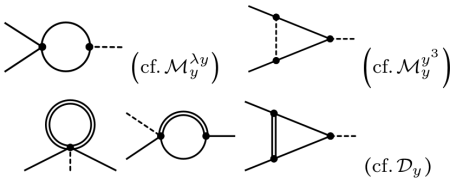

(b) Diagramatic contributions to β_y: pure-matter diagrams in the first row (cf. $\mathcal{M}_y^{\lambda y}$ and $\mathcal{M}_y^{y^3}$ in Eq. (4.18)); non-inducing gravitational diagrams in the second row (cf. $\mathcal{D}_y$ in Eq. (4.18)).

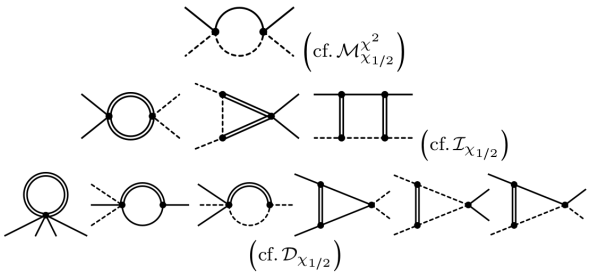

(c) Diagramatic contributions to β_{χ_i}: pure-matter diagrams in the first row (cf. $\mathcal{M}_{\chi_{1/2}}^{\chi^2}$ in Eq. (4.14) & (4.15)); gravity-induced diagrams in the second row (cf. $\mathcal{I}_{\chi_{1/2}}$ in Eq. (4.14) & (4.15)); non-inducing gravitational diagrams in the third row (cf. $\mathcal{D}_{\chi_{1/2}}$ in Eq. (4.14) & (4.15)). Symmetry-reduced contributions from $y \neq 0$ omitted.

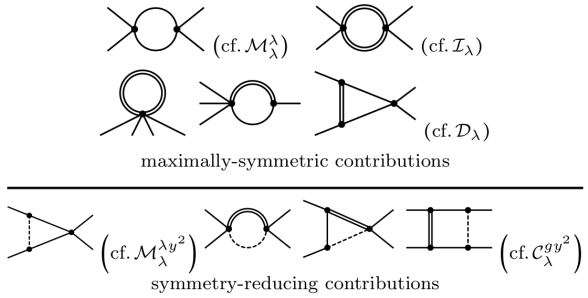

(d) Diagramatic contributions to β_{χ_i}: pure-matter (cf. $\mathcal{M}_\lambda^\lambda$ in Eq. (4.16),(4.17), and (4.19)) and gravity-induced diagrams (cf. $\mathcal{I}_\lambda$ in Eq. (4.16)) in the first row; non-induced gravitational diagrams in the second row (cf. $\mathcal{D}_\lambda$ in Eq. (4.16), (4.17) and (4.19)); symmetry-reducing diagrams in the third row vanish with $y = 0$ (cf. $\mathcal{M}_\lambda^{\lambda y^2}$ in Eq. (4.16), (4.17) and (4.19) and $\mathcal{C}_\lambda^{gy^2}$ in Eq. (4.19)).

Figure 36: Diagramatic expansion of the flow equation (2.5) for the effective action $\Gamma_k = \Gamma_{k\,\mathrm{grav}} + \Gamma_{k,\mathrm{MSAS}} + \Gamma_{k\,\mathrm{marginal}}$, cf. Eq. (4.4) and (4.12) in Sec. 4. Gravitational, fermionic, and scalar fluctuations are depicted as double, solid, and dashed lines, respectively. We do not show further vanishing diagrams.

C Matter in asymptotically safe gravity: Supplementary material

C.1 Diagramatic expansion of the flow equation

We present the diagramatic expansion for the effective action $\Gamma_k = \Gamma_{k\,\mathrm{grav}} + \Gamma_{k,\mathrm{MSAS}} + \Gamma_{k\,\mathrm{marginal}}$, cf. Eq. (4.4) and (4.12) in Sec. 4. Expanding the flow equation (2.5) by applying sufficiently many functional derivatives with respect to the fluctuation fields generates the diagrammatic structure represented in Fig. 36 where external momenta can be assigned arbitrarily. More specifically, the diagrams in Fig. 36a, Fig. 36d, Fig. 36c, and Fig. 36b contribute to the running of anomalous dimensions, i.e., $\eta_{\phi/\psi}$, four-fermion couplings, i.e., β_{λ_i}, mixed two-fermion–two-scalar couplings, i.e., $\chi_{1/2}$ and the Yukawa coupling y, respectively. We transition to momentum space, i.e., $\partial_\mu\phi(x) \to ip_\mu\tilde{\phi}(p)$ for bosons and $\partial_\mu\psi(x) \to ip_\mu\tilde{\psi}(p)$ as well as $\partial_\mu\bar{\psi}(x) \to -ip_\mu\tilde{\bar{\psi}}(p)$ for fermions with Fourier-transform conventions as in [676] and drop the tilde from hereon. It is always implied that all the remaining fluctuations are set to zero after the variations. To project on the two-scalar–two-fermion interactions we add an external $\gamma_\mu p_{\mathrm{ext}}^\mu$, as otherwise the Dirac

traces would vanish. The explicit projections read

$$\chi_1 = \frac{-9}{16\sqrt{2}}\left[\partial_{p_1}\partial_{p_2}\partial_{p_3}\partial_{p_{\text{ext}}}\left(\text{Tr}\left[\frac{\delta}{\delta\phi(p_1)}\frac{\delta}{\delta\phi(p_2)}\frac{\delta}{\delta\psi(p_3)}\frac{\delta}{\delta\bar{\psi}(+p_1+p_2+p_3)}\Gamma_k\gamma_\rho p_{\text{ext}}^\rho\right]\right)\right]^{p_i=0,\vartheta_{3,\text{ext}}=0}_{\vartheta_{1,\text{ext}}=\vartheta_{2,\text{ext}}=\sqrt{2}/3}, \tag{C.1}$$

$$\chi_2 = \frac{-9}{8\sqrt{2}}\left[\partial_{p_1}\partial_{p_2}\partial_{p_3}\partial_{p_{\text{ext}}}\left(\text{Tr}\left[\frac{\delta}{\delta\phi(p_1)}\frac{\delta}{\delta\phi(p_2)}\frac{\delta}{\delta\psi(p_3)}\frac{\delta}{\delta\bar{\psi}(+p_1+p_2+p_3)}\Gamma_k\gamma_\rho p_{\text{ext}}^\rho\right]\right)\right]^{p_i=0,\vartheta_{1,\text{ext}}=\vartheta_{2,\text{ext}}=0}_{\vartheta_{3,\text{ext}}=\sqrt{2}/3}, \tag{C.2}$$

where $\vartheta_{i,j}$ are the angles between the respective two momenta. An explicit choice of basis in momenta which realizes the respective angles can be found in [449, App. G]. The projection on the four-fermion interactionscan be infered from [447, App. A]. The projection on the Yukawa coupling is simply given by $\frac{\delta}{\delta\phi(p_1)}\frac{\delta}{\delta\psi(p_2)}\frac{\delta}{\delta\bar{\psi}(+p_1+p_2)}\Gamma_k$.

C.2 Threshold integrals

This appendix presents the explicit contributions to the β-functions in Eq. (4.14)-(4.19) in terms of threshold integrals. All tensor structure has been traced out and confirmed by use of the FormTracer package [677]. Threshold integrals of the form $I = I[n_{\text{TT}}, n_{\text{Tr}}, n_\psi, n_\phi; n_p]$ count the numbers n_{TT}, n_{Tr}, n_ψ, and n_ϕ of propagators of the TT-, trace-, fermionic, and scalar mode in a diagram, respectively. Due to the 1-loop structure of the flow equation (2.5), the sum $n_{\text{TT}} + n_{\text{Tr}} + n_\psi + n_\phi$ corresponds to the number of vertices in a diagram. Further, n_p denotes the number of additional momenta arising from the vertices. For some of the projections the traced momentum structure depends on which mode the scale derivative ∂_t acts. We, therefore, denote with round brackets, i.e., (n_i), a corresponding mode i which is not hit by the scale derivative ∂_t. In diagrammatic notation, the diagram with the respective regulator insertion on the i-mode leg is excluded.
The pure matter contributions (independent of the gravitational couplings) are given by

$$\mathcal{M}_y^{\lambda y} = \mathcal{M}_\lambda^{\lambda} = I[0,0,2,0;0]\,, \qquad \mathcal{M}_y^{y^3} = \mathcal{M}_\lambda^{\lambda y^2} = -I[0,0,2,1;0] \tag{C.3}$$

$$\mathcal{M}_{\chi_1}^{\chi^2} = -\frac{\left(121\chi_1^2 + 64\chi_1\chi_2 + 4\chi_2^2\right)}{24} I[0,0,(1),1;3] - \frac{(\chi_1 - 2\chi_2)\,(5\chi_1 + 2\chi_2)}{4} I[0,0,1,(1);3]\,, \tag{C.4}$$

$$\mathcal{M}_{\chi_2}^{\chi^2} = \frac{\left(59\chi_1^2 - 52\chi_1\chi_2 - 76\chi_2^2\right)}{48} I[0,0,(1),1;3] + \frac{(\chi_1 - 2\chi_2)\,(\chi_1 + \chi_2)}{2} I[0,0,1,(1);3]\,, \tag{C.5}$$

$$\mathcal{M}_{\eta_\phi}^{\chi} = 4(\chi_1 + 4\chi_2)\, I[0,0,1,0;1]\,, \qquad \mathcal{M}_{\eta_\psi}^{\chi} = -\frac{\chi_1 + 4\chi_2}{2} I[0,0,0,1;2]\,, \tag{C.6}$$

$$\mathcal{M}_{\eta_\phi}^{y^2} = \frac{y^2\left(4 - \eta_\psi\right)}{16\pi^2}\,, \qquad \mathcal{M}_{\eta_\psi}^{y^2} = y^2\frac{\left(5 - \eta_\phi\right)}{80\pi^2}\,. \tag{C.7}$$

Moreover, induced gravitational contributions are given by

$$\mathcal{I}_{\chi_1} = -\frac{5}{72}I[2,0,0,0;0] - \frac{3}{32768}I[0,2,(1),1;3] + \frac{9}{16384}I[0,(2),1,(1);3]\,, \tag{C.8}$$

$$\mathcal{I}_{\chi_2} = \frac{5}{288}I[2,0,0,0;0] + \frac{3}{16384}I[0,2,0,1;2] - \frac{57}{65536}I[0,2,(1),1;3] - \frac{9}{16384}I[0,(2),1,(1);3]\,, \tag{C.9}$$

$$\mathcal{I}_{\lambda} = -\frac{15}{1024}I[2,0,0,0;2]\,. \tag{C.10}$$

Further, gravity contributions contributing to the anomalous scaling dimension, i.e., not inducing the corresponding coupling read

$$\begin{aligned}\mathcal{D}_{\chi_1} = {}& \frac{5\,(31\chi_1+16\chi_2)}{288}I[1,0,0,0;0] + \frac{5\,(\chi_1-4\chi_2)}{72}I[1,0,1,0;1] - \frac{\chi_1}{128}I[0,1,0,0;0]\\ & - \frac{27\chi_1}{512}I[0,1,(1),0;1] - \frac{3\chi_1}{128}I[0,(1),1,0;1] - \frac{\chi_1}{64}I[0,1,0,1;2] + \frac{27\chi_1}{512}I[0,1,(2),0;2]\\ & + \frac{\chi_1}{192}I[0,1,0,2;4] + \frac{8\chi_1+\chi_2}{128}I[0,1,(1),1;3] - \frac{3(\chi_1+\chi_2)}{64}I[0,(1),1,(1);3]\,,\,,\end{aligned} \tag{C.11}$$

$$\begin{aligned}\mathcal{D}_{\chi_2} = {}& \frac{5\,(8\chi_1+23\chi_2)}{288}I[1,0,0,0;0] - \frac{5\,(\chi_1-4\chi_2)}{288}I[1,0,1,0;1] - \frac{\chi_2}{128}I[0,1,0,0;0]\\ & - \frac{3(\chi_1+13\chi_2)}{512}I[0,1,(1),0;1] - \frac{3(\chi_1+8\chi_2)}{512}I[0,(1),1,0;1] - \frac{\chi_2}{64}I[0,1,0,1;2]\\ & + \frac{9(\chi_1+7\chi_2)}{512}I[0,1,(2),0;2] + \frac{9(\chi_1+4\chi_2)}{512}I[0,(1),2,0;2] + \frac{\chi_1+6\chi_2}{384}I[0,1,0,2;4]\\ & + \frac{13\chi_1+38\chi_2}{512}I[0,1,(1),1;3] + \frac{3(\chi_1+4\chi_2)}{256}I[0,(1),1,(1);3]\,,\end{aligned} \tag{C.12}$$

$$\mathcal{D}_{y} = -\frac{5}{4}I[1,0,0,0;0] + \frac{1}{16}I[0,1,0,0;0] - \frac{3}{16}I[0,1,1,0;1] + \left(\frac{3}{16}\right)^2 I[0,1,2,0;2] \tag{C.13}$$

$$\mathcal{D}_{\lambda} = -\frac{5}{4}I[1,0,0,0;0] + \frac{1}{16}I[0,1,0,0;0] - \frac{3}{8}I[0,1,1,0;1] + \frac{27}{128}I[0,1,2,0;2] \tag{C.14}$$

$$\mathcal{D}_{\eta_\phi} = \frac{1}{64}I[0,1,0,1;2] \tag{C.15}$$

$$\begin{aligned}\mathcal{D}_{\eta_\psi} = {}& \frac{25}{32}I[1,0,0,0;0] - \frac{3}{128}I[0,1,0,0;0]\\ & + \frac{117}{1024}I[0,1,(1),0;1] + \frac{9}{128}I[0,(1),1,0;1]\,.\end{aligned} \tag{C.16}$$

Finally, the mixed contributions from gravitational and other matter fluctuations to another coupling are given by

$$\mathcal{C}_{\lambda}^{gy^2} = \frac{1}{4}I[0,1,0,1;0] + \frac{3}{8}I[0,1,1,1;1] + \frac{9}{64}I[0,1,2,1;2]\,. \tag{C.17}$$

The generic threshold integral reads,

$$I[n_{\mathrm{TT}}, n_{\mathrm{Tr}}, n_\psi, n_\phi; n_p] = \tilde{\partial}_t \int \frac{d^4p}{(2\pi)^4} \left(p^2\right)^{(n_p+n_\psi)/2} \left[\frac{1}{\left[Z_\psi p^2 \left(1 + r_{k,f}\left(\frac{p^2}{k^2}\right)\right)\right]^{n_\psi}} \times \right. \tag{C.18}$$
$$\left. \times \frac{1}{\left[Z_\phi p^2 \left(1 + r_{k,b}\left(\frac{p^2}{k^2}\right)\right)\right]^{n_\phi}} \times \frac{1}{\left[\Gamma^{(2)}_{\mathrm{k,TT}}\left(1 + r_{k,b}\left(\frac{p^2}{k^2}\right)\right)\right]^{n_{\mathrm{TT}}}} \times \frac{1}{\left[\Gamma^{(2)}_{\mathrm{k,Tr}}\left(1 + r_{k,b}\left(\frac{p^2}{k^2}\right)\right)\right]^{n_{\mathrm{Tr}}}} \right],$$

where $r_{k,b}$ and $r_{k,f}$ denote the regulator shape functions. Employing spectrally adjusted cutoff functions with a Litim regulator, the general threshold integral can be evaluated, i.e.,

$$\begin{aligned} I[n_{\mathrm{TT}}, n_{\mathrm{Tr}}, n_\psi, n_\phi; n_p] &= \frac{2^{8n_{\mathrm{Tr}}+5n_{\mathrm{TT}}-3}\pi^{n_{\mathrm{Tr}}+n_{\mathrm{TT}}-2}}{n_p+4} \times \\ &\left(\frac{1}{b-d+1-2\Lambda}\right)^{n_{\mathrm{TT}}} \times \left(\frac{1}{18a+6b-18c-6d+4\Lambda-3}\right)^{n_{\mathrm{Tr}}} \times \\ &\times \left[-\frac{2n_{\mathrm{TT}}\left(-\eta_h+n_p+6\right)}{\left(b-d+1-2\Lambda\right)}\mathbb{X}_1 - \frac{6n_{\mathrm{Tr}}\left(-\eta_h+n_p+6\right)}{\left(18a+6b-18c-6d+4\Lambda-3\right)}\mathbb{X}_2 \right. \\ &\left. - \frac{n_\psi\left(-\eta_\psi+n_p+5\right)}{n_p+5} - \frac{2n_\phi\left(-\eta_\phi+n_p+6\right)}{n_p+6} \right], \qquad \text{with} \end{aligned} \tag{C.19}$$

$$\mathbb{X}_1 = \frac{\left(2b\left(n_p+6\right)\left(n_p+10\right) - \left(n_p+8\right)\left(3d\left(n_p+6\right) - n_p - 10\right)\right)}{\left(n_p+6\right)\left(n_p+8\right)\left(n_p+10\right)} \tag{C.20}$$

$$\mathbb{X}_2 = \frac{\left(12a\left(n_p+6\right)\left(n_p+10\right) + 4b\left(n_p+6\right)\left(n_p+10\right) - \left(n_p+8\right)\left(18c\left(n_p+6\right) + 6d\left(n_p+6\right) + n_p + 10\right)\right)}{\left(n_p+6\right)\left(n_p+8\right)\left(n_p+10\right)}. \tag{C.21}$$

The terms in square brackets denote contributions for which the scale-derivative acts on respective mode i. Hence, whenever round brackets around a mode, i.e., (n_i), are given in Eqs. (C.3)-(C.17) one simply neglects the associated term in Eq. (C.19). The somewhat complicated prefactors arise from contractions of the gravitational modes. They can differ for the same diagram, depending on where the regulator is inserted.
The expressions in Eq. (C.3)-(C.17) can be substituted into Eq. (4.14)-Eq. (4.19) to obtain specific β-functions in the main text.

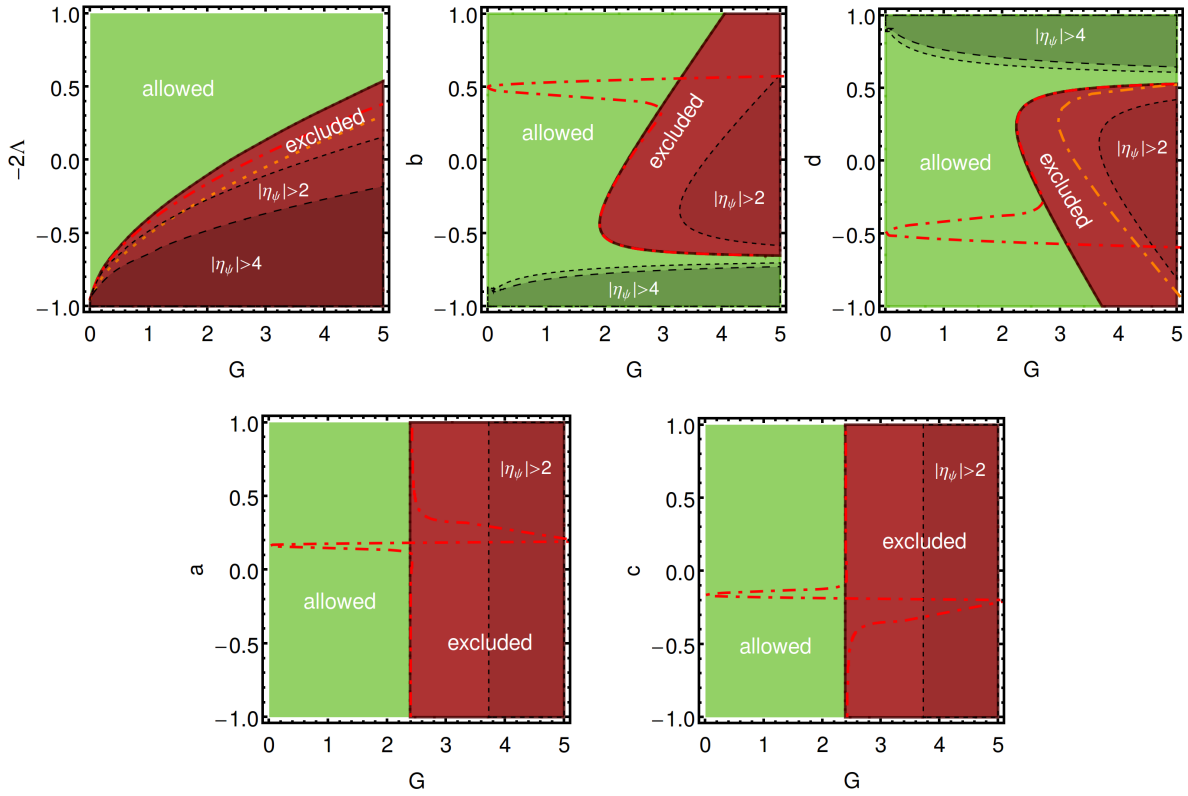

Figure 37: Weak-gravity bounds in slices through gravitational parameter space (G, Λ, a, b, c, d) based only on the TT mode including anomalous dimensions, cf. Eq. 4.4: In the darker-colored red region, gravitational fluctuations from the TT mode grow too strong and the fixed point in $\chi_{1/2}$ vanishes. A viable fixed point is possible in the lighter-colored green region.
The dashed orange lines (same as above but neglecting anomalous dimensions) indicate that the influence of the anomalous dimensions in Eq. (4.20) & (4.21) sharpens the weak-gravity bound. The thick red dot-dashed line marks the location of the weak-gravity bound without any approximations. The additional features arise due to the additional pole structure of the trace mode, cf. Eq. (C.23).

C.3 Bounds on gravitational parameter space

For a specific finite-order truncation in gravitational parameter space, the bounds on the propagator of metric fluctuations correspond to interrelated bounds on the dimensionless Newton coupling G, the dimensionless cosmological constant Λ, and all higher-order gravitational couplings which contribute to the propagating gravitational modes. In any such finite-order truncation, the higher-order couplings could be accompanied by a truncation-ghost scale, at which the truncated theory develops inconsistencies because of unitarity violations of the associated higher-derivative ghost modes, cf. Sec. 1.3.1. Without a proper analysis of unitarity of the respective higher-derivative truncations, it is unclear which effects of the higher-order couplings should be attributed to their physical contributions in a potential unitary infinite-order truncation and which effects are unphysical phenomena induced by unitarity-violating truncation ghosts.
With this word of caution, the higher-order couplings contribute to the propagator of metric fluctuations. For the given choice of gauge, i.e., $\beta = 0$ and $\alpha \to 0$ subsequently, only the traceless-transverse spin-2 mode and the trace mode are non-vanishing. We observe from Eq. (C.19) that for spectrally adjusted cutoffs this results in two pole-structures arising from the spin-2 and

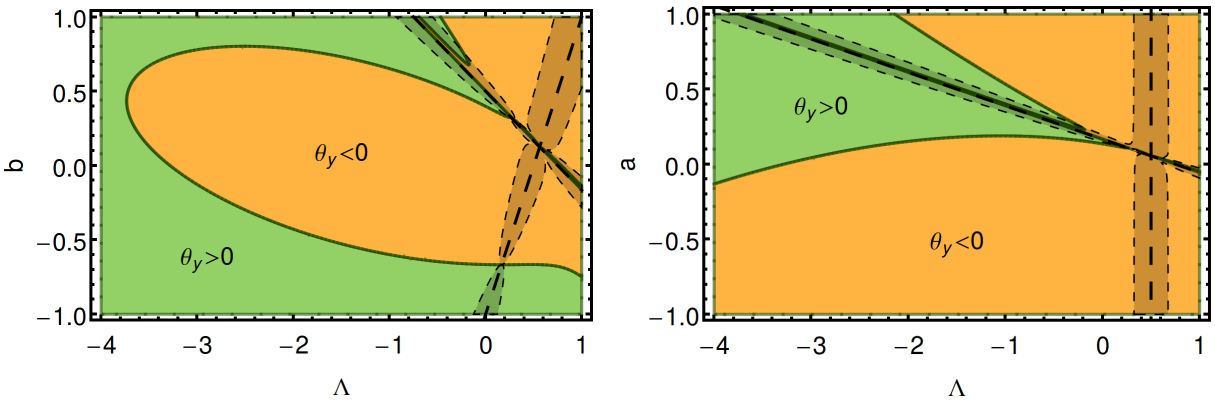

Figure 38: Slices through the Yukawa structure-bound in gravitational higher-derivative coupling space. Green (yellow) areas show where a non-trivial Yukawa coupling can (cannot) emerge in a flow towards the IR. The Newton coupling does not influence the viability bound significantly as long as it remains below the weak-gravity bound. Left-hand panel: slice in the Λ–b plane where b is the $R_{\mu\nu}R^{\mu\nu}$-coupling; all other couplings set to zero. Right-hand panel: slice in the Λ–a plane where b is the R^2-coupling; all other couplings set to zero.

trace mode, respectively, i.e.

$$\text{pole}_{\text{TT}} = \frac{g}{(1+\mu_h+b-d)}\,, \tag{C.22}$$

$$\text{pole}_{\text{Tr}} = \frac{g}{(3+2\mu_h-18(a-c)-6(b-d))}\,. \tag{C.23}$$

In the vicinity of these poles, anomalous dimensions, for instance, η_ψ, grow large. Even if the results are assumed to not be driven by truncation ghosts, this indicates a breakdown of the present approximation.

Fig. 37 and Fig. 38 show the weak-gravity bound and the viability bound in higher-order gravitational parameter space, respectively.

C.4 Suppression of matter-mediated effects

In Eq. (4.14)-(4.21), finite g results in finite fixed-point values for the corresponding couplings and anomalous dimensions. We aim at analyzing the impact of these induced interactions on β_y, i.e., ultimately on the value of y at the Planck scale which is linked to $\theta_y = \left(-\frac{\beta_y}{y}\right)|_{y^*=0}$. Specifically,

$$\theta_y = -\left(\eta_\psi + \frac{\eta_\phi}{2}\right) - g\,\mathcal{D}_y + 4\lambda_A \mathcal{M}_y^{\lambda y} \tag{C.24}$$

In the absence of gravity, *all* contributions vanish at the free fixed point. Thus, the critical exponent of the Yukawa coupling at the free fixed point depends on the gravitational coupling directly, through $\mathcal{D}_1$, and indirectly: Gravity induces nontrivial anomalous dimensions η_ϕ, η_ψ, which enter θ_y, and also induces a finite four-fermion coupling λ_A, which enters θ_y. The direct and the anomalous-dimension-mediated spin-2 contributions dominate the result, cf. Fig. 39.
In the spin-2 approximation (where $\mathcal{D}_y = \mathcal{D}_{\lambda_A} = -5/8\mathcal{D}_{\eta_\psi}$ and $\mathcal{D}_{\eta_\phi} = 0$) the suppression of matter-mediated effects can be demonstrated explicitly by solving Eq. (4.16) and plugging the result back into Eq. (C.24). In a regime where gravity is not strongly dynamically suppressed by a

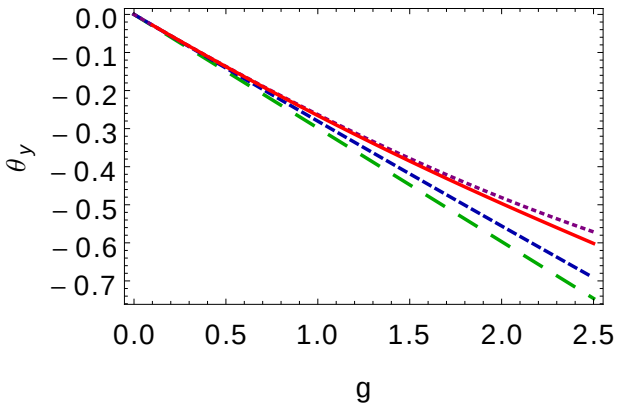

Figure 39: Comparison of the critical exponent of the Yukawa coupling θ_y (with $a = b = c = d = \mu_h = 0$) for different approximations: the green wide-dashed line shows the spin-2 contributions (including anomalous dimensions) only; the blue narrow-dashed line includes trace-contributions; the purple dotted line includes trace-contributions and matter-mediated effects from the induced four-fermion coupling λ_A; the red continuous line additionally includes matter-mediated contributions from the χ-sector that contribute to the Yukawa coupling via anomalous dimensions. The comparison shows that trace-mode and matter-mediated effects are subleading in the regime of g that obeys the weak-gravity bound.

large effective mass of the TT-propagator (i.e., $\mu_h + b - d < 2$), matter contributions are typically subleading by a factor of $\frac{1}{16\pi^2}$ occurring in pure-matter loops. Therefore, Eq. (C.24) can be expanded for small $\mathcal{M}_y^{\lambda y}$ and we find

$$\theta_y = \left(\frac{g\mathcal{D}_y - 32}{8} + \frac{|g\mathcal{D}_y - 8|}{2}\right) - \frac{16\mathcal{M}_y^{\lambda y}\mathcal{D}_\lambda\, g^2}{|g\mathcal{D}_y - 8|} + \mathcal{O}\left(\left(\mathcal{M}_y^{\lambda y}\right)^2\right), \tag{C.25}$$

where we have also exploited that $\mathcal{M}_y^{\lambda y} = \mathcal{M}_\lambda^{\lambda}$. For small $g \ll 1$ the matter-mediated $\mathcal{M}_y^{\lambda y}$-term is suppressed by the canonical dimensionality of the induced coupling λ_A. For large $g \gg 1$ the suppression relies solely on the matter-loop suppression

$$\mathcal{M}_y^{\lambda y} \simeq \frac{\mathcal{D}_{y/\lambda}}{16\pi^2}\,. \tag{C.26}$$

This explicit example is in accordance with the expectation that the gravity loop, which features several modes, dominates over the matter loops in β_y, with only one matter mode. We conclude that it is sufficient to consider only the direct contribution from the TT-mode to obtain a good understanding of the bound on the gravitational parameter space in our model. However, the suppression of matter-mediated contributions might not hold in models with many fermions and scalars.

D CKM running in three generations

For the parameterization in Eq. 5.19, the 1-loop running of the 3-generation CKM-matrix elements can be obtained from the general case in Eq. (5.14). The result reads

$$\begin{aligned}\frac{dX}{dt} = -\frac{3}{(4\pi)^2}\Bigg[&\frac{y_u^2+y_c^2}{y_u^2-y_c^2}\left\{(y_d^2-y_b^2)XZ+\frac{(y_b^2-y_s^2)}{2}(W(1-X)+X-(1-Y)(1-Z))\right\} \\ &+\frac{y_u^2+y_t^2}{y_u^2-y_t^2}\left\{(y_d^2-y_b^2)X(1-X-Z)+\frac{(y_b^2-y_s^2)}{2}((1-Y)(1-Z)-X(1-2Y)-W(1-X))\right\} \\ &+\frac{y_d^2+y_s^2}{y_d^2-y_s^2}\left\{(y_u^2-y_t^2)XY+\frac{y_t^2-y_c^2}{2}(W(1-X)+X-(1-Y)(1-Z))\right\} \\ &+\frac{y_d^2+y_b^2}{y_d^2-y_b^2}\left\{(y_u^2-y_t^2)X(1-X-Y)+\frac{y_t^2-y_c^2}{2}((1-Y)(1-Z)-X(1-2Z)-W(1-X))\right\}\Bigg],\end{aligned} \tag{D.1}$$

$$\begin{aligned}\frac{dY}{dt} = -\frac{3}{(4\pi)^2}\Bigg[&\frac{y_u^2+y_c^2}{y_u^2-y_c^2}\left\{\frac{(y_b^2-y_d^2)}{2}(W(1-X)+X-(1-Y)(1-Z))+(y_s^2-y_b^2)YW\right\} \\ &+\frac{y_u^2+y_t^2}{y_u^2-y_t^2}\left\{\frac{(y_b^2-y_d^2)}{2}((1-Y)(1-Z)-W(1-X)-X(1-2Y))+(y_s^2-y_b^2)Y(1-Y-W)\right\} \\ &+\frac{y_s^2+y_d^2}{y_s^2-y_d^2}\left\{(y_u^2-y_t^2)XY+\frac{y_t^2-y_c^2}{2}(W(1-X)+X-(1-Y)(1-Z))\right\} \\ &+\frac{y_s^2+y_b^2}{y_s^2-y_b^2}\left\{(y_u^2-y_t^2)Y(1-X-Y)+\frac{(y_c^2-y_t^2)}{2}(W(1-X-2Y)+X-(1-Z)(1-Y))\right\}\Bigg],\end{aligned} \tag{D.2}$$

$$\begin{aligned}\frac{dZ}{dt} = -\frac{3}{(4\pi)^2}\Bigg[&\frac{y_c^2+y_u^2}{y_c^2-y_u^2}\left\{(y_d^2-y_b^2)XZ+\frac{(y_b^2-y_s^2)}{2}(W(1-X)+X-(1-Z)(1-Y))\right\} \\ &+\frac{y_c^2+y_t^2}{y_c^2-y_t^2}\left\{(y_d^2-y_b^2)Z(1-X-Z)+\frac{(y_s^2-y_b^2)}{2}(W(1-X-2Z)+X-(1-Y)(1-Z))\right\} \\ &+\frac{y_d^2+y_s^2}{y_d^2-y_s^2}\left\{\frac{(y_u^2-y_t^2)}{2}((1-Y)(1-Z)-X-W(1-X))+(y_c^2-y_t^2)ZW\right\} \\ &+\frac{y_d^2+y_b^2}{y_d^2-y_b^2}\left\{\frac{(y_t^2-y_u^2)}{2}((1-Z)(1-Y)-W(1-X)-X(1-2Z))+(y_c^2-y_t^2)Z(1-Z-W)\right\}\Bigg],\end{aligned} \tag{D.3}$$

$$\begin{aligned}\frac{dW}{dt} = -\frac{3}{(4\pi)^2}\Bigg[&\frac{y_c^2+y_u^2}{y_c^2-y_u^2}\left\{(y_s^2-y_b^2)WY+\frac{(y_b^2-y_d^2)}{2}((1-X)W+X-(1-Y)(1-Z))\right\} \\ &+\frac{y_c^2+y_t^2}{y_c^2-y_t^2}\left\{(y_s^2-y_b^2)W(1-Y-W)+\frac{(y_b^2-y_d^2)}{2}((1-Y)(1-Z)-X-W(1-X-2Z))\right\} \\ &+\frac{y_s^2+y_d^2}{y_s^2-y_d^2}\left\{(y_c^2-y_t^2)WZ+\frac{(y_t^2-y_u^2)}{2}Z((1-X)W+X-(1-Y)(1-Z))\right\} \\ &+\frac{y_s^2+y_b^2}{y_s^2-y_b^2}\left\{(y_c^2-y_t^2)W(1-Z-W)+\frac{(y_t^2-y_u^2)}{2}((1-Y)(1-Z)-X-W(1-X-2Y))\right\}\Bigg].\end{aligned} \tag{D.4}$$

E RG-flow of the scalar potential in a simple gauge-Yukawa model

We present the full RG flow for the simple abelian $U(1)$-gauge model including a complex scalar degree of freedom ϕ charged under the $U(1)$ and a Dirac fermion with left- and right-handed components $\psi_{L,R}$ which is neutral under the $U(1)$. The scalar and fermion are coupled via a Yukawa term, i.e.,

$$\mathcal{L}_{\text{Yukawa}} = y\,(\bar{\psi}_R\,\phi^*\,\psi_L - \bar{\psi}_L\,\phi\,\psi_R)\,, \tag{E.1}$$

with Yukawa coupling y. The model is utilized as a simple example for the Planck-scale fixed-point potential and subsequent symmetry-breaking for a GUT in Sec. 6.4.1.
We use the gauge-invariant flow equation [514] corresponding to a so-called physical gauge fixing in the background-field formalism employing a linear metric split. The RG flow of the dimensionless scalar potential $U = \bar{U}/k^4$ evaluated for $\rho = \phi^*\phi/k^2$ reads

$$k\,\partial_k U(\rho) = -4U(\rho) + (2+\eta_\phi)\rho U'(\rho) + \tilde{\pi}_g + \tilde{\pi}_f + \tilde{\pi}_2 + \tilde{\pi}_0 + \tilde{\eta}\,, \tag{E.2}$$

where primes denote derivatives with respect to ρ. The traceless-transverse and scalar-gravitational mode contributions $\tilde{\pi}_2$ and $\tilde{\pi}_0$, respectively, have been calculated in [481, 504, 678]. They are presented for the Litim-type regulator [371], i.e.,

$$\tilde{\pi}_2 = \frac{5}{24\pi^2}\frac{1}{1-v(\rho)}\,, \quad v(\rho) = 2U(\rho)/\tilde{M}_P^2\,. \tag{E.3}$$

$$\tilde{\pi}_0 = \frac{1}{24\pi^2}\frac{(1+U'(\rho)+2\rho U''(\rho)) + \frac{3}{4}\,(1-v(\rho)/4)}{(1-v(\rho)/4)\,(1+U'(\rho)+2\rho U''(\rho)) + 3\rho U'(\rho)^2/\tilde{M}_P^2}\,. \tag{E.4}$$

The constant measure contribution $\tilde{\eta} = -1/(8\pi^2)$, related to the gravitational gauge degrees of freedom, is not of importance in the present context. The gauge and Yukawa contributions, cf. [264, 317, 617] read, respectively,

$$\tilde{\pi}_g = \frac{1}{32\pi^2}\left(\frac{3}{1+g^2\rho} - 1\right)\,, \qquad \tilde{\pi}_f = -\frac{1}{8\pi^2}\frac{1}{1+y^2\rho}\,, \tag{E.5}$$

where again the constant term in $\tilde{\pi}_g$ corresponds to a measure contribution in the U(1)-gauge sector.

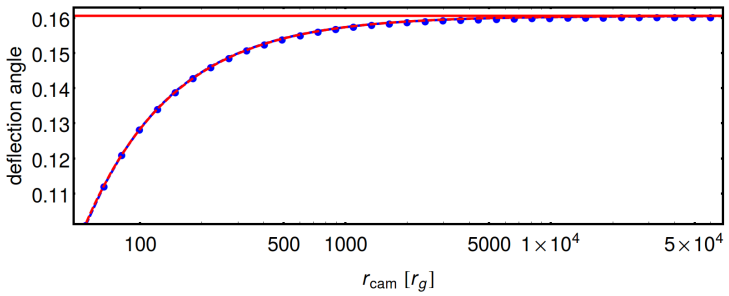

Figure 40: Numerical data (blue connected points), fit (red-dashed) and fitted value ϑ_0, cf. Eq. (F.7) (red continuous) for the deflection angle in RG-improved Kerr spacetime with $a = 0.9r_g$ and $\tilde{\gamma} = 0.11$ at an impact parameter corresponding to the outermost image point $(x, y) = (10, 0)$ in the equatorial plane. The plot shows the dependence on the radial distance $r_{\rm cam}$ at fixed precision $N_{\rm precision} = 10^{-20}$.

F Ray tracing in regular spacetimes

F.1 Simple Ray Tracer: A mathematica package

Generating an image of the horizon as seen by a distant observer requires tracing light rays through the corresponding black-hole geometry. Pioneering first approaches evolved geodesics forward in time from the source to the observer and considered radiative transfer from optically thick, geometrically thin accretion disks [679, 680]. [681] first traced geodesics backward in time from the observer to the source, which, in the case of homogeneous and non-localized sources, is far more efficient for a typically very localized observer. We will use similar techniques here. More recently, efficient methods [682, 683] for ray tracing involving both a localized source and localized observer have also been developed.

The geodesic equation. In a given spacetime the trajectories of light rays are governed by the null-geodesic equation

$$\frac{d^2x^\rho}{d\lambda^2} = -\Gamma^\rho_{\mu\nu}\frac{dx^\mu}{d\lambda}\frac{dx^\nu}{d\lambda} \,, \tag{F.1}$$

where x^ρ is the position of the photon, λ is an affine parameter parameterizing the photon's world line, and $\Gamma^\rho_{\mu\nu}$ is the metric-compatible Christoffel connection. We implement the geodesic equation (F.1) as eight coupled first-order ordinary differential equations

$$\frac{dx^\rho}{d\lambda} = k^\rho \,, \quad \frac{dk^\rho}{d\lambda} = -\Gamma^\rho_{\mu\nu}\, k^\mu\, k^\nu \,. \tag{F.2}$$

Here, $\Gamma^\rho_{\mu\nu}$ are given in an analytical form and since computation time is not critical, we use the native numerical integration techniques available in Mathematica [684]. Since the functional form, cf. Eq. (F.7), is known, we can test the convergence in radial distance in RG-improved Kerr spacetime explicitly, cf. Fig. 40.

Camera setup & image We position a distant virtual camera far away from the black hole where the geometry is well-approximated by flat spacetime. We will optimize this distance with respect to precision and computation time in the following section. The coordinates of the origin of the image plane in Boyer-Lindquist coordinates are given by $(r_{\rm cam}, i, \phi_{\rm cam})$. The image plane itself is spanned by two Cartesian coordinates (x, y). Each point in this image plane can be

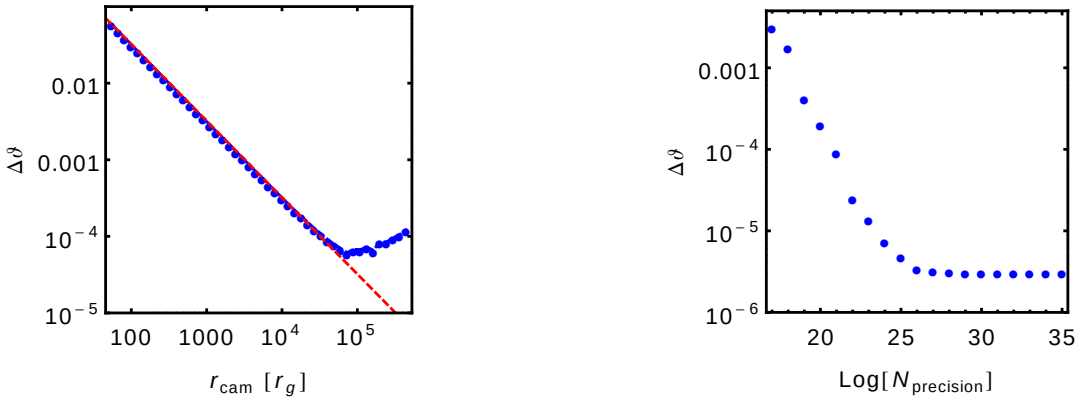

Figure 41: Deflection angle error $\Delta\vartheta = \vartheta_{\text{fit}}(r_{\text{cam}}) - \vartheta$, where ϑ is the exactly calculable deflection angle, as a function of radial camera distance r_{cam} at fixed $N_{\text{precision}} = 10^{-20}$ (left panel) and as a function of numerical precision $N_{\text{precision}}$ at fixed radial camera distance $r_{\text{cam}} = 10^6$ (right panel) for $a = 0.99\,r_g$ in classical Kerr spacetime. Blue points show explicit numerical data points. For the radial distance, we also show the fitted function (red dashed), cf. Eq. (F.7).

expressed in Boyer-Lindquist coordinates (r, θ, ϕ) of the black-hole spacetime by the following transformation

$$r^2 = \sigma + \sqrt{\sigma^2 + a^2\,Z^2)^{1/2}}\ ,\ \cos\theta = Z/r\ ,\ \tan\phi = Y/X\ , \tag{F.3}$$

where $\sigma = \left(X^2 + Y^2 + Z^2 - a^2\right)/2$. Here, (X, Y, Z) are Cartesian coordinates centred around the black hole. They are in turn related to the image coordinates (x, y) by

$$X = \mathcal{D}\,\cos\phi_{\text{cam}} - x\,\sin\phi_{\text{cam}}\ , \tag{F.4}$$

$$Y = \mathcal{D}\,\sin\phi_{\text{cam}} + x\,\cos\phi_{\text{cam}}\ , \tag{F.5}$$

$$Z = r_{\text{cam}}\,\cos(i) + y\,\sin(i)\ , \tag{F.6}$$

where $\mathcal{D} = \sin(i)\sqrt{r_{\text{cam}}^2 + a^2} - y\,\cos(i)$.
All the light rays are initialized perpendicular to the screen in which case their initial momentum vector can be calculated by differentiating Eqs. (F.3).
We parameterize the shadow boundary in the $x - y$ image plane by its radial distance from the origin $\rho(\psi)$ in the image plane as a function of the angle ψ between the x-Axis and the radial vector, cf. right-hand panel in Fig. 32. The resulting shadow boundary is determined by bisecting nested radial intervals for each ψ: Depending on whether the light ray crosses the horizon (and metric components in Boyer-Lindquist coordinates diverge), or escapes to large radii, the outer or inner interval is chosen for the next iteration.
To obtain the intensity distribution generated by a homogeneous background source, we employ the affine-parameter emissivity approximation [685]. We normalize the resulting intensity to the image point with the smallest affine parameter.

Error control. We use the deflection angle ϑ in the equatorial plane as a benchmark value for our error control. In classical Kerr spacetime, this angle can be obtained from an analytical form with arbitrary precision [686]. In controlling the initial-data error, the discretization error (due to a finite stepsize), and the computational errors due to finite numerical precision, we rely on standardized and well-known error control of the native ODE-solver.

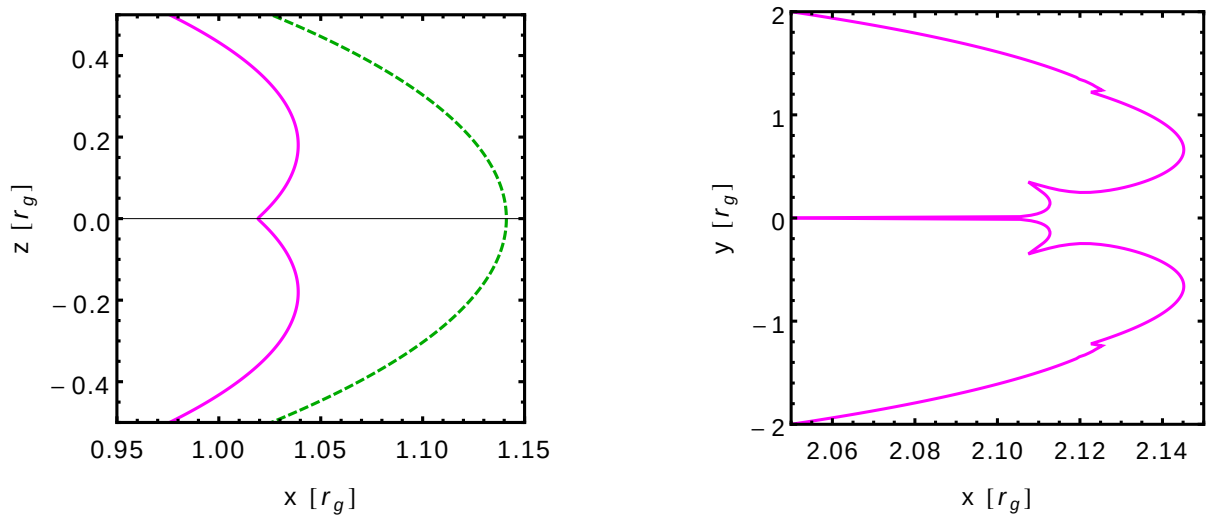

Figure 42: Horizon for the classical and RG-improved Kerr spacetime (left panel) and the RG-improved shadow boundary (right panel) in the equatorial plane for a critical $\tilde{\gamma} = 0.010242$ ($a = 0.99\, r_g$) just before the horizon disappears.

Additionally, there is an error due to the finite radial camera distance. At large distance $r_{\rm cam} \gg r_g$ all investigated black-hole metrics converge to flat space. In this regime, the dependence of the deflection angle ϑ on the radial distance is therefore expected to obey the functional form

$$\vartheta_{\rm fit}(r_{\rm cam}) = \vartheta_0 - b/r_{\rm cam} \,. \tag{F.7}$$

We fit this function to a series of data points obtained at increasing values of $r_{\rm cam}$ to determine the parameters ϑ_0 and b. Specifying a chosen maximal error $\Delta\vartheta = \vartheta_{\rm fit}(r_{\rm cam}) - \vartheta_0$ determines the required radial distance $r_{\rm cam}(\Delta\vartheta)$. We apply this procedure to fit the exact known result for Kerr spacetime, cf. Fig. 41. The exact form for θ in the equatorial plane allows us to also benchmark the required numerical precision. In Fig. 40, we also demonstrate the radial distance error control for an explicit deflection angle in the equatorial plane of the RG-improved spacetime. Kerr-like spacetimes exhibit three constants of motion: the energy E, the angular momentum along the black-hole rotation axis L_Z, and the celebrated Carter constant $\mathcal{Q}$ [664]. We use the conservation of energy and the angular momentum as independent checks of our numerical error.

We demonstrate how to obtain the minimal required radial distance and numerical precision given a desired error-tolerance in the deflection angle in Kerr spacetime. As a point of reference, we choose the outermost image point $(x, y) = (10\, r_g, 0)$ within the equatorial plane. Within the latter, the deflection angle is exactly calculable with arbitrary precision [686]. Therefore, we use it as a benchmark test for the required numerical precision. Fig. 41 shows how the numerical results (blue points) and the exact result (red continuous) develop with increasing radial distance and numerical precision. In both plots, we explicitly show how the error convergence stalls due to dominance of the respective other error. In practice, we avoid this by choosing both a large enough camera distance and numerical precision at the same time. Assuming that both errors do not significantly change for the RG-improved metric, we require a maximal error of the deflection angle $\Delta\vartheta = 0.001$ and therefore use $r_{\rm cam} = 10^4\, r_g$ and $\mathrm{Log}[N_{\rm precision}] = -20$ throughout all computations.

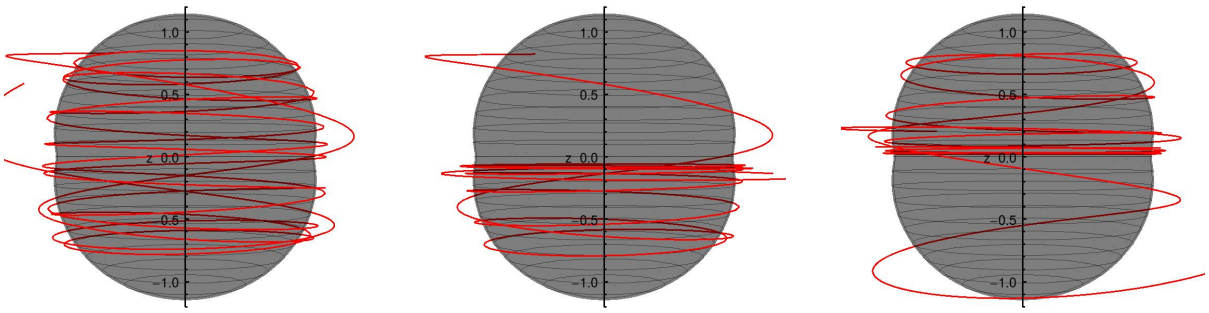

Figure 43: Marginally stable light-like trajectories in the RG-improved black-hole spacetime (thick red lines) for an extreme $\tilde{\gamma} = 0.010242$ ($a = 0.99\, r_g$) just before the horizon (transparent surface) disappears. The left panel shows an image angle $\psi > \psi_{\mathrm{crit},1}$. The middle panel shows an image angle $\psi_{\mathrm{crit},1} > \psi > \psi_{\mathrm{crit},2}$. The right panel shows an image angle $\psi < \psi_{\mathrm{crit},2}$.

F.2 Secondary features in the shadow boundary for near-critical $\tilde{\gamma}$

Close to critical $\tilde{\gamma}$, the horizon and the resulting shadow image develop additional distinct features. Such features are non-generic in the sense that they only appear for $\tilde{\gamma}$ close to $\tilde{\gamma}_{\mathrm{crit}}$. In the near-critical ($\tilde{\gamma} \approx \tilde{\gamma}_{\mathrm{crit}}$) regime, the dent in the RG-improved horizon at $\theta = \pi/2$ becomes very pronounced, cf. left panel of figure 42. This leads to a more pointy appearance of the dent-like feature in the shadow boundary at $\psi = 0$. Loosely speaking, the horizon takes on the appearance of two largely but not fully overlapping spheres (while remaining differentiable at $\theta = \pi/2$). Further, it results in two sets of distinct, novel features at two intermediate image angles, e.g. for $a = 0.99\, r_g$ and $\tilde{\gamma} \approx \tilde{\gamma}_{\mathrm{crit}} = 0.010242$, these occur at $\psi_{\mathrm{crit},1} \approx \frac{16}{100}\pi$ and $\psi_{\mathrm{crit},2} = \frac{4}{100}\pi$, cf. right panel of figure 42.

These secondary features are a consequence of three different regimes for near-horizon null geodesics, cf. figure 43. For $\psi > \psi_{\mathrm{crit},1}$ the light rays closest to the horizon probe the entire horizon. At $|\psi| = \psi_{\mathrm{crit},1}$, the null geodesics transition from wrapping around the entire horizon to wrapping around roughly half of the horizon. Loosely speaking, they probe just one of the two spheres that make up the horizon. Accordingly, the shadow diameter grows significantly at $|\psi| \approx \psi_{\mathrm{crit},1}$. In other words, a smooth, step-like feature appears in the shadow for $|\psi| = \psi_{\mathrm{crit},1}$. As the dent in the shadow is rather prominent for $\tilde{\gamma} \approx \tilde{\gamma}_{\mathrm{crit}}$, it can "trap" trajectories that exist for $|\psi| < \psi_{\mathrm{crit},2}$. As shown in figure 43, these mainly wrap around the dented region of the horizon and cover a significantly smaller interval in the affine parameter in exploring other parts of the horizon. Accordingly, these probe the smallest values of r of all trajectories and therefore arrive at values closer to the origin in the image plane.

For less extreme cases, i.e. $\tilde{\gamma} < \tilde{\gamma}_{\mathrm{crit}}$, these features in the shadow-boundary become less pronounced. Nevertheless, traces of these features remain present in the shadow boundary. We stress that we do not consider such features universal, in the sense that they can depend on the RG improvement that is used. The existence of the dent in the horizon and shadow, however, is robust.

References

[1] Astrid Eichhorn, Aaron Held, and Christof Wetterich. Predictive power of grand unification from quantum gravity. 2019.

[2] Senarath de Alwis, Astrid Eichhorn, Aaron Held, Jan M. Pawlowski, Marc Schiffer, and Fleur Versteegen. Asymptotic safety, string theory and the weak gravity conjecture. 2019.

[3] Aaron Held, Roman Gold, and Astrid Eichhorn. Asymptotic safety casts its shadow. 2019.

[4] Aaron Held and René Sondenheimer. Higgs stability-bound and fermionic dark matter. *JHEP*, 02:166, 2019.

[5] Astrid Eichhorn and Aaron Held. Mass difference for charged quarks from asymptotically safe quantum gravity. *Phys. Rev. Lett.*, 121(15):151302, 2018.

[6] Astrid Eichhorn, Aaron Held, and Peter Vander Griend. Asymptotic safety in the dark. *JHEP*, 08:147, 2018.

[7] Astrid Eichhorn, Aaron Held, and Christof Wetterich. Quantum-gravity predictions for the fine-structure constant. *Phys. Lett.*, B782:198–201, 2018.

[8] Astrid Eichhorn and Aaron Held. Top mass from asymptotic safety. *Phys. Lett.*, B777:217–221, 2018.

[9] Astrid Eichhorn and Aaron Held. Viability of quantum-gravity induced ultraviolet completions for matter. *Phys. Rev.*, D96(8):086025, 2017.

[10] Nicolai Christiansen, Astrid Eichhorn, and Aaron Held. Is scale-invariance in gauge-Yukawa systems compatible with the graviton? *Phys. Rev.*, D96(8):084021, 2017.

[11] Max Planck. On the Law of Distribution of Energy in the Normal Spectrum. *Annalen Phys.*, 4:553, 1901.

[12] Peter J. Mohr, David B. Newell, and Barry N. Taylor. CODATA Recommended Values of the Fundamental Physical Constants: 2014. *Rev. Mod. Phys.*, 88(3):035009, 2016.

[13] Lyndon Evans and Philip Bryant. LHC Machine. *JINST*, 3:S08001, 2008.

[14] Floyd W. Stecker. PeV neutrinos observed by IceCube from cores of active galactic nuclei. *Phys. Rev.*, D88(4):047301, 2013.

[15] Laurent Canetti, Marco Drewes, and Mikhail Shaposhnikov. Matter and Antimatter in the Universe. *New J. Phys.*, 14:095012, 2012.

[16] Guillermo Ballesteros, Javier Redondo, Andreas Ringwald, and Carlos Tamarit. Standard Model—axion—seesaw—Higgs portal inflation. Five problems of particle physics and cosmology solved in one stroke. *JCAP*, 1708(08):001, 2017.

[17] Steven Weinberg. *The Quantum theory of fields. Vol. 1: Foundations.* Cambridge University Press, 2005.

[18] Steven Weinberg. *The quantum theory of fields. Vol. 2: Modern applications.* Cambridge University Press, 2013.

[19] Michael E. Peskin and Daniel V. Schroeder. *An Introduction to quantum field theory*. Addison-Wesley, Reading, USA, 1995.

[20] Matthew D. Schwartz. *Quantum Field Theory and the Standard Model*. Cambridge University Press, 2014.

[21] C. Q. Geng and R. E. Marshak. Uniqueness of Quark and Lepton Representations in the Standard Model From the Anomalies Viewpoint. *Phys. Rev.*, D39:693, 1989.

[22] K. S. Babu and Rabindra N. Mohapatra. Quantization of Electric Charge From Anomaly Constraints and a Majorana Neutrino. *Phys. Rev.*, D41:271, 1990.

[23] J. A. Minahan, Pierre Ramond, and R. C. Warner. A Comment on Anomaly Cancellation in the Standard Model. *Phys. Rev.*, D41:715, 1990.

[24] Robert Foot, H. Lew, and R. R. Volkas. Electric charge quantization. *J. Phys.*, G19:361–372, 1993. [Erratum: J. Phys.G19,1067(1993)].

[25] Jean Zinn-Justin. Quantum field theory and critical phenomena. *Int. Ser. Monogr. Phys.*, 113:1–1054, 2002.

[26] Ingo Schienbein, Florian Staub, Tom Steudtner, and Kseniia Svirina. Revisiting RGEs for general gauge theories. *Nucl. Phys.*, B939:1–48, 2019.

[27] Georges Aad et al. Measurement of the top-quark mass in $t\bar{t}$ + 1-jet events collected with the ATLAS detector in pp collisions at $\sqrt{s}$ = 8 TeV. 2019.

[28] Albert M Sirunyan et al. Measurement of $t\bar{t}$ normalised multi-differential cross sections in pp collisions at $\sqrt{s}$ = 13 TeV, and simultaneous determination of the strong coupling strength, top quark pole mass, and parton distribution functions. *Submitted to: Eur. Phys. J.*, 2019.

[29] Fedor Bezrukov, Mikhail Yu. Kalmykov, Bernd A. Kniehl, and Mikhail Shaposhnikov. Higgs Boson Mass and New Physics. *JHEP*, 10:140, 2012. [,275(2012)].

[30] Giuseppe Degrassi, Stefano Di Vita, Joan Elias-Miro, Jose R. Espinosa, Gian F. Giudice, Gino Isidori, and Alessandro Strumia. Higgs mass and vacuum stability in the Standard Model at NNLO. *JHEP*, 08:098, 2012.

[31] Dario Buttazzo, Giuseppe Degrassi, Pier Paolo Giardino, Gian F. Giudice, Filippo Sala, Alberto Salvio, and Alessandro Strumia. Investigating the near-criticality of the Higgs boson. *JHEP*, 12:089, 2013.

[32] Fedor Bezrukov and Mikhail Shaposhnikov. Why should we care about the top quark Yukawa coupling? *J. Exp. Theor. Phys.*, 120:335–343, 2015. [Zh. Eksp. Teor. Fiz.147,389(2015)].

[33] Jose R. Espinosa, Gian F. Giudice, Enrico Morgante, Antonio Riotto, Leonardo Senatore, Alessandro Strumia, and Nikolaos Tetradis. The cosmological Higgstory of the vacuum instability. *JHEP*, 09:174, 2015.

[34] Mikhail Shaposhnikov and Christof Wetterich. Asymptotic safety of gravity and the Higgs boson mass. *Phys. Lett.*, B683:196–200, 2010.

[35] C. D. Froggatt and Holger Bech Nielsen. Standard model criticality prediction: Top mass 173 +- 5-GeV and Higgs mass 135 +- 9-GeV. *Phys. Lett.*, B368:96–102, 1996.

[36] B. Pontecorvo. Mesonium and anti-mesonium. *Sov. Phys. JETP*, 6:429, 1957. [Zh. Eksp. Teor. Fiz.33,549(1957)].

[37] Ziro Maki, Masami Nakagawa, and Shoichi Sakata. Remarks on the unified model of elementary particles. *Prog. Theor. Phys.*, 28:870–880, 1962. [,34(1962)].

[38] Raymond Davis, Jr., Don S. Harmer, and Kenneth C. Hoffman. Search for neutrinos from the sun. *Phys. Rev. Lett.*, 20:1205–1209, 1968.

[39] B. T. Cleveland, Timothy Daily, Raymond Davis, Jr., James R. Distel, Kenneth Lande, C. K. Lee, Paul S. Wildenhain, and Jack Ullman. Measurement of the solar electron neutrino flux with the Homestake chlorine detector. *Astrophys. J.*, 496:505–526, 1998.

[40] Y. Fukuda et al. Solar neutrino data covering solar cycle 22. *Phys. Rev. Lett.*, 77:1683–1686, 1996.

[41] W. Hampel et al. GALLEX solar neutrino observations: Results for GALLEX IV. *Phys. Lett.*, B447:127–133, 1999.

[42] S. Fukuda et al. Determination of solar neutrino oscillation parameters using 1496 days of Super-Kamiokande I data. *Phys. Lett.*, B539:179–187, 2002.

[43] Q. R. Ahmad et al. Direct evidence for neutrino flavor transformation from neutral current interactions in the Sudbury Neutrino Observatory. *Phys. Rev. Lett.*, 89:011301, 2002.

[44] M. Altmann et al. Complete results for five years of GNO solar neutrino observations. *Phys. Lett.*, B616:174–190, 2005.

[45] J. N. Abdurashitov et al. Measurement of the solar neutrino capture rate with gallium metal. III: Results for the 2002–2007 data-taking period. *Phys. Rev.*, C80:015807, 2009.

[46] Y. Fukuda et al. Evidence for oscillation of atmospheric neutrinos. *Phys. Rev. Lett.*, 81:1562–1567, 1998.

[47] Y. Ashie et al. Evidence for an oscillatory signature in atmospheric neutrino oscillation. *Phys. Rev. Lett.*, 93:101801, 2004.

[48] K. Eguchi et al. First results from KamLAND: Evidence for reactor anti-neutrino disappearance. *Phys. Rev. Lett.*, 90:021802, 2003.

[49] T. Araki et al. Measurement of neutrino oscillation with KamLAND: Evidence of spectral distortion. *Phys. Rev. Lett.*, 94:081801, 2005.

[50] M. H. Ahn et al. Measurement of Neutrino Oscillation by the K2K Experiment. *Phys. Rev.*, D74:072003, 2006.

[51] D. G. Michael et al. Observation of muon neutrino disappearance with the MINOS detectors and the NuMI neutrino beam. *Phys. Rev. Lett.*, 97:191801, 2006.

[52] M. C. Gonzalez-Garcia and Michele Maltoni. Phenomenology with Massive Neutrinos. *Phys. Rept.*, 460:1–129, 2008.

[53] Carlo Giunti and Chung W. Kim. *Fundamentals of Neutrino Physics and Astrophysics*. 2007.

[54] Ettore Majorana. Teoria simmetrica dell'elettrone e del positrone. *Nuovo Cim.*, 14:171–184, 1937.

[55] C. S. Wu, E. Ambler, R. W. Hayward, D. D. Hoppes, and R. P. Hudson. Experimental Test of Parity Conservation in Beta Decay. *Phys. Rev.*, 105:1413–1414, 1957.

[56] Steven Weinberg. Baryon and Lepton Nonconserving Processes. *Phys. Rev. Lett.*, 43:1566–1570, 1979.

[57] W. H. Furry. On transition probabilities in double beta-disintegration. *Phys. Rev.*, 56:1184–1193, 1939.

[58] Takehiko Asaka, Steve Blanchet, and Mikhail Shaposhnikov. The nuMSM, dark matter and neutrino masses. *Phys. Lett.*, B631:151–156, 2005.

[59] Takehiko Asaka and Mikhail Shaposhnikov. The nuMSM, dark matter and baryon asymmetry of the universe. *Phys. Lett.*, B620:17–26, 2005.

[60] B. Pontecorvo. Inverse beta processes and nonconservation of lepton charge. *Sov. Phys. JETP*, 7:172–173, 1958. [Zh. Eksp. Teor. Fiz.34,247(1957)].

[61] R. N. Cahn, D. A. Dwyer, S. J. Freedman, W. C. Haxton, R. W. Kadel, Yu. G. Kolomensky, K. B. Luk, P. McDonald, G. D. Orebi Gann, and A. W. P. Poon. White Paper: Measuring the Neutrino Mass Hierarchy. In *Proceedings, 2013 Community Summer Study on the Future of U.S. Particle Physics: Snowmass on the Mississippi (CSS2013): Minneapolis, MN, USA, July 29-August 6, 2013*, 2013.

[62] Susanne Mertens. Direct Neutrino Mass Experiments. *J. Phys. Conf. Ser.*, 718(2):022013, 2016.

[63] A. Gando et al. Limit on Neutrinoless $\beta\beta$ Decay of ^{136}Xe from the First Phase of KamLAND-Zen and Comparison with the Positive Claim in ^{76}Ge. *Phys. Rev. Lett.*, 110(6):062502, 2013.

[64] A. Osipowicz et al. KATRIN: A Next generation tritium beta decay experiment with sub-eV sensitivity for the electron neutrino mass. Letter of intent. 2001.

[65] Nathalie Palanque-Delabrouille et al. Neutrino masses and cosmology with Lyman-alpha forest power spectrum. *JCAP*, 1511(11):011, 2015.

[66] N. Aghanim et al. Planck intermediate results. XLVI. Reduction of large-scale systematic effects in HFI polarization maps and estimation of the reionization optical depth. *Astron. Astrophys.*, 596:A107, 2016.

[67] Michael Levi et al. The DESI Experiment, a whitepaper for Snowmass 2013. 2013.

[68] Peter Minkowski. $\mu \to e\gamma$ at a Rate of One Out of 10^9 Muon Decays? *Phys. Lett.*, 67B:421–428, 1977.

[69] Tsutomu Yanagida. Horizontal gauge symmetry and masses of neutrinos. *Conf. Proc.*, C7902131:95–99, 1979.

[70] Rabindra N. Mohapatra and Goran Senjanovic. Neutrino Mass and Spontaneous Parity Nonconservation. *Phys. Rev. Lett.*, 44:912, 1980. [,231(1979)].

[71] Murray Gell-Mann, Pierre Ramond, and Richard Slansky. Complex Spinors and Unified Theories. *Conf. Proc.*, C790927:315–321, 1979.

[72] P. A. M. Dirac. The Quantum Theory of the Electron. *Proceedings of the Royal Society of London Series A*, 117:610–624, February 1928.

[73] Carl D. Anderson. The Apparent Existence of Easily Deflectable Positives. *Science*, 76:238–239, 1932.

[74] C. D. Anderson. The Positive Electron. *Phys. Rev.*, 43:491–494, 1933.

[75] A. D. Sakharov. Violation of CP Invariance, C asymmetry, and baryon asymmetry of the universe. *Pisma Zh. Eksp. Teor. Fiz.*, 5:32–35, 1967. [Usp. Fiz. Nauk161,no.5,61(1991)].

[76] V. A. Kuzmin, V. A. Rubakov, and M. E. Shaposhnikov. On the Anomalous Electroweak Baryon Number Nonconservation in the Early Universe. *Phys. Lett.*, 155B:36, 1985.

[77] V. A. Rubakov and M. E. Shaposhnikov. Electroweak baryon number nonconservation in the early universe and in high-energy collisions. *Usp. Fiz. Nauk*, 166:493–537, 1996. [Phys. Usp.39,461(1996)].

[78] Stephen L. Adler. Axial vector vertex in spinor electrodynamics. *Phys. Rev.*, 177:2426–2438, 1969. [,241(1969)].

[79] J. S. Bell and R. Jackiw. A PCAC puzzle: $\pi^0 \to \gamma\gamma$ in the σ model. *Nuovo Cim.*, A60:47–61, 1969.

[80] Gerard 't Hooft. Symmetry Breaking Through Bell-Jackiw Anomalies. *Phys. Rev. Lett.*, 37:8–11, 1976. [,226(1976)].

[81] M. E. Shaposhnikov. Anomalous fermion number nonconservation. In *Proceedings, Summer School in High-energy Physics and Cosmology: Trieste, Italy, June 17-August 9, 1991. Vol. 1, 2*, pages 338–374, 1991.

[82] M. E. Shaposhnikov. Structure of the High Temperature Gauge Ground State and Electroweak Production of the Baryon Asymmetry. *Nucl. Phys.*, B299:797–817, 1988.

[83] M. E. Shaposhnikov. Possible Appearance of the Baryon Asymmetry of the Universe in an Electroweak Theory. *JETP Lett.*, 44:465–468, 1986. [Pisma Zh. Eksp. Teor. Fiz.44,364(1986)].

[84] M. E. Shaposhnikov. Baryon Asymmetry of the Universe in Standard Electroweak Theory. *Nucl. Phys.*, B287:757–775, 1987.

[85] Jan Ambjorn, M. L. Laursen, and M. E. Shaposhnikov. Baryon Asymmetry Generation in the Electroweak Theory: A Lattice Study. *Nucl. Phys.*, B316:483–508, 1989.

[86] Glennys R. Farrar and M. E. Shaposhnikov. Baryon asymmetry of the universe in the standard electroweak theory. *Phys. Rev.*, D50:774, 1994.

[87] M. B. Gavela, P. Hernandez, J. Orloff, O. Pene, and C. Quimbay. Standard model CP violation and baryon asymmetry. Part 2: Finite temperature. *Nucl. Phys.*, B430:382–426, 1994.

[88] Patrick Huet and Eric Sather. Electroweak baryogenesis and standard model CP violation. *Phys. Rev.*, D51:379–394, 1995.

[89] Tomas Brauner, Olli Taanila, Anders Tranberg, and Aleksi Vuorinen. Temperature Dependence of Standard Model CP Violation. *Phys. Rev. Lett.*, 108:041601, 2012.

[90] A. E. Nelson, D. B. Kaplan, and Andrew G. Cohen. Why there is something rather than nothing: Matter from weak interactions. *Nucl. Phys.*, B373:453–478, 1992.

[91] Andrew G. Cohen, D. B. Kaplan, and A. E. Nelson. Progress in electroweak baryogenesis. *Ann. Rev. Nucl. Part. Sci.*, 43:27–70, 1993.

[92] K. Kajantie, M. Laine, K. Rummukainen, and Mikhail E. Shaposhnikov. Is there a hot electroweak phase transition at m(H) larger or equal to m(W)? *Phys. Rev. Lett.*, 77:2887–2890, 1996.

[93] K. Rummukainen, M. Tsypin, K. Kajantie, M. Laine, and Mikhail E. Shaposhnikov. The Universality class of the electroweak theory. *Nucl. Phys.*, B532:283–314, 1998.

[94] David E. Morrissey and Michael J. Ramsey-Musolf. Electroweak baryogenesis. *New J. Phys.*, 14:125003, 2012.

[95] Steve Blanchet and Pasquale Di Bari. The minimal scenario of leptogenesis. *New J. Phys.*, 14:125012, 2012.

[96] M. Fukugita and T. Yanagida. Baryogenesis Without Grand Unification. *Phys. Lett.*, B174:45–47, 1986.

[97] Evgeny K. Akhmedov, V. A. Rubakov, and A. Yu. Smirnov. Baryogenesis via neutrino oscillations. *Phys. Rev. Lett.*, 81:1359–1362, 1998.

[98] Laurent Canetti, Marco Drewes, Tibor Frossard, and Mikhail Shaposhnikov. Dark Matter, Baryogenesis and Neutrino Oscillations from Right Handed Neutrinos. *Phys. Rev.*, D87:093006, 2013.

[99] Motohiko Yoshimura. Unified Gauge Theories and the Baryon Number of the Universe. *Phys. Rev. Lett.*, 41:281–284, 1978. [Erratum: Phys. Rev. Lett.42,746(1979)].

[100] A. Yu. Ignatiev, N. V. Krasnikov, V. A. Kuzmin, and A. N. Tavkhelidze. Universal CP Noninvariant Superweak Interaction and Baryon Asymmetry of the Universe. *Phys. Lett.*, 76B:436–438, 1978.

[101] Steven Weinberg. Cosmological Production of Baryons. *Phys. Rev. Lett.*, 42:850–853, 1979.

[102] A. D. Dolgov. NonGUT baryogenesis. *Phys. Rept.*, 222:309–386, 1992.

[103] A. D. Dolgov. QUANTUM EVAPORATION OF BLACK HOLES AND THE BARYON ASYMMETRY OF THE UNIVERSE. *Sov. Phys. JETP*, 52:169–175, 1980. [Zh. Eksp. Teor. Fiz.79,337(1980)].

[104] Scott Dodelson and Lawrence M. Widrow. BARYON SYMMETRIC BARYOGENESIS. *Phys. Rev. Lett.*, 64:340–343, 1990.

[105] Scott Dodelson and Lawrence M. Widrow. Baryogenesis in a Baryon Symmetric Universe. *Phys. Rev.*, D42:326–342, 1990.

[106] Gerard 't Hooft, C. Itzykson, A. Jaffe, H. Lehmann, P. K. Mitter, I. M. Singer, and R. Stora. Recent Developments in Gauge Theories. Proceedings, Nato Advanced Study Institute, Cargese, France, August 26 - September 8, 1979. *NATO Sci. Ser. B*, 59:pp.1–438, 1980.

[107] Christof Wetterich and Masatoshi Yamada. Gauge hierarchy problem in asymptotically safe gravity–the resurgence mechanism. *Phys. Lett.*, B770:268–271, 2017.

[108] S. Hossenfelder. Screams for Explanation: Finetuning and Naturalness in the Foundations of Physics. 2018.

[109] Event Horizon Telescope. First M87 Event Horizon Telescope Results. I. The Shadow of the Supermassive Black Hole. *Astrophys. J.*, 875(1):L1, 2019.

[110] Event Horizon Telescope. First M87 Event Horizon Telescope Results. II. Array and Instrumentation. *Astrophys. J.*, 875(1):L2, 2019.

[111] Event Horizon Telescope. First M87 Event Horizon Telescope Results. III. Data Processing and Calibration. *Astrophys. J.*, 875(1):L3, 2019.

[112] Event Horizon Telescope. First M87 Event Horizon Telescope Results. IV. Imaging the Central Supermassive Black Hole. *Astrophys. J.*, 875(1):L4, 2019.

[113] Event Horizon Telescope. First M87 Event Horizon Telescope Results. V. Physical Origin of the Asymmetric Ring. *Astrophys. J.*, 875(1):L5, 2019.

[114] Event Horizon Telescope. First M87 Event Horizon Telescope Results. VI. The Shadow and Mass of the Central Black Hole. *Astrophys. J.*, 875(1):L6, 2019.

[115] Steven Weinberg. *Cosmology*. 2008.

[116] A. Friedman. On the Curvature of space. *Z. Phys.*, 10:377–386, 1922. [Gen. Rel. Grav.31,1991(1999)].

[117] H. P. Robertson. Kinematics and World-Structure. *Astrophys. J.*, 82:284–301, 1935.

[118] A. G. Walker. On Milne's Theory of World-Structure. *Proceedings of the London Mathematical Society, (Series 2) volume 42, p. 90-127*, 42:90–127, 1937.

[119] R. R. Caldwell, Rahul Dave, and Paul J. Steinhardt. Cosmological imprint of an energy component with general equation of state. *Phys. Rev. Lett.*, 80:1582–1585, 1998.

[120] Neta A. Bahcall, Jeremiah P. Ostriker, Saul Perlmutter, and Paul J. Steinhardt. The Cosmic triangle: Assessing the state of the universe. *Science*, 284:1481–1488, 1999.

[121] Austin Joyce, Bhuvnesh Jain, Justin Khoury, and Mark Trodden. Beyond the Cosmological Standard Model. *Phys. Rept.*, 568:1–98, 2015.

[122] Adam G. Riess et al. Observational evidence from supernovae for an accelerating universe and a cosmological constant. *Astron. J.*, 116:1009–1038, 1998.

[123] S. Perlmutter et al. Measurements of Ω and Λ from 42 high redshift supernovae. *Astrophys. J.*, 517:565–586, 1999.

[124] E. Komatsu et al. Seven-Year Wilkinson Microwave Anisotropy Probe (WMAP) Observations: Cosmological Interpretation. *Astrophys. J. Suppl.*, 192:18, 2011.

[125] P. A. R. Ade et al. Planck 2015 results. XIII. Cosmological parameters. *Astron. Astrophys.*, 594:A13, 2016.

[126] Bharat Ratra and P. J. E. Peebles. Cosmological Consequences of a Rolling Homogeneous Scalar Field. *Phys. Rev.*, D37:3406, 1988.

[127] C. Wetterich. Cosmology and the Fate of Dilatation Symmetry. *Nucl. Phys.*, B302:668–696, 1988.

[128] Edmund J. Copeland, M. Sami, and Shinji Tsujikawa. Dynamics of dark energy. *Int. J. Mod. Phys.*, D15:1753–1936, 2006.

[129] Jose Luis Bernal, Licia Verde, and Adam G. Riess. The trouble with H_0. *JCAP*, 1610(10):019, 2016.

[130] Alexei A. Starobinsky. A New Type of Isotropic Cosmological Models Without Singularity. *Phys. Lett.*, 91B:99–102, 1980. [,771(1980)].

[131] Alan H. Guth. The Inflationary Universe: A Possible Solution to the Horizon and Flatness Problems. *Phys. Rev.*, D23:347–356, 1981. [Adv. Ser. Astrophys. Cosmol.3,139(1987)].

[132] Viatcheslav F. Mukhanov and G. V. Chibisov. Quantum Fluctuations and a Nonsingular Universe. *JETP Lett.*, 33:532–535, 1981. [Pisma Zh. Eksp. Teor. Fiz.33,549(1981)].

[133] Andrei D. Linde. A New Inflationary Universe Scenario: A Possible Solution of the Horizon, Flatness, Homogeneity, Isotropy and Primordial Monopole Problems. *Phys. Lett.*, 108B:389–393, 1982. [Adv. Ser. Astrophys. Cosmol.3,149(1987)].

[134] Andreas Albrecht and Paul J. Steinhardt. Cosmology for Grand Unified Theories with Radiatively Induced Symmetry Breaking. *Phys. Rev. Lett.*, 48:1220–1223, 1982. [Adv. Ser. Astrophys. Cosmol.3,158(1987)].

[135] Andrei D. Linde. Chaotic Inflation. *Phys. Lett.*, 129B:177–181, 1983.

[136] S. W. Hawking. The Development of Irregularities in a Single Bubble Inflationary Universe. *Phys. Lett.*, 115B:295, 1982.

[137] Alexei A. Starobinsky. Dynamics of Phase Transition in the New Inflationary Universe Scenario and Generation of Perturbations. *Phys. Lett.*, 117B:175–178, 1982.

[138] Misao Sasaki. Large Scale Quantum Fluctuations in the Inflationary Universe. *Prog. Theor. Phys.*, 76:1036, 1986.

[139] Viatcheslav F. Mukhanov. Quantum Theory of Gauge Invariant Cosmological Perturbations. *Sov. Phys. JETP*, 67:1297–1302, 1988. [Zh. Eksp. Teor. Fiz.94N7,1(1988)].

[140] Javier Rubio. Higgs inflation. *Front. Astron. Space Sci.*, 5:50, 2019.

[141] Alexei A. Starobinsky. Spectrum of relict gravitational radiation and the early state of the universe. *JETP Lett.*, 30:682–685, 1979. [,767(1979)].

[142] Vera C. Rubin and W. Kent Ford, Jr. Rotation of the Andromeda Nebula from a Spectroscopic Survey of Emission Regions. *Astrophys. J.*, 159:379–403, 1970.

[143] V. C. Rubin, N. Thonnard, and W. K. Ford, Jr. Rotational properties of 21 SC galaxies with a large range of luminosities and radii, from NGC 4605 /R = 4kpc/ to UGC 2885 /R = 122 kpc/. *Astrophys. J.*, 238:471, 1980.

[144] Douglas Clowe, Marusa Bradac, Anthony H. Gonzalez, Maxim Markevitch, Scott W. Randall, Christine Jones, and Dennis Zaritsky. A direct empirical proof of the existence of dark matter. *Astrophys. J.*, 648:L109–L113, 2006.

[145] Scott Dodelson and Lawrence M. Widrow. Sterile-neutrinos as dark matter. *Phys. Rev. Lett.*, 72:17–20, 1994.

[146] Y. B. Zel'dovich and I. D. Novikov. The Hypothesis of Cores Retarded during Expansion and the Hot Cosmological Model. *Astronomicheskii Zhurnal*, 43:758, 1966.

[147] Bernard J. Carr and S. W. Hawking. Black holes in the early Universe. *Mon. Not. Roy. Astron. Soc.*, 168:399–415, 1974.

[148] P. Meszaros. The behaviour of point masses in an expanding cosmological substratum. *Astron. Astrophys.*, 37:225–228, 1974.

[149] G. F. Chapline. Cosmological effects of primordial black holes. *Nature*, 253:251, January 1975.

[150] Bernard J. Carr. The Primordial black hole mass spectrum. *Astrophys. J.*, 201:1–19, 1975.

[151] I. D. Novikov, A. G. Polnarev, A. A. Starobinskii, and I. B. Zeldovich. Primordial black holes. *Astronomy and Astrophysics*, 80:104–109, November 1979.

[152] M. Khlopov, B. A. Malomed, and Ia. B. Zeldovich. Gravitational instability of scalar fields and formation of primordial black holes. *Mon. Not. Roy. Astron. Soc.*, 215:575–589, 1985.

[153] Sébastien Clesse and Juan García-Bellido. Massive Primordial Black Holes from Hybrid Inflation as Dark Matter and the seeds of Galaxies. *Phys. Rev.*, D92(2):023524, 2015.

[154] Luca Amendola, Javier Rubio, and Christof Wetterich. Primordial black holes from fifth forces. *Phys. Rev.*, D97(8):081302, 2018.

[155] B. J. Carr, Kazunori Kohri, Yuuiti Sendouda, and Jun'ichi Yokoyama. New cosmological constraints on primordial black holes. *Phys. Rev.*, D81:104019, 2010.

[156] M. A. Monroy-Rodriguez and C. Allen. The End of the MACHO Era, Revisited: New Limits on MACHO Masses from Halo Wide Binaries. *ApJ*, 790:159, August 2014.

[157] B. P. Abbott et al. Observation of Gravitational Waves from a Binary Black Hole Merger. *Phys. Rev. Lett.*, 116(6):061102, 2016.

[158] Simeon Bird, Ilias Cholis, Julian B. Muñoz, Yacine Ali-Haïmoud, Marc Kamionkowski, Ely D. Kovetz, Alvise Raccanelli, and Adam G. Riess. Did LIGO detect dark matter? *Phys. Rev. Lett.*, 116(20):201301, 2016.

[159] Yacine Ali-Haïmoud and Marc Kamionkowski. Cosmic microwave background limits on accreting primordial black holes. *Phys. Rev.*, D95(4):043534, 2017.

[160] Yacine Ali-Haïmoud, Ely D. Kovetz, and Marc Kamionkowski. Merger rate of primordial black-hole binaries. *Phys. Rev.*, D96(12):123523, 2017.

[161] Juan García-Bellido and Sebastien Clesse. Constraints from microlensing experiments on clustered primordial black holes. *Phys. Dark Univ.*, 19:144–148, 2018.

[162] Julian B. Muñoz, Ely D. Kovetz, Liang Dai, and Marc Kamionkowski. Lensing of Fast Radio Bursts as a Probe of Compact Dark Matter. *Phys. Rev. Lett.*, 117(9):091301, 2016.

[163] Lingyuan Ji, Ely D. Kovetz, and Marc Kamionkowski. Strong Lensing of Gamma Ray Bursts as a Probe of Compact Dark Matter. *Phys. Rev.*, D98(12):123523, 2018.

[164] Jane H. MacGibbon. Can Planck-mass relics of evaporating black holes close the universe? *Nature*, 329:308–309, 1987.

[165] Pisin Chen and Ronald J. Adler. Black hole remnants and dark matter. *Nucl. Phys. Proc. Suppl.*, 124:103–106, 2003. [,103(2002)].

[166] Kourosh Nozari and S. Hamid Mehdipour. Gravitational uncertainty and black hole remnants. *Mod. Phys. Lett.*, A20:2937–2948, 2005.

[167] Fabio Scardigli, Christine Gruber, and Pisin Chen. Black Hole Remnants in the Early Universe. *Phys. Rev.*, D83:063507, 2011.

[168] Bernard J. Carr, Jonas Mureika, and Piero Nicolini. Sub-Planckian black holes and the Generalized Uncertainty Principle. *JHEP*, 07:052, 2015.

[169] Tomohiro Nakama and Jun'ichi Yokoyama. Micro black holes formed in the early Universe and their cosmological implications. *Phys. Rev.*, D99(6):061303, 2019.

[170] Martti Raidal, Sergey Solodukhin, Ville Vaskonen, and Hardi Veermäe. Light Primordial Exotic Compact Objects as All Dark Matter. *Phys. Rev.*, D97(12):123520, 2018.

[171] Syksy Rasanen and Eemeli Tomberg. Planck scale black hole dark matter from Higgs inflation. *JCAP*, 1901(01):038, 2019.

[172] Karl Schwarzschild. On the gravitational field of a mass point according to Einstein's theory. *Sitzungsber. Preuss. Akad. Wiss. Berlin (Math. Phys.)*, 1916:189–196, 1916.

[173] J. Droste. The field of a single centre in Einstein's theory of gravitation, and the motion of a particle in that field. *Koninklijke Nederlandse Akademie van Wetenschappen Proceedings Series B Physical Sciences*, 19:197–215, 1917.

[174] Richard C. Tolman. Effect of imhomogeneity on cosmological models. *Proc. Nat. Acad. Sci.*, 20:169–176, 1934. [Gen. Rel. Grav.29,935(1997)].

[175] J. R. Oppenheimer and H. Snyder. On Continued gravitational contraction. *Phys. Rev.*, 56:455–459, 1939.

[176] R. Penrose. Gravitational collapse: The role of general relativity. *Riv. Nuovo Cim.*, 1:252–276, 1969. [Gen. Rel. Grav.34,1141(2002)].

[177] Douglas M. Eardley and Larry Smarr. Time function in numerical relativity. Marginally bound dust collapse. *Phys. Rev.*, D19:2239–2259, 1979.

[178] Demetrios Christodoulou. Violation of cosmic censorship in the gravitational collapse of a dust cloud. *Commun. Math. Phys.*, 93:171–195, 1984.

[179] Richard P. A. C. Newman. Strengths of naked singularities in Tolman-Bondi space-times. *Class. Quant. Grav.*, 3:527–539, 1986.

[180] Amos Ori and Tsvi Piran. Naked Singularities in Selfsimilar Spherical Gravitational Collapse. *Phys. Rev. Lett.*, 59:2137, 1987.

[181] D. Christodoulou. The instability of naked singularities in the gravitational collapse of a scalar field. *arXiv Mathematics e-prints*, December 1999.

[182] S. W. Hawking and G. F. R. Ellis. *The Large Scale Structure of Space-Time*. Cambridge Monographs on Mathematical Physics. Cambridge University Press, 2011.

[183] E. Eichten, Kenneth D. Lane, and Michael E. Peskin. New Tests for Quark and Lepton Substructure. *Phys. Rev. Lett.*, 50:811–814, 1983. [,369(1983)].

[184] W. E. Caswell and G. P. Lepage. Effective Lagrangians for Bound State Problems in QED, QCD, and Other Field Theories. *Phys. Lett.*, 167B:437–442, 1986.

[185] W. Buchmuller and D. Wyler. Effective Lagrangian Analysis of New Interactions and Flavor Conservation. *Nucl. Phys.*, B268:621–653, 1986.

[186] G. P. Lepage and B. A. Thacker. Effective Lagrangians for Simulating Heavy Quark Systems. *Nucl. Phys. Proc. Suppl.*, 4:199, 1988.

[187] H. David Politzer and Mark B. Wise. Effective Field Theory Approach to Processes Involving Both Light and Heavy Fields. *Phys. Lett.*, B208:504–507, 1988.

[188] Howard Georgi. An Effective Field Theory for Heavy Quarks at Low-energies. *Phys. Lett.*, B240:447–450, 1990.

[189] Ilaria Brivio and Michael Trott. The Standard Model as an Effective Field Theory. *Phys. Rept.*, 793:1–98, 2019.

[190] Marcel Froissart. Asymptotic behavior and subtractions in the Mandelstam representation. *Phys. Rev.*, 123:1053–1057, 1961.

[191] E. Fermi. An attempt of a theory of beta radiation. 1. *Z. Phys.*, 88:161–177, 1934.

[192] S. L. Glashow. Partial Symmetries of Weak Interactions. *Nucl. Phys.*, 22:579–588, 1961.

[193] Steven Weinberg. A Model of Leptons. *Phys. Rev. Lett.*, 19:1264–1266, 1967.

[194] Abdus Salam. Weak and Electromagnetic Interactions. *Conf. Proc.*, C680519:367–377, 1968.

[195] John M. Cornwall, David N. Levin, and George Tiktopoulos. Uniqueness of spontaneously broken gauge theories. *Phys. Rev. Lett.*, 30:1268–1270, 1973. [Erratum: Phys. Rev. Lett.31,572(1973)].

[196] C. H. Llewellyn Smith. High-Energy Behavior and Gauge Symmetry. *Phys. Lett.*, 46B:233–236, 1973.

[197] Satish D. Joglekar. S matrix derivation of the Weinberg model. *Annals Phys.*, 83:427, 1974.

[198] John M. Cornwall, David N. Levin, and George Tiktopoulos. Derivation of Gauge Invariance from High-Energy Unitarity Bounds on the s Matrix. *Phys. Rev.*, D10:1145, 1974. [Erratum: Phys. Rev.D11,972(1975)].

[199] Georges Aad et al. Observation of a new particle in the search for the Standard Model Higgs boson with the ATLAS detector at the LHC. *Phys. Lett.*, B716:1–29, 2012.

[200] Serguei Chatrchyan et al. Observation of a New Boson at a Mass of 125 GeV with the CMS Experiment at the LHC. *Phys. Lett.*, B716:30–61, 2012.

[201] D. A. Dicus and V. S. Mathur. Upper bounds on the values of masses in unified gauge theories. *Phys. Rev.*, D7:3111–3114, 1973.

[202] Murray Gell-Mann and F. E. Low. Quantum electrodynamics at small distances. *Phys. Rev.*, 95:1300–1312, 1954.

[203] M. Gockeler, R. Horsley, V. Linke, Paul E. L. Rakow, G. Schierholz, and H. Stuben. Is there a Landau pole problem in QED? *Phys. Rev. Lett.*, 80:4119–4122, 1998.

[204] M. Gockeler, R. Horsley, V. Linke, Paul E. L. Rakow, G. Schierholz, and H. Stuben. Resolution of the Landau pole problem in QED. *Nucl. Phys. Proc. Suppl.*, 63:694–696, 1998. [,290(1997)].

[205] Holger Gies and Joerg Jaeckel. Renormalization flow of QED. *Phys. Rev. Lett.*, 93:110405, 2004.

[206] L. Maiani, G. Parisi, and R. Petronzio. Bounds on the Number and Masses of Quarks and Leptons. *Nucl. Phys.*, B136:115–124, 1978.

[207] N. Cabibbo, L. Maiani, G. Parisi, and R. Petronzio. Bounds on the Fermions and Higgs Boson Masses in Grand Unified Theories. *Nucl. Phys.*, B158:295–305, 1979.

[208] Roger F. Dashen and Herbert Neuberger. How to Get an Upper Bound on the Higgs Mass. *Phys. Rev. Lett.*, 50:1897, 1983.

[209] David J. E. Callaway. Nontriviality of Gauge Theories With Elementary Scalars and Upper Bounds on Higgs Masses. *Nucl. Phys.*, B233:189–203, 1984.

[210] M. A. B. Beg, C. Panagiotakopoulos, and A. Sirlin. Mass of the Higgs Boson in the Canonical Realization of the Weinberg-Salam Theory. *Phys. Rev. Lett.*, 52:883, 1984.

[211] M. Lindner. Implications of Triviality for the Standard Model. *Z. Phys.*, C31:295, 1986.

[212] Julius Kuti, Lee Lin, and Yue Shen. Upper Bound on the Higgs Mass in the Standard Model. *Phys. Rev. Lett.*, 61:678, 1988.

[213] Thomas Hambye and Kurt Riesselmann. Matching conditions and Higgs mass upper bounds revisited. *Phys. Rev.*, D55:7255–7262, 1997.

[214] Gerard 't Hooft and M. J. G. Veltman. One loop divergencies in the theory of gravitation. *Ann. Inst. H. Poincare Phys. Theor.*, A20:69–94, 1974.

[215] Marc H. Goroff and Augusto Sagnotti. The Ultraviolet Behavior of Einstein Gravity. *Nucl. Phys.*, B266:709–736, 1986.

[216] G. 't Hooft. Perturbative quantum gravity. *Subnucl. Ser.*, 40:249–269, 2003.

[217] Bryce S. DeWitt. Quantum Theory of Gravity. 2. The Manifestly Covariant Theory. *Phys. Rev.*, 162:1195–1239, 1967. [,298(1967)].

[218] K. S. Stelle. Classical Gravity with Higher Derivatives. *Gen. Rel. Grav.*, 9:353–371, 1978.

[219] Philip D. Mannheim. Conformal Cosmology With No Cosmological Constant. *Gen. Rel. Grav.*, 22:289–298, 1990.

[220] Philip D. Mannheim. Making the Case for Conformal Gravity. *Found. Phys.*, 42:388–420, 2012.

[221] K. S. Stelle. Renormalization of Higher Derivative Quantum Gravity. *Phys. Rev.*, D16:953–969, 1977.

[222] E. S. Fradkin and Arkady A. Tseytlin. Renormalizable Asymptotically Free Quantum Theory of Gravity. *Phys. Lett.*, 104B:377–381, 1981.

[223] E. S. Fradkin and Arkady A. Tseytlin. Renormalizable asymptotically free quantum theory of gravity. *Nucl. Phys.*, B201:469–491, 1982.

[224] M. Ostrogradsky. Mémoires sur les équations différentielles, relatives au problème des isopérimètres. *Mem. Acad. St. Petersbourg*, 6(4):385–517, 1850.

[225] John F. Donoghue and Gabriel Menezes. The arrow of causality and quantum gravity. 2019.

[226] T. D. Lee and G. C. Wick. Negative Metric and the Unitarity of the S Matrix. *Nucl. Phys.*, B9:209–243, 1969. [,83(1969)].

[227] S. Coleman. Acausality. In *7th International School of Subnuclear Physics (Ettore Majorana): Subnuclear Phenomena Erice, Italy, July 3-19, 1969*, pages 282–327, 1969.

[228] S. W. Hawking and Thomas Hertog. Living with ghosts. *Phys. Rev.*, D65:103515, 2002.

[229] Alberto Salvio and Alessandro Strumia. Agravity. *JHEP*, 06:080, 2014.

[230] Bob Holdom and Jing Ren. Quadratic gravity: from weak to strong. *Int. J. Mod. Phys.*, D25(12):1643004, 2016.

[231] John F. Donoghue. Quartic propagators, negative norms and the physical spectrum. *Phys. Rev.*, D96(4):044007, 2017.

[232] Daniel Becker, Chris Ripken, and Frank Saueressig. On avoiding Ostrogradski instabilities within Asymptotic Safety. *JHEP*, 12:121, 2017.

[233] Damiano Anselmi and Marco Piva. The Ultraviolet Behavior of Quantum Gravity. *JHEP*, 05:027, 2018.

[234] John F. Donoghue. General relativity as an effective field theory: The leading quantum corrections. *Phys. Rev.*, D50:3874–3888, 1994.

[235] John F. Donoghue. Introduction to the effective field theory description of gravity. In *Advanced School on Effective Theories Almunecar, Spain, June 25-July 1, 1995*, 1995.

[236] Frits A. Berends and R. Gastmans. On the High-Energy Behavior in Quantum Gravity. *Nucl. Phys.*, B88:99–108, 1975.

[237] Yugo Abe, Takeo Inami, Keisuke Izumi, and Tomotaka Kitamura. Matter scattering in quadratic gravity and unitarity. *PTEP*, 2018(3):031E01, 2018.

[238] E. T. Tomboulis. Superrenormalizable gauge and gravitational theories. 1997.

[239] J. W. Moffat. Ultraviolet Complete Quantum Gravity. *Eur. Phys. J. Plus*, 126:43, 2011.

[240] Leonardo Modesto. Super-renormalizable Quantum Gravity. *Phys. Rev.*, D86:044005, 2012.

[241] Tirthabir Biswas, Erik Gerwick, Tomi Koivisto, and Anupam Mazumdar. Towards singularity and ghost free theories of gravity. *Phys. Rev. Lett.*, 108:031101, 2012.

[242] Steven Weinberg. ULTRAVIOLET DIVERGENCES IN QUANTUM THEORIES OF GRAVITATION. In *General Relativity: An Einstein Centenary Survey*, pages 790–831. 1980.

[243] M. Reuter. Nonperturbative evolution equation for quantum gravity. *Phys. Rev.*, D57:971–985, 1998.

[244] J. Polchinski. *String theory. Vol. 1: An introduction to the bosonic string.* Cambridge Monographs on Mathematical Physics. Cambridge University Press, 2007.

[245] J. Polchinski. *String theory. Vol. 2: Superstring theory and beyond.* Cambridge Monographs on Mathematical Physics. Cambridge University Press, 2007.

[246] Abhay Ashtekar and Jerzy Lewandowski. Background independent quantum gravity: A Status report. *Class. Quant. Grav.*, 21:R53, 2004.

[247] Luca Bombelli, Rabinder K. Koul, Joohan Lee, and Rafael D. Sorkin. A Quantum Source of Entropy for Black Holes. *Phys. Rev.*, D34:373–383, 1986.

[248] R. Loll. Quantum Gravity from Causal Dynamical Triangulations: A Review. 2019.

[249] L. P. Kadanoff. Scaling laws for Ising models near T(c). *Physics Physique Fizika*, 2:263–272, 1966.

[250] Kenneth G. Wilson. Renormalization group and critical phenomena. 1. Renormalization group and the Kadanoff scaling picture. *Phys. Rev.*, B4:3174–3183, 1971.

[251] Kenneth G. Wilson. Renormalization group and critical phenomena. 2. Phase space cell analysis of critical behavior. *Phys. Rev.*, B4:3184–3205, 1971.

[252] K. G. Wilson and John B. Kogut. The Renormalization group and the epsilon expansion. *Phys. Rept.*, 12:75–199, 1974.

[253] Curtis G. Callan, Jr. Broken scale invariance in scalar field theory. *Phys. Rev.*, D2:1541–1547, 1970.

[254] K. Symanzik. Small distance behavior in field theory and power counting. *Commun. Math. Phys.*, 18:227–246, 1970.

[255] Christof Wetterich. Exact evolution equation for the effective potential. *Phys. Lett.*, B301:90–94, 1993.

[256] Ulrich Ellwanger. FLow equations for N point functions and bound states. *Z. Phys.*, C62:503–510, 1994. [,206(1993)].

[257] Tim R. Morris. The Exact renormalization group and approximate solutions. *Int. J. Mod. Phys.*, A9:2411–2450, 1994.

[258] N. Tetradis and C. Wetterich. Critical exponents from effective average action. *Nucl. Phys.*, B422:541–592, 1994.

[259] Stefan Bornholdt and Christof Wetterich. Average action for models with fermions. *Z. Phys.*, C58:585–594, 1993.

[260] M. Salmhofer and C. Honerkamp. Fermionic renormalization group flows: Technique and theory. *Prog. Theor. Phys.*, 105:1–35, 2001.

[261] Manfred Salmhofer. Renormalization in condensed matter: Fermionic systems – from mathematics to materials. *Nucl. Phys.*, B941:868–899, 2019.

[262] M. Reuter and C. Wetterich. Average action for the Higgs model with Abelian gauge symmetry. *Nucl. Phys.*, B391:147–175, 1993.

[263] M. Reuter and C. Wetterich. Running gauge coupling in three-dimensions and the electroweak phase transition. *Nucl. Phys.*, B408:91–132, 1993.

[264] M. Reuter and C. Wetterich. Effective average action for gauge theories and exact evolution equations. *Nucl. Phys.*, B417:181–214, 1994.

[265] Juergen Berges, Nikolaos Tetradis, and Christof Wetterich. Nonperturbative renormalization flow in quantum field theory and statistical physics. *Phys. Rept.*, 363:223–386, 2002.

[266] Jan M. Pawlowski. Aspects of the functional renormalisation group. *Annals Phys.*, 322:2831–2915, 2007.

[267] Holger Gies. Introduction to the functional RG and applications to gauge theories. *Lect. Notes Phys.*, 852:287–348, 2012.

[268] Jan Ambjorn and Jerzy Jurkiewicz. Four-dimensional simplicial quantum gravity. *Phys. Lett.*, B278:42–50, 1992.

[269] P. Bialas, Z. Burda, A. Krzywicki, and B. Petersson. Focusing on the fixed point of 4-D simplicial gravity. *Nucl. Phys.*, B472:293–308, 1996.

[270] Bas V. de Bakker. Further evidence that the transition of 4-D dynamical triangulation is first order. *Phys. Lett.*, B389:238–242, 1996.

[271] J. Laiho and D. Coumbe. Evidence for Asymptotic Safety from Lattice Quantum Gravity. *Phys. Rev. Lett.*, 107:161301, 2011.

[272] Daniel Coumbe and John Laiho. Exploring Euclidean Dynamical Triangulations with a Non-trivial Measure Term. *JHEP*, 04:028, 2015.

[273] J. Laiho, S. Bassler, D. Coumbe, D. Du, and J. T. Neelakanta. Lattice Quantum Gravity and Asymptotic Safety. *Phys. Rev.*, D96(6):064015, 2017.

[274] J. Laiho, S. Bassler, D. Du, J. T. Neelakanta, and D. Coumbe. Recent results in Euclidean dynamical triangulations. *Acta Phys. Polon. Supp.*, 10:317–320, 2017.

[275] Raghav G. Jha, Jack Laiho, and Judah Unmuth-Yockey. Lattice quantum gravity with scalar fields. *PoS*, LATTICE2018:043, 2018.

[276] Simon Catterall, Jack Laiho, and Judah Unmuth-Yockey. Kähler-Dirac fermions on Euclidean dynamical triangulations. *Phys. Rev.*, D98(11):114503, 2018.

[277] Jan Ambjorn, J. Jurkiewicz, and R. Loll. A Nonperturbative Lorentzian path integral for gravity. *Phys. Rev. Lett.*, 85:924–927, 2000.

[278] Jan Ambjorn, J. Jurkiewicz, and R. Loll. Dynamically triangulating Lorentzian quantum gravity. *Nucl. Phys.*, B610:347–382, 2001.

[279] J. Ambjorn, S. Jordan, J. Jurkiewicz, and R. Loll. A Second-order phase transition in CDT. *Phys. Rev. Lett.*, 107:211303, 2011.

[280] J. Ambjorn, D. Coumbe, J. Gizbert-Studnicki, A. Gorlich, and J. Jurkiewicz. New higher-order transition in causal dynamical triangulations. *Phys. Rev.*, D95(12):124029, 2017.

[281] Ezra Newman and Roger Penrose. An Approach to gravitational radiation by a method of spin coefficients. *J. Math. Phys.*, 3:566–578, 1962.

[282] Carlo Rovelli and Lee Smolin. Spin networks and quantum gravity. *Phys. Rev.*, D52:5743–5759, 1995.

[283] John C. Baez. Spin foam models. *Class. Quant. Grav.*, 15:1827–1858, 1998.

[284] Alejandro Perez. Spin foam models for quantum gravity. *Class. Quant. Grav.*, 20:R43, 2003.

[285] Laurent Freidel and Kirill Krasnov. A New Spin Foam Model for 4d Gravity. *Class. Quant. Grav.*, 25:125018, 2008.

[286] Benjamin Bahr and Bianca Dittrich. Improved and Perfect Actions in Discrete Gravity. *Phys. Rev.*, D80:124030, 2009.

[287] Bianca Dittrich. The continuum limit of loop quantum gravity - a framework for solving the theory. In Abhay Ashtekar and Jorge Pullin, editors, *Loop Quantum Gravity: The First 30 Years*, pages 153–179. 2017.

[288] Benjamin Bahr, Bianca Dittrich, and Marc Geiller. A new realization of quantum geometry. 2015.

[289] Thorsten Lang, Klaus Liegener, and Thomas Thiemann. Hamiltonian renormalisation I: derivation from Osterwalder–Schrader reconstruction. *Class. Quant. Grav.*, 35(24):245011, 2018.

[290] Valentin Bonzom and Bianca Dittrich. 3D holography: from discretum to continuum. *JHEP*, 03:208, 2016.

[291] Astrid Eichhorn and Tim Koslowski. Continuum limit in matrix models for quantum gravity from the Functional Renormalization Group. *Phys. Rev.*, D88:084016, 2013.

[292] Astrid Eichhorn and Tim Koslowski. Towards phase transitions between discrete and continuum quantum spacetime from the Renormalization Group. *Phys. Rev.*, D90(10):104039, 2014.

[293] Astrid Eichhorn and Tim Koslowski. Flowing to the continuum in discrete tensor models for quantum gravity. *Ann. Inst. H. Poincare Comb. Phys. Interact.*, 5(2):173–210, 2018.

[294] Astrid Eichhorn, Tim Koslowski, Johannes Lumma, and Antonio D. Pereira. Towards background independent quantum gravity with tensor models. 2018.

[295] Astrid Eichhorn, Tim Koslowski, and Antonio D. Pereira. Status of background-independent coarse-graining in tensor models for quantum gravity. *Universe*, 5(2):53, 2019.

[296] Astrid Eichhorn. Towards coarse graining of discrete Lorentzian quantum gravity. *Class. Quant. Grav.*, 35(4):044001, 2018.

[297] Astrid Eichhorn. Steps towards Lorentzian quantum gravity with causal sets. In *9th International Conference: Spacetime - Matter - Quantum Mechanics: From discrete structures and dynamics to top-down causation (DICE2018) Castiglioncello , Tuscany , Italy, September 17-21, 2018*, 2019.

[298] Stefan Floerchinger. Analytic Continuation of Functional Renormalization Group Equations. *JHEP*, 05:021, 2012.

[299] I. Herbut. *A Modern Approach to Critical Phenomena*. Cambridge University Press, 2007.

[300] B. Pendleton and Graham G. Ross. Mass and Mixing Angle Predictions from Infrared Fixed Points. *Phys. Lett.*, 98B:291–294, 1981.

[301] C. Wetterich. GAUGE HIERARCHY DUE TO STRONG INTERACTIONS? *Phys. Lett.*, 104B:269–276, 1981.

[302] C. Wetterich. THE MASS OF THE HIGGS PARTICLE. In *Search for Scalar Particles: Experimental and Theoretical Aspects Trieste, Italy, July 23-24, 1987*, 1987.

[303] S. Bornholdt and C. Wetterich. Selforganizing criticality, large anomalous mass dimension and the gauge hierarchy problem. *Phys. Lett.*, B282:399–405, 1992.

[304] David J. Gross and Frank Wilczek. Ultraviolet Behavior of Nonabelian Gauge Theories. *Phys. Rev. Lett.*, 30:1343–1346, 1973. [,271(1973)].

[305] Jose M. Martin-Garcia, David Yllanes, and Renato Portugal. The Invar tensor package: Differential invariants of Riemann. *Comput. Phys. Commun.*, 179:586–590, 2008.

[306] Marie E. Machacek and Michael T. Vaughn. Two Loop Renormalization Group Equations in a General Quantum Field Theory. 1. Wave Function Renormalization. *Nucl. Phys.*, B222:83–103, 1983.

[307] Tom Banks and A. Zaks. On the Phase Structure of Vector-Like Gauge Theories with Massless Fermions. *Nucl. Phys.*, B196:189–204, 1982.

[308] Holger Gies. Running coupling in Yang-Mills theory: A flow equation study. *Phys. Rev.*, D66:025006, 2002.

[309] Daniel F. Litim and Francesco Sannino. Asymptotic safety guaranteed. *JHEP*, 12:178, 2014.

[310] Kenneth G. Wilson and Michael E. Fisher. Critical exponents in 3.99 dimensions. *Phys. Rev. Lett.*, 28:240–243, 1972.

[311] David J. Gross and Andre Neveu. Dynamical Symmetry Breaking in Asymptotically Free Field Theories. *Phys. Rev.*, D10:3235, 1974.

[312] Chen-Ning Yang and Robert L. Mills. Conservation of Isotopic Spin and Isotopic Gauge Invariance. *Phys. Rev.*, 96:191–195, 1954. [,150(1954)].

[313] M. F. Sohnius. Introducing Supersymmetry. *Phys. Rept.*, 128:39–204, 1985.

[314] J. Wess and J. Bagger. *Supersymmetry and supergravity.* Princeton University Press, Princeton, NJ, USA, 1992.

[315] Stephen P. Martin. A Supersymmetry primer. pages 1–98, 1997. [Adv. Ser. Direct. High Energy Phys.18,1(1998)].

[316] Holger Gies and Michael M. Scherer. Asymptotic safety of simple Yukawa systems. *Eur. Phys. J.*, C66:387–402, 2010.

[317] Holger Gies, Stefan Rechenberger, and Michael M. Scherer. Towards an Asymptotic-Safety Scenario for Chiral Yukawa Systems. *Eur. Phys. J.*, C66:403–418, 2010.

[318] Gian Paolo Vacca and Luca Zambelli. Multimeson Yukawa interactions at criticality. *Phys. Rev.*, D91(12):125003, 2015.

[319] Andrew D. Bond, Daniel F. Litim, Gustavo Medina Vazquez, and Tom Steudtner. UV conformal window for asymptotic safety. *Phys. Rev.*, D97(3):036019, 2018.

[320] G. Veneziano. U(1) Without Instantons. *Nucl. Phys.*, B159:213–224, 1979.

[321] Andrew D. Bond and Daniel F. Litim. Theorems for Asymptotic Safety of Gauge Theories. *Eur. Phys. J.*, C77(6):429, 2017. [Erratum: Eur. Phys. J.C77,no.8,525(2017)].

[322] Andrew D. Bond and Daniel F. Litim. More asymptotic safety guaranteed. *Phys. Rev.*, D97(8):085008, 2018.

[323] Andrew D. Bond and Daniel F. Litim. Price of Asymptotic Safety. *Phys. Rev. Lett.*, 122(21):211601, 2019.

[324] Daniel F. Litim, Matin Mojaza, and Francesco Sannino. Vacuum stability of asymptotically safe gauge-Yukawa theories. *JHEP*, 01:081, 2016.

[325] Kenneth Intriligator and Francesco Sannino. Supersymmetric asymptotic safety is not guaranteed. *JHEP*, 11:023, 2015.

[326] Andrew D. Bond and Daniel F. Litim. Asymptotic safety guaranteed in supersymmetry. *Phys. Rev. Lett.*, 119(21):211601, 2017.

[327] J. A. Gracey. Large N_f quantum field theory. *Int. J. Mod. Phys.*, A33(35):1830032, 2019.

[328] Jens Braun. Fermion Interactions and Universal Behavior in Strongly Interacting Theories. *J. Phys.*, G39:033001, 2012.

[329] Peter Kopietz, Lorenz Bartosch, and Florian Schütz. Introduction to the functional renormalization group. *Lect. Notes Phys.*, 798:1–380, 2010.

[330] Walter Metzner, Manfred Salmhofer, Carsten Honerkamp, Volker Meden, and Kurt Schonhammer. Functional renormalization group approach to correlated fermion systems. *Rev. Mod. Phys.*, 84:299, 2012.

[331] Robert Percacci. *An Introduction to Covariant Quantum Gravity and Asymptotic Safety*, volume 3 of *100 Years of General Relativity*. World Scientific, 2017.

[332] Martin Reuter and Frank Saueressig. *Quantum Gravity and the Functional Renormalization Group*. Cambridge University Press, 2019.

[333] Martin Reuter and Frank Saueressig. Quantum Einstein Gravity. *New J. Phys.*, 14:055022, 2012.

[334] Astrid Eichhorn. Status of the asymptotic safety paradigm for quantum gravity and matter. *Found. Phys.*, 48(10):1407–1429, 2018.

[335] Elisa Manrique, Stefan Rechenberger, and Frank Saueressig. Asymptotically Safe Lorentzian Gravity. *Phys. Rev. Lett.*, 106:251302, 2011.

[336] Stefan Rechenberger and Frank Saueressig. A functional renormalization group equation for foliated spacetimes. *JHEP*, 03:010, 2013.

[337] Jorn Biemans, Alessia Platania, and Frank Saueressig. Quantum gravity on foliated spacetimes: Asymptotically safe and sound. *Phys. Rev.*, D95(8):086013, 2017.

[338] Jorn Biemans, Alessia Platania, and Frank Saueressig. Renormalization group fixed points of foliated gravity-matter systems. *JHEP*, 05:093, 2017.

[339] Benjamin Knorr. Lorentz symmetry is relevant. *Phys. Lett.*, B792:142–148, 2019.

[340] R. Gastmans, R. Kallosh, and C. Truffin. Quantum Gravity Near Two-Dimensions. *Nucl. Phys.*, B133:417–434, 1978.

[341] S. M. Christensen and M. J. Duff. Quantum Gravity in Two + ϵ Dimensions. *Phys. Lett.*, 79B:213–216, 1978.

[342] Toshiaki Aida and Yoshihisa Kitazawa. Two loop prediction for scaling exponents in (2+epsilon)-dimensional quantum gravity. *Nucl. Phys.*, B491:427–460, 1997.

[343] Pietro Donà, Astrid Eichhorn, and Roberto Percacci. Matter matters in asymptotically safe quantum gravity. *Phys. Rev.*, D89(8):084035, 2014.

[344] Ivan Donkin and Jan M. Pawlowski. The phase diagram of quantum gravity from diffeomorphism-invariant RG-flows. 2012.

[345] Daniel Becker and Martin Reuter. En route to Background Independence: Broken split-symmetry, and how to restore it with bi-metric average actions. *Annals Phys.*, 350:225–301, 2014.

[346] Benjamin Knorr and Stefan Lippoldt. Correlation functions on a curved background. *Phys. Rev.*, D96(6):065020, 2017.

[347] Holger Gies, Benjamin Knorr, and Stefan Lippoldt. Generalized Parametrization Dependence in Quantum Gravity. *Phys. Rev.*, D92(8):084020, 2015.

[348] Nobuyoshi Ohta, Roberto Percacci, and Gian Paolo Vacca. Renormalization Group Equation and scaling solutions for f(R) gravity in exponential parametrization. *Eur. Phys. J.*, C76(2):46, 2016.

[349] Gustavo P. De Brito, Nobuyoshi Ohta, Antonio D. Pereira, Anderson A. Tomaz, and Masatoshi Yamada. Asymptotic safety and field parametrization dependence in the $f(R)$ truncation. *Phys. Rev.*, D98(2):026027, 2018.

[350] M. Reuter and Frank Saueressig. Renormalization group flow of quantum gravity in the Einstein-Hilbert truncation. *Phys. Rev.*, D65:065016, 2002.

[351] Natália Alkofer and Frank Saueressig. Asymptotically safe $f(R)$-gravity coupled to matter I: the polynomial case. *Annals Phys.*, 396:173–201, 2018.

[352] Jan Meibohm, Jan M. Pawlowski, and Manuel Reichert. Asymptotic safety of gravity-matter systems. *Phys. Rev.*, D93(8):084035, 2016.

[353] Peter Labus, Roberto Percacci, and Gian Paolo Vacca. Asymptotic safety in $O(N)$ scalar models coupled to gravity. *Phys. Lett.*, B753:274–281, 2016.

[354] Roberto Percacci and Gian Paolo Vacca. Search of scaling solutions in scalar-tensor gravity. *Eur. Phys. J.*, C75(5):188, 2015.

[355] Pietro Donà, Astrid Eichhorn, Peter Labus, and Roberto Percacci. Asymptotic safety in an interacting system of gravity and scalar matter. *Phys. Rev.*, D93(4):044049, 2016. [Erratum: Phys. Rev.D93,no.12,129904(2016)].

[356] Nicolai Christiansen, Daniel F. Litim, Jan M. Pawlowski, and Manuel Reichert. Asymptotic safety of gravity with matter. *Phys. Rev.*, D97(10):106012, 2018.

[357] Astrid Eichhorn, Stefan Lippoldt, Jan M. Pawlowski, Manuel Reichert, and Marc Schiffer. How perturbative is quantum gravity? *Phys. Lett.*, B792:310–314, 2019.

[358] Giulia Gubitosi, Robin Ooijer, Chris Ripken, and Frank Saueressig. Consistent early and late time cosmology from the RG flow of gravity. *JCAP*, 1812(12):004, 2018.

[359] Paul Joseph Steinhardt. Gravitation and experiment. In *Critical problems in physics. Proceedings, Conference celebrating the 250th Anniversary of Princeton University, Princeton, USA, October 31-November 2, 1996*, 1997.

[360] Alessandro Codello and Roberto Percacci. Fixed points of higher derivative gravity. *Phys. Rev. Lett.*, 97:221301, 2006.

[361] Dario Benedetti, Pedro F. Machado, and Frank Saueressig. Asymptotic safety in higher-derivative gravity. *Mod. Phys. Lett.*, A24:2233–2241, 2009.

[362] Dario Benedetti, Pedro F. Machado, and Frank Saueressig. Taming perturbative divergences in asymptotically safe gravity. *Nucl. Phys.*, B824:168–191, 2010.

[363] Nobuyoshi Ohta and Roberto Percacci. Higher Derivative Gravity and Asymptotic Safety in Diverse Dimensions. *Class. Quant. Grav.*, 31:015024, 2014.

[364] N. Ohta, R. Percacci, and A. D. Pereira. Gauges and functional measures in quantum gravity II: Higher derivative gravity. *Eur. Phys. J.*, C77(9):611, 2017.

[365] Dario Benedetti and Francesco Caravelli. The Local potential approximation in quantum gravity. *JHEP*, 06:017, 2012. [Erratum: JHEP10,157(2012)].

[366] Nobuyoshi Ohta, Roberto Percacci, and Gian Paolo Vacca. Flow equation for $f(R)$ gravity and some of its exact solutions. *Phys. Rev.*, D92(6):061501, 2015.

[367] Kevin Falls, Callum R. King, Daniel F. Litim, Kostas Nikolakopoulos, and Christoph Rahmede. Asymptotic safety of quantum gravity beyond Ricci scalars. *Phys. Rev.*, D97(8):086006, 2018.

[368] K. Falls, D. F. Litim, K. Nikolakopoulos, and C. Rahmede. A bootstrap towards asymptotic safety. 2013.

[369] Kevin Falls, Daniel F. Litim, Konstantinos Nikolakopoulos, and Christoph Rahmede. Further evidence for asymptotic safety of quantum gravity. *Phys. Rev.*, D93(10):104022, 2016.

[370] Kevin G. Falls, Daniel F. Litim, and Jan Schröder. Aspects of asymptotic safety for quantum gravity. *Phys. Rev.*, D99(12):126015, 2019.

[371] Daniel F. Litim. Optimized renormalization group flows. *Phys. Rev.*, D64:105007, 2001.

[372] Juergen A. Dietz and Tim R. Morris. Asymptotic safety in the f(R) approximation. *JHEP*, 01:108, 2013.

[373] Juergen A. Dietz and Tim R. Morris. Redundant operators in the exact renormalisation group and in the f(R) approximation to asymptotic safety. *JHEP*, 07:064, 2013.

[374] I. Hamzaan Bridle, Juergen A. Dietz, and Tim R. Morris. The local potential approximation in the background field formalism. *JHEP*, 03:093, 2014.

[375] Maximilian Demmel, Frank Saueressig, and Omar Zanusso. A proper fixed functional for four-dimensional Quantum Einstein Gravity. *JHEP*, 08:113, 2015.

[376] Sergio Gonzalez-Martin, Tim R. Morris, and Zoë H. Slade. Asymptotic solutions in asymptotic safety. *Phys. Rev.*, D95(10):106010, 2017.

[377] Benjamin Knorr, Chris Ripken, and Frank Saueressig. Form Factors in Asymptotic Safety: conceptual ideas and computational toolbox. 2019.

[378] Hikaru Kawai, Yoshihisa Kitazawa, and Masao Ninomiya. Scaling exponents in quantum gravity near two-dimensions. *Nucl. Phys.*, B393:280–300, 1993.

[379] Jan M. Pawlowski. Geometrical effective action and Wilsonian flows. 2003.

[380] Elisa Manrique and Martin Reuter. Bimetric Truncations for Quantum Einstein Gravity and Asymptotic Safety. *Annals Phys.*, 325:785–815, 2010.

[381] Nicolai Christiansen, Daniel F. Litim, Jan M. Pawlowski, and Andreas Rodigast. Fixed points and infrared completion of quantum gravity. *Phys. Lett.*, B728:114–117, 2014.

[382] Elisa Manrique, Martin Reuter, and Frank Saueressig. Matter Induced Bimetric Actions for Gravity. *Annals Phys.*, 326:440–462, 2011.

[383] Elisa Manrique, Martin Reuter, and Frank Saueressig. Bimetric Renormalization Group Flows in Quantum Einstein Gravity. *Annals Phys.*, 326:463–485, 2011.

[384] Nicolai Christiansen, Benjamin Knorr, Jan M. Pawlowski, and Andreas Rodigast. Global Flows in Quantum Gravity. *Phys. Rev.*, D93(4):044036, 2016.

[385] Nicolai Christiansen, Benjamin Knorr, Jan Meibohm, Jan M. Pawlowski, and Manuel Reichert. Local Quantum Gravity. *Phys. Rev.*, D92(12):121501, 2015.

[386] Tobias Denz, Jan M. Pawlowski, and Manuel Reichert. Towards apparent convergence in asymptotically safe quantum gravity. *Eur. Phys. J.*, C78(4):336, 2018.

[387] M. Reuter and C. Wetterich. Gluon condensation in nonperturbative flow equations. *Phys. Rev.*, D56:7893–7916, 1997.

[388] Daniel F. Litim and Jan M. Pawlowski. Wilsonian flows and background fields. *Phys. Lett.*, B546:279–286, 2002.

[389] Tim R. Morris. Large curvature and background scale independence in single-metric approximations to asymptotic safety. *JHEP*, 11:160, 2016.

[390] Roberto Percacci and Gian Paolo Vacca. The background scale Ward identity in quantum gravity. *Eur. Phys. J.*, C77(1):52, 2017.

[391] Peter Labus, Tim R. Morris, and Zoë H. Slade. Background independence in a background dependent renormalization group. *Phys. Rev.*, D94(2):024007, 2016.

[392] Nobuyoshi Ohta. Background Scale Independence in Quantum Gravity. *PTEP*, 2017(3):033E02, 2017.

[393] Carlos M. Nieto, Roberto Percacci, and Vedran Skrinjar. Split Weyl transformations in quantum gravity. *Phys. Rev.*, D96(10):106019, 2017.

[394] Richard L. Arnowitt, Stanley Deser, and Charles W. Misner. The Dynamics of general relativity. *Gen. Rel. Grav.*, 40:1997–2027, 2008.

[395] Alessio Baldazzi, Roberto Percacci, and Vedran Skrinjar. Quantum fields without Wick rotation. *Symmetry*, 11(3):373, 2019.

[396] Mathias Butenschoen, Bahman Dehnadi, Andre H. Hoang, Vicent Mateu, Moritz Preisser, and Iain W. Stewart. Top Quark Mass Calibration for Monte Carlo Event Generators. *Phys. Rev. Lett.*, 117(23):232001, 2016.

[397] S. Alekhin, J. Blümlein, S. Moch, and R. Placakyte. Parton distribution functions, α_s, and heavy-quark masses for LHC Run II. *Phys. Rev.*, D96(1):014011, 2017.

[398] M. Tanabashi et al. Review of Particle Physics. *Phys. Rev.*, D98(3):030001, 2018.

[399] A. Abada et al. HE-LHC: The High-Energy Large Hadron Collider. *Eur. Phys. J. ST*, 228(5):1109–1382, 2019.

[400] P. Azzi et al. Standard Model Physics at the HL-LHC and HE-LHC. 2019.

[401] J. de Blas et al. The CLIC Potential for New Physics. 2018.

[402] A. Abada et al. FCC Physics Opportunities. *Eur. Phys. J.*, C79(6):474, 2019.

[403] Holger Gies, Clemens Gneiting, and René Sondenheimer. Higgs Mass Bounds from Renormalization Flow for a simple Yukawa model. *Phys. Rev.*, D89(4):045012, 2014.

[404] Holger Gies and René Sondenheimer. Higgs Mass Bounds from Renormalization Flow for a Higgs-top-bottom model. *Eur. Phys. J.*, C75(2):68, 2015.

[405] Astrid Eichhorn, Holger Gies, Joerg Jaeckel, Tilman Plehn, Michael M. Scherer, and René Sondenheimer. The Higgs Mass and the Scale of New Physics. *JHEP*, 04:022, 2015.

[406] Holger Gies, René Sondenheimer, and Matthias Warschinke. Impact of generalized Yukawa interactions on the lower Higgs mass bound. *Eur. Phys. J.*, C77(11):743, 2017.

[407] Manuel Reichert, Astrid Eichhorn, Holger Gies, Jan M. Pawlowski, Tilman Plehn, and Michael M. Scherer. Probing baryogenesis through the Higgs boson self-coupling. *Phys. Rev.*, D97(7):075008, 2018.

[408] René Sondenheimer. Nonpolynomial Higgs interactions and vacuum stability. *Eur. Phys. J.*, C79(1):10, 2019.

[409] J. R. Espinosa, D. Racco, and A. Riotto. Cosmological Signature of the Standard Model Higgs Vacuum Instability: Primordial Black Holes as Dark Matter. *Phys. Rev. Lett.*, 120(12):121301, 2018.

[410] Sally Dawson, Christoph Englert, and Tilman Plehn. Higgs Physics: It ain't over till it's over. *Phys. Rept.*, 816:1–85, 2019.

[411] Vanda Silveira and A. Zee. SCALAR PHANTOMS. *Phys. Lett.*, 161B:136–140, 1985.

[412] John McDonald. Gauge singlet scalars as cold dark matter. *Phys. Rev.*, D50:3637–3649, 1994.

[413] C. P. Burgess, Maxim Pospelov, and Tonnis ter Veldhuis. The Minimal model of nonbaryonic dark matter: A Singlet scalar. *Nucl. Phys.*, B619:709–728, 2001.

[414] Brian Patt and Frank Wilczek. Higgs-field portal into hidden sectors. 2006.

[415] Vernon Barger, Paul Langacker, Mathew McCaskey, Michael J. Ramsey-Musolf, and Gabe Shaughnessy. LHC Phenomenology of an Extended Standard Model with a Real Scalar Singlet. *Phys. Rev.*, D77:035005, 2008.

[416] Christoph Englert, Tilman Plehn, Dirk Zerwas, and Peter M. Zerwas. Exploring the Higgs portal. *Phys. Lett.*, B703:298–305, 2011.

[417] Astrid Eichhorn and Michael M. Scherer. Planck scale, Higgs mass, and scalar dark matter. *Phys. Rev.*, D90(2):025023, 2014.

[418] Emidio Gabrielli, Matti Heikinheimo, Kristjan Kannike, Antonio Racioppi, Martti Raidal, and Christian Spethmann. Towards Completing the Standard Model: Vacuum Stability, EWSB and Dark Matter. *Phys. Rev.*, D89(1):015017, 2014.

[419] A. V. Bednyakov, B. A. Kniehl, A. F. Pikelner, and O. L. Veretin. Stability of the Electroweak Vacuum: Gauge Independence and Advanced Precision. *Phys. Rev. Lett.*, 115(20):201802, 2015.

[420] Giuseppe Iacobellis and Isabella Masina. Stationary configurations of the Standard Model Higgs potential: electroweak stability and rising inflection point. *Phys. Rev.*, D94(7):073005, 2016.

[421] M. C. Bento, O. Bertolami, R. Rosenfeld, and L. Teodoro. Selfinteracting dark matter and invisibly decaying Higgs. *Phys. Rev.*, D62:041302, 2000.

[422] M. C. Bento, O. Bertolami, and R. Rosenfeld. Cosmological constraints on an invisibly decaying Higgs boson. *Phys. Lett.*, B518:276–281, 2001.

[423] John McDonald. Thermally generated gauge singlet scalars as selfinteracting dark matter. *Phys. Rev. Lett.*, 88:091304, 2002.

[424] Vernon Barger, Paul Langacker, Mathew McCaskey, Michael Ramsey-Musolf, and Gabe Shaughnessy. Complex Singlet Extension of the Standard Model. *Phys. Rev.*, D79:015018, 2009.

[425] K. Holland and J. Kuti. How light can the Higgs be? *Nucl. Phys. Proc. Suppl.*, 129:765–767, 2004. [,765(2003)].

[426] Vincenzo Branchina and Hugo Faivre. Effective potential (in)stability and lower bounds on the scalar (Higgs) mass. *Phys. Rev.*, D72:065017, 2005.

[427] Zoltan Fodor, Kieran Holland, Julius Kuti, Daniel Nogradi, and Chris Schroeder. New Higgs physics from the lattice. *PoS*, LATTICE2007:056, 2007.

[428] Vincenzo Branchina, Hugo Faivre, and Vincent Pangon. Effective potential and vacuum stability. *J. Phys.*, G36:015006, 2009.

[429] Julia Borchardt, Holger Gies, and René Sondenheimer. Global flow of the Higgs potential in a Yukawa model. *Eur. Phys. J.*, C76(8):472, 2016.

[430] Ankit Beniwal, Filip Rajec, Christopher Savage, Pat Scott, Christoph Weniger, Martin White, and Anthony G. Williams. Combined analysis of effective Higgs portal dark matter models. *Phys. Rev.*, D93(11):115016, 2016.

[431] Andrew D. Bond, Gudrun Hiller, Kamila Kowalska, and Daniel F. Litim. Directions for model building from asymptotic safety. *JHEP*, 08:004, 2017.

[432] Gudrun Hiller, Clara Hormigos-Feliu, Daniel F. Litim, and Tom Steudtner. Asymptotically safe extensions of the Standard Model with flavour phenomenology. In *54th Rencontres de Moriond on Electroweak Interactions and Unified Theories (Moriond EW 2019) La Thuile, Italy, March 16-23, 2019*, 2019.

[433] Borut Bajc and Francesco Sannino. Asymptotically Safe Grand Unification. *JHEP*, 12:141, 2016.

[434] Robert Mann, Julia Meffe, Francesco Sannino, Tom Steele, Zhi-Wei Wang, and Chen Zhang. Asymptotically Safe Standard Model via Vectorlike Fermions. *Phys. Rev. Lett.*, 119(26):261802, 2017.

[435] Oleg Antipin and Francesco Sannino. Conformal Window 2.0: The large N_f safe story. *Phys. Rev.*, D97(11):116007, 2018.

[436] Giulio Maria Pelaggi, Alexis D. Plascencia, Alberto Salvio, Francesco Sannino, Juri Smirnov, and Alessandro Strumia. Asymptotically Safe Standard Model Extensions? *Phys. Rev.*, D97(9):095013, 2018.

[437] E. Molinaro, F. Sannino, and Z. W. Wang. Asymptotically safe Pati-Salam theory. *Phys. Rev.*, D98(11):115007, 2018.

[438] Giacomo Cacciapaglia, Shahram Vatani, Teng Ma, and Yongcheng Wu. Towards a fundamental safe theory of composite Higgs and Dark Matter. 2018.

[439] Francesco Sannino, J. Smirnov, and Zhi-Wei Wang. Safe Clockwork. 2019.

[440] Chengfeng Cai and Hong-Hao Zhang. Minimal asymptotically safe dark matter. 2019.

[441] Tommi Alanne, Simone Blasi, and Nicola Andrea Dondi. A critical look at β-function singularities at large N. 2019.

[442] Thomas A. Ryttov and Kimmo Tuominen. Safe Glueballs and Baryons. *JHEP*, 04:173, 2019.

[443] Francesco Sannino and Zhi-Wei Wang. Comment on "A critical look at β-function singularities at large N" by Alanne, Blasi and Dondi. 2019.

[444] Astrid Eichhorn. An asymptotically safe guide to quantum gravity and matter. *Front. Astron. Space Sci.*, 5:47, 2019.

[445] Daniele Barducci, Marco Fabbrichesi, Carlos M. Nieto, Roberto Percacci, and Vedran Skrinjar. In search of a UV completion of the standard model — 378,000 models that don't work. *JHEP*, 11:057, 2018.

[446] Mohamed M. Anber, John F. Donoghue, and Mohamed El-Houssieny. Running couplings and operator mixing in the gravitational corrections to coupling constants. *Phys. Rev.*, D83:124003, 2011.

[447] Astrid Eichhorn and Holger Gies. Light fermions in quantum gravity. *New J. Phys.*, 13:125012, 2011.

[448] Astrid Eichhorn. Quantum-gravity-induced matter self-interactions in the asymptotic-safety scenario. *Phys. Rev.*, D86:105021, 2012.

[449] Astrid Eichhorn, Aaron Held, and Jan M. Pawlowski. Quantum-gravity effects on a Higgs-Yukawa model. *Phys. Rev.*, D94(10):104027, 2016.

[450] Nicolai Christiansen and Astrid Eichhorn. An asymptotically safe solution to the U(1) triviality problem. *Phys. Lett.*, B770:154–160, 2017.

[451] Astrid Eichhorn, Stefan Lippoldt, and Vedran Skrinjar. Nonminimal hints for asymptotic safety. *Phys. Rev.*, D97(2):026002, 2018.

[452] Astrid Eichhorn, Stefan Lippoldt, and Marc Schiffer. Zooming in on fermions and quantum gravity. *Phys. Rev.*, D99(8):086002, 2019.

[453] Astrid Eichhorn and Marc Schiffer. $d = 4$ as the critical dimensionality of asymptotically safe interactions. *Phys. Lett.*, B793:383–389, 2019.

[454] Stephen L. Adler. A Formula for the Induced Gravitational Constant. *Phys. Lett.*, 95B:241, 1980. [,536(1980)].

[455] A. Zee. Spontaneously Generated Gravity. *Phys. Rev.*, D23:858, 1981.

[456] A. Zee. Calculating Newton's Gravitational Constant in Infrared Stable Yang-Mills Theories. *Phys. Rev. Lett.*, 48:295, 1982.

[457] Stephen L. Adler. Einstein Gravity as a Symmetry-Breaking Effect in Quantum Field Theory. *Rev. Mod. Phys.*, 54:729, 1982. [,539(1982)].

[458] John F. Donoghue and Gabriel Menezes. Gauge Assisted Quadratic Gravity: A Framework for UV Complete Quantum Gravity. *Phys. Rev.*, D97(12):126005, 2018.

[459] Holger Gies and Christof Wetterich. Renormalization flow of bound states. *Phys. Rev.*, D65:065001, 2002.

[460] Holger Gies. Renormalizability of gauge theories in extra dimensions. *Phys. Rev.*, D68:085015, 2003.

[461] Tim R. Morris. Renormalizable extra-dimensional models. *JHEP*, 01:002, 2005.

[462] Michael Creutz. Confinement and the Critical Dimensionality of Space-Time. *Phys. Rev. Lett.*, 43:553–556, 1979. [Erratum: Phys. Rev. Lett.43,890(1979)].

[463] Shinji Ejiri, Jisuke Kubo, and Michika Murata. A Study on the nonperturbative existence of Yang-Mills theories with large extra dimensions. *Phys. Rev.*, D62:105025, 2000.

[464] Francesco Knechtli and Enrico Rinaldi. Extra-dimensional models on the lattice. *Int. J. Mod. Phys.*, A31(22):1643002, 2016.

[465] P. Donà, Astrid Eichhorn, and Roberto Percacci. Consistency of matter models with asymptotically safe quantum gravity. *Can. J. Phys.*, 93(9):988–994, 2015.

[466] Yves Decanini and Antoine Folacci. FKWC-bases and geometrical identities for classical and quantum field theories in curved spacetime. 2008.

[467] James W. York, Jr. Conformatlly invariant orthogonal decomposition of symmetric tensors on Riemannian manifolds and the initial value problem of general relativity. *J. Math. Phys.*, 14:456–464, 1973.

[468] Ulrich Ellwanger, Manfred Hirsch, and Axel Weber. Flow equations for the relevant part of the pure Yang-Mills action. *Z. Phys.*, C69:687–698, 1996.

[469] Daniel F. Litim and Jan M. Pawlowski. Flow equations for Yang-Mills theories in general axial gauges. *Phys. Lett.*, B435:181–188, 1998.

[470] Astrid Eichhorn and Holger Gies. Ghost anomalous dimension in asymptotically safe quantum gravity. *Phys. Rev.*, D81:104010, 2010.

[471] Astrid Eichhorn, Peter Labus, Jan M. Pawlowski, and Manuel Reichert. Effective universality in quantum gravity. *SciPost Phys.*, 5(4):031, 2018.

[472] Jan Meibohm and Jan M. Pawlowski. Chiral fermions in asymptotically safe quantum gravity. *Eur. Phys. J.*, C76(5):285, 2016.

[473] Astrid Eichhorn. Faddeev-Popov ghosts in quantum gravity beyond perturbation theory. *Phys. Rev.*, D87(12):124016, 2013.

[474] Gustavo P. De Brito, Astrid Eichhorn, and Antonio D. Pereira. A link that matters: Towards phenomenological tests of unimodular asymptotic safety. 2019.

[475] Astrid Eichhorn. On unimodular quantum gravity. *Class. Quant. Grav.*, 30:115016, 2013.

[476] Astrid Eichhorn. The Renormalization Group flow of unimodular f(R) gravity. *JHEP*, 04:096, 2015.

[477] Dario Benedetti. Essential nature of Newton's constant in unimodular gravity. *Gen. Rel. Grav.*, 48(5):68, 2016.

[478] Holger Gies, Joerg Jaeckel, and Christof Wetterich. Towards a renormalizable standard model without fundamental Higgs scalar. *Phys. Rev.*, D69:105008, 2004.

[479] Holger Gies and Joerg Jaeckel. Chiral phase structure of QCD with many flavors. *Eur. Phys. J.*, C46:433–438, 2006.

[480] Jens Braun and Holger Gies. Chiral phase boundary of QCD at finite temperature. *JHEP*, 06:024, 2006.

[481] Gaurav Narain and Roberto Percacci. Renormalization Group Flow in Scalar-Tensor Theories. I. *Class. Quant. Grav.*, 27:075001, 2010.

[482] Astrid Eichhorn and Stefan Lippoldt. Quantum gravity and Standard-Model-like fermions. *Phys. Lett.*, B767:142–146, 2017.

[483] Sean P. Robinson and Frank Wilczek. Gravitational correction to running of gauge couplings. *Phys. Rev. Lett.*, 96:231601, 2006.

[484] Artur R. Pietrykowski. Gauge dependence of gravitational correction to running of gauge couplings. *Phys. Rev. Lett.*, 98:061801, 2007.

[485] David J. Toms. Quantum gravity and charge renormalization. *Phys. Rev.*, D76:045015, 2007.

[486] Dietmar Ebert, Jan Plefka, and Andreas Rodigast. Absence of gravitational contributions to the running Yang-Mills coupling. *Phys. Lett.*, B660:579–582, 2008.

[487] Yong Tang and Yue-Liang Wu. Gravitational Contributions to the Running of Gauge Couplings. *Commun. Theor. Phys.*, 54:1040–1044, 2010.

[488] David J. Toms. Cosmological constant and quantum gravitational corrections to the running fine structure constant. *Phys. Rev. Lett.*, 101:131301, 2008.

[489] David J. Toms. Quantum gravity, gauge coupling constants, and the cosmological constant. *Phys. Rev.*, D80:064040, 2009.

[490] Hong-Jian He, Xu-Feng Wang, and Zhong-Zhi Xianyu. Gauge-Invariant Quantum Gravity Corrections to Gauge Couplings via Vilkovisky-DeWitt Method and Gravity Assisted Gauge Unification. *Phys. Rev.*, D83:125014, 2011.

[491] David J. Toms. Quantum gravitational contributions to quantum electrodynamics. *Nature*, 468:56–59, 2010.

[492] Mohamed M. Anber and John F. Donoghue. On the running of the gravitational constant. *Phys. Rev.*, D85:104016, 2012.

[493] John Ellis and Nick E. Mavromatos. On the Interpretation of Gravitational Corrections to Gauge Couplings. *Phys. Lett.*, B711:139–142, 2012.

[494] J. C. C. Felipe, L. C. T. Brito, Marcos Sampaio, and M. C. Nemes. Quantum gravitational contributions to the beta function of quantum electrodynamics. *Phys. Lett.*, B700:86–89, 2011.

[495] David J. Toms. Quadratic divergences and quantum gravitational contributions to gauge coupling constants. *Phys. Rev.*, D84:084016, 2011.

[496] Jan-Eric Daum, Ulrich Harst, and Martin Reuter. Running Gauge Coupling in Asymptotically Safe Quantum Gravity. *JHEP*, 01:084, 2010.

[497] J. E. Daum, U. Harst, and M. Reuter. Non-perturbative QEG Corrections to the Yang-Mills Beta Function. *Gen. Relativ. Gravit.*, 2010. [Gen. Rel. Grav.43,2393(2011)].

[498] Sarah Folkerts, Daniel F. Litim, and Jan M. Pawlowski. Asymptotic freedom of Yang-Mills theory with gravity. *Phys. Lett.*, B709:234–241, 2012.

[499] U. Harst and M. Reuter. QED coupled to QEG. *JHEP*, 05:119, 2011.

[500] Astrid Eichhorn and Fleur Versteegen. Upper bound on the Abelian gauge coupling from asymptotic safety. *JHEP*, 01:030, 2018.

[501] O. Zanusso, L. Zambelli, G. P. Vacca, and R. Percacci. Gravitational corrections to Yukawa systems. *Phys. Lett.*, B689:90–94, 2010.

[502] Kin-ya Oda and Masatoshi Yamada. Non-minimal coupling in Higgs–Yukawa model with asymptotically safe gravity. *Class. Quant. Grav.*, 33(12):125011, 2016.

[503] Yuta Hamada and Masatoshi Yamada. Asymptotic safety of higher derivative quantum gravity non-minimally coupled with a matter system. *JHEP*, 08:070, 2017.

[504] Astrid Eichhorn, Yuta Hamada, Johannes Lumma, and Masatoshi Yamada. Quantum gravity fluctuations flatten the Planck-scale Higgs potential. *Phys. Rev.*, D97(8):086004, 2018.

[505] Jan M. Pawlowski, Manuel Reichert, Christof Wetterich, and Masatoshi Yamada. Higgs scalar potential in asymptotically safe quantum gravity. *Phys. Rev.*, D99(8):086010, 2019.

[506] Christof Wetterich and Masatoshi Yamada. Variable Planck mass from gauge invariant flow equation. 2019.

[507] Ralf Hempfling and Bernd A. Kniehl. On the relation between the fermion pole mass and MS Yukawa coupling in the standard model. *Phys. Rev.*, D51:1386–1394, 1995.

[508] Ulrich Ellwanger. Flow equations and BRS invariance for Yang-Mills theories. *Phys. Lett.*, B335:364–370, 1994.

[509] Tim R. Morris. Noncompact pure gauge QED in 3-D is free. *Phys. Lett.*, B357:225–231, 1995.

[510] Tim R. Morris. A Gauge invariant exact renormalization group. 1. *Nucl. Phys.*, B573:97–126, 2000.

[511] Yuji Igarashi, Katsumi Itoh, and Hiroto So. Exact symmetries realized on the renormalization group flow. *Phys. Lett.*, B479:336–342, 2000.

[512] Tim R. Morris and Oliver J. Rosten. Manifestly gauge invariant QCD. *J. Phys.*, A39:11657–11681, 2006.

[513] Kevin Falls and Tim R. Morris. Conformal anomaly from gauge fields without gauge fixing. *Phys. Rev.*, D97(6):065013, 2018.

[514] C. Wetterich. Gauge invariant flow equation. *Nucl. Phys.*, B931:262–282, 2018.

[515] Shimasadat Asnafi, Holger Gies, and Luca Zambelli. BRST invariant RG flows. *Phys. Rev.*, D99(8):085009, 2019.

[516] Joseph J. Atick and Edward Witten. The Hagedorn Transition and the Number of Degrees of Freedom of String Theory. *Nucl. Phys.*, B310:291–334, 1988.

[517] J. Ambjorn, J. Jurkiewicz, and R. Loll. Spectral dimension of the universe. *Phys. Rev. Lett.*, 95:171301, 2005.

[518] Leonardo Modesto. Fractal Structure of Loop Quantum Gravity. *Class. Quant. Grav.*, 26:242002, 2009.

[519] Steven Carlip. Spontaneous Dimensional Reduction in Short-Distance Quantum Gravity? *AIP Conf. Proc.*, 1196(1):72, 2009.

[520] Astrid Eichhorn and Sebastian Mizera. Spectral dimension in causal set quantum gravity. *Class. Quant. Grav.*, 31:125007, 2014.

[521] S. Carlip. Dimensional reduction in causal set gravity. *Class. Quant. Grav.*, 32(23):232001, 2015.

[522] O. Lauscher and M. Reuter. Fractal spacetime structure in asymptotically safe gravity. *JHEP*, 10:050, 2005.

[523] Martin Reuter and Frank Saueressig. Fractal space-times under the microscope: A Renormalization Group view on Monte Carlo data. *JHEP*, 12:012, 2011.

[524] Gianluca Calcagni, Astrid Eichhorn, and Frank Saueressig. Probing the quantum nature of spacetime by diffusion. *Phys. Rev.*, D87(12):124028, 2013.

[525] S. Carlip. Dimension and Dimensional Reduction in Quantum Gravity. *Universe*, 5:83, 2019.

[526] Marie E. Machacek and Michael T. Vaughn. Two Loop Renormalization Group Equations in a General Quantum Field Theory. 2. Yukawa Couplings. *Nucl. Phys.*, B236:221–232, 1984.

[527] C. Patrignani et al. Review of Particle Physics. *Chin. Phys.*, C40(10):100001, 2016.

[528] Gustavo P. De Brito, Yuta Hamada, Antonio D. Pereira, and Masatoshi Yamada. On the impact of Majorana masses in gravity-matter systems. 2019.

[529] T. P. Cheng, E. Eichten, and Ling-Fong Li. Higgs Phenomena in Asymptotically Free Gauge Theories. *Phys. Rev.*, D9:2259, 1974.

[530] K. Sasaki. Renormalization Group Equations for the Kobayashi-Maskawa Matrix. *Z. Phys.*, C32:149–152, 1986.

[531] K. S. Babu. Renormalization Group Analysis of the Kobayashi-Maskawa Matrix. *Z. Phys.*, C35:69, 1987.

[532] Vernon D. Barger, M. S. Berger, and P. Ohmann. Universal evolution of CKM matrix elements. *Phys. Rev.*, D47:2038–2045, 1993.

[533] P. Kielanowski, S. Rebeca Juarez Wysozka, and J. H. Montes de Oca Y. Renormalization Group Equations for the CKM matrix. *Phys. Rev.*, D78:116010, 2008.

[534] P. F. Harrison, R. Krishnan, and W. G. Scott. Exact One-Loop Evolution Invariants in the Standard Model. *Phys. Rev.*, D82:096004, 2010.

[535] Thorsten Feldmann, Thomas Mannel, and Steffen Schwertfeger. Renormalization Group Evolution of Flavour Invariants. *JHEP*, 10:007, 2015.

[536] S. Rebeca Juárez W., Piotr Kielanowski, Gerardo Mora, and Arno Bohm. Renormalization group: new relations between the parameters of the Standard Model. *Phys. Lett.*, B772:294–299, 2017.

[537] Jogesh C. Pati and Abdus Salam. Lepton Number as the Fourth Color. *Phys. Rev.*, D10:275–289, 1974. [Erratum: Phys. Rev.D11,703(1975)].

[538] H. Georgi. LIE ALGEBRAS IN PARTICLE PHYSICS. FROM ISOSPIN TO UNIFIED THEORIES. *Front. Phys.*, 54:1–255, 1982.

[539] R. Slansky. Group Theory for Unified Model Building. *Phys. Rept.*, 79:1–128, 1981.

[540] John M. Gipson and R. E. Marshak. Intermediate Mass Scales in the New SO(10) Grand Unification in the One Loop Approximation. *Phys. Rev.*, D31:1705, 1985.

[541] D. Chang, R. N. Mohapatra, J. Gipson, R. E. Marshak, and M. K. Parida. Experimental Tests of New SO(10) Grand Unification. *Phys. Rev.*, D31:1718, 1985.

[542] N. G. Deshpande, E. Keith, and Palash B. Pal. Implications of LEP results for SO(10) grand unification. *Phys. Rev.*, D46:2261–2264, 1993.

[543] N. G. Deshpande, E. Keith, and Palash B. Pal. Implications of LEP results for SO(10) grand unification with two intermediate stages. *Phys. Rev.*, D47:2892–2896, 1993.

[544] Stefano Bertolini, Luca Di Luzio, and Michal Malinsky. Intermediate mass scales in the non-supersymmetric SO(10) grand unification: A Reappraisal. *Phys. Rev.*, D80:015013, 2009.

[545] Jeffrey A. Harvey, D. B. Reiss, and Pierre Ramond. Mass Relations and Neutrino Oscillations in an SO(10) Model. *Nucl. Phys.*, B199:223–268, 1982.

[546] K. S. Babu and R. N. Mohapatra. Predictive neutrino spectrum in minimal SO(10) grand unification. *Phys. Rev. Lett.*, 70:2845–2848, 1993.

[547] K. Matsuda, Y. Koide, and T. Fukuyama. Can the SO(10) model with two Higgs doublets reproduce the observed fermion masses? *Phys. Rev.*, D64:053015, 2001.

[548] K. Matsuda, Y. Koide, T. Fukuyama, and H. Nishiura. How far can the SO(10) two Higgs model describe the observed neutrino masses and mixings? *Phys. Rev.*, D65:033008, 2002. [Erratum: Phys. Rev.D65,079904(2002)].

[549] Borut Bajc, Alejandra Melfo, Goran Senjanovic, and Francesco Vissani. Yukawa sector in non-supersymmetric renormalizable SO(10). *Phys. Rev.*, D73:055001, 2006.

[550] Stefano Bertolini, Luca Di Luzio, and Michal Malinsky. On the vacuum of the minimal nonsupersymmetric SO(10) unification. *Phys. Rev.*, D81:035015, 2010.

[551] Guido Altarelli and Gianluca Blankenburg. Different $SO(10)$ Paths to Fermion Masses and Mixings. *JHEP*, 03:133, 2011.

[552] Stefano Bertolini, Luca Di Luzio, and Michal Malinsky. Seesaw Scale in the Minimal Renormalizable SO(10) Grand Unification. *Phys. Rev.*, D85:095014, 2012.

[553] K. S. Babu and S. Khan. Minimal nonsupersymmetric $SO(10)$ model: Gauge coupling unification, proton decay, and fermion masses. *Phys. Rev.*, D92(7):075018, 2015.

[554] K. S. Babu, Borut Bajc, and Shaikh Saad. Yukawa Sector of Minimal SO(10) Unification. *JHEP*, 02:136, 2017.

[555] Takeshi Fukuyama and Nobuchika Okada. Alternative renormalizable minimal SO(10) GUT and Seesaw Scale. *Mod. Phys. Lett.*, A33(29):1850167, 2018.

[556] Tommy Ohlsson and Marcus Pernow. Running of Fermion Observables in Non-Supersymmetric SO(10) Models. *JHEP*, 11:028, 2018.

[557] Jakob Schwichtenberg. Gauge Coupling Unification without Supersymmetry. *Eur. Phys. J.*, C79(4):351, 2019.

[558] Tommy Ohlsson and Marcus Pernow. Fits to Non-Supersymmetric SO(10) Models with Type I and II Seesaw Mechanisms Using Renormalization Group Evolution. *JHEP*, 06:085, 2019.

[559] Borut Bajc, Goran Senjanovic, and Francesco Vissani. b - tau unification and large atmospheric mixing: A Case for noncanonical seesaw. *Phys. Rev. Lett.*, 90:051802, 2003.

[560] Takeshi Fukuyama and Nobuchika Okada. Neutrino oscillation data versus minimal supersymmetric SO(10) model. *JHEP*, 11:011, 2002.

[561] H. S. Goh, R. N. Mohapatra, and Siew-Phang Ng. Minimal SUSY SO(10), b tau unification and large neutrino mixings. *Phys. Lett.*, B570:215–221, 2003.

[562] H. S. Goh, R. N. Mohapatra, and Siew-Phang Ng. Minimal SUSY SO(10) model and predictions for neutrino mixings and leptonic CP violation. *Phys. Rev.*, D68:115008, 2003.

[563] Stefano Bertolini, Michele Frigerio, and Michal Malinsky. Fermion masses in SUSY SO(10) with type II seesaw: A Non-minimal predictive scenario. *Phys. Rev.*, D70:095002, 2004.

[564] K. S. Babu and Cosmin Macesanu. Neutrino masses and mixings in a minimal SO(10) model. *Phys. Rev.*, D72:115003, 2005.

[565] Stefano Bertolini, Thomas Schwetz, and Michal Malinsky. Fermion masses and mixings in SO(10) models and the neutrino challenge to SUSY GUTs. *Phys. Rev.*, D73:115012, 2006.

[566] Anjan S. Joshipura and Ketan M. Patel. Fermion Masses in SO(10) Models. *Phys. Rev.*, D83:095002, 2011.

[567] Guido Altarelli and Davide Meloni. A non supersymmetric SO(10) grand unified model for all the physics below M_{GUT}. *JHEP*, 08:021, 2013.

[568] Alexander Dueck and Werner Rodejohann. Fits to SO(10) Grand Unified Models. *JHEP*, 09:024, 2013.

[569] Borut Bajc, Ilja Dorsner, and Miha Nemevsek. Minimal SO(10) splits supersymmetry. *JHEP*, 11:007, 2008.

[570] K. S. Babu, Borut Bajc, and Shaikh Saad. Resurrecting Minimal Yukawa Sector of SUSY SO(10). *JHEP*, 10:135, 2018.

[571] H. Georgi and S. L. Glashow. Unity of All Elementary Particle Forces. *Phys. Rev. Lett.*, 32:438–441, 1974.

[572] Harald Fritzsch and Peter Minkowski. Unified Interactions of Leptons and Hadrons. *Annals Phys.*, 93:193–266, 1975.

[573] Naoki Yamatsu. Finite-Dimensional Lie Algebras and Their Representations for Unified Model Building. 2015.

[574] Howard Georgi and Sheldon L. Glashow. Gauge theories without anomalies. *Phys. Rev.*, D6:429, 1972.

[575] L. Michel. MINIMA OF HIGGS-LANDAU POLYNOMIALS. In *Colloquium on Fundamental Interactions, in honor of A. Visconti Marseille, France, July 5-6, 1979*, page 157, 1979.

[576] L. Michel and L. A. Radicati. Properties of the breaking of hadronic internal symmetry. *Annals Phys.*, 66:758–783, 1971.

[577] L. Michel. SYMMETRY DEFECTS AND BROKEN SYMMETRY. CONFIGURATIONS - HIDDEN SYMMETRY. *Rev. Mod. Phys.*, 52:617–651, 1980. [,316(1980)].

[578] Ling-Fong Li. Group Theory of the Spontaneously Broken Gauge Symmetries. *Phys. Rev.*, D9:1723–1739, 1974.

[579] H. Ruegg. Extremas of SU(N) Higgs Potentials and Symmetry Breaking Pattern. *Phys. Rev.*, D22:2040, 1980.

[580] F. Buccella, H. Ruegg, and Carlos A. Savoy. Spontaneous Symmetry Breaking of SU(n). *Nucl. Phys.*, B169:68–76, 1980.

[581] F. Buccella, H. Ruegg, and Carlos A. Savoy. Spontaneous Symmetry Breaking in O(10). *Phys. Lett.*, 94B:491–494, 1980.

[582] F. Buccella, H. Ruegg, and Carlos A. Savoy. Symmetry Breaking Patterns for Unitary and Orthogonal Groups. In *First Workshop on Grand Unification Durham, New Hampshire, April 10-12, 1980*, pages 23–32, 1980.

[583] Masaki Yasue. HOW TO BREAK SO(10) VIA SO(4) x SO(6) DOWN TO SU(2)(L) x SU(3)(C) x U(1). *Phys. Lett.*, 103B:33–38, 1981.

[584] Masaki Yasue. Symmetry Breaking of SO(10) and Constraints on Higgs Potential. 1. Adjoint (45) and Spinorial (16). *Phys. Rev.*, D24:1005, 1981.

[585] George Lazarides, M. Magg, and Q. Shafi. Phase Transitions and Magnetic Monopoles in SO(10). *Phys. Lett.*, 97B:87–92, 1980.

[586] Dan-di Wu. The Symmetry Breaking Pattern of Scalars in Low Dimension Representations. *Nucl. Phys.*, B199:523, 1982. [Erratum: Nucl. Phys.B213,545(1983)].

[587] F. Buccella, L. Cocco, and C. Wetterich. An SO(10) Model With 54 + 126 + 10 Higgs. *Nucl. Phys.*, B243:273–284, 1984.

[588] K. S. Babu and Ernest Ma. Symmetry Breaking in SO(10): Higgs Boson Structure. *Phys. Rev.*, D31:2316, 1985.

[589] M. Abud, F. Buccella, A. Della Selva, A. Sciarrino, R. Fiore, and G. Immirzi. Stability of Spontaneous Symmetry Breaking in SO(10). *Nucl. Phys.*, B263:336–346, 1986.

[590] H. Nishino et al. Search for Proton Decay via $p \to e^+ \pi_0$ and $p \to \mu^+ \pi_0$ in a Large Water Cherenkov Detector. *Phys. Rev. Lett.*, 102:141801, 2009.

[591] Ugo Amaldi, Wim de Boer, and Hermann Furstenau. Comparison of grand unified theories with electroweak and strong coupling constants measured at LEP. *Phys. Lett.*, B260:447–455, 1991.

[592] Paul Langacker and Ming-xing Luo. Implications of precision electroweak experiments for M_t, ρ_0, $\sin^2\theta_W$ and grand unification. *Phys. Rev.*, D44:817–822, 1991.

[593] Hitoshi Murayama and Aaron Pierce. Not even decoupling can save minimal supersymmetric SU(5). *Phys. Rev.*, D65:055009, 2002.

[594] Frank Wilczek and A. Zee. Families from Spinors. *Phys. Rev.*, D25:553, 1982.

[595] Rabindra N. Mohapatra and B. Sakita. SO(2n) Grand Unification in an SU(N) Basis. *Phys. Rev.*, D21:1062, 1980. [,283(1979)].

[596] Howard Georgi and C. Jarlskog. A New Lepton - Quark Mass Relation in a Unified Theory. *Phys. Lett.*, 86B:297–300, 1979.

[597] H. David Politzer. Reliable Perturbative Results for Strong Interactions? *Phys. Rev. Lett.*, 30:1346–1349, 1973. [,274(1973)].

[598] D. J. Gross and Frank Wilczek. Asymptotically Free Gauge Theories - I. *Phys. Rev.*, D8:3633–3652, 1973.

[599] D. J. Gross and Frank Wilczek. ASYMPTOTICALLY FREE GAUGE THEORIES. 2. *Phys. Rev.*, D9:980–993, 1974.

[600] Sidney R. Coleman and David J. Gross. Price of asymptotic freedom. *Phys. Rev. Lett.*, 31:851–854, 1973.

[601] Reinhard Oehme and Wolfhart Zimmermann. Relation Between Effective Couplings for Asymptotically Free Models. *Commun. Math. Phys.*, 97:569, 1985.

[602] J. Kubo, K. Sibold, and W. Zimmermann. Higgs and Top Mass from Reduction of Couplings. *Nucl. Phys.*, B259:331–350, 1985.

[603] Jisuke Kubo, Klaus Sibold, and Wolfhart Zimmermann. New Results in the Reduction of the Standard Model. *Phys. Lett.*, B220:185–190, 1989.

[604] W. Zimmermann. Scheme independence of the reduction principle and asymptotic freedom in several couplings. *Commun. Math. Phys.*, 219:221–245, 2001.

[605] E. S. Fradkin and O. K. Kalashnikov. Asymptotically Free SU(5) Model of Unified Interaction. *Phys. Lett.*, 64B:177–180, 1976.

[606] O. K. Kalashnikov. Asymptotically Free SU(2) x SU(2) x SU(4) Model of Unified Interaction. *Phys. Lett.*, 72B:65–69, 1977.

[607] Gian F. Giudice, Gino Isidori, Alberto Salvio, and Alessandro Strumia. Softened Gravity and the Extension of the Standard Model up to Infinite Energy. *JHEP*, 02:137, 2015.

[608] Bob Holdom, Jing Ren, and Chen Zhang. Stable Asymptotically Free Extensions (SAFEs) of the Standard Model. *JHEP*, 03:028, 2015.

[609] Holger Gies and Luca Zambelli. Asymptotically free scaling solutions in non-Abelian Higgs models. *Phys. Rev.*, D92(2):025016, 2015.

[610] Holger Gies and Luca Zambelli. Non-Abelian Higgs models: Paving the way for asymptotic freedom. *Phys. Rev.*, D96(2):025003, 2017.

[611] Holger Gies, René Sondenheimer, Alessandro Ugolotti, and Luca Zambelli. Asymptotic freedom in $\mathbb{Z}_2$ -Yukawa-QCD models. *Eur. Phys. J.*, C79(2):101, 2019.

[612] J. Julve and M. Tonin. Quantum Gravity with Higher Derivative Terms. *Nuovo Cim.*, B46:137–152, 1978.

[613] Michael S. Chanowitz, John R. Ellis, and Mary K. Gaillard. The Price of Natural Flavor Conservation in Neutral Weak Interactions. *Nucl. Phys.*, B128:506–536, 1977.

[614] A. J. Buras, John R. Ellis, M. K. Gaillard, and Dimitri V. Nanopoulos. Aspects of the Grand Unification of Strong, Weak and Electromagnetic Interactions. *Nucl. Phys.*, B135:66–92, 1978.

[615] R. D. Peccei and Helen R. Quinn. CP Conservation in the Presence of Instantons. *Phys. Rev. Lett.*, 38:1440–1443, 1977. [,328(1977)].

[616] Florian Staub. SARAH 4 : A tool for (not only SUSY) model builders. *Comput. Phys. Commun.*, 185:1773–1790, 2014.

[617] C. Wetterich. Quadratic Renormalization of the Average Potential and the Naturalness of Quadratic Mass Relations for the Top Quark. *Z. Phys.*, C48:693–705, 1990.

[618] Julia Borchardt and Benjamin Knorr. Global solutions of functional fixed point equations via pseudospectral methods. *Phys. Rev.*, D91(10):105011, 2015. [Erratum: Phys. Rev.D93,no.8,089904(2016)].

[619] Marie E. Machacek and Michael T. Vaughn. Two Loop Renormalization Group Equations in a General Quantum Field Theory. 3. Scalar Quartic Couplings. *Nucl. Phys.*, B249:70–92, 1985.

[620] E. A. Uehling. Polarization effects in the positron theory. *Phys. Rev.*, 48:55–63, 1935.

[621] Willis E. Lamb and Robert C. Retherford. Fine Structure of the Hydrogen Atom by a Microwave Method. *Phys. Rev.*, 72:241–243, 1947.

[622] Alfio Bonanno and Martin Reuter. Quantum gravity effects near the null black hole singularity. *Phys. Rev.*, D60:084011, 1999.

[623] Alfio Bonanno and Martin Reuter. Renormalization group improved black hole space-times. *Phys. Rev.*, D62:043008, 2000.

[624] Sean A. Hayward. Formation and evaporation of regular black holes. *Phys. Rev. Lett.*, 96:031103, 2006.

[625] J. M. Bardeen. . *Conference Proceedings of GR5, Tbilisi, USSR*, page 174, 1968.

[626] A. Bonanno and M. Reuter. Spacetime structure of an evaporating black hole in quantum gravity. *Phys. Rev.*, D73:083005, 2006.

[627] Kevin Falls, Daniel F. Litim, and Aarti Raghuraman. Black Holes and Asymptotically Safe Gravity. *Int. J. Mod. Phys.*, A27:1250019, 2012.

[628] Kevin Falls and Daniel F. Litim. Black hole thermodynamics under the microscope. *Phys. Rev.*, D89:084002, 2014.

[629] Ramón Torres. Singularity-free gravitational collapse and asymptotic safety. *Phys. Lett.*, B733:21–24, 2014.

[630] Ramon Torres and Francesc Fayos. On the quantum corrected gravitational collapse. *Phys. Lett.*, B747:245–250, 2015.

[631] Alfio Bonanno, Benjamin Koch, and Alessia Platania. Cosmic Censorship in Quantum Einstein Gravity. *Class. Quant. Grav.*, 34(9):095012, 2017.

[632] Alfio Bonanno, Benjamin Koch, and Alessia Platania. Gravitational collapse in Quantum Einstein Gravity. *Found. Phys.*, 48(10):1393–1406, 2018.

[633] Daniel F. Litim and Konstantinos Nikolakopoulos. Quantum gravity effects in Myers-Perry space-times. *JHEP*, 04:021, 2014.

[634] Yi-Fu Cai and Damien A. Easson. Black holes in an asymptotically safe gravity theory with higher derivatives. *JCAP*, 1009:002, 2010.

[635] Benjamin Koch and Frank Saueressig. Structural aspects of asymptotically safe black holes. *Class. Quant. Grav.*, 31:015006, 2014.

[636] Benjamin Koch and Frank Saueressig. Black holes within Asymptotic Safety. *Int. J. Mod. Phys.*, A29(8):1430011, 2014.

[637] Cristopher González and Benjamin Koch. Improved Reissner–Nordström–(A)dS black hole in asymptotic safety. *Int. J. Mod. Phys.*, A31(26):1650141, 2016.

[638] Georgios Kofinas and Vasilios Zarikas. Avoidance of singularities in asymptotically safe Quantum Einstein Gravity. *JCAP*, 1510(10):069, 2015.

[639] Jan M. Pawlowski and Dennis Stock. Quantum-improved Schwarzschild-(A)dS and Kerr-(A)dS spacetimes. *Phys. Rev.*, D98(10):106008, 2018.

[640] Ademola Adeifeoba, Astrid Eichhorn, and Alessia Platania. Towards conditions for black-hole singularity-resolution in asymptotically safe quantum gravity. *Class. Quant. Grav.*, 35(22):225007, 2018.

[641] Lando Bosma, Benjamin Knorr, and Frank Saueressig. Resolving Spacetime Singularities within Quantum Gravity. 2019.

[642] Dao-Jun Liu, Bin Yang, Yong-Jia Zhai, and Xin-Zhou Li. Quasinormal modes for asymptotic safe black holes. *Class. Quant. Grav.*, 29:145009, 2012.

[643] M. Reuter and E. Tuiran. Quantum Gravity Effects in Rotating Black Holes. In *Recent developments in theoretical and experimental general relativity, gravitation and relativistic field theories. Proceedings, 11th Marcel Grossmann Meeting, MG11, Berlin, Germany, July 23-29, 2006. Pt. A-C*, pages 2608–2610, 2006.

[644] M. Reuter and E. Tuiran. Quantum Gravity Effects in the Kerr Spacetime. *Phys. Rev.*, D83:044041, 2011.

[645] Alessia Platania. Dynamical renormalization of black-hole spacetimes. *Eur. Phys. J.*, C79(6):470, 2019.

[646] I. Dymnikova. Vacuum nonsingular black hole. *Gen. Rel. Grav.*, 24:235–242, 1992.

[647] I. G. Dymnikova. De Sitter-Schwarzschild Black Hole:. its Particlelike Core and Thermodynamical Properties. *International Journal of Modern Physics D*, 5:529–540, 1996.

[648] Abhay Ashtekar, Tomasz Pawlowski, and Parampreet Singh. Quantum Nature of the Big Bang: An Analytical and Numerical Investigation. I. *Phys. Rev.*, D73:124038, 2006.

[649] Leonardo Modesto. Semiclassical loop quantum black hole. *Int. J. Theor. Phys.*, 49:1649–1683, 2010.

[650] Rodolfo Gambini and Jorge Pullin. Black holes in loop quantum gravity: The Complete space-time. *Phys. Rev. Lett.*, 101:161301, 2008.

[651] Rodolfo Gambini and Jorge Pullin. Loop quantization of the Schwarzschild black hole. *Phys. Rev. Lett.*, 110(21):211301, 2013.

[652] Carlo Rovelli and Francesca Vidotto. Planck stars. *Int. J. Mod. Phys.*, D23(12):1442026, 2014.

[653] Piero Nicolini, Anais Smailagic, and Euro Spallucci. Noncommutative geometry inspired Schwarzschild black hole. *Phys. Lett.*, B632:547–551, 2006.

[654] Piero Nicolini, Euro Spallucci, and Michael F. Wondrak. Quantum Corrected Black Holes from String T-Duality. *Phys. Lett.*, B797:134888, 2019.

[655] Ronald J. Adler, Pisin Chen, and David I. Santiago. The Generalized uncertainty principle and black hole remnants. *Gen. Rel. Grav.*, 33:2101–2108, 2001.

[656] Sushant G. Ghosh. A nonsingular rotating black hole. *Eur. Phys. J.*, C75(11):532, 2015.

[657] Rahul Kumar, Balendra Pratap Singh, and Sushant G. Ghosh. Rotating black hole shadow in asymptotically safe gravity. 2019.

[658] Irina Dymnikova and Kirill Kraav. Identification of a Regular Black Hole by Its Shadow. *Universe*, 5(7):163, 2019.

[659] Ernesto Contreras, Ángel Rincón, Grigoris Panotopoulos, Pedro Bargueño, and Benjamin Koch. Black hole shadow of a rotating scale–dependent black hole. 2019.

[660] Cosimo Bambi. *Black Holes: A Laboratory for Testing Strong Gravity*. Springer, 2017.

[661] Yosuke Mizuno, Ziri Younsi, Christian M. Fromm, Oliver Porth, Mariafelicia De Laurentis, Hector Olivares, Heino Falcke, Michael Kramer, and Luciano Rezzolla. The Current Ability to Test Theories of Gravity with Black Hole Shadows. *Nat. Astron.*, 2(7):585–590, 2018.

[662] Jonelle L. Walsh, Aaron J. Barth, Luis C. Ho, and Marc Sarzi. The M87 Black Hole Mass from Gas-dynamical Models of Space Telescope Imaging Spectrograph Observations. *Astrophys. J.*, 770:86, 2013.

[663] Robert H. Boyer and Richard W. Lindquist. Maximal analytic extension of the Kerr metric. *J. Math. Phys.*, 8:265, 1967.

[664] Brandon Carter. Global structure of the Kerr family of gravitational fields. *Phys. Rev.*, 174:1559–1571, 1968.

[665] J. M. Bardeen. Timelike and null geodesics in the Kerr metric. In *Proceedings, Ecole d'Eté de Physique Théorique: Les Astres Occlus: Les Houches, France, August, 1972*, pages 215–240, 1973.

[666] Subrahmanyan Chandrasekhar. The mathematical theory of black holes. In *Oxford, UK: Clarendon (1992) 646 p., OXFORD, UK: CLARENDON (1985) 646 P.*, 1985.

[667] James M. Bardeen, William H. Press, and Saul A Teukolsky. Rotating black holes: Locally nonrotating frames, energy extraction, and scalar synchrotron radiation. *Astrophys. J.*, 178:347, 1972.

[668] E. T. Newman and A. I. Janis. Note on the Kerr spinning particle metric. *J. Math. Phys.*, 6:915–917, 1965.

[669] F. Staub. SARAH. 2008.

[670] F. Lyonnet, I. Schienbein, F. Staub, and A. Wingerter. PyR@TE: Renormalization Group Equations for General Gauge Theories. *Comput. Phys. Commun.*, 185:1130–1152, 2014.

[671] Hong Lü, A. Perkins, C. N. Pope, and K. S. Stelle. Lichnerowicz Modes and Black Hole Families in Ricci Quadratic Gravity. *Phys. Rev.*, D96(4):046006, 2017.

[672] David R. Noakes. The initial value formulation of higher derivative gravity. *Journal of Mathematical Physics*, 24(7):1846–1850, 1983.

[673] Peter J. Mohr, Barry N. Taylor, and David B. Newell. CODATA Recommended Values of the Fundamental Physical Constants: 2010. *Rev. Mod. Phys.*, 84:1527–1605, 2012.

[674] J. Beringer et al. Review of Particle Physics (RPP). *Phys. Rev.*, D86:010001, 2012.

[675] Daniel F. Litim. Optimization of the exact renormalization group. *Phys. Lett.*, B486:92–99, 2000.

[676] Holger Gies and Christof Wetterich. Universality of spontaneous chiral symmetry breaking in gauge theories. *Phys. Rev.*, D69:025001, 2004.

[677] Anton K. Cyrol, Mario Mitter, and Nils Strodthoff. FormTracer - A Mathematica Tracing Package Using FORM. *Comput. Phys. Commun.*, 219:346–352, 2017.

[678] C. Wetterich. Graviton fluctuations erase the cosmological constant. *Phys. Lett.*, B773:6–19, 2017.

[679] J. M. Bardeen. Timelike and null geodesics in the Kerr metric. In C. Dewitt and B. S. Dewitt, editors, *Black Holes (Les Astres Occlus)*, pages 215–239, 1973.

[680] C. T. Cunningham. The effects of redshifts and focusing on the spectrum of an accretion disk around a Kerr black hole. *Astrophys. J.*, 202:788–802, 1975.

[681] J.-P. Luminet. Image of a spherical black hole with thin accretion disk. *Astronomy and Astrophysics*, 75:228–235, May 1979.

[682] S. U. Viergutz. Image generation in Kerr geometry. I. Analytical investigations on the stationary emitter-observer problem. *Astronomy and Astrophysics*, 272:355, May 1993.

[683] Kris Beckwith and Chris Done. Extreme gravitational lensing near rotating black holes. *Mon. Not. Roy. Astron. Soc.*, 359:1217–1228, 2005.

[684] Inc. Wolfram Research. Mathematica, version 11.2. *Champaign, Illinois*, 2017.

[685] Jason Dexter and Eric Agol. A Fast New Public Code for Computing Photon Orbits in a Kerr Spacetime. *Astrophys. J.*, 696:1616–1629, 2009.

[686] S. V. Iyer and E. C. Hansen. Light's Bending Angle in the Equatorial Plane of a Kerr Black Hole. *Phys. Rev.*, D80:124023, 2009.